DOCTORAL THESIS

Presented to the Department of Pharmacy
Graduate School of Pharmaceutical Science

University of Naples Federico II
For the Degree of

DOCTOR OF PHILOSOPHY

ADVANCED STRATEGIES TO DELIVER BIOACTIVE MOLECULES IN NUTRACEUTICALS

by

DILETTA ESPOSITO

Approved by

Ph.D. Supervisor: Prof. Fabiana Quaglia, PhD

Ph.D. Program Coordinator: Prof. Maria Valeria D'Auria, PhD

University of Naples Federico II, Naples, Italy

January 2020

TABLE OF CONTENT

Chapter 1

Background and aims

1.1 Nutraceuticals: the future of intelligent food

Nowadays, nutraceuticals have received considerable interest due to their potential nutritional, safety and therapeutic effects (Nasri, 2013). It has been highlighted that the worldwide dietary supplement market is widely expanding and reaching $250 billion by 2018, roughly five times larger than in 1999. This size is notable when compared with the $ 900 billion pharmaceuticals market, but it is still small compared to the $5 trillion worldwide food industry (KPGM report, Partners 2015).

Followed by Germany (13% market share), France (9%) and Great Britain (8%), with 23% market share and €3.3 billion revenues in 2018, Italy's nutraceutical industry is the largest in Europe (www.statista.com/Value of the dietary supplements market in Europe 2015 and 2020, by country Published by StatistaResearchDepartment, Jan17,2018).

The term 'nutraceuticals' is a syncretic neologism initially coined in the late 1980s by Stephen DeFelice (DeFelice, 1995) and has since been used to describe a wide variety of non-pharmaceutical compounds that may have an impact on health and disease conditions, general well-being and human performance. The term is poorly defined and has been used by consumers, producers and even healthcare professionals to refer to many different types of compounds, including (semi)-purified substances from natural sources, plant extracts, dietary supplements, vitamins and minerals, phytonutrients, various products combined with functional ingredients and even modified whole foods. Conceptually, this area of interest can be positioned between medicinal drugs and basic nutrition, emphasizing the 'nutri-' (towards basic nutritional concepts) or the '-ceutical' (resembling pharmaceuticals approaches) parts of the word 'nutraceuticals' (Schmitt & Ferro, 2013).

Nutraceuticals may be used to improve health, delay the aging process, prevent chronic diseases, increase life expectancy or support the structure or function of the body. If a substance contributes only to the maintenance of healthy tissues and organs, then it may be considered as food ingredient. On the other hand, if it shows a modifying effect on the body's physiological functions and is supported by a positive scientific opinion, it is classified as nutraceutical (Vozza, Khalid, Byrne, Ryan, & Frias, 2017).

Differently from drugs, which are subjected to strict pre-clinical and clinical trials before receiving the marketing authorization, nutraceuticals are often used in the absence of clinical studies proving their effectiveness and safety in humans. Hence, there is an increasing need to conduct clinical trials in accordance with the established rules to determine their effectiveness,

safety and the long-term effects (Santini, Cammarata, Capone, Ianaro, Tenore, Pani, et al., 2018).

In this scenario, in 2002 the General Food Law Regulation (Regulation (EC) No. 178/2002 of the European Parliament and of the Council 2002), established the principle and foresaw the creation of an independent organization called the European Food Safety Authority (EFSA) with the specific task of giving scientific advice based upon scientific assessment of the beneficial health effects and associated risks related to food intake (Santini, et al., 2018).

In Europe, any product that claims to be a nutraceutical has to be certified first by the EFSA, which checks the supporting documentation and establish whether it lives up to its claims. The EFSA also sets maximum and minimum levels of ingredients to be added to food supplements and packaging requirements. Labels cannot contain claims that nutraceuticals will diagnose, cure, mitigate, treat a disease, nutrition, and health claims must be authorized at the European level (KPGM report, Partners 2015).

Recently many studies have shown promising results for several bioactive compounds in various pathological complications such as diabetes (Balandrán-Quintana, Ana, Miguel, & Rogerio, 2013), atherosclerosis (Nasri, 2013), cardiovascular diseases (CVDs) (Khosravi-Boroujeni, Sarrafzadegan, Mohammadifard, Sajjadi, Maghroun, Asgari, et al., 2013), cancer (Shirzad, Kordyazdi, Shahinfard, & Nikokar, 2013), and neurological disorders (Roohafza, Sarrafzadegan, Sadeghi, Rafieian-kopaei, Sajjadi, & khosravi-boroujeni, 2013).

Nevertheless, sometimes the claimed health benefits can induce false expectations missing the target for a product to be useful as claimed and may not be appropriately substantiated by appropriate experimental trials (Santini, et al., 2018). Furthermore, the association of components is almost always employed in nutraceuticals and attribution of a specific physiological activity, and thus claim, to one component erroneously cover the other components in the formula. This creates novel opportunities for the market but is misleading from a scientific standpoint.

Under EU regulations, any food that was not consumed “significantly” before May 1997 is considered as a novel food. The category covers new foods, food from new sources, new substances used in food as well as new ways and technologies for producing food. As of 1 January 2018, the new Regulation (EU) 2015/2283 on novel foods repeals and replaces Regulation (EC) No 258/97 and Regulation (EC) No 1852/2001, which were in force until 31 December 2017. In this frame, a novel food can be a newly developed food, innovative food, food produced using new technologies and production processes, as well as food which is or has been traditionally eaten outside of Europe.

A novel food does not present a safety risk, its use does not mislead consumers, and it is not nutritionally disadvantageous for them. For a centralized safety evaluation of novel foods, the European Commission requested the EFSA to update and develop scientific and technical guidance for the preparation and presentation of applications for their authorization and risk assessment. In this regard, even foods originating from plants, animals, microorganisms, cell cultures, and specific categories of foods (insects) are considered as a novel food. To ensure a high level of protection of human health and consumers' interests, food consisting of engineered nanomaterials should also be considered a novel food under this European regulation.

In the last years, the interest of the scientific community has been focused not only on the evaluation of their beneficial properties but also on the optimization of nutraceutical dosage forms, which can preserve the provisions on their efficacy overcoming the hurdles of their administration. Although nutraceutical products have wide diffusion, some critical aspects like absorption of bioactive compounds, their bioavailability, stability, and shelf-life have been poorly addressed so far.

In this context, the development of new tools seems central to resolve the issues related to their delivery and to demonstrate the real advantageous effects on human health also given the growing market demand.

1.2 Lights and shadows on nutraceutical dosage forms

The exclusive route for the administration of nutraceuticals is the oral one because of patient compliance, long-term acceptance, and painless/non-invasive administration (Sastry, Nyshadham, & Fix, 2000). The dosage forms intended for oral nutraceutical administration include solid forms such as tablets, capsules, and liquid formulations. Tablets can be coated to control the release rate of the bioactive compounds, to cover bad odor/taste, to facilitate administration (sugar-coated tablets, film-coated tablets, multiple compressed tablets, enteric coated-tablet), can be effervescent or chewable. Capsules can be made of either gelatin or hydroxypropyl cellulose (vegetal capsules). They can be gastro-resistant and contain solid or liquid inside. Liquid dosage forms include syrups, drops, solutions, and suspensions (Kumar, 2015).

After ingestion, a series of physical and chemical changes may occur to a delivery system as it moves from the mouth to the large intestine, including changes in pH, ionic composition, surface activity, enzyme activity, agitation, and temperature (D. J. McClements & Li, 2010) (Fig. 1). Common drawbacks with solid dosage forms are i) long disaggregation time; ii) too slow release of the bioactive component from the dosage form; iii) sub-optimal dissolution and

in small intestinal fluids (bioaccessibility); iv) reduced diffusion across mucus layer and low intestinal epithelial permeability; v) pH- and enzymatic degradation in gastrointestinal (GI) environment, vi) biotransformation during GI transit.

All of these issues must be taken into account in designing the dosage form to get an efficient absorption into the bloodstream and, in turn, physiological effects (Braithwaite, Tyagi, Tomar, Kumar, Choonara, & Pillay, 2014). Furthermore, hampered absorption due to dietary factors interferences can occur. The bitter or bad taste of some bioactive compounds and their degradation, when exposed to detrimental conditions during processing and storage (presence of oxygen, humidity, temperature and light), should be considered too. These conditions lead to undesirable changes in the product and organoleptic features (color, taste, appearance) (Aditya, Espinosa, & Norton, 2017).

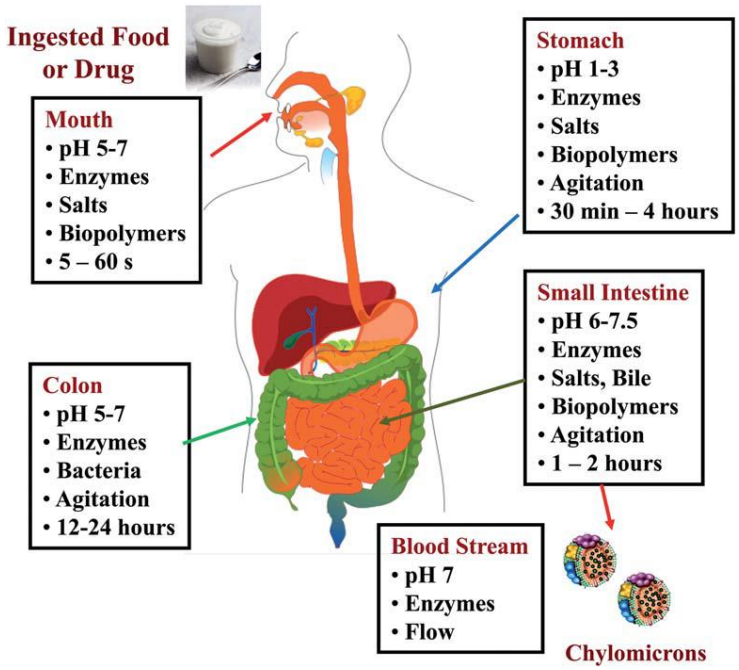

Fig. 1. Schematic representation of the physiological conditions in different regions of the human gastrointestinal tract affecting the liberation, absorption, metabolism, and distribution of bioactive compounds (D. McClements & Xiao, 2014).

Nutraceutical manufacturing involves several main steps, starting with raw material harvesting and storage through processing to get the final products. The process production commonly employed include extraction, purification, thermal process, extrusion, the application of freeze-drying, and spray drying technologies. After that, ingredients are processed to give the dosage form, which represents another critical step to ensure the proper

quality of the final product. The development of a nutraceutical production matching quality criteria is thus hard and problematic, and especially standardization of operative procedures seems to be complicated. Besides, the manufactures must overcome the issues related to process validation, including the reproducibility of the applied methods, the lack of studies on the compatibility of bioactive compounds and ingredients, the stability of the compounds, and the packaging materials which can be employed in the production process.

Dietary supplements are evaluated considering different features such as their identity (conformity to the recognized standards of identity and the level of quality claimed on the label), strength (the product contains the amount of ingredient claimed on the label), purity (absence of contaminants) and disintegration in the human body (the product properly break apart). In particular, most supplements presented as solid dosage forms must first disintegrate and dissolve the active ingredient in the gut to allow its absorption and enter the bloodstream. This requirement is needed from regulatory agencies only in some countries such as the USA, while in Europe, the approval conditions are so different so that producers do not always fulfill all the requirements cited above. This is also because supplements are not considered as pharmaceutical dosage forms, and reference to quality tests reported in the country Pharmacopoeia is not mandatory.

For example, the standard laboratory test for disintegration (part of the test known as the United States Pharmacopeia [USP] "Disintegration and Dissolution of Dietary Supplements" method <2040>), is an essential test of product quality. However, passing this test alone does not assure bioavailability – which depends on additional factors such as how well ingredients are absorbed. During the test, the product under investigation is continuously agitated in water. In that time, a tablet should have dissolved or fallen apart to the extent that, if touched, there is no hardcore remaining. Some manufacturers claim their products meet the USP specification, although the claim should not be taken as certainty (www.consumerlab.com).

In this scenario, it is evident that several drawbacks to formulation development are related to the manufacturing process.

During this decade, the regulatory requirements are changing rapidly for nutraceutical products. The FDA's (Food and Drug Administration) Good Manufacturing Practices (GMPs) for dietary supplements allow each manufacturer to determine the quality standards and analytical methods it uses to evaluate the quality of its products. The holder of market authorization is also responsible for vigilance on dietary supplements after their launch.

The FDA is issuing a final rule regarding current good manufacturing practice (cGMP) for dietary supplements. The final rule establishes the minimum cGMPs necessary for activities

related to manufacturing, packaging, labeling, or holding dietary supplements to ensure their quality. The general food cGMPs in part 110 (21 CFR part 110) mostly address practices designed to ensure that food is manufactured, processed, packed, and held under sanitary conditions and that the food is safe, clean, and wholesome.

Dietary supplements are a type of food product for which specific food cGMPs also are needed (21 CFR part 111). Well-established principles of cGMP require process controls at each step of the manufacturing process as early in the production process as possible because the quality cannot be tested into the product only at the end. Instead, the quality of the dietary supplement must be built into the product throughout the manufacturing process; quality begins with the starting material and continues with the product being manufactured in a reproducible manner according to established specifications.

It is not sufficient nor adequate to rely solely on end-product testing to assure the quality of the individual dietary supplement product sold to the consumer. cGMPs are intended to establish a comprehensive system of process controls, including operators, machines involved, and documentation of each stage of the manufacturing process, that can minimize the likelihood of detect problems and variances in manufacturing as they occur and before the product is in its finished form. These process controls that are a part of cGMPs are essential to ensure that the dietary supplement is manufactured, packaged, held, and labeled in a consistent and reproducible manner.

FDA regulations and GMP guidelines are under constant implementation as for the pharmaceutical industry, so the cost of manufacturing is expected to increase rapidly with sudden changes in nutraceutical market (www.fda.gov/food/current-good-manufacturing-practices-cgmps/current-good-manufacturing-practices-cgmps-dietary-supplements).

1.3 Delivery technologies and nutraceuticals: a route for innovation

1.3.1 Delivery platforms for nutraceuticals: a new route for innovation

Lately, the research efforts are focusing on the design of innovative strategies that could improve nutraceutical products through the application of delivery technologies.

There has been a growing interest in delivery systems able to encapsulate and protect poorly-stable bioactive molecules using food approved ingredients and processing procedures. In particular, the application of micro-nano technology has been considered a valid strategy to address these challenges. The composition and structure of micro/nano-systems can be carefully tailored to control functional properties, such as improved dispersibility, enhanced chemical stability, increased bioavailability, and finally control the release rate of the active

component to get “high performance” products that may satisfy patient’s needs (D. J. McClements, 2015).

While micro-technologies are consolidated in the food industry, moving to the nanoscale represents a potential risk for people. The regulation of nanotechnology application to food products is thus a dynamic and evolving area and is focused on the development of new approaches to risk assessment on human health. In the United States, the FDA is involved in this process and operates in concert with the National Nanotechnology Initiative (NNI). In Europe, the Institute for Health and Consumer Protection (IHCP) is the regulatory body proactively involved in nanomaterials safety, identification, and detection. Both agencies focus their attention on the potential risks and benefits of nanomaterials on human health and the environment. In the food sector, EFSA works closely with the IHCP to explore the behavior of engineered nanomaterials and to validate the standard operative procedure for their characterization (Vozza, Khalid, Byrne, Ryan, & Frias, 2017). Recently, due to the emerging use of nanomaterials in foods, EU legislation (No. 1169/2011) on novel foods has introduced obligatory labeling of nanomaterials on packaging (European Parliament, 2011) and EFSA has published guidance for assessing the risks of nanotechnologies in food and feed. In order to show the wide variety of systems developed in the last years, the most frequently applied nanoformulations are reported in Fig. 2.

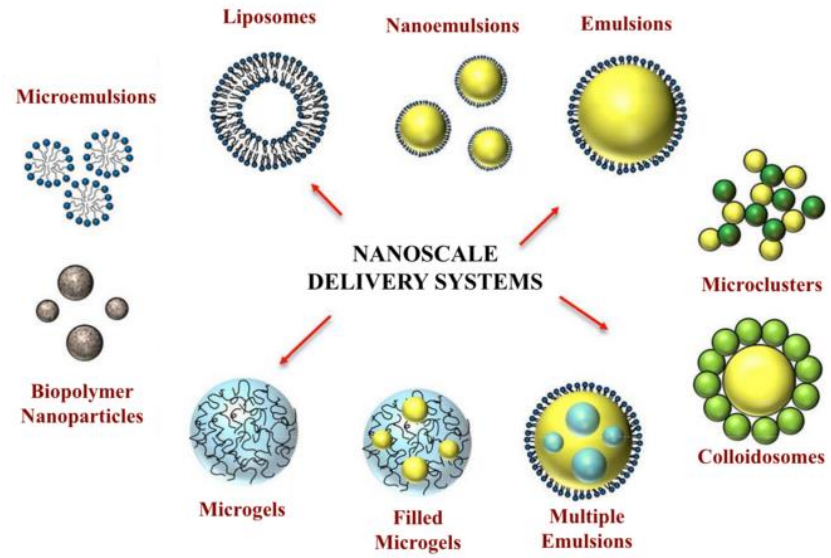

Fig. 2. Nanoplatfoms can be applied in the dietary supplements field for different medical purposes.

1.3.2 Design of particle-based formulations

Recently a new classification system, nutraceutical bioavailability classification scheme (NuBACS) has been devoloped for food bioactives. It is an extension and modification of biopharmaceutical classification system (BCS), wherein, it takes into consideration the complex factors that limit the oral bioavailability of bioactives other than just solubility and permeability. Liberation from food matrices, interaction with gastrointestinal components, degradation and metabolism of the molecules and their epithelium cell permeability were considered to provide a rational design of the delivery systems.

Oral bioavailability can be defined as the fraction of a specific ingested substance that eventually reaches an individual's circulatory system in an active form (Parada & Aguilera, 2007). The overall bioavailability (BA) is determined by three main factors (D. McClements & Xiao, 2014):

$$BA = B* \times A* \times T*$$

$B*$ is the bioaccessibility of the substance within the intestinal fluids. For hydrophilic compounds, it is the fraction that is released from the food matrix and dissolved in the intestinal fluids, whereas for hydrophobic substances, this is the fraction that is solubilized within mixed micelles in the small intestinal fluids. $A*$ is the absorption of the substance from the GI fluids into the systemic circulation, that is, the fraction that passes through the mucus layer, across the epithelium cells, and reaches the bloodstream. $T*$ is the fraction of the absorbed substance that reaches the site of action in an active state.

As reported in Fig. 3 for the case of bioactive compounds formulated in nanoparticles, different strategies can be exploited for spatiotemporal control of the delivered dose and, in turn, affect physiological effects.

As compared with unprocessed bioactive compounds, a nanotech bioactive can take benefit of particle behavior in the GI tract, such as interaction with mucosa or responsiveness to environmental conditions. The increase of $B*$ can be thus be attained via modulation of dissolution/release rate, the extension of the residence time of the system at the absorption site, and protection of the cargo to minimize its inactivation.

The composition and structure of a delivery system for a special bioactive compound can be thus designed to improve bioavailability by altering $B*$, $A*$, and $T*$ (F. Liu, Ma, Gao, & McClements, 2017).

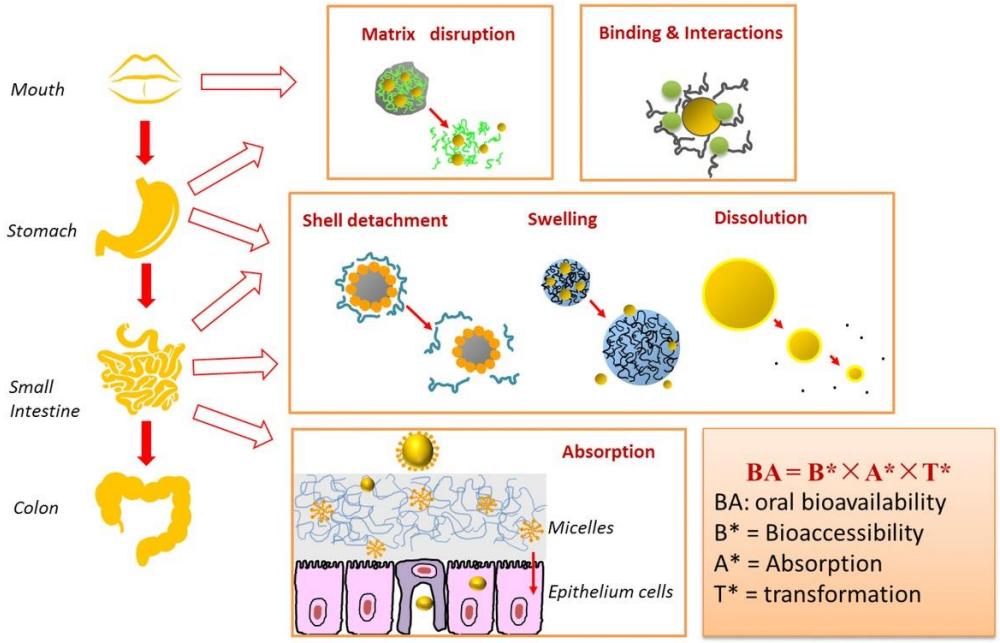

Fig. 3. Possible design of a nanoparticulate system designed to improve the oral bioavailability of bioactive compounds in the GI tract (F. Liu, Ma, Gao, & McClements, 2017).

1.3.3 Nanotech-based nutraceutical formulations

Over the last decade, various types of raw materials have been used as carrier excipient for nutraceuticals, and several research papers are published annually by scientists both from industry and academia where the application of nanotechnologies for food fortification is reported (Yao, McClements, & Xiao, 2015). Food formulators are restricted to using edible biopolymers and approved as Generally Recognized As Safe (GRAS) synthetic polymers. Besides, the awareness of naturalness among general consumers has put enormous pressure on the identification of novel biopolymers useful in food formulations.

Some of the biopolymers that can be used in the design of innovative colloidal delivery systems include polysaccharides (alginic acid, dextran, xanthan gum, chitosan), polysaccharides from plant sources (pectin, starch, arabic gum, carrageenan), polysaccharides from microbial origin (xanthan gum, dextran), food proteins (soy proteins, albumin, casein, zein, gelatin, whey proteins), lipids and low molecular weight surfactants (Table 1). Their rational combination to deliver bioactive compounds with high impact in the nutraceutical field is currently the research core for the development of innovative products that can respond to the expected benefits for patient care.

Since most of these materials are hydrophilic, delivery systems are designed based on protein-polysaccharide interactions, bioactive molecule-biopolymer binding, self-assembling, pH-dependent solubility differences, cross-linking and hydrophobic modifications (A. R. Patel & Velikov, 2011). Their appropriate combinations can potentiate the properties of micro- and nano delivery systems in terms of mechanical, thermal and barrier resistance, encapsulation efficiency, stability and absorption of bioactive compounds, in comparison with those obtained by using a single material (de Souza Simões, Madalena, Pinheiro, Teixeira, Vicente, & Ramos, 2017).

In this scenario, polysaccharides are central due to crucial properties such as excellent stability, safety profile and biodegradability (O. Ramos, Pereira, Rodrigues, Teixeira, Vicente, & Malcata, 2014). Some polysaccharides show mucoadhesive properties, which is a desirable feature to improve the residence time of a delivery system at the mucosal level and promote effective absorption of the bioactive cargo (Livney, 2010). Moreover, they can form protective shells which are stable to high-temperature processes, due to their higher stability as compared to lipid- or protein-based delivery systems that melt or denature (Vega-Baudrit, 2019).

On the other hand, proteins hold a high nutritional value and notable functional properties (Augustin & Hemar, 2009). Due to their structural versatility, several delivery systems can be produced (film, particles, fibers, and hydrogels), providing the delivery of either lipophilic or hydrophilic compounds (Wan, Guo, & Yang, 2015). Due to their amphiphilic structure, several binding sites establishing electrostatic and hydrophobic interactions with the carried bioactive component can guarantee a high loading of the delivery platform (O. L. Ramos, Pereira, Martins, Rodrigues, Fuciños, Teixeira, et al., 2017). Nowadays, proteins nanoencapsulation may provide a new approach for targeted and controlled delivery of bioactive compounds in the human gut by avoiding nanoparticle aggregation and degradation during storage or in the stomach environment (C. Wang, Tian, Chen, Temelli, Liu, & Wang, 2010).

Lipid-based delivery systems represent another class uniquely suited for bioactive with poor solubility and intestinal permeability. Nanoemulsions, solid lipid nanoparticles, and liposomes are widely used for this purpose (Bhushani, Harish, & Anandharamakrishnan, 2017).

Oil-in-water (o/w) nanoemulsions are kinetically stable systems containing two immiscible liquids stabilized by surfactant materials. They are useful to encapsulate lipophilic compounds such as polyphenols, vitamins, fatty acids, and sterols, while the second one has been considered to deliver water-soluble compounds like folic acid (X. Wang, Jiang, Wang, Huang, Ho, & Huang, 2008). Recently, poorly water-soluble nutraceuticals such as vitamin A palmitate, vitamin K2, coenzyme Q_{10}, quercetin, and *trans*-resveratrol were formulated using

monoglyceride (Capmul MCM), triglyceride (Captex 355) and Tween 80 (Shah, Desai, Thool, Dalrymple, & Serajuddin, 2018).

Self-emulsifying drug delivery systems usually comprise an isotropic mixture of oils, surfactants and nutrients. Their smaller size and large surface area enhance the aqueous solubility of hydrophobic compounds loaded. In fact, after the administration, SEDDS-based formulations get rapidly dispersed in the gastrointestinal tract and deliver their cargo (Singh, Kumari, & Kumar, 2017). Solid SEDDS of coenzyme Q_{10} with high photostability and oral bioavailability were produced by spray-drying to enhance the nutraceutical value of coenzyme Q_{10}. Silymarin oil was formulated in self-emulsifying drug delivery systems (SMEDDS) and proposed as a treatment of induced hepatotoxicity in mice (Garg, Sharma, Rath, & Goyal, 2017).

Solid lipid nanoparticles are prepared through hot or cold homogenization. The solubility of the bioactive compounds in melted lipids and the miscibility with the lipidic phase affect its loading capacity in the matrix. Curcumin (Wang 2015), β-carotene and α-tocopherol (Trombino, Cassano, Muzzalupo, Pingitore, Cione, & Picci, 2009), quercetin (Aditya, Espinosa, & Norton, 2017), resveratrol (Pandita, Kumar, Poonia, & Lather, 2014), were efficiently delivered in those nanosystems.

Among vesicular carriers, liposomes are the most diffused in the formulation of nutraceuticals. Liposomes are phospholipid vesicles composed of a lipid bilayer formed by hydrophilic-hydrophobic interactions that segregate the inner aqueous phase from the external continuous water phase. The lipid bilayer acts as a semi-permeable membrane containing a hydrophilic head (polar) and a hydrophobic tail (non-polar). The most common methods to produce liposomes are high-pressure homogenization, microfluidization, electro-spraying. Besides, liposomes show excellent ability to encapsulate hydrophobic, hydrophilic, and amphiphilic bioactive compounds. However, several significant shortcomings limit their commercial application, like, high cost, low physicochemical stability, drug leakage, and fast release in the gastrointestinal tract.

Liposomes are commonly termed phytosomes in nutraceutical formulation. Phytosomes are, in fact, complex (and not well-structured and characterized vesicles) of natural bioactive materials and phospholipids, mostly phosphatidylcholine, which should increase the absorption of herbal extracts or isolated active ingredients when applied topically or orally. Phytosome technology has been effectively used to increase the bioavailability of herbal extracts, including ginkgo, milk thistle, green tea successfully as well as phytochemicals such as curcumin and silybin. In the phytosome, the bioactive compounds are an integral part of the membrane, being

the molecules stabilized through non-covalent bonds to the polar head or lipophilic chains of the phospholipids (Karimi, Ghanbarzadeh, Hamishehkar, Pezeshki, Mostafayi, & Gholian, 2015).

Table 1. An overview of the component which can be employed to design food-grade delivery systems (D. McClements & Xiao, 2014).

Structural component	Examples	Critical features	Delivery systems
Biopolymers	*Globular proteins*: whey, soy, egg *Flexible proteins*: casein, gelatin *Nonionic polysaccharides:* starch, dextran, agar, galactomannans, cellulose *Anionic polysaccharides:* alginate, pectin, xanthan, carrageenan, gellan, gum Arabic *Cationic polysaccharides*: chitosan	• Molecular weight • Polarity and charge • Solubility • Conformation and flexibility • Surface activity and load • Adsorption kinetics	Molecular complexes Hydrogel particles Polymeric particles Polymeric fibers
Surfactants	*Non-ionic*: Tween, Span *Anionic:* SLS, DATEM, CITREM *Cationic*: Lauric arginate *Zwitterionic*: lecithin	• Head group/tail group • Polarity and charge • Molecular geometry • Solubility • Surface activity and load • Adsorption kinetics	Liposomes Micelles
Lipids	*Animal fats*: beef, pork, chicken *Fish oils*: cod liver, menhaden, salmon, tuna *Plant oils:* palm, coconut, sunflower, safflower, corn, flaxseed, soybean *Flavor and essential oils:* lemon, lime, orange, thyme, clove *Indigestible oils*: paraffin oils, olestra	• Polarity • Rheology • Chemical stability • Physical state • Digestibility	Nanoemulsion Solid lipid nanoparticles

Among the self-assembled ‘systems, micelles are aggregates of molecules with amphiphilic properties, which organize as hydrophobic cores surrounded by a hydrophilic shell.

Hydrophobic regions can be useful to accommodate lipophilic compounds. In the food field, micelles were employed to deliver curcumin, catechins, and omega-3-fatty acids (Bhushani, Harish, & Anandharamakrishnan, 2017).

1.4 Zein: a promising plant-based protein for nutraceuticals product

1.4.1 Zein properties

The raw materials employed as excipients to formulate nutraceutical products must show some mandatory attributes such as the state of GRAS (Generally Recognized As Safe), natural origin, biocompatibility, low cost, full availability and a long history of their use (A. R. Patel & Velikov, 2011).

Among biopolymers, proteins offer numerous benefits as compared to lipids, polysaccharides, synthetic, and inorganic polymers (Labib, 2018). Biodegradability, high capacity to incorporate active molecules, and to interact with other natural polymers characterized by different polarity, make natural proteins promising excipients for nutraceuticals delivery (Paliwal & Palakurthi, 2014). Then, plant-based proteins are renewable sources that have received a broad consensus by the scientific community as compared with animal proteins because their use avoids the risk of infection and biological contamination (Reddy & Yang, 2011).

Nevertheless, most protein polymers that are currently used for drug delivery applications are water-soluble, which poses some drawbacks mainly if the delivery strategy is aimed to attain sustained-release features (G. Wang & Uludag, 2008). Thus, the identification of hydrophobic protein is a crucial point in designing nutraceutical products modulating the release of their bioactive cargo.

Zein, a plant-based protein extracted from corn (*Zea mays L.)* (MW =35 kDa), is water-insoluble due to the presence of a high number of hydrophobic amino acids. It is formed by three different fractions which present different solubility and molecular weight (α-zein MW 19–24 kDa 75–80% of the total protein; β-zein MW 17–18 kDa 10–15% and γ-zein MW 27 kDa 5–10%) (S.-Z. Wang & Esen, 1986). Commercial zein is made up of α-zeins (Wilson 1988). Only α-zein is found in commercial zein in large amounts because the other types of zeins (β, γ, and δ) are thought to contribute to gelling, which is a shortcoming of commercial zein products, and can be eliminated during the extraction process from corn (Lawton, 2002).

Since 1985, zein has been approved by FDA as GRAS excipient, and it is used as coating material and as a carrier of bioactive compounds in the form of film, fibers, and colloidal

particles. As a natural polymer, it can be employed in the food field and is a promising candidate for the delivery of functional ingredients due to its hydrophobicity and bioadhesive properties (Ashok R. Patel & Velikov, 2014). In Fig. 4, the platforms developed with this plant-based protein are reported.

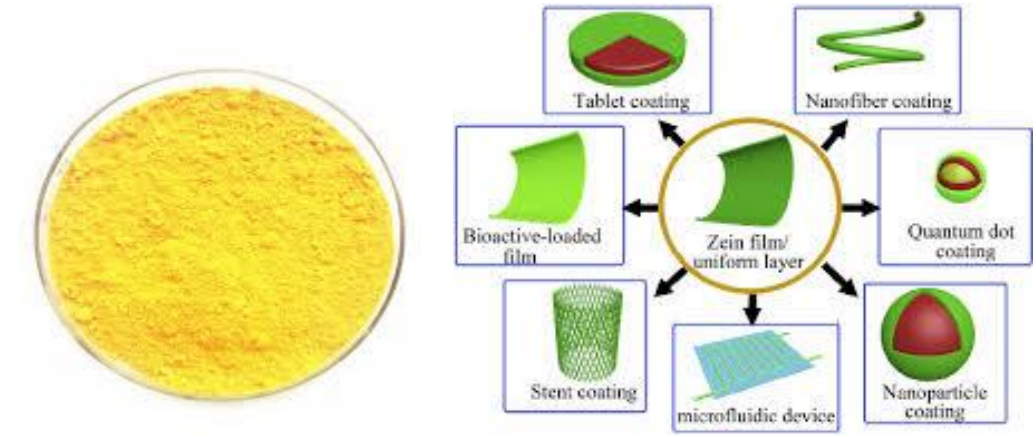

Fig. 4. Zein appearance and use as a delivery platform (Ashok R. Patel & Velikov, 2014).

During the ’80s, electrophoresis and chromatographic methods were used for the characterization of zein after extraction and purification to clarify the presence of different molecular weight fractions. In the last decades, efforts were devoted to also elucidating the zein structure. Zein is formed of helical wheel conformation with nine homologous repeating units arranged in an antiparallel form and is stabilized by hydrogen bonds. In another following study, a small-angle X-ray scattering technique (SAXS) demonstrated that the monomeric structure of zein is formed of ten successively folded helical segments. However, a relatively recent study has proposed that zein structure is composed of 9 α-helices arranged in super-helical structures, each stacked end to end of 3 helices (Fig. 5) (Labib, 2018).

Zein comes from the protein group known as prolamines (Demir, Ramos-Rivera, Silva, Nazhat, & Boccaccini, 2017) and its hydrophobicity is linked to the high percentage of apolar amino acids such as glutamic acid (21–26%) and nonpolar amino acids such as leucine (20%), proline (10%) and alanine (10%) which altogether constitute the 60% of its total amino acid content. Due to its peculiar composition, zein is soluble in binary mixture of water and aliphatic alcohol such as methanol, ethanol and propanol, aqueous acetone, and aqueous alkaline solutions with pH ≥ 11.5.

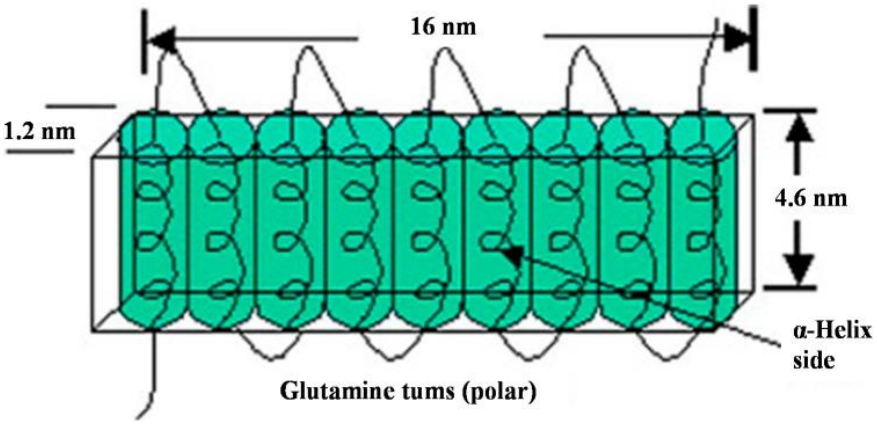

Fig. 5. Possible α-zein structural model (Q. Wang, Xian, Li, Liu, & Padua, 2008).

The solubility behavior of zein is shown in its ternary phase diagram in Fig. 6. At constant temperature, the protein solubility spans in the range from 2 to 60 % (w/w), depending on ethanol concentration. In fact, at low ethanol concentration (<40 %) and at high concentration (> 90 %), two liquid phases appear, both containing zein, water, and ethanol. This corresponds to a transition state between the complete zein solubilization and its precipitation (Shukla & Cheryan, 2001).

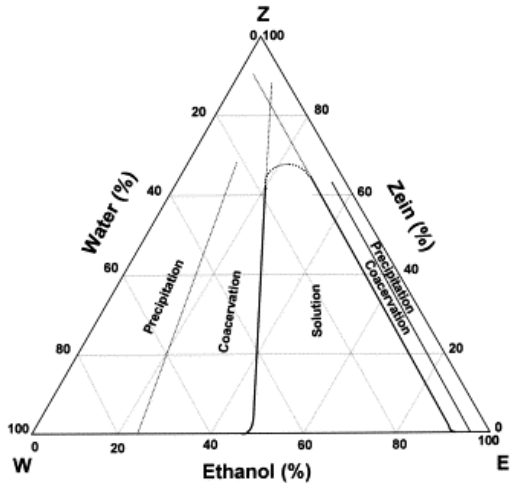

Fig. 6. Ternary diagram phase indicating zein solubility (Shukla & Cheryan, 2001).

1.4.2 Zein-based platforms for nutraceutical delivery

Since the '90s, zein-based delivery systems received extensive research interest in the field of biomedicine and drug delivery due to its GRAS regulatory status and secure preparation procedures. According to recent pieces of evidence, the potential of zein is underestimated, and

it will always attract significant interest in the next future with many applications in different sectors (Luo & Wang, 2014).

As widely reported in the literature, zein is mostly employed to develop fibers, films, gels, and micro/nano delivery systems (Fig. 7) (Labib, 2018).

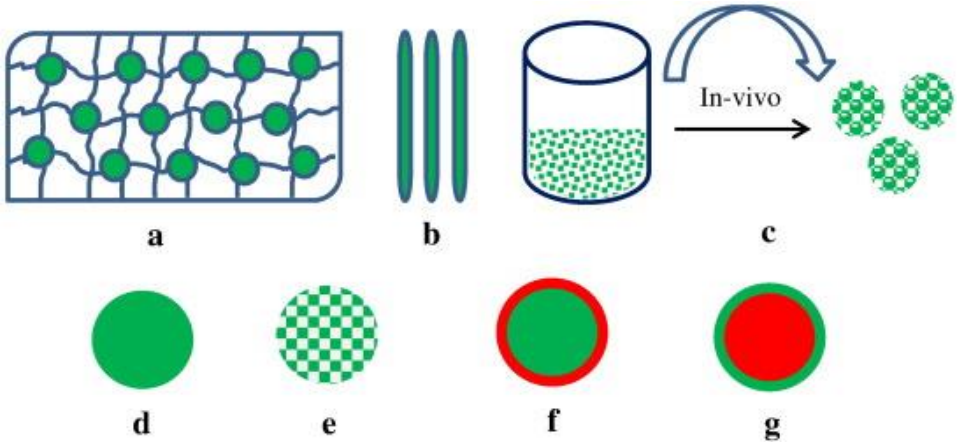

Fig. 7. Schematic representation of zein-based delivery systems (A) film; (B) fibers; (C) gel; (D) matrix-type micro/nanospheres; (E) porous micro/nanospheres; (F) core in surface-modified nanoparticles (G) zein as surface modifier of nanoparticles.

Moreover, zein is also used as a coating material due to resistance to high temperatures and humidity, which allows prolonging shelf-life of the final products (Paliwal & Palakurthi, 2014). Thanks to the presence of many lateral chains of aminoacidic residues, zein can be easily processed as films either through interaction with other materials or by chemical procedures of cross-linking. Zein films have a regular surface, are hydrophobic, biodegradable, and resistant to microbial attacks (Paliwal & Palakurthi, 2014). Surfactant-free aqueous zein pseudo-latex was developed for the coating of both tablets and pellets. The system contained propylene glycol as plasticizers to eliminate surface defects of the coated layer while improving film flexibility, as well as methyl or propylparaben as preservatives (O'Donnell, Wu, Wang, Wang, Oshlack, Chasin, et al., 1997).

The fibers produced by electrospray/electrospinning can mimic the extracellular matrix and can provide a large surface for loading selected bioactive molecules. The incorporation of antibacterial agents into zein fibers to prevent the proliferation of bacteria is one type of active food packaging (Aytac, Keskin, Tekinay, & Uyar, 2017). Zein nanofibers have found applications also in other biomedical fields such as tissue engineering due to their superior mechanical resistance.

For its hydrophobic nature, zein can be easily used to form nanoparticles through desolvation or coacervation in which the solubilizing capacity of the primary solvent (commonly it is ethanol at 70-80 % w/v) is modified by the addition of a non-solvent phase (water). Thus, nanoparticles can be purified (filtration) or dried (freeze-drying or spray-drying).

Considering the zein solubility profile, anti-solvent co-precipitation was used as a master method to produce zein micro- or nano-particles exploiting the switch of the polarity of the liquid phase in which the material is initially dissolved. The formation of zein micro-nano particles occurs after mixing the organic phase of zein in ethanol/water and a second phase, usually water, miscible with the first one (Ashok R. Patel & Velikov, 2014).

Due to the excellent miscibility of ethanol and water, ethanol in the dispersed droplets diffuses into the bulk water. Zein becomes insoluble and precipitates to form spherical colloidal particles when the ethanol concentration in the dispersed droplets decreases below the solubilization limit (Fig. 8) (Ashok R. Patel & Velikov, 2014).

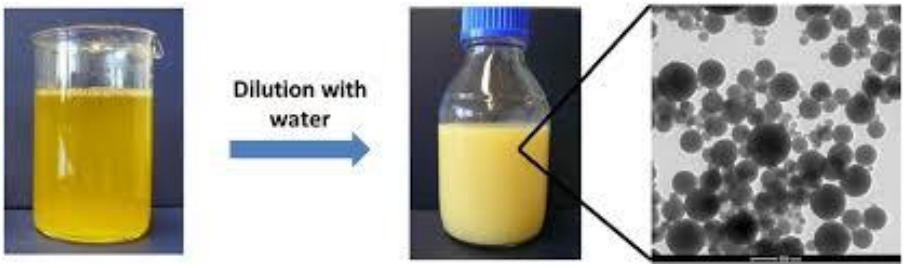

Fig. 8. Zein dissolved in a hydroalcoholic solution (ethanol/water) and diluted with water to get spherical colloidal particles (Ashok R. Patel & Velikov, 2014).

The first category of bioactive compounds encapsulated in zein nanoparticles were essential oils (Parris, Cooke, & Hicks, 2005) and since then zein was considered to entrap many lipophilic compounds including fish oil (Zhong & Jin, 2009b), vitamins (Luo, Teng, & Wang, 2012) and polyphenols (Zou & Gu, 2013). Zein nanoparticles can encapsulate lipophilic compounds due to strong hydrophobic interactions and thus providing a sustained release rate of cargo. Another in vivo study demonstrated that zein nanoparticles could remarkably improve the bioavailability of daidzin 2- folds as compared with that of a daidzin solution when orally administered into mice improving the solubility of a poorly absorbed nutrient (Zou & Gu, 2013).

A smart modification of the anti-solvent precipitation method has been proposed to form hollow nanoparticles for the delivery of short nucleic acid. The process involves precipitation

of zein in the presence of a calcium carbonate dispersion, which leads to the precipitation of zein on calcium carbonate particles. The subsequent dissolution of calcium carbonate cores gives rise to hollow nanoparticles of zein. The potential of the hollow nanoparticles was demonstrated in terms of sustained release and cell delivery of the hydrophilic cargo (Xu, Jiang, Reddy, & Yang, 2011).

Remarkably, hollow zein nanoparticles provide a larger space to load bioactive compounds, although their multi-step production process could be difficult to transfer in an industrial environment (Paliwal & Palakurthi, 2014).

Core-shell zein nanoparticles were found non-immunogenic in the rats and showed long retention in their gastrointestinal tract after the oral administration due to mucoadhesion. In fact, zein-caseinate nanoparticles remained in the GI tract for 24 h, as demonstrated through in vivo biodistribution studies in rats (Alqahtani, Islam, Podaralla, Kaushik, Reineke, Woyengo, et al., 2017).

However, due to its hydrophobic nature, zein colloidal particles are susceptible to aggregation during processing in aqueous media or a possible drying step (Irache & González-Navarro, 2017) (Irache et al., 2017). Zein nanoparticles exhibit aggregation and precipitation since zein is close to its isoelectric point (pH 6.2) in solutions with pH above 5 (Hu & McClements, 2015). Regarding the influence of the ionic strength, these nanoparticles have been shown to be highly susceptible to aggregation at low concentrations of sodium chloride (NaCl). In fact, the salt added to formulations increases the ionic strength, with consequent increases in van der Waals interactions and hydrophobic effects among the protein chains, favoring aggregation and precipitation of the proteins (Dai, Sun, Wang, & Gao, 2016). Solutions proposed for overcoming the problems of aggregation and precipitation of zein nanoparticles have involved coating the particles with emulsifiers such as carrageenan, gum arabic, lecithin, pluronic, sodium caseinate, pectin, and chitosan, in order to maintain repulsion among the particles (Pascoli, Lima, & Fraceto, 2018).

Based on these considerations, zein nanoparticles are demonstrated to be a safe and innovative oral delivery systems for several compounds, from nutraceuticals components to drugs. Their mucoadhesive properties, hydrophobic features, as well as their high resistance to the digestion process, can be successfully exploited for controlled-release purposes (Irache & González-Navarro, 2017).

1.4.3 Combination of zein with polysaccharides in nanoparticle formulation

The combination of proteins and polysaccharides represents a valuable solution to design efficient oral drug delivery systems (Matalanis, Jones, & McClements, 2011). While proteins show nutritional properties even if they are easily hydrolyzed from digestive protease, polysaccharides have high stability in the harsh gastric conditions, and some of them are characterized by a remarkable bioadhesion on the surface of the intestinal mucosa (Fang & Bhandari, 2012). Moreover, proteins and polysaccharides are characterized by an opposite charge in physiological conditions, and it contributes to establishing their associative interactions through an electrostatic attraction (Luo, Zhang, Whent, Yu, & Wang, 2011).

The combined use with polysaccharides resulted in a "winning strategy" to stabilize zein nanoparticles because of their tendency to aggregation in water, at acidic pH, or high ionic strength (Huang, Dai, Cai, Zhong, Xiao, McClements, et al., 2017). The formation of protein-polysaccharide complexes is based on the interaction of ionized groups, mainly the amine groups in zein and the carboxyl groups in the polysaccharide, which gives polyelectrolytes (Dobrynin & Rubinstein, 2005). The use of anionic polysaccharides (Luo, Zhang, Whent, Yu, & Wang, 2011) represent a valuable option to change surface properties of nanoparticles, improve the physical stability to environmental stress and protect nanoparticles within the GI tract (Luo, Wang, Teng, Chen, Sun, & Wang, 2013).

Different techniques were employed to combine zein with anionic polysaccharides such as layer-by-layer electrostatic deposition, liquid dispersion, anti-solvent precipitation, electrospray/electrospinning. The advantage of the layer-by-layer technique is that it can be coupled to other particle forming methods. The layer-by-layer electrostatic deposition of polyelectrolytes onto oppositely charged surfaces formed relatively thick and highly charged shell interfaces may increase the electrostatic and steric repulsion between particles, which may increase the particle stability against the environmental stresses. The investigation on the utilization of layer-by-layer electrostatic deposition technique to coat zein nanoparticles with a negative polyelectrolyte layer is recently receiving an increasing interest by the scientific community. Nanocores can be prepared by different techniques and then coated with the polysaccharides.

For example, zein nanoparticles entrapping the bioactive molecules can be formed, followed by the electrostatic deposition of the polysaccharide on zein nanocore. The liquid-liquid dispersion technique involves the formation of droplets by the dispersion of a liquid inside another immiscible liquid. This technique consists of two phases: a first phase comprises the zein solubilization in the hydroalcoholic solution also adding the bioactive compound to

encapsulate (Zhong & Jin, 2009b) and a second phase that consists of placing the nanoparticles in a solution containing the polysaccharide to form the protein-polysaccharide complexes. The electrospray technique allows nanoparticle formation through the application of an electric field. The properties of the material forming the conductive polymer solution is critical in the process. The experimental set-up consists of a syringe pump with a polymer solution connected to the high voltage power supply that represents the functional electrode. The liquid emerging from the nozzle of the syringe pump into the electric field forms a tailored cone because of the surface tension, which breaks into highly charged droplets close to the micro or nano-size level (Sridhar & Ramakrishna, 2013).

In another strategy (Fig. 9), zein is heat-treated to improve the stability of the nanocore and then coated. A short heat treatment (15 min) partially unravels the tertiary structures of zein molecules, resulting in a monodisperse nanoparticle formulation with a small size. Heat treatment for longer times leads to complete unraveling of the zein molecules, which can then aggregate, hence increasing interactions among the polypeptide chains (Sun, Dai, He, Liu, Yuan, & Gao, 2016).

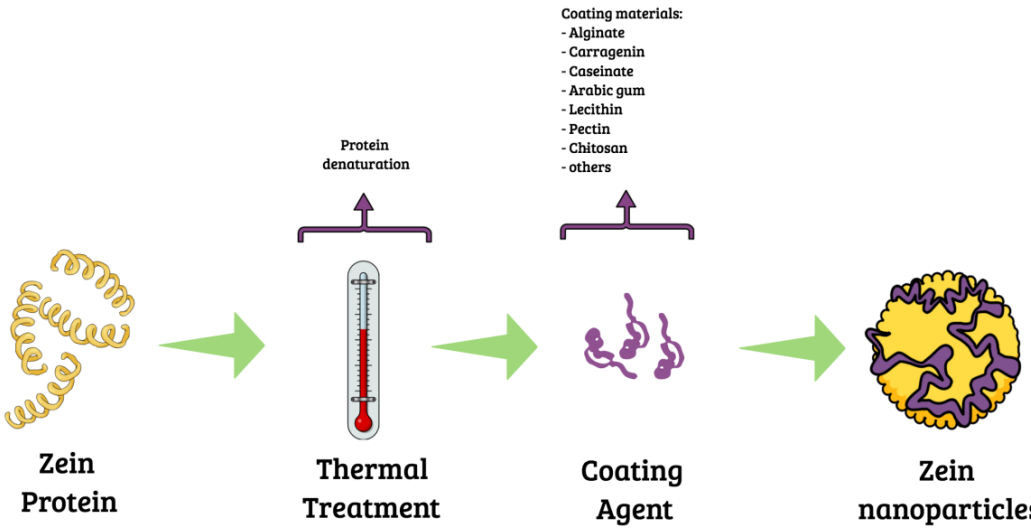

Fig. 9. Proposed strategies to increase the stability of zein nanoparticles (Pascoli, Lima, & Fraceto, 2018).

Zein-polysaccharide nanoparticles can also be formed in one-step by the anti-solvent co-precipitation method, which consists in the co-precipitation of dissolved polymers in an ideal solvent by incorporating an antisolvent, which provides the driving force to precipitate the solute. Zein-polysaccharide nanoparticles are formed by adding zein in the solvent (ethanol or ethanol/water) and the polysaccharide in an anti-solvent such as water, causing the precipitation

of zein-polysaccharide particles (Ashok R. Patel & Velikov, 2014). Nanoparticles with a zein-core were produced by the antisolvent co-precipitation method, and then an alginate shell was formed via electrostatic deposition to improve the overall stability of the nanosystem (Hu & McClements, 2015).

As a negatively charged polyelectrolyte, carrageenan can form a negative charged outer layer on zein positively-charged nanoparticles over a wide pH range acting as a stabilizer against flocculation and gravitational separation (C. J. Cheng & Jones, 2017). Gum arabic was proposed to stabilize zein nanoparticles by steric and electrostatic repulsions to get complexes for the encapsulation and controlled release of peppermint oil (H. Cheng, Khan, Xie, Tao, Li, & Liang, 2020). Very recently, dextran sulfate, a sulfated anionic polysaccharide, was employed with the same role of carrageenan and gum arabic, to deliver curcumin in zein/dextran nanoparticles (Yuan, Li, Zhu, Liu, Sun, Wang, et al., 2019).

Alginate, pectins, chitosan, cellulose derivatives are all polysaccharides that have been tested in combination with zein. Recently, alginate was combined with zein and caseinate to produce propolis-loaded zein/caseinate/alginate nanoparticles able to increase the bioaccessibility of the active cargo and to improve nanoparticle stability against aggregation phenomena (Zhang, Fu, Xu, Niu, Li, Ba, et al., 2019). Pectin is the most studied polysaccharide to fabricate a variety of zein-based delivery systems, such as core-shell nanoparticles (Hu & McClements, 2015), microspheres (Mukhidinov, Kasimova, Bobokalonov, Khalikov, Teshaev, Khalikova, et al., 2011), hydrogel beads (L. Liu, Fishman, Kost, & Hicks, 2003), and soft gels (Soltani & Madadlou, 2015).

The biocompatible and biodegradable polymer chitosan is currently employed to prepare nanoparticles with mucoadhesive properties due to its positive charge, which allows a secure interaction with negatively-charged sites of mucin, the main protein in the mucous layer lining oral epithelium. The previously described electrospray technique was employed to adsorb chitosan on zein nanoparticles forming a core-shell nanosystem that can encapsulate bioactive compounds in both portions. Electrospray apparatus provides an opportunity to spray two fluids separately at the same time, an inner fluid and an outer fluid. The materials used for the core of the nanoparticles were curcumin as the active and zein as biopolymer and for the shell piperine as the active and chitosan (Baspinar, Üstündas, Bayraktar, & Sezgin, 2018).

Regardless of the technique employed, the mixed systems provide useful properties to the nanoplatforms in the GI tract in terms of protection from enzymes and pH, as well as improved stability (Lee, Kim, & Park, 2016).

Based on the research findings published so far, the combination between zein and polysaccharides plays a vital role in a wide range of applications where the controlled delivery of the bioactive cargo can impact bioavailability/physiological effects.

1.5 Cyclodextrins as helping ingredients in formulation development

Cyclodextrins (CDs) are cyclic oligosaccharides produced by enzymatic degradation of starch, a renewable natural material. The most common CDs are the natural α, β, γ, constituted respectively by 6, 7, and 8 glucopyranose units. The CDs structure forms a torus or doughnut ring, and the molecule exists as a truncated cone. The outer side of the toroid is hydrophilic for the presence of the hydroxyl groups of the glucopyranose units, while the internal cavity is relatively apolar (Rachmawati, Edityaningrum, & Mauludin, 2013).

The chemical structure of α, β, γ cyclodextrins is reported in Fig. 10.

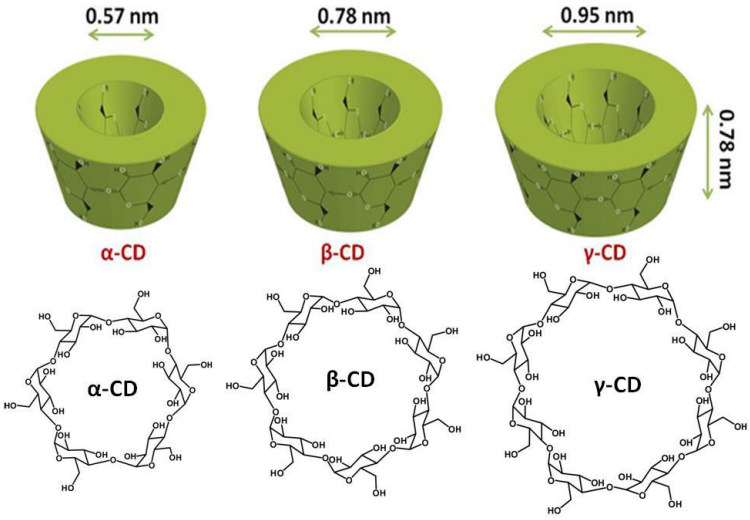

Fig. 10. Chemical structure of α, β and γ cyclodextrins.

CDs have the intrinsic capacity to complex a wide variety of bioactive compounds acting as "host" and conferring to the "guest" molecule new physicochemical features. The main applications of CDs in the pharmaceutical field include the protection of oxidizable and labile molecules, the improvement of aqueous solubility for poorly water-soluble compounds, mask bad taste and odor, and increase of their stability prolonging the shelf- life of the final complexed products. Nowadays, many drugs with solubility-limited bioavailability (Class II in BCS scheme) are complexed with CDs to make their dissolution faster in the biological environment and encourage oral absorption. βCD is neutral in terms of aroma and flavor and,

although it is made of glucose units, has no sweet taste. Their complexation ability makes CDs a helpful and versatile excipient with a shining future as reflected by the increasing number of publications and patents. Because it is a colorless powder, βCD is highly suitable for industrial production processes (da Silva, 2018).

Another aspect to take into account is the ability of CDs to form supramolecular complexes with proteins through interaction with hydrophobic amino acids (tyrosine, phenylalanine, and tryptophan) and change protein properties. This is the reason why CDs have been proposed to inhibit protein aggregation, increase the thermal stability of liquid protein formulations, and as stabilizers during the spray- and freeze-drying processes (Serno, Geidobler, & Winter, 2011).

Natural CDs are already used as food additives in the USA, where they are considered GRAS excipients, and in Japan, while only β-cyclodextrin (βCD) is approved in Europe as an additive in food supplements (da Silva, 2018). Moreover, αCD and γCD are still recognized as novel foods in the EU. βCD (E 459) is authorized as a food additive in the EU under Annex II, and Annex III to Regulation (EC) No 1333/2008 on food additives, and specific purity criteria have been defined in the Commission Regulation (EU) No 231/2012. It is also authorized, according to Annex III to Regulation (EC) No 1333/2008 as a carrier for all food additives (Part 1) up to 1,000 mg/kg in the final food. According to Part 4 of Annex III to Regulation (EC) No 1333/2008, βCD (E 459) is authorized for use in encapsulated flavorings up to 500 mg/L in 'Flavoured teas and flavored powdered instant drinks' (FCS 14.1.5) and up to 1,000 mg/kg in 'Flavoured snacks' (FCS 15.1), and according to Part 5 Section A in nutrients up to 100,000 mg/kg in their preparation and 1,000 mg/kg in final food. Its acceptable daily intake (ADI) is 5 mg/kg/day.

After oral administration, it is not toxic, not absorbed in the digestive tract, and is completely metabolized by the intestinal microflora. Depending on the extent of stability constant, the host-guest complex can dissociate upon dilution in the GI fluids and allow quick absorption of free guest molecules (Yang, Lin, Chen, & Liu, 2009).

βCD is sparingly soluble in water, freely soluble in hot water, and slightly soluble in ethanol. Due to its peculiar properties, it can be host inside its cavity lipophilic moieties of bioactive compounds used in food supplements and, when associated to polymers, as a modifier of the overall platform features (Esposito, Dal Poggetto, Demont, Kraut, Miro, Ungaro, et al., 2020).

Given the limited number of materials useful to design a delivery platform for nutrients, the rational combination of raw materials already approved as food ingredients and its processing through nano-micro technology can offer a unique tool for innovation. As described

previously, the combination of zein with different polysaccharides may represent a valid strategy to expand the manipulation space for zein-based delivery platforms and to develop innovative oral delivery systems (Tapia-Hernández, Rodríguez-Felix, Juárez-Onofre, Ruiz-Cruz, Robles-García, Borboa-Flores, et al., 2018). Prospectively, zein/βCDs association can be promising in the formulation of bioactive compounds in food supplements. In this context, the combination of zein, which sustains the release of its cargo due to its high hydrophobicity, and of β-cyclodextrin that can promote the encapsulation and improve the solubility of lipophilic bioactive molecules, seems to be a powerful tool for nutraceutical delivery. βCD was therefore already employed to modify different zein-based platforms such as antimicrobial fibers for food packaging (Aytac, Keskin, Tekinay, & Uyar, 2017; Dias Antunes, da Silva Dannenberg, Fiorentini, Pinto, Lim, da Rosa Zavareze, et al., 2017; Kayaci & Uyar, 2012), microparticles entrapping α-tocopherol (Saldanha do Carmo, Maia, Poejo, Lychko, Gamito, Nogueira, et al., 2017) to ensure color stability and shelf-life of fruit beverages and powders for oral bioavailability improvement.

Quercetin-loaded zein nanoparticles containing 2-hydroxypropyl-β-cyclodextrin (HP-β-CD) improved the oral bioavailability of the free flavonoid significantly. At the dose of 25 mg/kg every two days for 2 consecutive months, the system improved the cognition and memory impairments and reduced the astrogliosis shown by SAMP8 mice thus representing a potential oral treatment for Alzheimer's disease (Moreno, Puerta, Suárez-Santiago, Santos-Magalhães, Ramirez, & Irache, 2017).

1.6 Microencapsulation technologies in the food industry: focus on Spray-drying process

1.6.1 Microencapsulation with spray-drying

Recently, considerable advances have been achieved in engineering and manufacturing micro-nano systems to increase the oral bioavailability of nutraceuticals. Researchers in the food industry have realized that the microencapsulation for nutrients is one of the strategic ways for their better delivery in humans.

An efficient delivery system should show different features to guarantee the incorporation of the encapsulated bioactive compounds and its advantageous delivery. The ability to retain the active molecules during processing, storage, and transport, to prevent its chemical degradation and oxidation is critical to get the effectiveness of the product.

Through microencapsulation, the bioactive compounds must be incorporated in and easily mixed with a food/beverage matrix without alteration of the texture, taste, and appearance. The encapsulated micronutrients, coated with safe materials, were protected from pH, light, heat, and less exposed to harsh environmental conditions. Moreover, the encapsulation can also guarantee an increase in the solubility of poorly-soluble soluble compounds, thus increasing their absorption and bioavailability (Karunaratne, Surandika Siriwardhana, Ariyarathna, Indunil Rajakaruna, Banu, & Karunaratne, 2017).

Several techniques are available for the encapsulation of food ingredients, and some of them comprise a drying step. The selection of a suitable encapsulation procedure is a crucial step since most of the bioactive compounds are sensitive to heat and to a high temperature, which could cause degradation and, in turn, the loss of their efficacy (Vega-Baudrit, 2019). Encapsulation technologies as spray drying, spray-bed-drying, fluid-bed coating, spray-chilling, spray-cooling, or melt injection, have gained momentum in the last few decades.

Amid them, spray-drying remains the most current technology in the food industry, and a series of bioactive components have been successfully co-process with support ingredients like maltodextrins ("Encapsulation of bioactive ingredients by spray drying,"). Spray-drying is indeed a well-established method to convert liquid materials into powders, which has not only contributed to the drying of fluids but also has played a vital role in encapsulation and microencapsulation of valuable foods and functional nutraceutical ingredients (Murugesan & Orsat, 2011).

Among the materials that can benefit from microencapsulation, lipids, vitamins, minerals, salts, amino acids, flavors, colorings, enzymes, and micro-organisms can be cited (Tolve, Galgano, Caruso, Tchuenbou-Magaia, Condelli, Favati, et al., 2016).

The working principle in spray-drying is solvent removal by application of heat to the product feed. The exclusivity of the method is that the evaporation is promoted by spraying the feed into a heated atmosphere, resulting in an improved drying rate. Four stages are involved in the process: 1) atomization of the liquid feed; 2) contact of sprayed droplets with the hot gas; 3) evaporation of the solvent; 4) particle separation from the gas (Fig. 11).

Each phase can influence the quality of the final product collected ("Introduction to spray drying,"). The first transformation process is the atomization/nebulization that the liquid feed undergoes during spray drying. Liquid feed is transported to the atomization device by different types of pumps. Samuel Percy was the first to describe the principle of spray drying in a US patent dated back in 1872, and he is considered to be the inventor of this technology. He gave

a precise definition of this stage considered as a process that consists of “bringing fluid or solid substances into a state of minute division”.

The breakup of bulk liquid into many droplets through its nebulization drives the rest of the spray drying process by reducing the internal resistances to moisture transfer from the droplet to the surrounding medium. This is because of the enormous increase in surface area of the bulk fluid as the droplet fission proceeds, with its instability increasing under the intensity of atomization. Atomization influences the shape, structure, velocity, and size distribution of the droplets and, in turn, the particle size and the morphology obtained.

This higher surface-to-volume ratio enables spray drying to achieve a faster drying rate (as drying time is proportional to the square of the particle dimension). Consequently, there is minimal loss of heat-sensitive compounds. It does not require a final drying phase, as is the case of most conventional methods and allows us to deal with heat-sensitive materials. The second step is the close contact of the droplets into the hot gas. This enables rapid evaporation of moisture from the surface of all the droplets in a uniform manner. Herein, the critical factor is a uniform gas flow to all parts of the drying chamber. During spray-air contact, the droplets usually meet hot air in the spraying chamber, either in co-current flow or counter-current flow ("Introduction to spray drying,"). Then, reaching a large surface liquid area during atomization facilitates heat transfer from the heated drying gas to the atomized fluid particles. The solvent is evaporated in a few seconds, and the mass is transferred back into the gas phase.

Most of the water is evaporated from the droplet surface, and the droplets are transformed into dry powder. The drying medium carries the dried particles through the dryer into the cyclone, in which a powder is separated from the humid air. Spray dryers are commonly equipped with bag filters, which are used to remove the finest powder ("Novel polymer systems and additives to protect bioactive substances applied in spray-drying,").

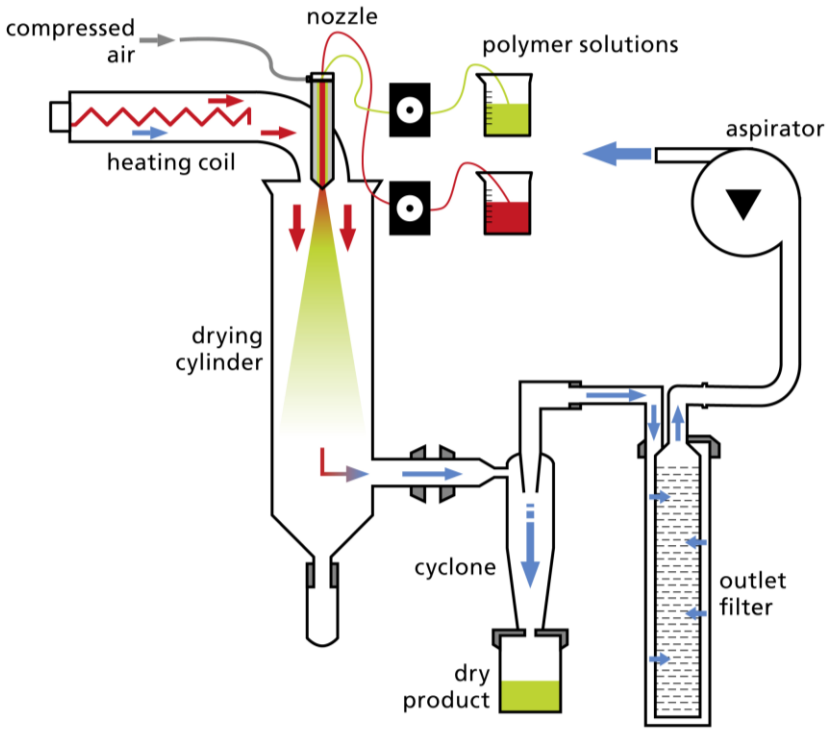

Fig. 11. Schematic representation of the spray-drying process.

Many features of spray-dried products such as morphology, particle size, and shape are affected by spray-drying conditions. The morphology of the powder affects particle size distribution, flowability, friability, moisture content, and bulk and particle density and can be modified modulating spray-drying parameters.

Particle morphology is affected by drying kinetics. After the crust formation, the droplet may follow one of the two principal pathways, leading to either small, solid particles or large, hollow particles. The first is the "dry shell" route, which is comparable to a shrinking core, producing particles which are susceptible to shattering when dried at high temperature. The second route is the "wet shell" type and tends to form hollow particles that may inflate or collapse. Thus, the morphology of the spray-dried particles also depends on the nature of the shell formed (Handscomb, Kraft, & Bayly, 2009).

Particle size can be manipulated by controlling specific parameters such as the size of nozzle orifices or the difference between inlet and outlet air temperature. A profound difference between inlet and outlet air temperatures will produce slightly larger particles than slow drying (Jafari, Assadpoor, He, & Bhandari, 2008).

On the other hand, the shape of particles influences solubility and packaging properties of dried powders, and in this sense, a spherical shape is highly desirable.

The main advantage of spray-drying respect to other methods is i) the possibility to collect the final powder in one-step; ii) the fact that it is a continuous process; iii) the opportunity to manipulate the features of the feeding liquid. This rapid, continuous, and single-step method displays excellent versatility and reproducibility. Considering these attributes, the use of the spray-drying in the production of several particles or polymeric carriers with well-defined particle size comes as no surprise.

Spray-drying can be considered a green industrial process because of the use of solvents, which can be recovered and recycled, thus reducing the impact of solvents other than water. Other valuable aspects are cost-effectiveness and the scalability which extend the possibility to transfer a product from the bench to an industrial contest favoring a variety of applications within the food, chemical, polymeric, pharmaceutical, biotechnology and medical industries (Santos, Maurício, Sencadas, Santos, Fernandes, & Gomes, 2018).

Although it shows several advantages, spray drying presents some issues like product loss associated with particle deposition inside the walls of the drying chamber, as well as due to the inability of the separation devices to collect the smallest particles. As a consequence, the process yield tends to decrease, and it is difficult to set parameters to get a high yield of the collected product. Moreover, small particles are hardly obtained not only due to the inefficiency of the collecting devices but also due to the problem of disintegrating the feedstock solution (atomization step) into submicron droplets (Sosnik & Seremeta, 2015). This has led to the introduction in the market of equipment like nano-spray-dryer (Büchi).

1.6.2 Zein microencapsulation with spray-drying

Encapsulation of a bioactive compound through spray-drying comprises an initial step where a liquid feed containing the bioactive compounds is prepared (Jain, Ganesh, Manoj, Randhir, Shashikant, & Chirag, 2012). Depending on the solubility profile of the bioactive compound and the matrix, the feed can be a solution, a dispersion or an emulsion in which water or a volatile organic solvent is employed. The type of feed will impact on the morphology/structure of the final dry product. In the particular case of dispersions, it is evident that the size of dispersed particles needs to meet the criteria for effective nebulization (Fang & Bhandari, 2012).

Among the excipients employed in spray-drying, plant proteins are more hydrophobic and easy to assemble without involving harsh processing conditions such as thermal treatment and/or toxic crosslinkers (Elzoghby, Samy, & Elgindy, 2012). In the last decades, there has

been, therefore, an increasing interest in the development of zein-based micro-nano systems to encapsulate bioactive molecules through the application of spray-drying technology.

In the food area, the production of zein platforms loaded with antimicrobial was in the limelight due to their insolubility in food products. To this regard, thymol was loaded in a spray-dried zein-microcapsule matrix providing a sustained release of the antimicrobial over long periods that may be important to enhance the efficacy of antimicrobials against pathogenic and spoilage microorganisms attack (Zhong & Jin, 2009a).

Considering that the addition of ω-3 and ω-6 polyunsaturated fatty acids (PUFA) to functional food ingredients and their consumption in dietary supplements have experienced significant increases, flax oil-loaded microcapsules were efficiently produced by spray-drying using zein as a coating material and overcoming the issues of the freeze-drying of these capsules (Quispe-Condori, Saldaña, & Temelli, 2011).

α-Tocopherol is considered an important food additive due to its antioxidant effect and capacity to increase the shelf-life of products. However, its hydrophobicity compromises its applicability in soft drinks and fruit beverages. The development of zein/βCD spray-dried powders allowed to get a sustained release of this bioactive and represent a promising carrier which could be applied in fruit beverage products to improve product shelf-life (Saldanha do Carmo, et al., 2017).

Nevertheless, due to the strong hydrophobicity of zein, some hurdles related to powder difficult dispersibility and tendency to the agglomeration/aggregation must be overcome. In this regard, the use of cyclodextrin for protein stabilization in the dried state represents a valuable tool to develop innovative formulations and robust manufacturing processes (Serno, Geidobler, & Winter, 2011). Recently, the co-encapsulation of quercetin and 2-hydroxypropyl-β-cyclodextrin (HP-β-CD) in zein nanoparticles as oral carriers for this flavonoid was investigated. This combination has demonstrated a significant efficiency in improving the oral bioavailability of quercetin and in providing high and sustained plasma levels of the flavonoid for at least 2 days (Penalva, Esparza, Larraneta, González-Navarro, Gamazo, & Irache, 2015).

Nowadays, the rational combination between zein and cyclodextrins has been only partially investigated for food applications and represents an attractive topic to ameliorate the oral delivery of nutraceuticals in the human body.

1.7 Aim of work

In the frame of "PON RI 2014-2020-Dottorati innovativi con caratterizzazione industriale" the proposed research project deals with the development of novel strategies to deliver bioactive products and their transfer to an industrial setting. The research is focused on the formulation of those bioactive compounds that have high impact in food supplement field, with polymer materials, generally approved as food ingredients, opportunely processed through the application of nano-micro technology to get innovative oral delivery systems with implemented properties.

The strategy pursued was to employ micro-nano technologies to develop oral zein-based platforms for the delivery of bioactive compounds with high impact in nutraceutical field. The primary specific objective was to setting-up a nano-in-micro strategy to produce powders combining the hydrophobic protein zein and β-cyclodextrin. The potential of the platform was tested in the delivery of both hydrophilic and lipophilic compounds with different requirements for bioavailability improvement.

The bioactive compounds of interest were selected in collaboration with the industrial partner Neilos s.r.l. considering the market trend in the food supplements field. An iron source (iron bisglycinate), employed in the treatment of anemic patients, and Curcumin, the "golden powder" in the nutraceutical sector, which offers potent antimicrobial, antioxidant, anti-infiammatory, and antitumor properties, were selected.

The second objective was the development of bioadhesive nanoparticles suitable for buccal delivery. Again, the combination of zein and β-cyclodextrin was explored to obtain liquid dispersions for the delivery of curcumin which can potentially overcome bioavailability issues.

The third objective was the industrialization of the developed products taking advantage of our industrial partners. The technological transfer of the iron-powders from the bench to an industrial setting was carried out in collaboration with Neilos s.r.l, and the optimization of the spray-drying process was tried with the support of the product specialists working at BUCHI Labortechnik AG. This allowed close contact with the hurdles of the scale-up process and a proof of concept of the translation of the final product on a large-scale.

This research activity has been summarized in four chapters and two annexes entitled:

- Zein beta-cyclodextrin micropowders for iron bisglycinate delivery (Chapter 2)
- Zein beta-cyclodextrin platforms for curcumin oral delivery (Chapter 3)
- From the bench to the market: industrial partnership and product development (Chapter 4)

The work has been carried out also in collaboration with the Institute of Polymers, Composites, and Biomaterials (Italian National Research Council, Pozzuoli, Napoli, Italy), which contributed to powder characterization in the solid-state.

In the annex, the contribution to the development of positively-charged nanoparticles for the delivery of chemotherapeutics in solid tumors is reported. The design and application of a panel of amine-bearing PEGylated biodegradable nanoparticles (NPs) is reported and their behaviour toward protein-rich biological media and in terms of in vivo biodistribution is illustrated.

References

Aditya, N. P., Espinosa, Y. G., & Norton, I. T. (2017). Encapsulation systems for the delivery of hydrophilic nutraceuticals: Food application. *Biotechnology Advances, 35*(4), 450-457.

Alqahtani, M. S., Islam, M. S., Podaralla, S., Kaushik, R. S., Reineke, J., Woyengo, T., & Perumal, O. (2017). Food Protein Based Core–Shell Nanocarriers for Oral Drug Delivery: Effect of Shell Composition on in Vitro and in Vivo Functional Performance of Zein Nanocarriers. *Molecular Pharmaceutics, 14*(3), 757-769.

Augustin, M. A., & Hemar, Y. (2009). Nano- and micro-structured assemblies for encapsulation of food ingredients. *Chemical Society Reviews, 38*(4), 902-912.

Aytac, Z., Keskin, N. O. S., Tekinay, T., & Uyar, T. (2017). Antioxidant α-tocopherol/γ-cyclodextrin–inclusion complex encapsulated poly(lactic acid) electrospun nanofibrous web for food packaging. *Journal of Applied Polymer Science, 134*(21).

Balandrán-Quintana, R. R., Ana, M. M.-W., Miguel, A. V. z.-C., & Rogerio, R. S.-M. (2013). α-Lactalbumin hydrolysate spontaneously produces disk-shaped nanoparticles. *International dairy journal, 32*(2), 133-135.

Baspinar, Y., Üstündas, M., Bayraktar, O., & Sezgin, C. (2018). Curcumin and piperine loaded zein-chitosan nanoparticles: Development and in-vitro characterisation. *Saudi pharmaceutical journal : SPJ : the official publication of the Saudi Pharmaceutical Society, 26*(3), 323-334.

Bhushani, A., Harish, U., & Anandharamakrishnan, C. (2017). 10 - Nanodelivery of nutrients for improved bioavailability. In A. M. Grumezescu (Ed.), *Nutrient Delivery*, (pp. 369-411): Academic Press.

Braithwaite, M. C., Tyagi, C., Tomar, L. K., Kumar, P., Choonara, Y. E., & Pillay, V. (2014). Nutraceutical-based therapeutics and formulation strategies augmenting their efficiency to complement modern medicine: An overview. *Journal of Functional Foods, 6*, 82-99.

Cheng, C. J., & Jones, O. G. (2017). Stabilizing zein nanoparticle dispersions with ι-carrageenan. *Food Hydrocolloids, 69*, 28-35.

Cheng, H., Khan, M. A., Xie, Z., Tao, S., Li, Y., & Liang, L. (2020). A peppermint oil emulsion stabilized by resveratrol-zein-pectin complex particles: Enhancing the chemical stability and antimicrobial activity in combination with the synergistic effect. *Food Hydrocolloids*, 105675.

da Silva, A. M. (2018). Room at the Top as well as at the Bottom: Structure of Functional Food Inclusion Compounds. In P. A. a. N. Dhingra (Ed.), *Cyclodextrin - A Versatile Ingredient*): IntechOpen.

Dai, L., Sun, C., Wang, D., & Gao, Y. (2016). The Interaction between Zein and Lecithin in Ethanol-Water Solution and Characterization of Zein-Lecithin Composite Colloidal Nanoparticles. *PloS one, 11*(11), e0167172-e0167172.

de Souza Simões, L., Madalena, D. A., Pinheiro, A. C., Teixeira, J. A., Vicente, A. A., & Ramos, Ó. L. (2017). Micro- and nano bio-based delivery systems for food applications: In vitro behavior. *Advances in Colloid and Interface Science, 243*, 23-45.

DeFelice, S. L. (1995). The nutraceutical revolution: its impact on food industry R&D. *Trends in Food Science & Technology, 6*(2), 59-61.

Demir, M., Ramos-Rivera, L., Silva, R., Nazhat, S. N., & Boccaccini, A. R. (2017). Zein-based composites in biomedical applications. *Journal of Biomedical Materials Research Part A, 105*(6), 1656-1665.

Dias Antunes, M., da Silva Dannenberg, G., Fiorentini, Â. M., Pinto, V. Z., Lim, L.-T., da Rosa Zavareze, E., & Dias, A. R. G. (2017). Antimicrobial electrospun ultrafine fibers from zein containing eucalyptus essential oil/cyclodextrin inclusion complex. *International Journal of Biological Macromolecules, 104*(Pt A), 874-882.

Dobrynin, A. V., & Rubinstein, M. (2005). Theory of polyelectrolytes in solutions and at surfaces. *Progress in Polymer Science, 30*(11), 1049-1118.

Elzoghby, A. O., Samy, W. M., & Elgindy, N. A. (2012). Protein-based nanocarriers as promising drug and gene delivery systems. *Journal of Controlled Release, 161*(1), 38-49.

. Encapsulation of bioactive ingredients by spray drying. In. *Spray Drying Techniques for Food Ingredient Encapsulation*, (pp. 156-179).

Esposito, D., Dal Poggetto, G., Demont, A., Kraut, N., Miro, A., Ungaro, F., Laurienzo, P., & Quaglia, F. (2020). Zein Beta-Cyclodextrin Micropowders for Iron Bisglycinate Delivery. *Pharmaceutics, 12*(1).

Fang, Z., & Bhandari, B. (2012). 4 - Spray drying, freeze drying and related processes for food ingredient and nutraceutical encapsulation. In N. Garti & D. J. McClements (Eds.), *Encapsulation Technologies and Delivery Systems for Food Ingredients and Nutraceuticals*, (pp. 73-109): Woodhead Publishing.

Garg, T., Sharma, G., Rath, G., & Goyal, A. K. (2017). 18 - Colloidal systems: an excellent carrier for nutrient delivery. In A. M. Grumezescu (Ed.), *Nutrient Delivery*, (pp. 681-712): Academic Press.

Handscomb, C. S., Kraft, M., & Bayly, A. (2009). A New Model for the Drying of Droplets Containing Suspended Solids After Shell Formation. *Chemical Engineering Science, 64*, 228-246.

Hu, K., & McClements, D. J. (2015). Fabrication of biopolymer nanoparticles by antisolvent precipitation and electrostatic deposition: Zein-alginate core/shell nanoparticles. *Food Hydrocolloids, 44*, 101-108.

Huang, X., Dai, Y., Cai, J., Zhong, N., Xiao, H., McClements, D. J., & Hu, K. (2017). Resveratrol encapsulation in core-shell biopolymer nanoparticles: Impact on antioxidant and anticancer activities. *Food Hydrocolloids, 64*, 157-165.

. Introduction to spray drying. In. *Spray Drying Techniques for Food Ingredient Encapsulation*, (pp. 1-36).

Irache, J. M., & González-Navarro, C. J. (2017). Zein nanoparticles as vehicles for oral delivery purposes. *Nanomedicine, 12*(11), 1209-1211.

Jafari, S. M., Assadpoor, E., He, Y., & Bhandari, B. (2008). Encapsulation Efficiency of Food Flavours and Oils during Spray Drying. *Drying Technology, 26*(7), 816-835.

Jain, M., Ganesh, L., Manoj, B., Randhir, C., Shashikant, B., & Chirag, S. (2012). Spray Drying in Pharmaceutical Industry: A Review. *4*, 74-79.

Karimi, N., Ghanbarzadeh, B., Hamishehkar, H., Pezeshki, A., Mostafayi, H., & Gholian, M. M. (2015). Phytosome as novel delivery system for nutraceutical materials.

Karunaratne, D. N., Surandika Siriwardhana, D. A., Ariyarathna, I. R., Indunil Rajakaruna, R. M. P., Banu, F. T., & Karunaratne, V. (2017). 17 - Nutrient delivery through nanoencapsulation. In A. M. Grumezescu (Ed.), *Nutrient Delivery*, (pp. 653-680): Academic Press.

Kayaci, F., & Uyar, T. (2012). Electrospun zein nanofibers incorporating cyclodextrins. *Carbohydrate Polymers, 90*, 558–568.

Khosravi-Boroujeni, H., Sarrafzadegan, N., Mohammadifard, N., Sajjadi, F., Maghroun, M., Asgari, S., Rafieian-Kopaei, M., & Azadbakht, L. (2013). White rice consumption and CVD risk factors among Iranian population. *Journal of health, population, and nutrition, 31*(2), 252-261.

Kumar, D. S. (2015). *Herbal Bioactives and Food Fortification: Extraction and Formulation*.

Labib, G. (2018). Overview on zein protein: a promising pharmaceutical excipient in drug delivery systems and tissue engineering. *Expert Opinion on Drug Delivery, 15*(1), 65-75.

Lawton, J. W. (2002). Zein: A History of Processing and Use. *Cereal Chemistry, 79*(1), 1-18.

Lee, S., Kim, Y.-C., & Park, J.-H. (2016). Zein-alginate based oral drug delivery systems: Protection and release of therapeutic proteins. *International Journal of Pharmaceutics, 515*(1), 300-306.

Liu, F., Ma, C., Gao, Y., & McClements, D. J. (2017). Food-Grade Covalent Complexes and Their Application as Nutraceutical Delivery Systems: A Review. *Comprehensive Reviews in Food Science and Food Safety, 16*(1), 76-95.

Liu, L., Fishman, M. L., Kost, J., & Hicks, K. B. (2003). Pectin-based systems for colon-specific drug delivery via oral route. *Biomaterials, 24*(19), 3333-3343.

Livney, Y. D. (2010). Milk proteins as vehicles for bioactives. *Current Opinion in Colloid & Interface Science, 15*(1), 73-83.

Luo, Y., Teng, Z., & Wang, Q. (2012). Development of Zein Nanoparticles Coated with Carboxymethyl Chitosan for Encapsulation and Controlled Release of Vitamin D3. *Journal of Agricultural and Food Chemistry, 60*(3), 836-843.

Luo, Y., & Wang, Q. (2014). Zein-based micro- and nano-particles for drug and nutrient delivery: A review. *Journal of Applied Polymer Science, 131*(16).

Luo, Y., Wang, T. T. Y., Teng, Z., Chen, P., Sun, J., & Wang, Q. (2013). Encapsulation of indole-3-carbinol and 3,3′-diindolylmethane in zein/carboxymethyl chitosan nanoparticles with controlled release property and improved stability. *Food Chemistry, 139*(1), 224-230.

Luo, Y., Zhang, B., Whent, M., Yu, L., & Wang, Q. (2011). Preparation and characterization of zein/chitosan complex for encapsulation of α-tocopherol, and its in vitro controlled release study. *Colloids and Surfaces B: Biointerfaces, 85*(2), 145-152.

Matalanis, A., Jones, O. G., & McClements, D. J. (2011). Structured biopolymer-based delivery systems for encapsulation, protection, and release of lipophilic compounds. *Food Hydrocolloids $V 25*(8), 1865-1880.

McClements, D., & Xiao, H. (2014). Excipient foods: Designing food matrices that improve the oral bioavailability of pharmaceuticals and nutraceuticals. *Food & Function, 5*.

McClements, D. J. (2015). Nanoscale Nutrient Delivery Systems for Food Applications: Improving Bioactive Dispersibility, Stability, and Bioavailability. *Journal of Food Science, 80*(7), N1602-N1611.

McClements, D. J., & Li, Y. (2010). Structured emulsion-based delivery systems: Controlling the digestion and release of lipophilic food components. *Advances in Colloid and Interface Science, 159*(2), 213-228.

Moreno, L. C. G. e. I., Puerta, E., Suárez-Santiago, J. E., Santos-Magalhães, N. S., Ramirez, M. J., & Irache, J. M. (2017). Effect of the oral administration of nanoencapsulated quercetin on a mouse model of Alzheimer's disease. *International Journal of Pharmaceutics, 517*(1), 50-57.

Mukhidinov, Z. K., Kasimova, G. F., Bobokalonov, D. T., Khalikov, D. K., Teshaev, K. I., Khalikova, M. D., & Liu, L. S. (2011). Pectin–zein microspheres as drug delivery systems. *Pharmaceutical Chemistry Journal, 44*(10), 564-567.

Murugesan, R., & Orsat, V. (2011). Spray Drying for the Production of Nutraceutical Ingredients—A Review. *Food and Bioprocess Technology, 5*, 3-14.

Nasri, H. (2013). Impact of diabetes mellitus on parathyroid hormone in hemodialysis patients. *J parathyr dis, 1*(1), 9-11.

Novel polymer systems and additives to protect bioactive substances applied in spray-drying. In. *New Polymers for Encapsulation of Nutraceutical Compounds*, (pp. 97-119).

O'Donnell, P. B., Wu, C., Wang, J., Wang, L., Oshlack, B., Chasin, M., Bodmeier, R., & McGinity, J. W. (1997). Aqueous pseudolatex of zein for film coating of solid dosage forms. *European Journal of Pharmaceutics and Biopharmaceutics, 43*(1), 83-89.

Paliwal, R., & Palakurthi, S. (2014). Zein in controlled drug delivery and tissue engineering. *Journal of Controlled Release, 189*, 108-122.

Pandita, D., Kumar, S., Poonia, N., & Lather, V. (2014). Solid lipid nanoparticles enhance oral bioavailability of resveratrol, a natural polyphenol. *Food Research International, 62*, 1165-1174.

Parada, J., & Aguilera, J. M. (2007). Food Microstructure Affects the Bioavailability of Several Nutrients. *Journal of Food Science, 72*(2), R21-R32.

Parris, N., Cooke, P. H., & Hicks, K. B. (2005). Encapsulation of Essential Oils in Zein Nanospherical Particles. *Journal of Agricultural and Food Chemistry, 53*(12), 4788-4792.

Pascoli, M., Lima, R., & Fraceto, L. (2018). Zein nanoparticles and the strategies to improve the colloidal stability: a mini review. *Frontiers in Chemistry, 6*.

Patel, A. R., & Velikov, K. P. (2011). Colloidal delivery systems in foods: A general comparison with oral drug delivery. *LWT - Food Science and Technology, 44*(9), 1958-1964.

Patel, A. R., & Velikov, K. P. (2014). Zein as a source of functional colloidal nano- and microstructures. *Current Opinion in Colloid & Interface Science, 19*(5), 450-458.

Penalva, R., Esparza, I., Larraneta, E., González-Navarro, C. J., Gamazo, C., & Irache, J. M. (2015). Zein-Based Nanoparticles Improve the Oral Bioavailability of Resveratrol and Its Anti-inflammatory Effects in a Mouse Model of Endotoxic Shock. *Journal of Agricultural and Food Chemistry, 63*(23), 5603-5611.

Quispe-Condori, S., Saldaña, M. D. A., & Temelli, F. (2011). Microencapsulation of flax oil with zein using spray and freeze drying. *LWT - Food Science and Technology, 44*(9), 1880-1887.

Rachmawati, H., Edityaningrum, C. A., & Mauludin, R. (2013). Molecular inclusion complex of curcumin-β-cyclodextrin nanoparticle to enhance curcumin skin permeability from hydrophilic matrix gel. *AAPS PharmSciTech, 14*(4), 1303-1312.

Ramos, O., Pereira, R., Rodrigues, R. M., Teixeira, J., Vicente, A., & Malcata, F. (2014). Physical effects upon whey protein aggregation for nano-coating production. *Food Research International, 66*, 344-355.

Ramos, O. L., Pereira, R. N., Martins, A., Rodrigues, R., Fuciños, C., Teixeira, J. A., Pastrana, L., Malcata, F. X., & Vicente, A. A. (2017). Design of whey protein nanostructures for incorporation and release of nutraceutical compounds in food. *Critical Reviews in Food Science and Nutrition, 57*(7), 1377-1393.

Reddy, N., & Yang, Y. (2011). Potential of plant proteins for medical applications. *Trends in Biotechnology, 29*(10), 490-498.

Roohafza, H., Sarrafzadegan, N., Sadeghi, M., Rafieian-kopaei, M., Sajjadi, F., & khosravi-boroujeni, H. (2013). The Association between Stress Levels and Food Consumption among Iranian Population. *Archives of Iranian medicine, 16*, 145-148.

Saldanha do Carmo, C., Maia, C., Poejo, J., Lychko, I., Gamito, P., Nogueira, I., Bronze, M. R., Serra, A. T., & Duarte, C. M. M. (2017). Microencapsulation of α-tocopherol with zein and β-cyclodextrin using spray drying for colour stability and shelf-life improvement of fruit beverages. *RSC Advances, 7*(51), 32065-32075.

Santini, A., Cammarata, S. M., Capone, G., Ianaro, A., Tenore, G. C., Pani, L., & Novellino, E. (2018). Nutraceuticals: opening the debate for a regulatory framework. *British journal of clinical pharmacology, 84*(4), 659-672.

Santos, D., Maurício, A., Sencadas, V., Santos, J., Fernandes, M., & Gomes, P. (2018). Spray Drying: An Overview. In).

Sastry, S. V., Nyshadham, J. R., & Fix, J. A. (2000). Recent technological advances in oral drug delivery – a review. *Pharmaceutical Science & Technology Today, 3*(4), 138-145.

Schmitt, J., & Ferro, A. (2013). Nutraceuticals: is there good science behind the hype? *British journal of clinical pharmacology, 75*(3), 585-587.

Serno, T., Geidobler, R., & Winter, G. (2011). Protein stabilization by cyclodextrins in the liquid and dried state. *Advanced Drug Delivery Reviews, 63*(13), 1086-1106.

Shah, A. V., Desai, H. H., Thool, P., Dalrymple, D., & Serajuddin, A. T. M. (2018). Development of self-microemulsifying drug delivery system for oral delivery of poorly water-soluble nutraceuticals. *Drug Development and Industrial Pharmacy, 44*(6), 895-901.

Shirzad, M., Kordyazdi, R., Shahinfard, N., & Nikokar, M. (2013). Does Royal jelly affect tumor cells? *J Herbmed Pharmacol, 2*(2), 45-48.

Shukla, R., & Cheryan, M. (2001). Zein: The industrial protein from corn. *Industrial Crops and Products, 13*, 171-192.

Singh, R., Kumari, P., & Kumar, S. (2017). 11 - Nanotechnology for enhanced bioactivity of bioactive phytomolecules. In A. M. Grumezescu (Ed.), *Nutrient Delivery*, (pp. 413-456): Academic Press.

Soltani, S., & Madadlou, A. (2015). Gelation characteristics of the sugar beet pectin solution charged with fish oil-loaded zein nanoparticles. *Food Hydrocolloids, 43*, 664-669.

Sosnik, A., & Seremeta, K. P. (2015). Advantages and challenges of the spray-drying technology for the production of pure drug particles and drug-loaded polymeric carriers. *Advances in Colloid and Interface Science, 223*, 40-54.

Sridhar, R., & Ramakrishna, S. (2013). Electrosprayed nanoparticles for drug delivery and pharmaceutical applications. *Biomatter, 3*(3), e24281.

Sun, C., Dai, L., He, X., Liu, F., Yuan, F., & Gao, Y. (2016). Effect of heat treatment on physical, structural, thermal and morphological characteristics of zein in ethanol-water solution. *Food Hydrocolloids, 58*.

Tapia-Hernández, J. A., Rodríguez-Felix, F., Juárez-Onofre, J. E., Ruiz-Cruz, S., Robles-García, M. A., Borboa-Flores, J., Wong-Corral, F. J., Cinco-Moroyoqui, F. J., Castro-Enríquez, D. D., & Del-Toro-Sánchez, C. L. (2018). Zein-polysaccharide nanoparticles as matrices for

antioxidant compounds: A strategy for prevention of chronic degenerative diseases. *Food Research International, 111*, 451-471.

Tolve, R., Galgano, F., Caruso, M., Tchuenbou-Magaia, F. L., Condelli, N., Favati, F., & Zhang, Z. (2016). Encapsulation of health-promoting ingredients: applications in foodstuffs. *International journal of food sciences and nutrition, 67*, 1-31.

Trombino, S., Cassano, R., Muzzalupo, R., Pingitore, A., Cione, E., & Picci, N. (2009). Stearyl ferulate-based solid lipid nanoparticles for the encapsulation and stabilization of β-carotene and α-tocopherol. *Colloids and Surfaces B: Biointerfaces, 72*(2), 181-187.

Vega-Baudrit, J. (2019). Nutraceuticals: definition, applied nanoengineering in their production and applications. *International Journal of Biosensors & Bioelectronics, 5*.

Vozza, G., Khalid, M., Byrne, H. J., Ryan, S., & Frias, J. (2017). 1 - Nutrition—nutrient delivery. In A. M. Grumezescu (Ed.), *Nutrient Delivery*, (pp. 1-42): Academic Press.

Wan, Z.-L., Guo, J., & Yang, X.-Q. (2015). Plant protein-based delivery systems for bioactive ingredients in foods. *Food & Function, 6*(9), 2876-2889.

Wang, C., Tian, Z., Chen, L., Temelli, F., Liu, H., & Wang, Y. (2010). Functionality of Barley Proteins Extracted and Fractionated by Alkaline and Alcohol Methods. *Cereal Chemistry, 87*(6), 597-606.

Wang, G., & Uludag, H. (2008). Recent developments in nanoparticle-based drug delivery and targeting systems with emphasis on protein-based nanoparticles. *Expert Opinion on Drug Delivery, 5*(5), 499-515.

Wang, Q., Xian, W., Li, S., Liu, C., & Padua, G. W. (2008). Topography and biocompatibility of patterned hydrophobic/hydrophilic zein layers. *Acta Biomaterialia, 4*(4), 844-851.

Wang, S.-Z., & Esen, A. (1986). Primary Structure of a Proline-Rich Zein and Its cDNA. *Plant Physiology, 81*(1), 70-74.

Wang, X., Jiang, Y., Wang, Y.-W., Huang, M.-T., Ho, C.-T., & Huang, Q. (2008). Enhancing anti-inflammation activity of curcumin through O/W nanoemulsions. *Food Chemistry, 108*(2), 419-424.

Xu, H., Jiang, Q., Reddy, N., & Yang, Y. (2011). Hollow nanoparticles from zein for potential medical applications. *Journal of Materials Chemistry, 21*(45), 18227-18235.

Yang, B., Lin, J., Chen, Y., & Liu, Y. (2009). Artemether/hydroxypropyl-β-cyclodextrin host–guest system: Characterization, phase-solubility and inclusion mode. *Bioorganic & Medicinal Chemistry, 17*(17), 6311-6317.

Yao, M., McClements, D., & Xiao, H. (2015). Improving oral bioavailability of nutraceuticals by engineered nanoparticle-based delivery systems. *Current Opinion in Food Science, 2*, 14-19.

Yuan, Y., Li, H., Zhu, J., Liu, C., Sun, X., Wang, D., & Xu, Y. (2019). Fabrication and characterization of zein nanoparticles by dextran sulfate coating as vehicles for delivery of curcumin. *International Journal of Biological Macromolecules*.

Zhang, H., Fu, Y., Xu, Y., Niu, F., Li, Z., Ba, C., Jin, B., Chen, G., & Li, X. (2019). One-step assembly of zein/caseinate/alginate nanoparticles for encapsulation and improved bioaccessibility of propolis. *Food & Function, 10*(2), 635-645.

Zhong, Q., & Jin, M. (2009a). Nanoscalar Structures of Spray-Dried Zein Microcapsules and in Vitro Release Kinetics of the Encapsulated Lysozyme As Affected by Formulations. *Journal of Agricultural and Food Chemistry, 57*(9), 3886-3894.

Zhong, Q., & Jin, M. (2009b). Zein nanoparticles produced by liquid–liquid dispersion. *Food Hydrocolloids, 23*(8), 2380-2387.

Zou, T., & Gu, L. (2013). TPGS Emulsified Zein Nanoparticles Enhanced Oral Bioavailability of Daidzin: In Vitro Characteristics and In Vivo Performance. *Molecular Pharmaceutics, 10*(5), 2062-2070.

Chapter 2

Zein Beta-cyclodextrin micropowders for iron bisglycinate delivery*

* this work has been published as:

Diletta Esposito, Giovanni Dal Poggetto, Aurélie Demont, Nicolai Kraut, Agnese Miro, Francesca Ungaro, Paola Laurienzo, Fabiana Quaglia, ***Pharmaceutics*** **2020, 12(1), 60**

1.1 Introduction

Corn zein (α type) is soluble in 50–90% water/ethanol depending on the composition of the raw material (Shukla & Cheryan, 2001) and easily nano-precipitates from hydroalcoholic solution after the addition of water as anti-solvent. Thus, appropriate manipulation of experimental conditions allows the formation of zein nanoparticles loaded with hydrophobic bioactive components previously co-solubilized in the zein hydroalcoholic solution such as fish oil (Zhong, Tian, & Zivanovic, 2009), α-tocopherol (Luo, Zhang, Whent, Yu, & Wang, 2011), vitamin D3 (Luo, Teng, & Wang, 2012), daidzin (Zou & Gu, 2013), and curcumin (Gómez-Estaca, Balaguer, Gavara, & Hernandez-Munoz, 2012; A. Patel, Hu, Tiwari, & Velikov, 2010). On the other hand, the entrapment of hydrophilic compounds in zein-based nanoparticles is much more difficult to attain since their precipitation in the hydroalcoholic solution can occur, especially when high ratios between the bioactive molecule to load and the polymer are set. To this purpose, nanoparticle formation becomes much more complex, requiring multiple steps, which unavoidably makes the industrial scale-up challenging to attain. Another issue associated with zein nanoparticles is their poor stability in aqueous systems with pH close to the isoelectric point (pI) of zein (ca. 6.2) (A. Patel, Hu, Tiwari, & Velikov, 2010). The zein nanoparticle (NP) surface-stabilized with proteins (A. R. Patel, Bouwens, & Velikov, 2010), polysaccharides (Cheng, 2017), and other anionic polymers like gum arabic (Li, Xu, Chen, Wang, Lu, Hu, et al., 2018), pectin (Chang, Wang, Hu, & Luo, 2017), and alginate (Lee, Kim, & Park, 2016) can be proposed to overcome stability issues because of the possibility of obtaining a dry product.

Combination of zein with different polymers may represent a valid strategy to enlarge the manipulation space for zein-based delivery platforms and to develop novel oral delivery systems (Tapia-Hernández, Rodríguez-Felix, Juárez-Onofre, Ruiz-Cruz, Robles-García, Borboa-Flores, et al., 2018). In this regard, cyclodextrins are ideal candidates since they can form supramolecular complexes with hydrophobic amino acids and change protein properties (Serno, Geidobler, & Winter, 2011). In fact, cyclodextrins can inhibit protein aggregation, increase the thermal stability of liquid protein formulations, and act as stabilisers during the spray- and freeze-drying process (Serno, Geidobler, & Winter, 2011). Only β-cyclodextrin (βCD) is approved in Europe as an additive in food supplements, while different natural and semisynthetic cyclodextrins are already employed in marketed drugs (da Silva, 2018).

The combined use of zein and cyclodextrins as delivery platforms for poorly water-soluble compounds has been scarcely explored so far. Zein/βCD antimicrobial fibres for food packaging (Aytac, Ipek, Durgun, Tekinay, & Uyar, 2017; Dias Antunes, da Silva Dannenberg,

Fiorentini, Pinto, Lim, da Rosa Zavareze, et al., 2017; Kayaci & Uyar, 2012), microparticles entrapping α-tocopherol able to ensure colour stability and shelf-life of fruit beverages (Saldanha do Carmo, Maia, Poejo, Lychko, Gamito, Nogueira, et al., 2017), and powders delivering quercetin for oral bioavailability improvement (Ashok R. Patel & Velikov, 2014) have been developed so far. To our knowledge, the development of strategies for the delivery of hydrophilic molecules has been minimal.

Iron is a trace mineral that is naturally present in many foods, is added to some foods to achieve fortification, and is available as a dietary supplement. Frequently used forms of iron in supplements include ferrous and ferric iron salts such as ferrous sulfate, ferrous gluconate, ferric citrate, and ferric sulfate. Because of its higher solubility, ferrous iron in dietary supplements is more greatly bioavailable than ferric iron (Manoguerra, Erdman, Booze, Christianson, Wax, Scharman, et al., 2005). Despite its wide diffusion, most oral iron supplements have been associated with erosive mucosal injury in the upper gastrointestinal tract as well as nausea, vomiting and epigastric discomfort, diarrhoea, and constipation (Cancelo-Hidalgo, Castelo-Branco, Palacios, Haya-Palazuelos, Ciria-Recasens, Manasanch, et al., 2013). Side effects, bad taste, low bioavailability, and possible interactions with other components in the mouth or multimineral/multivitamin supplements have all prompted the investigation of appropriate delivery strategies (chelation, encapsulation) (Uberti, Morsanuto, Ghirlanda, & Molinari, 2017).

Herein, we explore the applicability of zein as a base material for the delivery of iron. A thorough survey on food-grade iron sources carried out during a first period of internship at Neilos s.r.l. allowed selection of iron bisglycinate as the derivative with the highest impact on supplement market (see chapter 4 for details). Iron-loaded micropowders were prepared through a two-steps nano-in-micro strategy consisting in forming a zein/βCD pseudolatex via antisolvent precipitation followed by a spray-drying step. Experimental conditions to obtain zein/βCD pseudolatexes and powders were preliminarily set and interactions between components clarified. After that, iron was incorporated at different loadings and the final powders fully characterised in the solid state and in simulated oral fluids to evaluate their potential in oral delivery.

1.2 Materials and Methods

1.2.1 Materials

Corn zein (Zein F4400C non-GMO/food grade) was a kind gift of Flo Chemical Corporation (Ashburnham, MA, USA). KLEPTOSE® (beta-cyclodextrin, βCD) was purchased by Roquette Italia SpA (Alessandria, Italy) and iron bisglycinate (FeBIS, total iron content of 26% by wt) was a kind gift from Giusto Faravelli SpA (Milan, Italy). Phenolphthalein, sodium chloride, sodium hydroxide, sodium carbonate, monobasic potassium phosphate, and pepsin from porcine gastric mucosa were from Sigma-Aldrich (Milan, Italy). Methanol and hydrochloric acid were from Carlo Erba Reagents (Milan, Italy), and ethanol was from Honeywell (Seelze, Germany). All the other chemicals were of analytical reagent grade. Ultrapure water was used for all experiments.

1.2.2 Production of Pseudolatexes

Zein pseudolatexes (PLs) were formed by the anti-solvent co-precipitation method (Joye, Davidov-Pardo, Ludescher, & McClements, 2015), adding 50 mL of a water solution of βCD (0.5–1.5% *w*/*v*) to 50 mL of a solution of zein in ethanol/water 80% *v*/*v* at room temperature and under magnetic stirring. The following process parameters were tested: (1) zein and βCD concentration in the hydroalcoholic and water solution, respectively, and (2) the ratio between hydroalcoholic and water phases.

In the first set of experiments, βCD concentration was fixed at 1% *w*/*v* while zein was employed in a concentration range of 2–6% *w*/*v* while maintaining a 1:1 volume ratio between the two solutions.

In the second set of experiments, zein concentration was fixed at 4% *w*/*v* while βCD was used in a concentration range of 0.5–1.5% *w*/*v*. Pseudolatex of zein alone were prepared analogously using water instead of the βCD solution.

1.2.3 Characterisation of Pseudolatexes

The hydrodynamic diameter (D_H) and polydispersity index (PI) of pseudolatex were assessed on a Zetasizer Nano ZS (Malvern Instruments Ltd., UK). The amount of βCD embedded in the pseudolatex was evaluated indirectly from the amount of βCD remaining in the water solution after pseudolatex formation. βCD quantification was carried out following two protocols: (1) a spectrophotometric assay based on the shift of colour of a phenolphthalein solution upon βCD complexation, and (2) by weighting the lyophilised βCD-containing aqueous phase after pseudolatex centrifugation. In the first method, βCD was quantified by UV analysis of the fading of a phenolphthalein alkaline solution (Giuseppe De Rosa, 2008).

Phenolphthalein/βCD form a colourless stable inclusion complex (molar ratio 1:1) which was directly related to the amount of βCD added to the solution (Zarzycki & Lamparczyk, 1998). Briefly, a stock phenolphthalein solution in methanol (3 mM) was diluted 1:100 in 0.05 M carbonate buffer at pH 10.5 just before use. Then, 1.3 mL of the phenolphthalein working solution were added to 200 µL of the sample, and the absorbance of the resulting solution was immediately measured at 553 nm (phenolphthalein λ_{max}) on an UV-1800 (Shimadzu Corporation, Tokyo, Japan). The linearity of the response was verified over the βCD concentration range of 0.1–1.00 mg/mL ($R^2 > 0.99$). All the measurements were performed in triplicate at room temperature.

In the second method, the amount of unbound βCD was evaluated by weighting the mass of lyophilised supernatant obtained after the centrifugation of pseudolatex at 5400 ×*g* for 30 min.

Both methods were performed considering the interference of zein in the pseudolatex prepared without CD.

1.2.4 Production of Micropowders

Micrometric powders were obtained by spray-drying the pseudolatex in a Büchi Mini Spray Dryer B-290 (BÜCHI Labortechnik AG, Flawil, Switzerland). Different process parameters were preliminarily tested on pseudolatex made only with zein to optimise the properties of the final products (yield, adhesiveness, flow properties). For pseudolatex including βCD the following operating conditions were maintained: (1) inlet drying temperature 115 °C, (2) outlet drying temperature 60 °C, (3) pump 10%, and (4) aspirator level 90%. After the drying process, the powders were collected, sieved, and stored at room temperature. The yield of the production process was calculated from the weight of collected micropowders.

FeBIS-loaded micropowders were produced by spray-drying a pseudolatex prepared from a zein hydroalchoholic solution at 4% *w*/*v* and a water solution containing βCD and FeBIS at 1% and 0.1% *w*/*v*, respectively. The volume ratio between phases was 1:1. The theoretical loading of the final powder was 2% *w*/*w* corresponding to 0.5% *w*/*w* Fe^{2+}. It was not possible to form pseudolatex of FeBIS in the absence of βCD.

To maximise the theoretical loading of FeBIS, component concentrations and volume of the solutions needed to be changed. Zein was used at 2% *w*/*v* in the hydroalcoholic solution, βCD was set at 0.1% *w*/*v* and FeBIS at 0.04% *w*/*v*, respectively. The volume ratio between the hydroalcoholic and water phases was 1:5. The theoretical loading of the final powder was 8% *w*/*w*, corresponding to 2% *w*/*w* Fe^{2+}.

1.2.5 Solid State Characterisation of Micropowders

Scanning electron microscopy (SEM) and energy dispersive X-ray (EDX) mapping analysis were performed to evaluate the morphology of micropowders and the distribution of iron in the solid, respectively. For SEM analysis, Quanta 200 FEG apparatus (FEI, Hillsboro, OR, USA) equipped with an Inca Energy 250 and an Inca-X-act LN2-free analytical silicon drift detector (Oxford Instruments, High Wycombe, UK) were used. Samples were coated with Au/Pd alloy. Micrographs were taken by using a beam intensity of 30 kV. For EDX analysis, a Phenom XL (Alfatest, Milan, Italy) was used. The distribution of iron was analysed with Phenom XL Desktop software.

The bulk/tapped density of the sieved powders was evaluated before/after a compaction process according to method 1 of the European Pharmacopoeia (9 ed. monograph 2.9.34., Bulk density and tapped density of powders). Accordingly, the flow properties of micropowders were estimated as Carr's Index.

The evaluation of the amount of uncomplexed βCD in the micropowders was carried out using the same protocols described above for the pseudolatex. An amount of micropowder (100 mg) was treated with water (4 mL) to solubilise free βCD. After centrifugation (5400 ×*g* for 30 min), the supernatant was collected and either treated with phenolphthalein (1) or freeze-dried and weighted (2).

Fourier transform infrared (FTIR) analysis was performed with a Paragon 500 spectrometer (Perkin Elmer, Shelton, CT, USA) equipped with a ZnSe attenuated total reflectance (ATR) crystal accessory. Samples were placed in direct contact with the ATR crystal and pressed with a pressure clamp positioned over the crystal/sample area to allow intimate interaction between the material and the crystal. Spectra were acquired in the 4000–400 cm^{-1} range, at a resolution of 2 cm^{-1} (average of 20 scans).

NIR spectra were collected in reflectance mode with an NIRFlex® N-500 FT-NIR spectrometer (BÜCHI Labortechnik AG, Flawil, Switzerland) over the range of 4000–10,000 cm^{-1}, with 4 cm^{-1} resolution. The micropowders were analysed in vials with 8 mm outer diameter. The results were reported as the percentage of reflactance.

Thermogravimetric analysis (TGA) was carried out on a Pyris Diamond TG-DTA (Perkin-Elmer, Shelton, CT, USA) apparatus from 25 to 400 °C under nitrogen flow (50 mL/min) at 10 °C/min heating rates.

Differential scanning calorimetry (DSC) analysis was carried out on a Q2000 (TA Instruments, Lukens Drive, New Castle, DE, USA) under nitrogen flow. Samples (about 4 mg)

sealed in an aluminium crucible were heated from 25 to 120 °C at 10°/min scanning rate, cooled to 25 °C at 20°/min and finally heated again up to 200 °C at 10°/min (second heating run).

1.2.6 Zein Quantification in the Micropowders

This method was carried out to assess the amount of zein in raw material and spray-dried products. Zein raw material or micropowders (40–250 mg) were weighted using Kjeldahl weighting boats (nitrogen-free) and placed in Kjeldahl tubes (300 mL) adding three tablets of titanium-micro as the catalyst and 10 mL of 98% *w*/*v* H_2SO_4. All samples were digested in KjelDigester K-449 for 2 h at 420 °C (one digestion cycle). After digestion (samples were clear-green digestate), the samples were cooled to room temperature. Then the acidic digestion mixtures were diluted with distilled water (25 mL), and the samples tubes were transferred in the KjelMasterK-375 distillation unit (BÜCHI Labortechnik AG, Flawil, Switzerland). The digestion mixtures were alkalinised with NaOH 32% *w*/*v* (45 mL) before distillation to free-up ammonia. Ammonia was steam-distilled into an acidic receiver solution of H_3BO_3 4% *w*/*v* with Sher indicator (60 mL). The nitrogen content was determined by the titration of the borate complex with H_2SO_4 0.1 M according to Equation (1):

$$\% N = [V(\mathrm{l}) - V(\mathrm{Bl})] \times F \times c \times f \times \frac{M(\mathrm{N})}{m \times 1000} \times 100 \quad (1)$$

where % *N* is the % of weight of *N*, *V*(l) is the consumption of titrant, sample (mL), *V*(Bl) is the average consumption of titrant, blank (mL), *F* is the molar reaction factor (1 = HCI, 2 = H_2SO_4), *c* is the concentration of titrant (0.1 mol/L), *f* is the factor of titrant (1), *M*(N) is the molecular weight of N (14,007 (g/mol)), and *m* is the sample weight (g).

A protein factor (PF) of 6.25 was used to calculate the protein content (% P).

1.2.7 Release of Iron Bisglycinate from Micropowders

The release properties of the micropowders loaded with FeBIS was assessed in simulated gastric fluid (SGF) pH 1.2 (2 g NaCl, 80 mL of 1 M HCl, 3.2 g pepsin powder from porcine gastric mucosa in 1 L of water) and in simulated intestinal fluid (SIF) pH 6.8 (77 mL of 0.2 M NaOH, 6.8 g KH_2PO_4, 10 g of pancreas powder in 1 L of water) according to European Pharmacopeia indications. Fifty milligrams of micropowders were placed in 4 mL of SGF or SIF under stirring. Samples were taken at different time points and centrifuged at 16300 ×*g* for 15 min. Iron content in the sample was assessed by inductively coupled plasma–mass spectrometry (ICP-MS). To this purpose, 100 µL of the supernatant were treated with 9.2 mL of ultrapure water and 0.7 mL of HNO_3 65% *w*/*v* and analysed with an Agilent 7500ce apparatus

(Agilent Technologies, Inc., Santa Clara, CA, USA) with a collision/octopole reaction system (ORS) to reduce polyatomic interferences. Instrument performances were checked using proper Tuning Solution (AGILENT®) until the setting related to sensitivity and interference parameters were optimised. Possible interferences were tested through Interference Check Solutions (AGILENT®).

1.2.8 Statistics

Data are expressed as the mean ± standard deviation (SD) of at least three experiments. Post hoc paired Student's *t*-test was used to investigate significant differences.

In all cases, $p < 0.05$ (one-tail) was considered to be statistically significant. All data processing was performed using Excel statistics.

1.3 Results and discussion

1.3.1 The Issue of Iron Entrapment in Zein-Based Nanoparticles

Processing of powders was attempted with a two-step method with the potential of industrial scale-up, where a zein-based pseudolatex incorporating the bioactive component is then processed by spray-drying giving a final solid product with controlled-release features. The general strategy proposed here to form zein powders consists in (1) preparing a stable colloidal dispersion (referred to as pseudolatex) through an anti-solvent precipitation method (first step), and (2) drying the pseudolatex by spray-drying to achieve a solid (second step). Experimental conditions were set to obtain pseudolatexes withstanding (1) size compatible with nebulisation process and (2) colloidal stability during spray-drying.

The most logical way to entrap FeBIS in the pseudolatex was to dissolve the iron salt in the hydroalcoholic zein solution and achieve particle hardening by adding water. Unfortunately, massive aggregation occurred at different zein/FeBIS concentrations (data not shown) due to the low solubility of FeBIS in the hydroalcholic solution.

As an alternative, we decided to dissolve FeBIS in the antisolvent and achieve encapsulation upon mixing with the hydroalcoholic zein solution. Again, massive aggregation occurred at different zein concentrations and solvent/antisolvent ratios. Thus, we introduced βCD as helping excipient in the antisolvent to alter zein conformation/solubility and, in so doing, to make zein and FeBIS compatible from a chemical-physical standpoint. The general procedure to prepare FeBIS-loaded powders is illustrated in Fig. 1.

A direct method to establish if a protein changes its conformation in the presence of an interacting species is to analyse UV and fluorescence spectra at different protein/complexant ratios. We found that βCD could interact with zein as demonstrated by the depression of UV maximum absorption for zein at 278 nm and a progressive decrease of baseline scattering (supplementary information, Fig. S1a). A depression of the emission band with a maximum at 305 nm typical of tyrosine and tryptophan was observed in parallel (supplementary information, Fig. S1b).

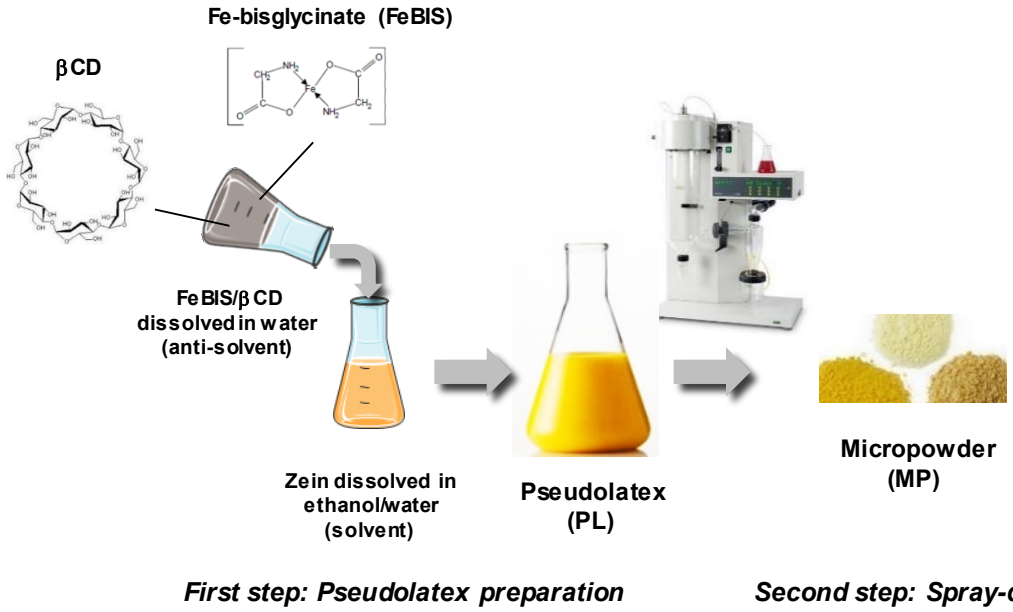

Fig. 1. Schematic representation of the powder production process through the nano-in-micro strategy.

Fluorescence results clearly showed that βCD interacts with zein, likely altering its conformation. Since zein contains a high amount of tyrosine residues (approx. 5.0% *w/w*) while the level of tryptophan residues is insignificant (Joye, Davidov-Pardo, Ludescher, & McClements, 2015), it is logical to assume that tyrosine is involved in such interaction with βCD.

1.3.2 First Step: Development of Zein/βCD Pseudolatex

In the first part of the study, we investigated the impact of zein concentration and βCD addition on pseudolatex hydrodynamic diameter (D_H) and polydispersity (PI) (Fig. 2). In the formulation approach, the concentration of βCD in water was maintained constant at 1% *w/v* while zein concentration was gradually increased. As illustrated in Fig. 2a, D_H and PI increased proportionally as the concentration of zein in the hydroalcoholic solution did. No macroscopic aggregation was also observed at large particle size and high PI. At each zein concentration tested, the addition of βCD 1% *w/v* in the aqueous phase did not impact significantly on the final size and PI (data not shown).

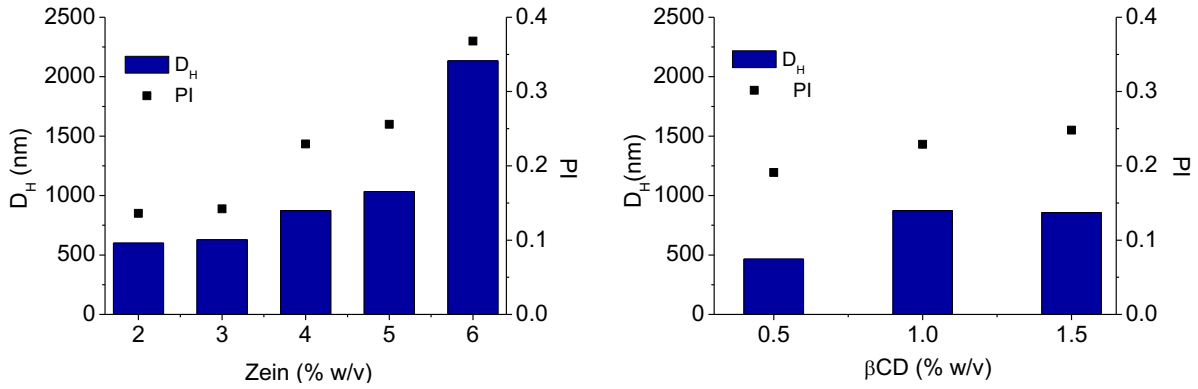

(**a**) (**b**)

Fig. 2. Size and polydispersity (PI) of zein/CD pseudolatexes. Effect of zein concentration (2–6% *w*/*v*) at a fixed CD concentration (1% *w*/*v*) (**a**); effect of increasing CD concentration (0.5–1.5% *w*/*v*) at a fixed zein concentration (4% *w*/*v*) (**b**). D_H: hydrodynamic diameter.

After that, the effect of increasing βCD amount at a fixed zein concentration (4% *w*/*v*) was evaluated (Fig. 2b). Zein concentration of 4% *w*/*v* gave, in fact, a pseudolatex with satisfactory colloidal stability along time (no change of size observed up to 4 h). An increase of βCD concentration in the antisolvent aqueous phase up to 1.5% *w*/*v* (which is very close to maximum βCD solubility in water) resulted in a pseudolatex with D_H increasing from ca 500 nm to ca 800 nm, suggesting that the incorporation of βCD in the zein solid matrix during solvent diffusion process reached a plateau. PI remained in the range 0.20–0.25, which can be satisfactory for a pseudolatex.

1.3.3 Second Step: Processing Pseudolatex by Spray-Drying

This step focused on setting-up suitable operation conditions for spray-drying zein and corresponding zein/βCD pseudolatexes developed in 3.2 (compositions in Table S1).

In a pilot experiment, a powder of zein (MP_Z_2) was produced by employing different process parameters to optimise process conditions. As shown in Table S2, the maximum yield around 60% was achieved by increasing the inlet temperature, which did not increase further at a doubled pumping rate of the feeding liquid. In the absence of βCD, the yield of the process was never higher than 60%. Based on these preliminary results the inlet drying temperature was set at 115 °C which gave an outlet value in the range 55–60 °C (i.e., the maximum temperature encountered by the powder during the drying process). The modulation of the *t* outlet below Tg of βCD was found crucial to reduce the humidity of the drying gas, thus avoiding the formation

of a sticky product and overall increasing the powder yield. In these operating conditions, the drying process gave a solid with yields above 70%, reaching even 90% for MP_Z_2/$CD_{0.5}$.

The produced powders were investigated by NIR to get preliminary insight in zein/βCD interactions. As evidenced in Fig. 3a, a different shift in the spectral bands was found as a function of βCD amount in the sample. In particular, the OH/NH stretch region (Fig. 3b), was changed depending on the βCD amount in the powder.

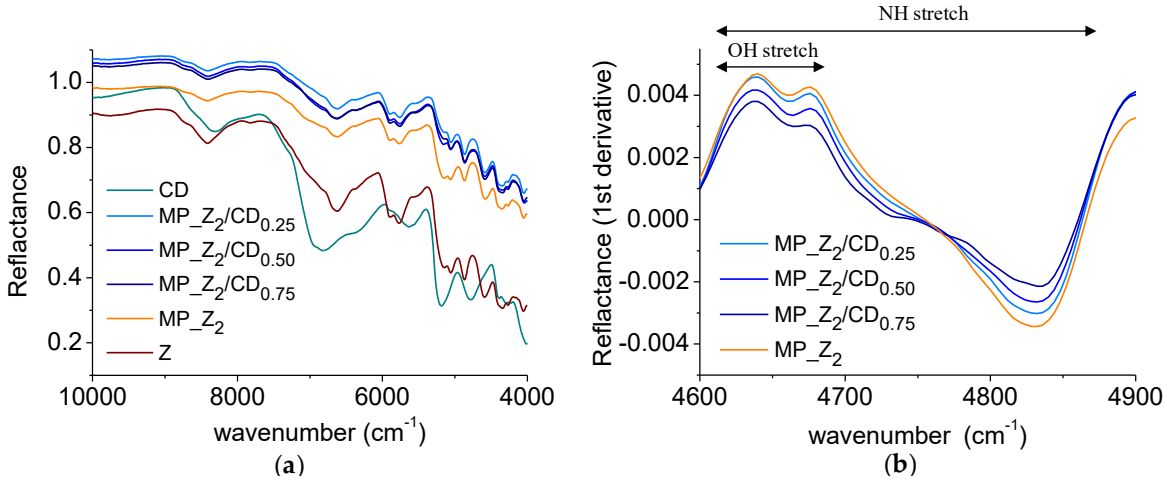

Fig. 3. NIR spectra of zein and zein/CD micropowders. Reflectance (**a**) and first derivative spectra in the interval 4600–4900 cm^{-1} (**b**).

Thus, it could be hypothesised that some chemical groups were involved in the formation of a supramolecular zein/βCD complex. The quantification of free βCD for MP_Z_2/$CD_{0.5}$ powder with the highest yield gave values around 50% of the total βCD employed (49 ± 5 and 49 ± 1 for βCD quantification via protocols 1 and 2 described in the experimental part). A similar amount of free CD was found in the aqueous phase of pseudolatex feeding (51 ± 11 and 45 ± 7 for βCD quantification via protocols 1 and 2 described in the experimental part) indicating that βCD is partly associated to zein matrix during pseudolatex formation and partly uncomplexed.

The flow properties were estimated after the evaluation of the bulk/tapped density of the sieved powders. The presence of βCD did not affect significantly the flowability of the powder expressed as Carr's Index (MP_Z_2 = 38 ± 2.8%; MP_Z_2/$CD_{0.25}$ = 37 ± 4.8%; MP_Z_2/$CD_{0.5}$ = 37 ± 8.0%; MP_Z_2/$CD_{0.75}$ = 38 ± 2.8%).

1.3.4 Development of Zein/βCD/FeBIS Micropowders

FeBIS was first dissolved in the βCD water solution (Fig. 1) and then added to the hydroalcoholic zein solution. The concentration of zein and βCD selected to prepare pseudolatex were those achieving a dispersion having a size compatible with nebulisation (<1 µm to avoid nozzle blocking) and at a high solid content for a shorter spray-drying process (PL_Z_2/$CD_{0.5}$). In parallel, we also tried to maximise FeBIS loading, which is a critical requirement when developing a successful drug delivery strategy. Loading should be as high as possible to reduce the amount of both carrier material employed for production and amount of processed product needed in the final dosage form.The maximum amount of FeBIS that could be loaded without causing massive aggregation of the pseudolatex was 2% *w*/*w* of the total solid. The D_H values of the FeBIS-containing pseudolatex at low FeBIS loading were unchanged as compared with those of unloaded pseudolatex (Fig. 4a).

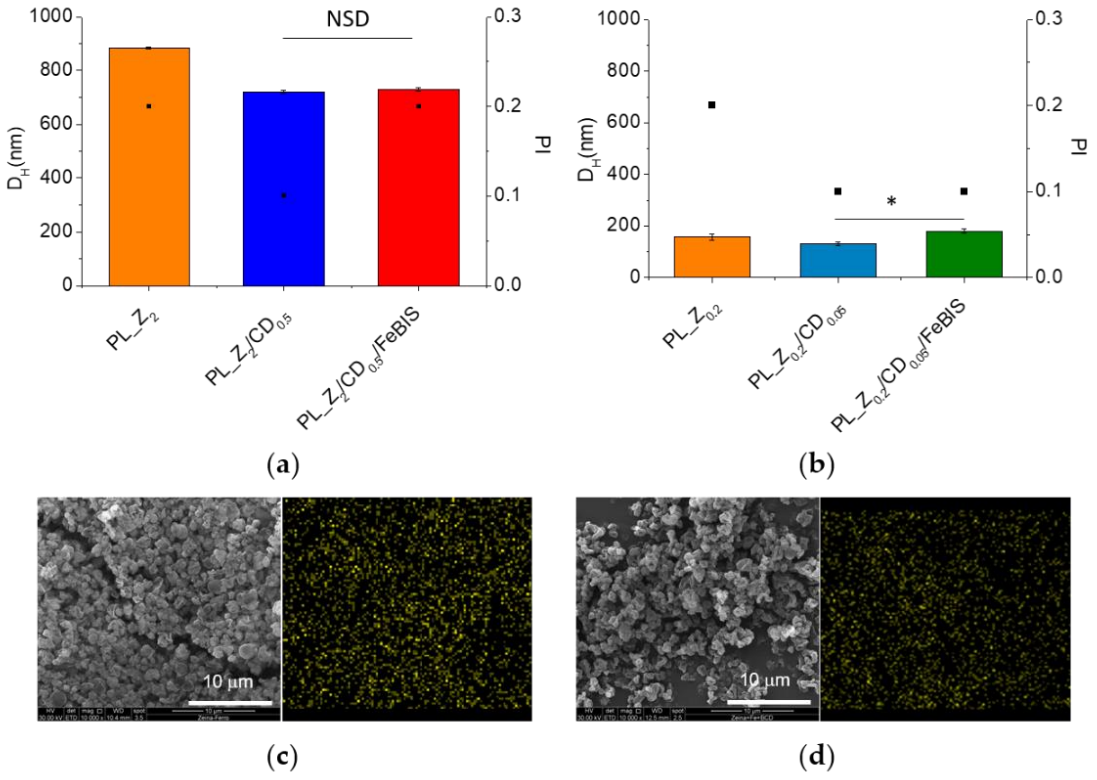

Fig. 4. D_H (bars) and PI (squares) of the pseudolatex employed to prepare powders at FeBIS theoretical loading of 2% (**a**) and 8% *w*/*w* (**b**). SEM images and corresponding energy dispersive X-ray (EDX) mapping of iron (yellow) in the MP_Z_2/$CD_{0.5}$/FeBIS (**c**) and MP_$Z_{0.2}$/$CD_{0.05}$/FeBIS (**d**). NSD: no significant difference. * $p < 0.02$.

To increase FeBIS theoretical loading, we needed to optimise formulation again. FeBIS loading of 8% *w*/*w* ($Z_{0.2}$/$CD_{0.05}$/FeBIS) could be attained by setting different zein and βCD initial concentration in the hydroalcoholic and aqueous phase (Zein and βCD concentrations

needed to be decreased ten times), respectively, as well as solvent/antisolvent ratio as detailed in 2.4. As shown in Fig. 4b, the increase of theoretical loading slightly increased the size of the pseudolatex formed. For both pseudolatexes at different theoretical loadings, size and PI were unchanged as compared with unloaded systems.

Both FeBIS-containing pseudolatexes were processed by spray-drying, and powders with different yields were collected. For MP_Z_2/$CD_{0.5}$/FeBIS, the yield remained very high (88%) while product recovered for MP_$Z_{0.2}$/$CD_{0.05}$/FeBIS was lower (45%). This result is expected if considering that solid content of the corresponding feeding liquid is lower (2.55 and 0.45% *w*/*v* for iron theoretical loading of 2% and 8%, respectively).SEM images in Fig. 4c,d show that micro-sized powders with irregular shape were obtained and, remarkably, a very homogeneous distribution of iron in the matrix was attained.

The Carr's Index calculated from the bulk/tapped density was 22 ± 0.1% for MP_Z_2/$CD_{0.5}$/FeBIS and 27 ± 1.8% for MP_$Z_{0.2}$/$CD_{0.05}$/FeBIS (FeBIS-loaded micropowders), whereas it was 37 ± 8.0% for MP_Z_2/$CD_{0.5}$ and 31 ± 1.7% for MP_$Z_{0.2}$/$CD_{0.05}$ (unloaded micropowders). Significantly higher flowability was found for FeBIS-loaded micropowders (MP_Z_2/$CD_{0.5}$/FeBIS vs. MP_Z_2/$CD_{0.5}$ and MP_$Z_{0.2}$/$CD_{0.05}$/FeBIS vs. MP_$Z_{0.2}$/$CD_{0.05}$, $p < 0.005$).

During spray-drying of a multicomponent feeding liquid, the final ratio between components can be altered due to a preferential loss of one component over the others. To check that the amount of zein was maintained throughout the entire drying process, that is to compare theoretical zein employed initially to prepare pseudolatex, and that found in the final micropowders, nitrogen content in the micropowder was assessed through Kjeldahl. The % *N* in zein as raw material was 13.82% in line with values reported in the technical data sheet (13–16%). This value corresponded to a measured % protein of 86.39 calculated on a dry basis (82–100% in the datasheet). As reported in Table 1, values of % *N* and % protein in the micropowder made only with zein were close to those of raw zein, demonstrating that the method can be applied to quantify the protein amount also after spray-drying. For micropowders of zein/βCD or zein/βCD/FeBIS, the theoretical protein content of zein was lower due to the presence of βCD or βCD/FeBIS. The % *N* and % protein in the micropowder made with different amounts of βCD (Table S3) also demonstrated that the actual zein content was always comparable to the theoretical value. Thus, the spray-drying process did not alter the original ratios of the components in the formulation, which can be a drawback when processing multicomponent systems.

Table 1. Nitrogen and protein content of zein micropowders.

Batch	% N (±SD) [a]	% Protein (±SD) [b]	% Theoretical Protein [c]
MP_Z_2	13.67 ± 0.43	85.46 ± 2.69	86
MP_Z_2/$CD_{0.50}$	11.53 ± 0.05	72.05 ± 0.28	80
MP_Z_2/$CD_{0.5}$/FeBIS	11.30 ± 0.01	69.91 ± 0.01	78
MP_$Z_{0.2}$	13.89 ± 0.05	86.81 ± 0.29	86
MP_$Z_{0.2}$/$CD_{0.05}$	11.25 ± 0.01	70.34 ± 0.08	80
MP_$Z_{0.2}$/$CD_{0.05}$/FeBIS	11.13 ± 0.02	69.57 ± 0.12	74

[a,b] calculated as reported in 2.9, [c] calculated from the ratio between the mass of zein and the mass of total components used to prepare pseudolatex × 100.

1.3.5 Solid State Interactions in the Micropowders

The micropowders were analysed in the solid state by ATR-FITR, TGA and DSC to investigate the interaction between zein, βCD and FeBIS. Analysis of βCD, FeBIS and zein (raw materials) was also carried out.

Attenuated total reflectance–Fourier transform infrared (ATR-FTIR) spectra of micropowders at different FeBIS loading and corresponding unloaded micropowders, βCD and FeBIS (raw materials) were collected over the range of 4000–500 cm^{-1} (Fig. 5a,b). Overall, the broad band between 3200 and 3400 cm^{-1} due to hydrogen bonds can be attributed to complex vibrational stretching, associated with free, inter- and intramolecular bound hydroxyl groups, including contributions from primary amides of zein at 3207 and 3450 cm^{-1} (Pascalau, Popescu, Liviu, Dudescu, Borodi, Dinescu, et al., 2012). Furthermore, characteristic FTIR bands for proteins with amide I at 1650 cm^{-1}, amide II at 1530–50 cm^{-1}, and a set of weaker bands that represent amide III vibration modes centred at 1245 cm^{-1} are present (Supplementary information, Fig. S2). For the βCD-containing micropowders, the spectrum trend remains similar independently of the presence of FeBIS and amount loaded. This trend is expected since βCD should complex the hydrophobic side chains of zein amino acid sequence. On the other hand, a shift of the bands from 1021 to 1030 and from 1077 to 1080 cm^{-1} (C-O and CO/CC stretches, respectively) is observed. ATR-FTIR spectra of micropowders suggested that interaction between zein and βCD involves the hydrophobic side chains of zein amino acid sequence, while novel zein/βCD and βCD/FeBIS interactions take place (Saldanha do Carmo, et al., 2017). In particular, the characteristic bands related to FeBIS are no more visible in the spectra, and this effect could be attributed to its interaction with βCD. βCD/FeBIS interactions would hinder these molecular vibrations, consequently diminishing the intensities of its absorption bands (Saldanha do Carmo, et al., 2017).

The thermogravimetric analysis (TGA) of micropowders at different FeBIS loading and corresponding unloaded micropowders, βCD and FeBIS was carried out to monitor the mass

loss of the products at an increasing temperature from 40 to 400 °C (Fig. 5c,d). TGA for raw zein is reported in supplementary material, Fig. S3. The micropowder composition did not significantly affect curve trends. It is worth to notice, however, an incipit of degradation at around 150 °C in the case of MP_$Z_{0.2}$/$CD_{0.05}$/FeBIS, which loads the highest amount of FeBIS. This effect can be attributed to the loss of volatile compounds in FeBIS samples, which contains labile components, and is recommended to be processed below 153 °C. The water content, which corresponds to the initial weight loss until around 100 °C, was found to be the same for all the samples (below 10%).

DSC analysis of the micropowders was run to highlight the occurrence of interactions at a molecular level between the components. Thermograms of the second heating run of micropowders at different FeBIS loading and corresponding unloaded micropowders, βCD and FeBIS are reported in Fig. 5e,f whereas glass transition temperature (Tg) values are summarised in Table S4. DSC thermograms in the range 30–200°C and corresponding Tg values (Supplementary information Fig. S4 and Table S5, respectively) are also reported. Tg of zein (Tg1) moves to slightly higher values in the micropowders containing βCD and βCD/FeBIS. The raw βCD shows a broad Tg at 84 °C, according to the literature (Zhou, Zhao, Wan, Liu, Liu, & Wang, 2015), which is no more visible in zein-based micropowders, confirming strong interactions with the protein. Interestingly, another glass transition at 128 °C (Tg2) was detected in all MP_Z_2 formulations and, at a lower extent, in MP_$Z_{0.2}$. Since Tg2 is present in spray-dried zein while it is absent in raw zein, it is supposed that the spray-drying process causes a separation between two fractions of zein, resulting in the appearance of the second Tg. This effect could be reasonably due to the presence of zein in different fractions. The relaxation enthalpy indicates that this second phase is in a *nonequilibrium* conformation, where chains have been “frozen” into high-energy conformations because of fast water evaporation during the spray-drying process. This transition is accompanied by a relaxation enthalpy well evident in MP_Z_2/$CD_{0.5}$ and MP_Z_2/$CD_{0.5}$/FeBIS.

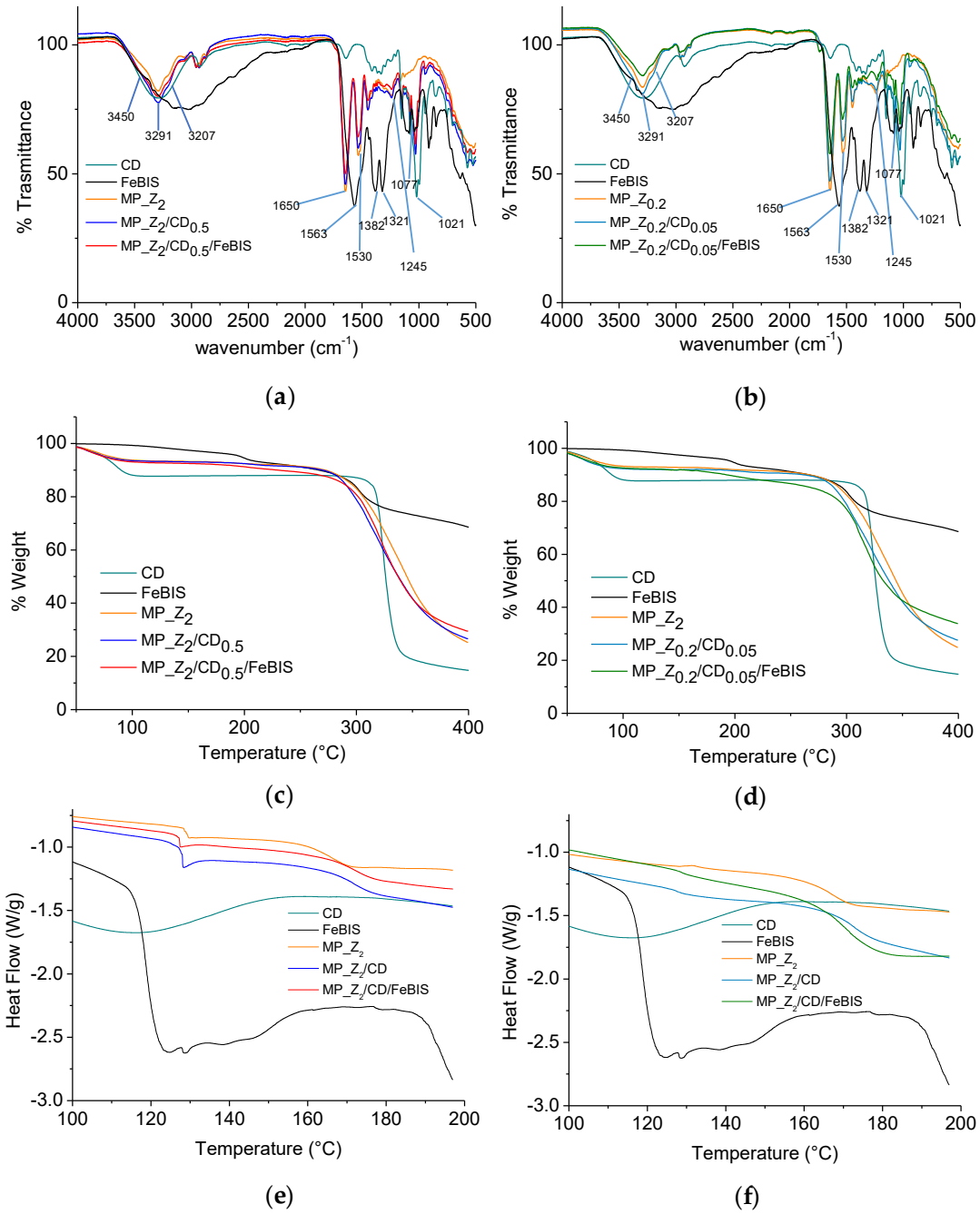

Fig. 5. Fourier transform infrared (FTIR) spectra (**a**,**b**), thermogravimetric analysis (TGA) thermograms (**c**,**d**), and differential scanning calorimetry (DSC) profiles (second run) (**e**,**f**) for micropowders prepared at FeBIS theoretical loading of 2% (**a**,**c**,**e**) and 8% *w*/*w* (**b**,**d**,**f**) with corresponding unloaded micropowders, CD and FeBIS (raw materials).

Furthermore, to investigate the melting behaviour of FeBIS in the complex, DSC measurements were acquired up to 250 °C for raw FeBIS and micropowders containing FeBIS (Supplementary information, Fig. S5). The thermogram of FeBIS taken in the first heating run shows a broad endotherm centred at around 75°, attributable to water evaporation, and two

endotherms at 125° and 220 °C, which can be reasonably attributed to the melting of some component of raw FeBIS (reasonably, citric acid tert-butyl ester, a mono-ester derivative of citric acid) and the melting of FeBIS, respectively. The broad transitions in the range 150–180 °C are related to degradation as found by TGA. Thermograms of MP_Z_2/$CD_{0.5}$/FeBIS and MP_$Z_{0.2}$/$CD_{0.05}$/FeBIS show, along with an expected remarkable increase of water evaporation, the absence of FeBIS melting endotherm at 220 °C, pointing out the formation of an amorphous complex.

1.3.6 Release of FeBIS from Micropowders

The release of FeBIS was studied in simulated gastric fluid (SGF) pH 1.2 and simulated intestinal fluid (SIF) pH 6.8, both supplemented with enzymes. As shown in Fig. 6, the micropowders loaded with different amount of FeBIS released an amount of total iron (Fe^{2+}/Fe^{3+}) below 30% after 2 h in SGF while free FeBIS was immediately dissolved, as expected for a water-soluble compound.

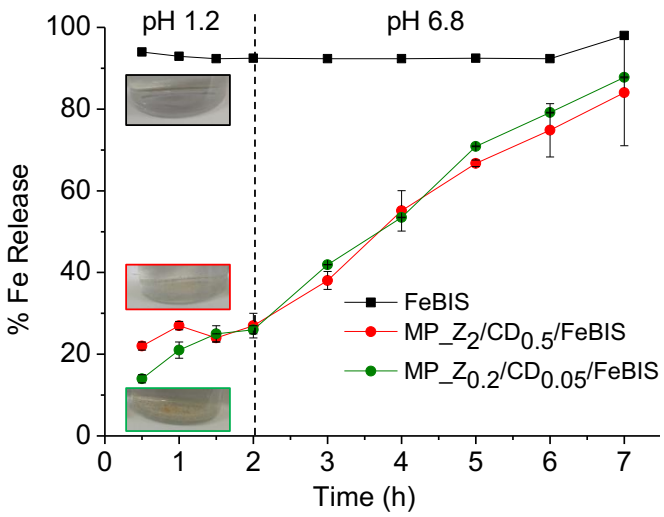

Fig. 6. Release of iron from micropowders prepared at FeBIS theoretical loading of 2% (red) and 8% *w*/*w* (green) in simulated gastric fluid (pH 1.2) and simulated intestinal fluid (pH 6.8). Free FeBIS is reported as control. Data are the mean of three separate experiments ± SD.

Limited FeBIS release in SGF further demonstrated that FeBIS was entrapped in the zein/βCD matrix. The protection of FeBIS can be useful to protect the chelate from dissociation at the low pH values in the stomach. FeBIS is in fact an iron chelate with pH-dependent stability. At acidic pH values, dissociation of the chelate occurs due to the increase of H^+ concentration, which results in significant ferrous glycinate destruction (Ding, Xia, Hayat, & Zhang, 2009) allowing free iron ions interaction with physiologically relevant anions with high affinity for

iron (i.e., phosphates). Furthermore, FeBIS protection may improve iron gastric tolerability and eventual iron precipitation in the gastric mucosa (Stokar-Regenscheit, Sydler, Bürgi, Lippuner, Naegeli, & Sidler, 2017), which is of utmost importance if considering the prolonged use of food supplements. In fact, it has been demonstrated that a severe gastric effect occurs in humans consuming iron tablets, with iron deposits found in the stomach causing mucosal erosions (Kaye, Abdulla, Wood, James, Foley, Ragunath, et al., 2008).

When the medium was changed to SIF, the iron release occurred at a sustained and constant rate, reaching 80% in 7 h. Similar results were obtained with spray-dried powders for resveratrol delivery obtained with a procedure similar to that proposed here (Penalva, Esparza, Larraneta, Gonzalez-Navarro, Gamazo, & Irache, 2015). The mechanism of release was closely related to water uptake of micropowders which activates FeBIS solubilisation in the matrix. A combination of Fickian diffusion and erosion of the matrix was hypothesised (Penalva, Esparza, Larraneta, Gonzalez-Navarro, Gamazo, & Irache, 2015). Since zein is equally ionised at both pH values tested here (Bouman, Belton, Venema, van der Linden, de Vries, & Qi, 2016), no relevant difference in water uptake and, in turn, on release rate is found. The impact of an extended and pH-independent FeBIS release on cell internalization and bioavailability cannot be derived a priori and will be the next step in our research activity.

1.4 Conclusions

In this work, we propose zein/beta-cyclodextrin powders as a delivery platform for bioactive compounds with possible application in food supplements. A two-step nano-in-micro strategy is set up where nanometer-size zein is formed in a first step and then spray-dried to form a micron-sized powder. We demonstrate the crucial role of beta-cyclodextrin as a helping excipient to process zein by spray-drying and to entrap a hydrophilic iron chelate effectively. Studies in the solid state have highlighted that βCD partially interacts with zein and in so doing it increases production yields of the spray-drying process, which is very relevant, taking into account an industrial scale-up. Entrapment of FeBIS in the micropowder is feasible only when βCD is employed in the first preparation step of the nano-in-micro process where modulation of component amount/volume phase ratio can allow achievement of different FeBIS loadings. FeBIS acquires desirable gastro resistance when formulated as micropowders, which avoids chelate destruction occurring at the low pH values in the stomach. In perspective, zein/βCD/FeBIS micropowders could allow efficient absorption of FeBIS in the intestine and can be considered as an innovative strategy for efficient delivery in the body.

References

Aytac, Z., Ipek, S., Durgun, E., Tekinay, T., & Uyar, T. (2017). Antibacterial electrospun zein nanofibrous web encapsulating thymol/cyclodextrin-inclusion complex for food packaging. *Food Chem, 233*, 117-124.

Bouman, J., Belton, P., Venema, P., van der Linden, E., de Vries, R., & Qi, S. (2016). Controlled Release from Zein Matrices: Interplay of Drug Hydrophobicity and pH. *Pharm Res, 33*(3), 673-685.

Cancelo-Hidalgo, M. J., Castelo-Branco, C., Palacios, S., Haya-Palazuelos, J., Ciria-Recasens, M., Manasanch, J., & Pérez-Edo, L. (2013). Tolerability of different oral iron supplements: a systematic review. *Current Medical Research and Opinion, 29*(4), 291-303.

Chang, C., Wang, T., Hu, Q., & Luo, Y. (2017). Zein/caseinate/pectin complex nanoparticles: Formation and characterization. *International Journal of Biological Macromolecules, 104*, 117-124.

Cheng, C. J. (2017). Stabilizing zein nanoparticle dispersions with ι-carrageenan. *Food Hydrocolloids, v. 69*, pp. 28-35-2017 v.2069.

da Silva, A. M. (2018). Room at the Top as well as at the Bottom: Structure of Functional Food Inclusion Compounds. In P. A. a. N. Dhingra (Ed.), *Cyclodextrin - A Versatile Ingredient*): IntechOpen.

Dias Antunes, M., da Silva Dannenberg, G., Fiorentini, Â. M., Pinto, V. Z., Lim, L.-T., da Rosa Zavareze, E., & Dias, A. R. G. (2017). Antimicrobial electrospun ultrafine fibers from zein containing eucalyptus essential oil/cyclodextrin inclusion complex. *International Journal of Biological Macromolecules, 104*, 874-882.

Ding, B., Xia, S., Hayat, K., & Zhang, X. (2009). Preparation and pH stability of ferrous glycinate liposomes. *J Agric Food Chem, 57*(7), 2938-2944.

Giuseppe De Rosa, M. I. L. R., Fabiana Quaglia, Francesca Ungaro. (2008). Use of Additives in the Design of Poly(Lactide-Co-Glycolide) Microspheres for Drug Delivery, . In M. N. V. R. Kumar (Ed.), *Handbook of Particulate Drug Delivery*, vol. 1): American Scientific Publishers.

Gómez-Estaca, J., Balaguer, M., Gavara, R., & Hernandez-Munoz, P. (2012). Formation of zein nanoparticles by electrohydrodynamic atomization: Effect of the main processing variables and suitability for encapsulating the food coloring and active ingredient curcumin. *Food Hydrocolloids, 28*, 82–91.

Joye, I. J., Davidov-Pardo, G., Ludescher, R. D., & McClements, D. J. (2015). Fluorescence quenching study of resveratrol binding to zein and gliadin: Towards a more rational approach to resveratrol encapsulation using water-insoluble proteins. *Food Chem, 185*, 261-267.

Kayaci, F., & Uyar, T. (2012). Electrospun zein nanofibers incorporating cyclodextrins. *Carbohydr Polym, 90*(1), 558-568.

Kaye, P., Abdulla, K., Wood, J., James, P., Foley, S., Ragunath, K., & Atherton, J. (2008). Iron-induced mucosal pathology of the upper gastrointestinal tract: a common finding in patients on oral iron therapy. *Histopathology, 53*(3), 311-317.

Labib, G. (2018). Overview on zein protein: a promising pharmaceutical excipient in drug delivery systems and tissue engineering. *Expert Opin Drug Deliv, 15*(1), 65-75.

Lee, S., Kim, Y. C., & Park, J. H. (2016). Zein-alginate based oral drug delivery systems: Protection and release of therapeutic proteins. *Int J Pharm, 515*(1-2), 300-306.

Li, J., Xu, X., Chen, Z., Wang, T., Lu, Z., Hu, W., & Wang, L. (2018). Zein/gum Arabic nanoparticle-stabilized Pickering emulsion with thymol as an antibacterial delivery system. *Carbohydr Polym, 200*, 416-426.

Luo, Y., Teng, Z., & Wang, Q. (2012). Development of zein nanoparticles coated with carboxymethyl chitosan for encapsulation and controlled release of vitamin D3. *J Agric Food Chem, 60*(3), 836-843.

Luo, Y., Zhang, B., Whent, M., Yu, L. L., & Wang, Q. (2011). Preparation and characterization of zein/chitosan complex for encapsulation of alpha-tocopherol, and its in vitro controlled release study. *Colloids Surf B Biointerfaces, 85*(2), 145-152.

Manoguerra, A. S., Erdman, A. R., Booze, L. L., Christianson, G., Wax, P. M., Scharman, E. J., Woolf, A. D., Chyka, P. A., Keyes, D. C., Olson, K. R., Caravati, E. M., & Troutman, W. G. (2005). Iron ingestion: an evidence-based consensus guideline for out-of-hospital management. *Clin Toxicol (Phila), 43*(6), 553-570.

McClements, D. J. (2015). Nanoscale Nutrient Delivery Systems for Food Applications: Improving Bioactive Dispersibility, Stability, and Bioavailability. *Journal of Food Science, 80*(7), N1602-N1611.

Pascalau, V., Popescu, V., Liviu, P., Dudescu, C., Borodi, G., Dinescu, A., Perhaiţa, I., & Paul, M. (2012). The alginate/k-Carrageenan ratio's influence on their cross-linked composite films properties. *Journal of Alloys and Compounds, 536*, S418.

Patel, A., Hu, Y., Tiwari, J. K., & Velikov, K. P. (2010). Synthesis and characterisation of zein–curcumin colloidal particles. *Soft Matter, 6*(24), 6192-6199.

Patel, A. R., Bouwens, E. C., & Velikov, K. P. (2010). Sodium caseinate stabilized zein colloidal particles. *J Agric Food Chem, 58*(23), 12497-12503.

Patel, A. R., & Velikov, K. P. (2014). Zein as a source of functional colloidal nano- and microstructures. *Current Opinion in Colloid & Interface Science, 19*(5), 450-458.

Penalva, R., Esparza, I., Larraneta, E., Gonzalez-Navarro, C. J., Gamazo, C., & Irache, J. M. (2015). Zein-Based Nanoparticles Improve the Oral Bioavailability of Resveratrol and Its Anti-inflammatory Effects in a Mouse Model of Endotoxic Shock. *J Agric Food Chem, 63*(23), 5603-5611.

Reddy, N., & Yang, Y. (2011). Potential of plant proteins for medical applications. *Trends in Biotechnology, 29*(10), 490-498.

Saldanha do Carmo, C., Maia, C., Poejo, J., Lychko, I., Gamito, P., Nogueira, I., Bronze, M., Serra, A., & Duarte, C. (2017). Microencapsulation of α-tocopherol with zein and β-cyclodextrin using spray drying for colour stability and shelf-life improvement of fruit beverages. *RSC Adv., 7*, 32065-32075.

Serno, T., Geidobler, R., & Winter, G. (2011). Protein stabilization by cyclodextrins in the liquid and dried state. *Advanced Drug Delivery Reviews, 63*(13), 1086-1106.

Shukla, R., & Cheryan, M. (2001). Zein: the industrial protein from corn. *Industrial Crops and Products, 13*(3), 171-192.

Stokar-Regenscheit, N., Sydler, T., Bürgi, E., Lippuner, A., Naegeli, H., & Sidler, X. (2017). Lethal Gastric Mucosal Necrosis due to Administration of Oral Ferrous Bisglycinate Chelate to Suckling Piglets. *Journal of Comparative Pathology, 157*(1), 39-45.

Tapia-Hernández, J. A., Rodríguez-Felix, F., Juárez-Onofre, J. E., Ruiz-Cruz, S., Robles-García, M. A., Borboa-Flores, J., Wong-Corral, F. J., Cinco-Moroyoqui, F. J., Castro-Enríquez, D. D., & Del-Toro-Sánchez, C. L. (2018). Zein-polysaccharide nanoparticles as matrices for antioxidant compounds: A strategy for prevention of chronic degenerative diseases. *Food Research International, 111*, 451-471.

Uberti, F., Morsanuto, V., Ghirlanda, S., & Molinari, C. (2017). Iron Absorption from Three Commercially Available Supplements in Gastrointestinal Cell Lines. *Nutrients, 9*(9).

Vozza, G., Khalid, M., Byrne, H. J., Ryan, S., & Frias, J. (2017). 1 - Nutrition—nutrient delivery. In A. M. Grumezescu (Ed.), *Nutrient Delivery*, (pp. 1-42): Academic Press.

Zarzycki, P. K., & Lamparczyk, H. (1998). The equilibrium constant of beta-cyclodextrin-phenolphtalein complex; influence of temperature and tetrahydrofuran addition. *J Pharm Biomed Anal, 18*(1-2), 165-170.

Zhong, Q., Tian, H., & Zivanovic, S. (2009). Encapsulation of fish oil in solid zein particles by liquid-liquid dispersion. *Journal of Food Processing and Preservation, 33*(2), 255-270.

Zhou, G., Zhao, T., Wan, J., Liu, C., Liu, W., & Wang, R. (2015). Predict the glass transition temperature and plasticization of beta-cyclodextrin/water binary system by molecular dynamics simulation. *Carbohydr Res, 401*, 89-95.

Zou, T., & Gu, L. (2013). TPGS Emulsified Zein Nanoparticles Enhanced Oral Bioavailability of Daidzin: In Vitro Characteristics and In Vivo Performance. *Molecular Pharmaceutics, 10*(5), 2062-2070.

Supplementary Materials

Table S1. Code and corresponding compositions of zein-based micropowders prepared from different pseudolatex.

Powder codes	Pseudolatex preparation			Powder composition	
	zein % w/v [a]	CD % w/v [b]	Antisolvent/ solvent ratio	zein % w/w	CD % w/w
MP_Z_2	4	-	1	2	-
MP_ Z_2/CD $_{0.25}$	4	0.25	1	2	0.25
MP_ Z_2/CD $_{0.50}$	4	1	1	2	0.50
MP_ Z_2/CD $_{0.75}$	4	1.5	1	2	0.75
MP_ $Z_{0.2}$	2	-	5	0.2	-
MP_ $Z_{0.2}$/CD $_{0.05}$	2	0.1	5	0.2	0.05

[a, b] % w/v components in the PL produced to obtain the correspondent MP.

Table S2. Set-up of spray drying conditions for MP_Z_2 powders.

Aspirator flow rate (%)	Pump Speed (%)	T inlet (° C)	T outlet[a] (° C)	Yield (%)
90	10	115	60	50
90	10	150	77	59
90	10	180	121	38
90	20	180	91	23

[a] T outlet is consequent to setting the other parameters.

Table S3. Nitrogen/protein content of zein micropowders using as reference standard zein raw material.

Batch	%N (±SD)	% Protein (±SD)	% Theoretical Protein
MP_ Z_2/CD $_{0.25}$	12.46±0.02	77.87±0.09	86
MP _Z_2/CD $_{0.75}$	10.29±0.05	64.29±0.38	73

Table S4. Glass transition temperatures (Tg) of zein-based micropowders taken in 2nd heating run.

Batch	Tg_1 (°C)	Tg_2 (°C)
MP_Z_2	165.88	128.47
MP_ Z_2/$CD_{0.50}$	171.64	128.06
MP_ Z_2/$CD_{0.5}$/FeBIS	172.28	127.35
MP_ $Z_{0.2}$	166.77	n.d.
MP_ $Z_{0.2}$/$CD_{0.05}$	171.48	128.79
MP_$Z_{0.2}$/$CD_{0.05}$/ FeBIS	172.60	127.40

Table S5. Glass transition temperatures (Tg1) of raw materials.

Sample	Tg (°C)
Zein	162
CD	84

S1. Zein/CD interactions in solution

The interaction between CD and zein was studied in solution by spectroscopic analysis. Zein (20 µg/mL) was dissolved in ethanol:water (8:2 v/v) solution containing different amounts of CD (0, 2 and 5 µg/mL) under magnetic stirring. UV-vis spectra were recorded in the wavelength range of 200-800 nm on a UV-1800; Shimadzu. The emission fluorescence spectra of the samples were collected at a fixed excitation wavelength (λ_{ex} 278 nm) in the range of 290-450 nm by a spectrofluorimeter (RF-6000, Shimadzu).

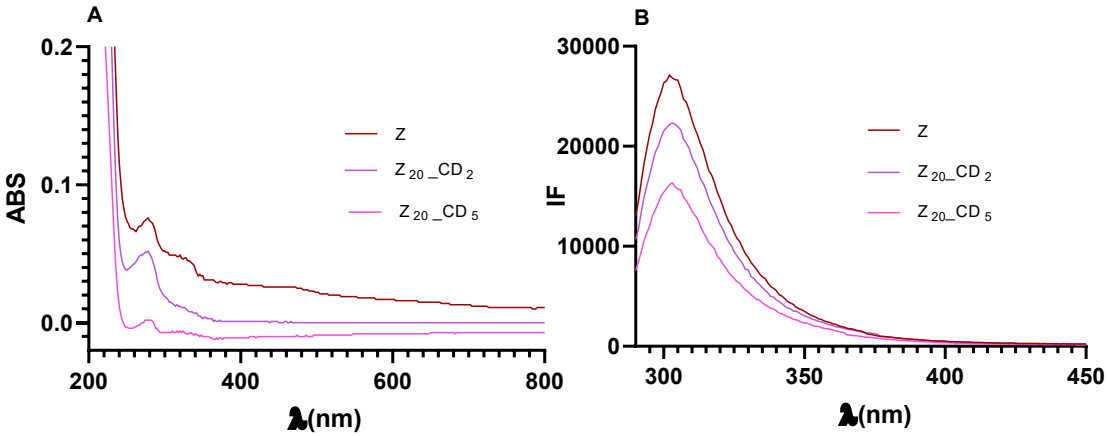

Fig. S1. UV and emission spectra of hydroalcoholic solutions containing zein (20 µg/mL) and CD (0, 2 and 5 µg/mL).

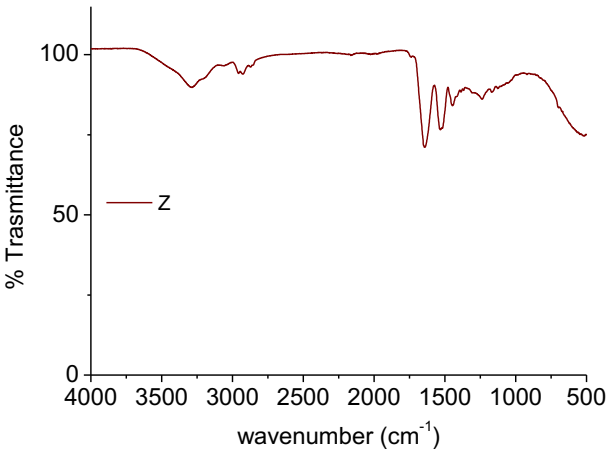

Fig. S2. FTIR spectra of zein (raw material).

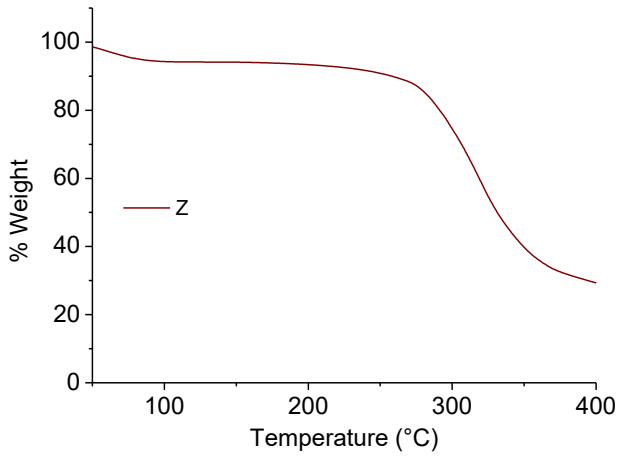

Fig. S3. TGA thermograms of zein (raw material).

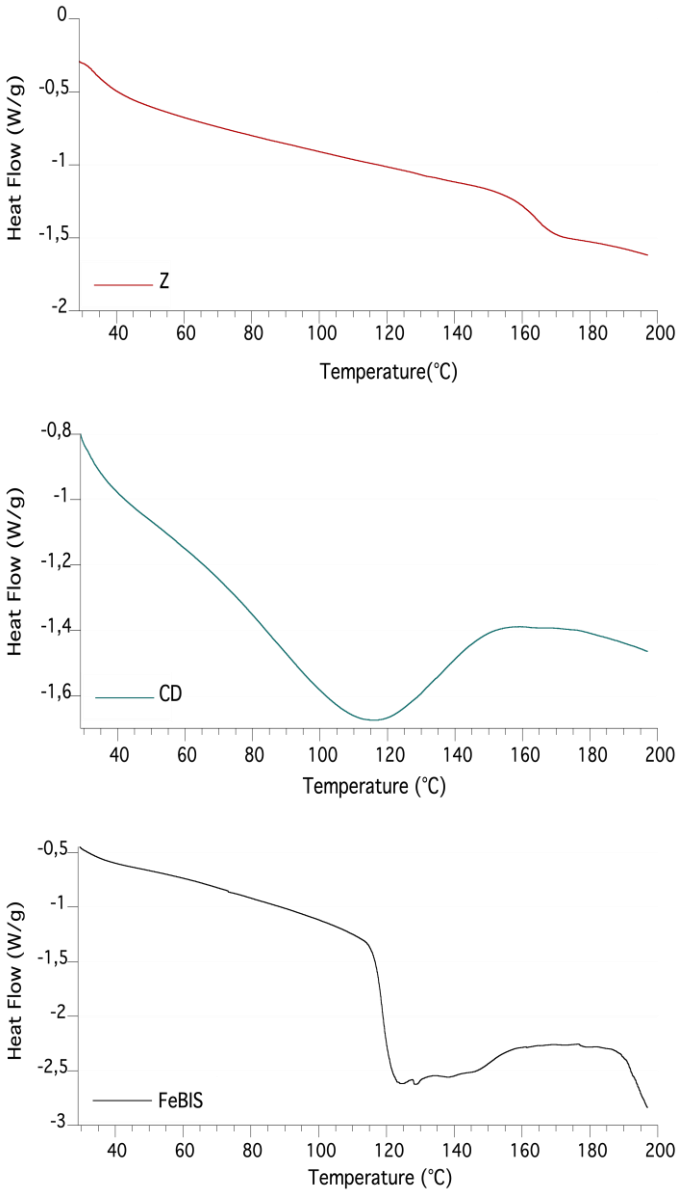

Fig. S4. 2nd run thermograms of zein, CD and FeBIS (raw materials). The transition observed in the thermogram of FeBIS is related to the incipit of degradation phenomena.

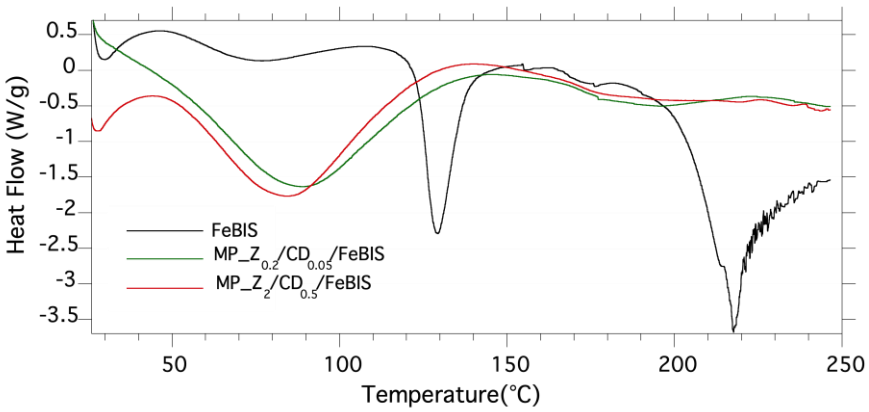

Fig. S5. DSC profiles (1st run) of FeBIS-loaded micropowders and raw FeBIS.

Chapter 3

Zein platforms
for curcumin oral delivery

1.1 Introduction

Among several bioactive food components with healthy effect on humans, polyphenols in particular are under investigation as both nutraceutical supplement and/or therapeutic agents (Vittorio, Curcio, Cojoc, Goya, Hampel, Iemma, et al., 2017).

In this category, curcumin (CUR) is a bioactive constituent found in turmeric rhizome of Curcuma Longa with a bis-α,β-unsaturated β-diketone structure. It contains two conjugated phenolic groups substituted with methoxy, hydroxyl, and carbonyl groups, which may contribute to its antioxidant activity (Wright, 2002).

Curcumin can exist in at least two tautomeric forms, such as a keto-enol and diketone form. These two forms can reach equilibrium in physiological conditions (Payton, Sandusky, & Alworth, 2007) (Fig. 1). The keto form of curcumin predominates in neutral and acidic solution as well as in solid states and it acts as a potent donor of H-atoms, whereas the enolic form predominates at pH>8 and prone to donate electrons.

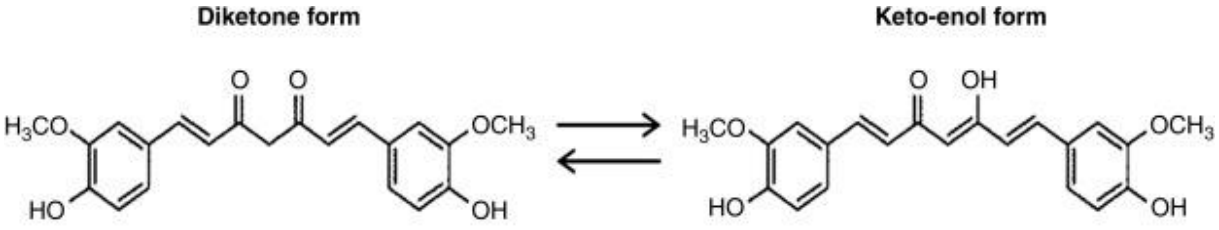

Fig. 1. Chemical structure of curcumin as diketone and keto-enol form.

CUR has demonstrated antioxidant and anti-inflammatory properties that have led to its application as a nutraceutical or pharmaceutical to prevent certain diseases, such as rheumatoid arthritis, cystic fibrosis, inflammatory bowel disease, and colon cancer (Zheng, Peng, Zhang, & McClements, 2018). Furthermore, a number of studies demonstrate that CUR possesses broad-spectrum antimicrobial activity against bacteria, virus, fungi, and parasites (Fig. 2).

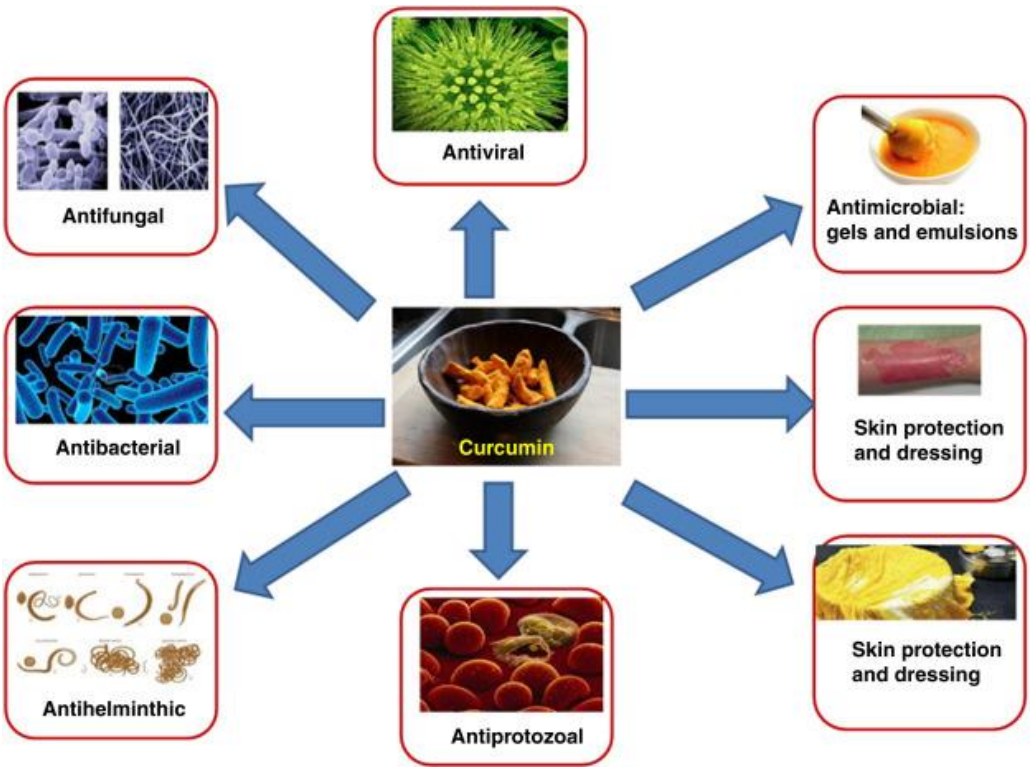

Fig. 2. Different antimicrobial actions of curcumin and proposed mode of delivery (Subramani, Panati, Lebaka, Reddy, & Narala, 2017).

In foods, curcumin is also used as a colour blend because of its yellow-orange pigmentation (Patel, Heussen, Dorst, Hazekamp, & Velikov, 2013).

Despite the potential beneficial activities and safety profile, CUR has not been approved yet as therapeutic agent mainly because of its relatively poor bioavailability. No CUR serum level can be detected after oral administration in a study on the fate of curcumin in the rat, while a few is found in the portal blood (Ravindranath & Chandrasekhara, 1980) and traces of CUR are found in the liver and kidney.

In fact, once tissues absorb curcumin, it is subjected to conjugations including sulfation and glucuronidation, being the enzymes responsible of the biotransformation mainly present in tissues of liver, kidney and intestinal mucosa (Asai & Miyazawa, 2000). Thereafter, several CUR metabolites have been identified (Fig. 3).

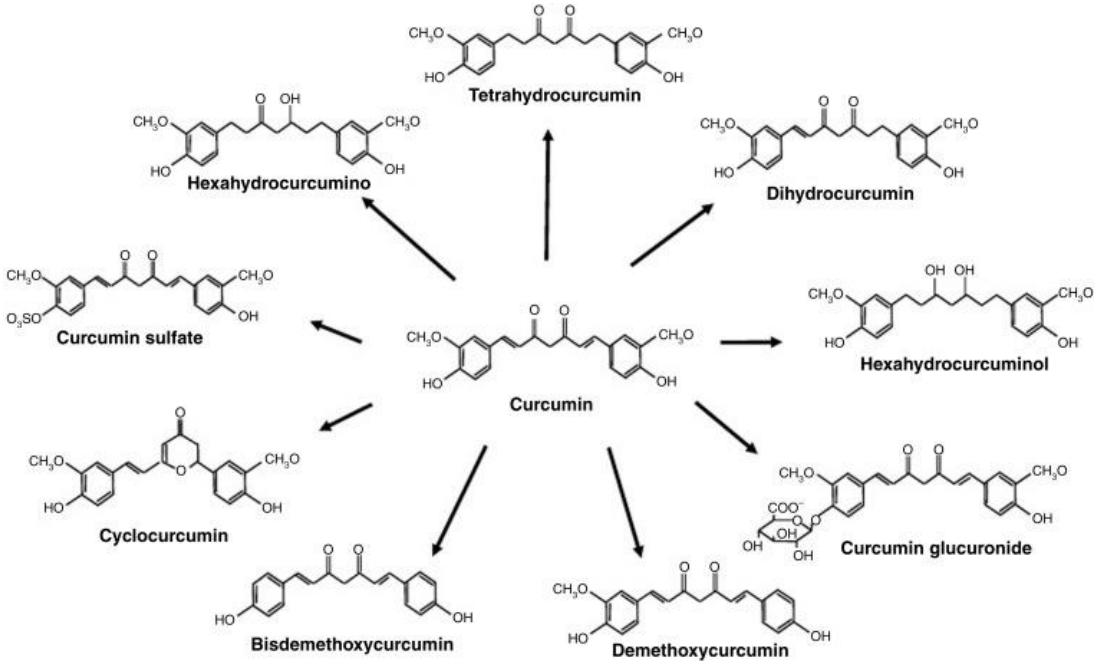

Fig. 3. Curcumin metabolites reported so far (Anand, Thomas, Kunnumakkara, Sundaram, Harikumar, Sung, et al., 2008).

In human subjects, 2 h after an oral intake of CUR (8 g), serum concentration of curcumin is only 1.8 μM (Cheng, Hsu, Lin, Hsu, Ho, Shen, et al., 2000). However, conjugates of curcumin like glucuronide and sulfate can be detected in plasma after oral administration (Vareed, Kakarala, Ruffin, Crowell, Normolle, Djuric, et al., 2008).

Nevertheless, after oral administration, unmodified CUR is found in faeces (Wahlström & Blennow, 1978).

In all these bioavailability studies, the variant of the type of formulation employed has not been properly considered, which overcomplicate their interpretation. Main obstacles to CUR absorption are summarize in Fig. 4 (Ma, Wang, He, & Tang, 2019).

The interest in CUR has led the pharmaceutical, supplement and food industries to develop forms suitable for oral ingestion, such as pills, capsules, powders, foods, and drinks. However, poor water-solubility and stability in neutral and alkaline solutions, light-sensitivity coupled with erratic oral bioavailability, represent the major hurdles in the development of innovative formulations (Zheng, Peng, Zhang, & McClements, 2018). The maximum solubility of CUR in aqueous buffer (pH 5.0) was reported to be as low as 11 ng/mL (Aggarwal, Kumar, & Bharti,

2002) and the degradation proceed so fast that after 10 min at pH 7.4 its maximum absorption band at 426 nm is depressed of a 90%.

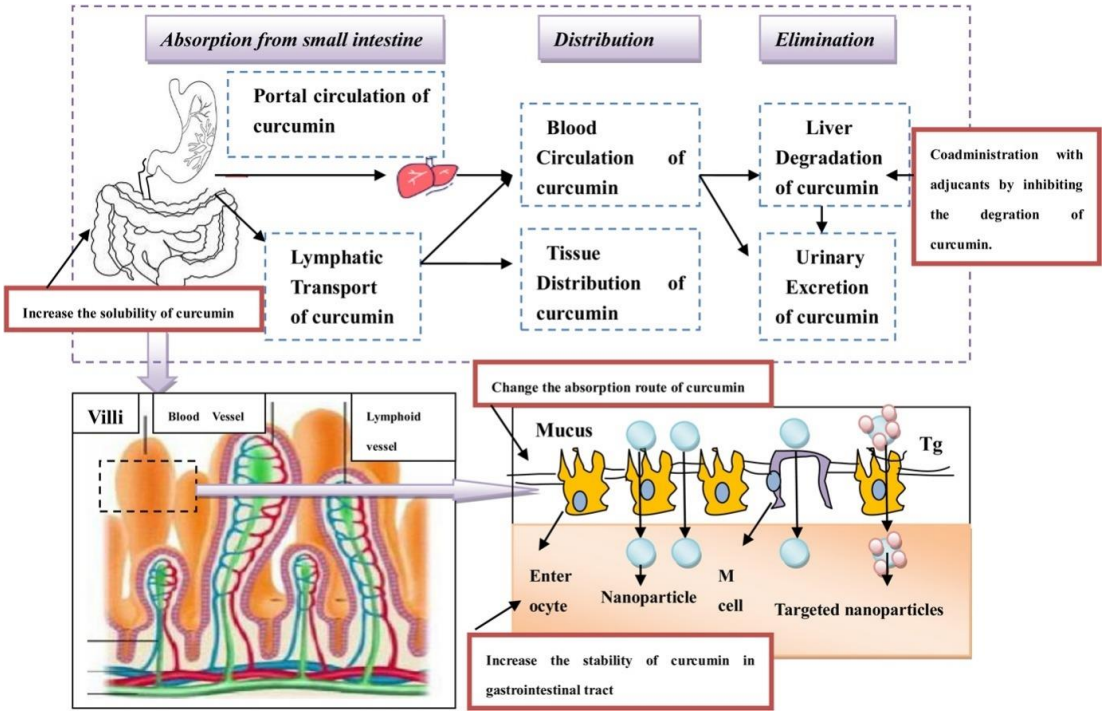

Fig. 4. Critical issues in CUR oral absorption. Absorption, distribution, metabolism and elimination (ADME) of curcumin preparations following oral administration. The curcumin oral bioavailability is increased by enhancing curcumin solubility, improving curcumin gastrointestinal stability, changing the absorption route of curcumin, coadministration with enhancers (Ma, Wang, He, & Tang, 2019).

In this context, micro- and nano-technologies can offer effective alternative to conventional formulations (Yallapu, Nagesh, Jaggi, & Chauhan, 2015). Arantal® is a patented CUR microemulsion which should consist in polysorbate, turmeric oil/curcumin and a weak acid. The formulation has demonstrated increased bioavailability in humans (Henrotin, Priem, & Mobasheri, 2013). In addition, other nano-based drug delivery systems for CUR delivery include nanocrystals, nanoparticles, nanoemulsions, liposomes, polymeric micelles, cyclodextrin complexes, nanosuspension, and solid-lipid nanoparticles (Subramani, Panati, Lebaka, Reddy, & Narala, 2017). Meriva® (Indena s.p.a.) is a commercial product based on phytosome technology and comprises a standardized mixture of natural curcuminoids and lecithin in a 1:2 ratio, with two parts of microcrystalline cellulose. Its superior performance as

compared with non-formulated CUR has been demonstrated in rats and in humans (Jurenka, 2009).

Based on these considerations, we developed two different platforms based on zein and zein/βCD for CUR oral delivery aimed at increasing its bioavailability. In the first strategy, CUR was entrapped in micropowders produced by the nano-in-micro methodology described in chapter 2 to overcome its poor aqueous solubility. In the second alternative strategy, mucoadhesive nanoparticles suitable for buccal delivery were developed and tested for their potential to improve CUR absorption and by-pass hepatic metabolism.

References

Aggarwal, B., Kumar, A., & Bharti, A. (2002). Anticancer Potential of Curcumin: Preclinical and Clinical Studies. *Anticancer research, 23*, 363-398.

Anand, P., Thomas, S. G., Kunnumakkara, A. B., Sundaram, C., Harikumar, K. B., Sung, B., Tharakan, S. T., Misra, K., Priyadarsini, I. K., Rajasekharan, K. N., & Aggarwal, B. B. (2008). Biological activities of curcumin and its analogues (Congeners) made by man and Mother Nature. *Biochemical Pharmacology, 76*(11), 1590-1611.

Asai, A., & Miyazawa, T. (2000). Occurrence of orally administered curcuminoid as glucuronide and glucuronide/sulfate conjugates in rat plasma. *Life Sciences, 67*(23), 2785-2793.

Cheng, A. L., Hsu, C.-H., Lin, J. K., Hsu, M., Ho, Y.-F., Shen, T. S., Ko, J. Y., Lin, J. T., Lin, B.-R., Ming-Shiang, W., Yu, H., Jee, S.-H., Chen, G., Chen, T., Chen, C., Lai, M.-K., Pu, Y. S., Pan, M., Wang, Y. J., & Hsieh, C.-Y. (2000). Phase I clinical trial of curcumin, a chemopreventive agent, in patients with high-risk or pre-malignant lesions. *Anticancer research, 21*, 2895-2900.

Henrotin, Y., Priem, F., & Mobasheri, A. (2013). Curcumin: a new paradigm and therapeutic opportunity for the treatment of osteoarthritis: curcumin for osteoarthritis management. *SpringerPlus, 2*(1), 56.

Jurenka, J. S. (2009). Anti-inflammatory properties of curcumin, a major constituent of Curcuma longa: a review of preclinical and clinical research. *Altern Med Rev, 14*(2), 141-153.

Ma, Z., Wang, N., He, H., & Tang, X. (2019). Pharmaceutical strategies of improving oral systemic bioavailability of curcumin for clinical application. *Journal of Controlled Release, 316*, 359-380.

Patel, A., Heussen, P., Dorst, E., Hazekamp, J., & Velikov, K. (2013). Colloidal approach to prepare colour blends from colourants with different solubility profiles. *Food chemistry, 141*, 1466-1471.

Payton, F., Sandusky, P., & Alworth, W. L. (2007). NMR Study of the Solution Structure of Curcumin. *Journal of Natural Products, 70*(2), 143-146.

Ravindranath, V., & Chandrasekhara, N. (1980). Absorption and tissue distribution of curcumin in rats. *Toxicology, 16*(3), 259-265.

Subramani, P. A., Panati, K., Lebaka, V. R., Reddy, D. D., & Narala, V. R. (2017). Chapter 21 - Nanostructures for Curcumin Delivery: Possibilities and Challenges. In A. M. Grumezescu (Ed.), *Nano- and Microscale Drug Delivery Systems*, (pp. 393-418): Elsevier.

Vareed, S. K., Kakarala, M., Ruffin, M. T., Crowell, J. A., Normolle, D. P., Djuric, Z., & Brenner, D. E. (2008). Pharmacokinetics of curcumin conjugate metabolites in healthy human subjects. *Cancer epidemiology, biomarkers & prevention : a publication of the American Association for Cancer Research, cosponsored by the American Society of Preventive Oncology, 17*(6), 1411-1417.

Vittorio, O., Curcio, M., Cojoc, M., Goya, G. F., Hampel, S., Iemma, F., Dubrovska, A., & Cirillo, G. (2017). Polyphenols delivery by polymeric materials: challenges in cancer treatment. *Drug Delivery, 24*(1), 162-180.

Wahlström, B., & Blennow, G. (1978). A Study on the Fate of Curcumin in the Rat. *Acta Pharmacologica et Toxicologica, 43*(2), 86-92.

Wright, J. (2002). Predicting the antioxidant activity of curcumin and curcuminoids. *Journal of Molecular Structure: THEOCHEM, 591*, 207-217.

Yallapu, M. M., Nagesh, P. K. B., Jaggi, M., & Chauhan, S. C. (2015). Therapeutic Applications of Curcumin Nanoformulations. *The AAPS Journal, 17*(6), 1341-1356.

Zheng, B., Peng, S., Zhang, X., & McClements, D. J. (2018). Impact of Delivery System Type on Curcumin Bioaccessibility: Comparison of Curcumin-Loaded Nanoemulsions with Commercial Curcumin Supplements. *Journal of Agricultural and Food Chemistry, 66*(41), 10816-10826.

Section 3A

Zein beta-cyclodextrin micropowders for curcumin oral delivery

1.1 Introduction

Nowadays, the major limitation of nutraceutical products is their low bioavailability, which affects their bioactivity and reduces their utility in the prevention of diseases as well as economic impact. Micro-nano delivery systems have an underestimated potential to "fill this gap," ameliorating the bioaccessibility of nutrients (Đorđević, Belščak-Cvitanović, Drvenica, Komes, Nedović, & Bugarski, 2017).

According to the biopharmaceutical classification system (BCS), curcumin (CUR) belongs to class II compounds for its low water-solubility and high permeability. However, the low oral bioavailability of curcumin is also attributed to instability in the GI tract and extensive metabolism in the intestine and liver (Kurita & Makino, 2013). In the last years, different strategies have been designed to overcome these issues, and numerous approaches proposed to enhance its solubility like using cosolvents, oily solutions, micronization, surfactant dispersions, permeation enhancers, salt formation.

Recently, micro-nano scale systems have been widely proposed for the delivery of the active form of curcumin to the target tissue. Several formulations, such as microspheres, solid lipid nanoparticles, liposomes, polymeric nanoparticles, nanocrystals, CD-inclusion complexes, can tremendously increase its absorption (Giri, 2016). This effect is mainly due to an increase in CUR dissolution rate coupled with protection in the GI tract.

Amid the different pharmaceutical strategies to increase CUR bioavailability, it seems that nanoparticles can be a valuable option as compared to other nanoplatforms (Siviero, 2015) (Ma, Wang, He, & Tang, 2019).

Amid the carriers employed so far, cyclodextrins (CDs) can sequester insoluble compounds within their hydrophobic cavity, resulting in improved solubility and enhanced chemical or enzymatic stability. A hydroxypropyl-β-CD inclusion compound with CUR showed enhanced oral absorption in rats (Ouyang, Fang, Zhu, Zhang, Ren, He, et al., 2012). Compared with a CUR suspension, its C_{max} (370 ng/ml) was about nine-times higher at a 500 mg/kg dose. A γ-CD inclusion compound of CUR led to 10-20-times higher amount of total curcumin in the plasma than pure curcumin powder after oral administration (Kurita & Makino, 2013).

On the other hand, several nanosystems have been developed using zein as an excipient to enhance the bioavailability of lipophilic drugs such as simvastatin (Ahmed, Hosny, Al-Sawahli, & Fahmy, 2015) and folic acid (Peñalva, Esparza, González-Navarro, Quincoces, Peñuelas, & Irache, 2015).

Since several supplements are supplied as solid dosage form, nano-formulated compounds need to be dried, often resulting in irreversible aggregation and poor dispersion in the GI tract after administration. As a result, the unabated research on novel and improved approaches to increase its bioavailability continues, although several strategies for curcumin oral delivery have been successfully developed (D'Souza & Devarajan, 2016).

Nano-in-micro particles contain nanoparticles encapsulated within the microparticles, and thus combine two different properties in one system, which make them a good candidate for the sustained gastrointestinal release. Nanoparticles dried in a solid product with distinct size/shape and excellent flow properties can be beneficial in the development of a dosage form.

As demonstrated in the previous chapter, spray drying allows the production of a micron-sized product from dispersions of zein nanoparticles, thus establishing a link between the nanoplatform development and the traditional processes which can give materials on the microscale.

Herein we propose the nano-in-micro strategy, explored in chapter 2 for the oral delivery of iron bysglicinate, to produce zein-based micropowders loaded with CUR. The increase of CUR poor aqueous solubility and dissolution rate in biological fluids represents the main scope of this part of the work.

1.2 Materials and methods

1.2.1 Materials

Corn zein (Z F4400C non-GMO/food grade) was a kind gift of Flo Chemical Corporation (Ashburnham, MA, USA), KLEPTOSE® (Beta-cyclodextrin, CD) was purchased by Roquette Italia SpA (Alessandria, Italy). Curcumin (CUR) >94% (curcuminoid content) >80 % (Curcumin), sodium chloride, potassium phosphate monobasic, sodium phosphate dibasic, sodium chloride, sodium hydroxide, sodium carbonate, potassium phosphate monobasic, pepsin from porcine gastric mucosa, pancreas powder protease BRP, dimethyl sulfoxide (DMSO) were purchased from Sigma-Aldrich (Italy), hydrochloric acid was from Carlo Erba Reagents (Milan, Italy) and ethanol was from Honeywell (Seelze, Germany). All the other chemicals were of analytical reagent grade. Ultrapure water was used for all experiments.

1.2.2 Production of pseudolatexes

Pseudolatexes (PL) of zein/curcumin were formed by the anti-solvent co-precipitation method (Joye & McClements, 2013) adding 50 mL of a water solution to 50 mL of a solution of Z_CUR in ethanol/water 80% v/v at room temperature and under magnetic stirring. Zein concentration was fixed at 2 % w/v while different CUR amount (25, 50, 100 mg) were added. PL including CD (Zein/CD_CUR) was formed following the process reported above by adding 50 mL of a water solution of βCD (0.5 % w/v) to 50 mL of the hydroalcoholic solution of zein/curcumin.

1.2.3 Production of micropowders

Micrometric powders were obtained by spray-drying PL in a Büchi Mini Spray Dryer B-290 (BÜCHI Labortechnik AG, Flawil, Switzerland). Different process parameters were preliminary set to optimize the properties of the final micropowders (yield, adhesiveness, flow properties). Then the following operating conditions were maintained: (1) inlet drying temperature 150 ºC, (2) outlet drying temperature 75-80 ºC, (3) pump 10 % and (4) aspirator level 90 %. After the drying process, the powders were collected, sieved and stored at room temperature. The yield of spray-drying process was easily calculated from the weight of the collected micropowders.

1.2.4 Characterization of the micropowders

CUR loading in the micropowders was evaluated by placing 2 mg of spray-dried powders in 1 mL of dimethyl sulfoxide for 1 h under magnetic stirring. The spectrophotometric analysis of samples was carried out at λ=434 nm (UV-1800, Shimadzu) versus the calibration curve of CUR in DMSO obtained in the concentration range of 0.3- μg/mL (R^2> 0.99).

Scanning Electron Microscopy (SEM) was performed to evaluate the morphology of the powders (FEI Quanta 200 FEG apparatus equipped with an Oxford Inca Energy System 250 and an Inca-X-act LN2-free analytical silicon drift detector). Samples were coated with Au/Pd alloy. Micrographs were taken by using a beam intensity of 30 kV.

The bulk/tapped density of the sieved powders were evaluated before/after compaction according to the method 1 of the European Pharmacopoeia 9 ed. monograph 2.9.34 *Bulk density and tapped density of powders*. Accordingly, the flow properties of micropowders were estimated as Carr's Index.

NIR spectra were collected in reflectance mode with an FT near-infrared spectrometer (BÜCHI NIRFlex® N-500) over the range of 4000 – 10.000 cm^{-1} with 4 cm^{-1} resolution. The micropowders were analyzed in vials with 8 mm outer diameter. The results were reported as reflectance value.

1.2.5 Zein quantification in the micropowders

This method was carried out to assess the amount of zein in the raw material and spray-dried products. Zein raw material or micropowders (200 mg) were weighted using Kjeldahl weighting boats (nitrogen-free) and placed in Kjeldahl tubes (300 mL) adding three tablets of titanium-micro as catalyst and 10 mL of 98 % w/v H_2SO_4. All samples were digested in KjelDigester K-449 for 2 h at 420 °C (one digestion cycle). After digestion (samples were clear-green digestate), the samples were cooled to room temperature. Then the acidic digestion mixtures were diluted with distilled water (25 mL), and the samples tubes were transferred in the KjelMasterK-375 distillation unit (BÜCHI Labortechnik AG, Flawil, Switzerland). The digestion mixtures were alkalinized with NaOH 32 % w/v (45 mL) prior to distillation to free-up ammonia. Ammonia was steam-distilled into an acidic receiver solution of H_3BO_3 4 % *w/v* with Sher indicator (60 mL). The nitrogen content was determined by the titration of the borate complex with H_2SO_4 0.1 M according to Equation (1):

$$\% N = [V(\mathrm{l}) - V(\mathrm{Bl})] \times F \times c \times f \times \frac{M(\mathrm{N})}{m \times 1000} \times 100 \qquad (2)$$

where % *N* is the % of weight of *N*, *V*(l) is the consumption of titrant, sample (mL), *V*(Bl) is the average consumption of titrant, blank (mL), *F* is the molar reaction factor (1 = HCI, 2 = H_2SO_4), *c* is the concentration of titrant (0.1 mol/L), *f* is the factor of titrant (1), *M*(N) is the molecular weight of N (14,007 (g/mol)), and *m* is the sample weight (g).

A protein factor (PF) of 6.25 was used to calculate the protein content (% P).

1.2.6 Release of CUR from the micropowders

The release properties of micropowders loaded with CUR were tested in simulated oral fluids. Twenty mg of each micropowder were placed in 20 mL of simulated gastric fluid (SGF, composed by 2 g NaCl, 80 mL of 1 M HCl, 3.2 g pepsin powder from porcine gastric mucosa in 1 L of water) under stirring at 37 °C. Samples were taken at different time points (time 0, 30, 60, 90, 120 minutes), centrifuged at 16300 x *g* for 15 min and analyzed at λ=434. After 2 h the SGF was removed and 20 mL of simulated intestinal fluid (SIF, composed by 77 mL of 0.2 M NaOH, 6.8 g KH_2PO_4 and 10 g of pancreas powder in 1 L of water) were added. Samples were taken at different time points (1, 2, 3, 4, 5, 6, 7 h), centrifuged at 16300 x*g* for 15 min and analyzed at λ=434 nm. The same protocol was used to assess the release of free CUR.

1.2.7 Micropowders oral administration in mice

Male adult CD1 mice (28-30 g) were purchased from Charles River Laboratories (Calco, Lecco, Italy) and maintained in the animal care facility at the University of Naples in polycarbonate cages under controlled temperature (23 ± 2°C), constant humidity (60%) and with a 12-h light, 12-h dark cycle. The animals were acclimatized to their environment at least one week under standard conditions, with free access to tap water and standard rodent diet.

Animals were fasted for 24 h to have the gastrointestinal tract completely free; subsequently, CUR (raw material) or a CUR-loaded micropowder suspended in sesame oil, were administered by oral gavage (250 µL/mice) at the dose of 100 mg/kg of CUR using a stainless-steel feeding needle. Only vehicle (sesame oil) was given to control mice.

After 45 minutes, animals were euthanized by asphyxiation with CO_2, and the mice abdomen was opened by a midline incision, blood collected by heart puncture and the gastrointestinal tract removed, isolated from surrounding tissues, length measured, divided in

12 sections (Table 1), rinsed with 1 ml of physiological solution (NaCl 0.9% w/v) and then processed.

Table 1. Portion of the G.I. tract recovered after animal sacrifice.

Portion of the G.I. tract	Divided in
Stomach	1 piece
Small intestine	8 pieces
Ileocecal valve	1 piece
Colon	2 pieces

Each portion of the gastrointestinal tract was observed under a fluorescence microscope (Leica DMRB) with an excitation of 480 nm, emission of 535 nm and 10X magnification to detect CUR present in different regions of the digestive tract. All the tissues were next immediately frozen at -80°C for further analysis.

The blood samples were immediately put in ice and stored at 4°C for 2 h. Then, blood serum was obtained by centrifugation for 10 minutes at 4000 x*g* at 4°C. The resulting supernatant was transferred to a new tube and stored at -80°C. CUR detection in the serum was performed by plating 50 µL of each sample in a 96 well black microplate and reading the fluorescence in a GloMax® Microplate Reader (Promega) at 480 nm excitation and 500-550 nm emission.

1.3 Results

1.3.1 Production of pseudolatexes and corresponding curcumin micropowders

CUR-powders were produced according to a nano-in-micro strategy, which consists 1) forming a stable colloidal dispersion (referred to as pseudolatex) through an anti-solvent precipitation method (1st step) and 2) drying the pseudolatex by spray-drying to achieve a solid (2nd step) (Esposito, Dal Poggetto, Demont, Kraut, Miro, Ungaro, et al., 2020). Experimental conditions were set to obtain pseudolatexes (PL) with size compatible with nebulization process and showing colloidal stability during drying step.

In the first step, CUR was entrapped in the PL after dissolution in the hydroalcoholic zein solution and matrix desolvation after the addition of water as anti-solvent. An in-depth formulation study was carried out at different CUR loading taking into consideration the maximum loading capacity of the PL to avoid particle aggregation phenomena. PL loaded with 25, 50, 100 mg of CUR were produced and the corresponding micropowders collected after spray-drying process (MP_Z_CUR25, MP_Z_CUR50, MP_Z_CUR100).

Moreover, in our previous publication (Esposito, et al., 2020), we have highlighted by different analytical technique that CD could interact with zein modifying its chemical features, processability and ability to incorporate bioactive molecules. Thus, we introduced again CD as useful excipient in formulation process to improve the properties of zein-based micropowders and to control the release of their cargo. In particular, the micropowder loaded with 50 mg of CUR was produced adding CD during the formulation process of the pseudolatex (MP_Z/CD_CUR50). All PL produced and powder compositions were reported in Table 2.

Table 2. Code and corresponding composition of CUR micropowders prepared from different pseudolatex.

	Pseudolatex preparation				Powder composition		
Powder codes	**Zein % w/v [a]**	**CD % w/v [a]**	**CUR % w/v [a]**	**Antisolvent/ solvent ratio**	**Zein % w/w [b]**	**CD % w/w [b]**	**CUR % w/w [b]**
MP_Z_CUR25	2	-	0.050	1	1	-	0.025
MP_ Z_CUR50	2	-	0.100	1	1	-	0.050
MP_ Z_CUR100	2	-	0.200	1	1	-	0.100
MP_ Z/CD_CUR50	2	0.5	0.100	1	1	0.250	0.050

[a] % w/v components in the PL produced to obtain the correspondent MP, [b]% w/w components in the MP.

In the second step, suitable operation conditions for spray-drying process were set up considering that the modulation of T inlet was found crucial to reduce the humidity of the drying gas increasing the powder yield. Remarkably, the inlet was maintained at 150 °C which gave a T outlet value in the range 75-80 °C that it is below zein Tg=129 °C (Notario-Pérez, Martín-Illana, Cazorla-Luna, Ruiz-Caro, Peña, & Veiga, 2018) thus avoiding the formation of a sticky product. In these operating conditions, the drying process gave a solid with yields always above 70% (as reported in Table 3) which is notably high considering the usual yield of this drying method.

Table 3. Set-up of spray drying to obtain CUR micropowders.

Batch	Aspirator flow rate (%)	Pump Speed (%)	T inlet (° C)	T outlet (° C) [a]	Yield (%)	Theoretical loading CUR (mg CUR/ 100 mg NPs	Actual loading CUR (mg CUR/ 100 mg NPs)
MP_Z_CUR25	90	10	150	81	72	2.5	2.4±0.1
MP_Z_CUR50	90	10	150	75	84	5.0	4.4±0.2
MP_Z_CUR100	90	10	150	80	78	10	8.4±1.0
MP_Z/CD_CUR50	90	10	150	83	79	4.9	4.6±0.2

[a] T outlet is consequent to setting the other parameters

1.3.2 Characterization of micropowders

The micropowders produced were fully characterized in term of actual loading of CUR, morphology and flow properties. As reported in Table 3, CUR loading inside the micropowders was almost complete. These results highlight the capacity of this platform to entrap efficiently a lipophilic compound possibly by accommodating it in the hydrophobic pockets of the protein.

SEM images (Fig. 1) show that a population of particles spanning in a pretty wide size range and with irregular shape were obtained.

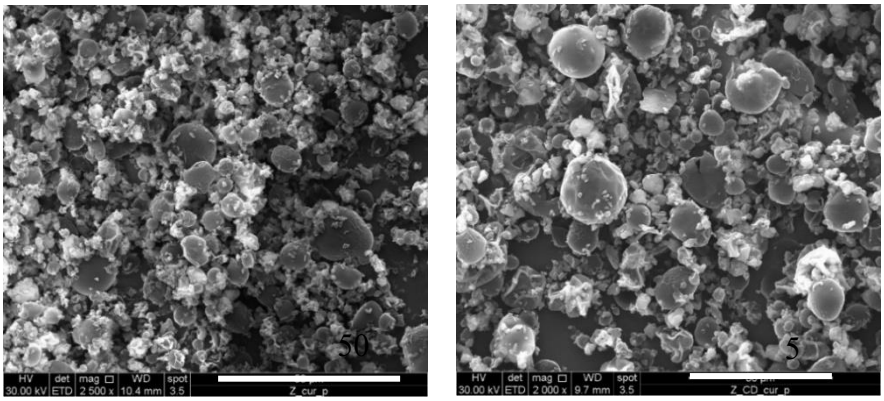

Fig. 1. SEM images of MP_Z_CUR50(A) and MP_Z/CD_CUR50(B). The scale bar correspond to 50 μm.

The Carr's Index calculated from bulk/tapped density (Table 4) underlined that the MP_Z/CD_CUR50 prepared with CD flowed better than other powders confirming that CD is a helpful excipient in controlling the solid-state properties of particles.

Table 4. Flow properties of CUR micropowders.

Batch	Bulk Density (g/ml)	Tapped Density (g/ml)	Carr's Index (%)
MP_Z_CUR25	0.30±0.03	0.34±0.03	37±11
MP_Z_CUR50	0.18±0.02	0.20±0.02	37±6.0
MP_Z_CUR100	0.16±0.02	0.18±0.02	38±8.0
MP_Z/CD_CUR50	0.17±0.01	0.19±0.01	30±6.0

The produced powders were explored also by NIR to confirm zein/CD interactions. As evidenced in Fig. 2, a different shift in the spectral bands was found in presence of CD in the sample. In particular, the OH/NH stretch region (Fig. 2B), was changed depending on the presence of CD in the powder.

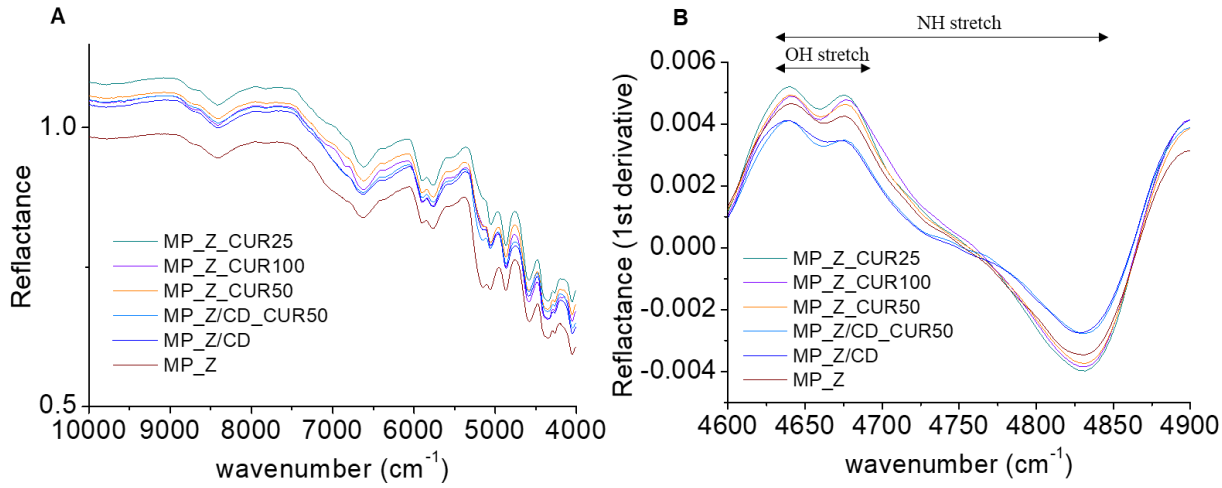

Fig. 2. NIR spectra of CUR micropowders reported as reflactance (A) and first derivative in the interval 4600-4900 cm^{-1} (B).

1.3.3 Zein quantification in the micropowders

To check that the amount of zein was maintained throughout the entire drying process, that is to compare theoretical zein employed initially to prepare pseudolatexes and that found in the final micropowders, nitrogen content in the micropowder was assessed through Kjeldahl.

The % N in zein in raw material was 13.82% in line with the values reported in its technical data sheet (13-16%). This value corresponded to a measured % protein of 86.39 calculated on a dry basis (82-100% in the datasheet). As reported in Table 5, % N and % Protein in the micropowder made with zein/CUR were close to that of raw zein, demonstrating that the method can be applied to quantify the protein amount also after spray-drying. For micropowders of zein/CD_CUR, the theoretical protein content of zein was lower due to the presence of CD.

Table 5. Nitrogen and protein content of zein micropowders.

Batch	% N (±SD)	% Protein (±SD)
MP_ Z_CUR25	13.91±0.04	86.78±0.26
MP_ Z_CUR50	13.60±0.07	84.99±0.46
MP _Z_CUR100	13.23±0.01	82.69±0.08
MP_Z/CD_CUR50	11.28±0.03	70.50±0.22

1.3.4 Release of curcumin from micropowders

The release of CUR loaded from MP_ Z_CUR50 and MP_ Z/CD_CUR50 was performed in continuous in simulated gastric fluid (SGF) pH 1.2 and then in simulated intestinal fluid (SIF) pH 6.8 both supplemented with enzymes. As shown in Fig. 3, the micropowders loaded with CUR released an amount of the bioactive compound below 30% after 2 h in SGF. The amount of CUR released in SGF from CD-containing micropowders was higher as compared to the CUR control and micropowder without CD demonstrating that CUR dissolution rate was enhanced by entrapment in zein/CD particles. When the medium was changed to SIF, CUR release occurred at a sustained and constant rate and was improved by the presence of CD in the powder reaching 100% in 8 h.

Similar results were obtained with zein spray-dried powders loaded with a very hydrophilic molecule like FeBIS reported in chapter 2. The mechanism of release was closely related to water uptake of micropowders which activates CUR solubilisation in the matrix. An increase

of the surface area due to formation of small micron-sized particles coupled with amorphization of crystalline CUR could contribute to faster release from zein-based powders.

A combination of Fickian diffusion and erosion of the matrix coupled with prompt dissolution of CUR in the matrix can be hypothesized in this case. Amorphisation of CUR in zein matrix needs will be investigated soon by X-ray and DSC in forthcoming studies.

The positive results obtained testing the MP_Z/CD_CUR50 in simulated gastrointestinal conditions underlines again the importance to introduce CD in the formulation development.

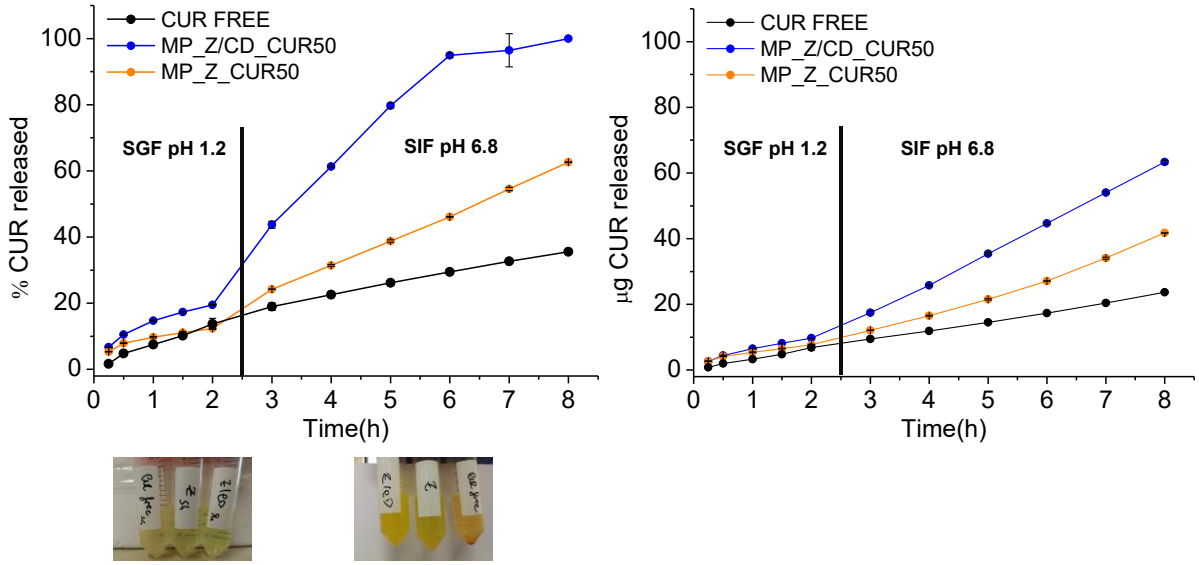

Fig. 3. Release of CUR from micropowders in simulated gastric fluid (SGF) added with pepsin (pH 1.2) and then in simulated intestinal fluid (SIF) added with pancreatin (pH 6.8). CUR sieved powder is reported as control. Data are the mean of three separate experiments ± SD.

These data confirm that zein/CD-based powders are a versatile platform to deliver both hydrophilic (FeBIS as reported in chapter 2) and lipophilic (CUR as reported in this chapter) compounds.

1.3.5 Oral administration of micropowders in mice

In a very preliminary experiment, we aimed at understanding if the distribution of CUR in the gastrointestinal tract of mice could be changed by micropowders.

To this purpose, free CUR and MP_Z/CD_CUR50 were administered by oral gavage and after 45 min the gastrointestinal tract was removed, isolated, divided in 12 sections (Table 1) and rinsed with physiological solution to remove the excess of CUR in the lumen. The pieces were then analyzed by fluorescence microscopy.

As shown in Fig. 4, MP_Z/CD_CUR50 is remarkably concentrated in the small intestine (Fig. 4 D, E, F) while it is scarcely localized at the end of gastrointestinal tract including the portions of the ileocecal valve (Fig. 4 L) and colon (Fig. 4 M, N).

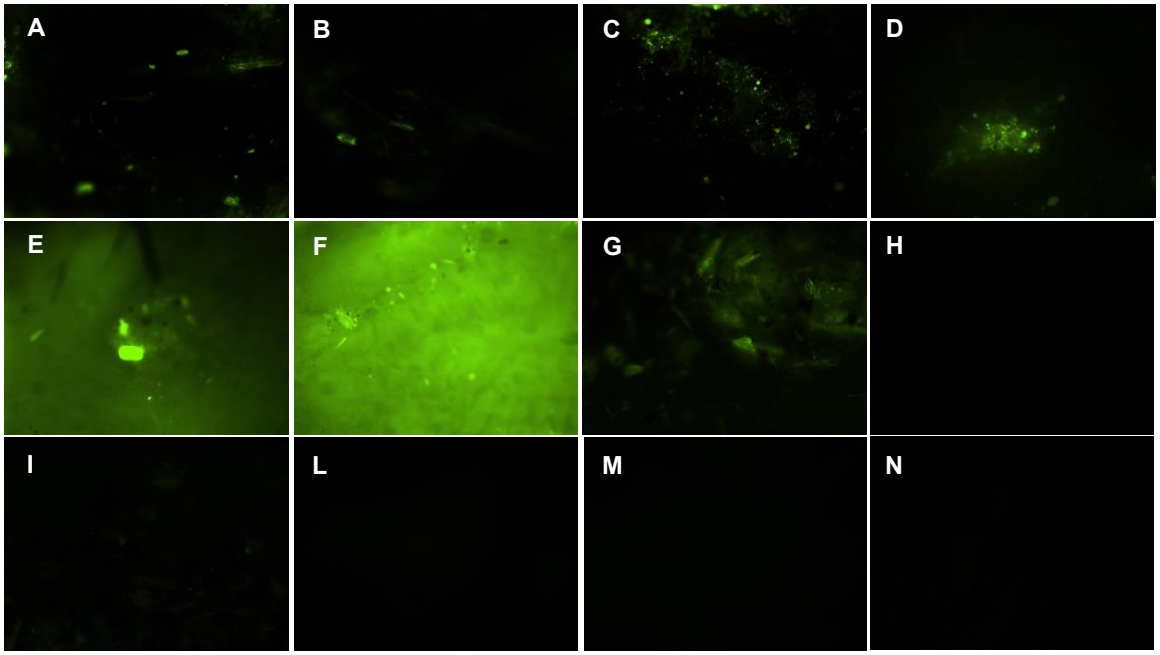

Fig. 4. Distribution of CUR (100 mg/kg) in the gastrointestinal tissues recovered from mice after 45 min from the oral administration of MP_Z/CD_CUR50. Gastrointestinal tract was divided in stomach (A), small intestine (B-I), ileocecal valve (L) and colon (M-N). This is a representative image of two animals.

The CUR control was instead mainly present in the upper part of the GI tract (mainly B-D sections, data not shown).

After 45 minutes from the oral gavage, blood collected by heart puncture was analyzed by fluorescence to get a rough idea of the overall CUR and eventual metabolites passed through the gastrointestinal barriers and absorbed in the bloodstream. The blood recovered was centrifuged and the resulting supernatant analyzed to compare the behavior of CUR dispersed directly in the vehicle and that encapsulated in MP_Z/CD_CUR$_{50}$. As visible from Fig. 5, when CUR is loaded in zein/cyclodextrin powder a fluorescence value higher than that of free CUR is obtained. These preliminary results suggest that the zein/CD micropowders could promote CUR absorption overcoming the issues related to its oral administration.

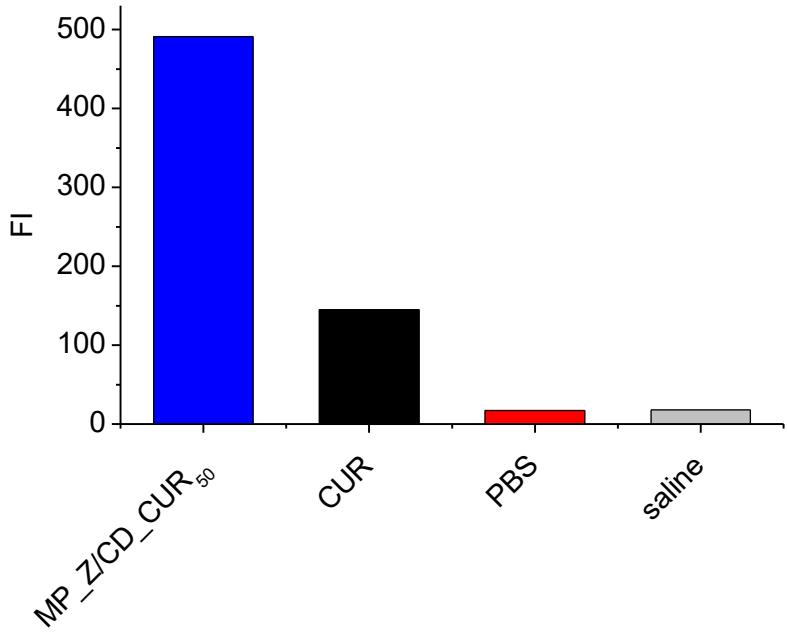

Fig. 5. Fluorescence intensity of supernatant recovered after the centrifugation of blood samples collected at 45 min from mice treated with CUR in solution and with the MP_Z/CD_CUR50 (100 mg/kg).

Nevertheless, these experimental evidences need to be confirmed through analytical methodologies such as high-performance liquid chromatography (HPLC) that can allow quantification of the amount of CUR and its metabolites in the tissues and can confirm the qualitative results collected by fluorescence microscopy.

1.4 Conclusions

Herein, zein/beta-cyclodextrin powders for the oral delivery of curcumin were developed in view of a possible application in food supplement field. CUR was entrapped through a nano-in-micro strategy comprising formation of a CUR-loaded pseudolatex that is then spray-dried. Micron-sized CUR-loaded powders are produced with a high yield of production and high loading efficiency. CD partially interacts with zein changing the overall organization of protein chains and ameliorating the flow properties of the spay-dried products. CUR-loaded micropowders with CD allow a full control of the release kinetics of the bioactive molecules providing its complete dissolution in a time-window typical for absorption in humans.

After oral administration in mice, preliminary results highlight that zein/CD micropowder has the potential to allow a CUR absorption in the bloodstream higher as compared with free CUR.

In perspective, the micropowders developed here could represent a novel option to formulate CUR in a high-bioavailability nutraceutical product.

References

Ahmed, O. A. A., Hosny, K. M., Al-Sawahli, M. M., & Fahmy, U. A. (2015). Optimization of caseinate-coated simvastatin-zein nanoparticles: improved bioavailability and modified release characteristics. *Drug design, development and therapy, 9*, 655-662.

D'Souza, A. A., & Devarajan, P. V. (2016). Bioenhanced oral curcumin nanoparticles: Role of carbohydrates. *Carbohydrate Polymers, 136*, 1251-1258.

Đorđević, V., Belščak-Cvitanović, A., Drvenica, I., Komes, D., Nedović, V., & Bugarski, B. (2017). 3 - Nanoscale nutrient delivery systems. In A. M. Grumezescu (Ed.), *Nutrient Delivery*, (pp. 87-139): Academic Press.

Esposito, D., Dal Poggetto, G., Demont, A., Kraut, N., Miro, A., Ungaro, F., Laurienzo, P., & Quaglia, F. (2020). Zein Beta-Cyclodextrin Micropowders for Iron Bisglycinate Delivery. *Pharmaceutics, 12*(1), 60.

Giri, T. K. (2016). 15 - Bioavailability enhancement of curcumin nutraceutical through nano-delivery systems. In A. M. Grumezescu (Ed.), *Nutraceuticals*, (pp. 593-625): Academic Press.

Joye, I., & McClements, D. (2013). Production of nanoparticles by anti-solvent precipitation for use in food systems. *Trends in Food Science & Technology, 34*.

Kurita, t., & Makino, Y. (2013). Novel Curcumin Oral Delivery Systems. *Anticancer research, 33*(7), 2807-2821.

Ma, Z., Wang, N., He, H., & Tang, X. (2019). Pharmaceutical strategies of improving oral systemic bioavailability of curcumin for clinical application. *Journal of Controlled Release, 316*, 359-380.

Notario-Pérez, F., Martín-Illana, A., Cazorla-Luna, R., Ruiz-Caro, R., Peña, J., & Veiga, M.-D. (2018). Improvement of Tenofovir vaginal release from hydrophilic matrices through

drug granulation with hydrophobic polymers. *European Journal of Pharmaceutical Sciences, 117*, 204-215.

Ouyang, H.-Z., Fang, L., Zhu, L., Zhang, L., Ren, X.-L., He, J., & Qi, A.-D. (2012). Effect of external factors on the curcumin/2-hydroxypropyl-β-cyclodextrin: in vitro and in vivo study. *Journal of Inclusion Phenomena and Macrocyclic Chemistry, 73*(1), 423-433.

Peñalva, R., Esparza, I., González-Navarro, C. J., Quincoces, G., Peñuelas, I., & Irache, J. M. (2015). Zein nanoparticles for oral folic acid delivery. *Journal of Drug Delivery Science and Technology, 30*, 450-457.

Siviero, A. (2015). Curcumin, a golden spice with a low bioavailability. *Journal of herbal medicine, v. 5*(no. 2), pp. 57-70-2015 v.2015 no.2012.

Section 3B

Bioadhesive zein beta-cyclodextrin nanoparticles for the buccal delivery of curcumin

1.1 Introduction

In the last years, the design of buccal formulations represented a considerable challenge in the drug delivery field. The buccal administration has been explored for decades as a site for drug absorption to attain systemic circulation in alternative to the conventional oral or intravenous routes (Morales & Brayden, 2017). The ability of the medication to achieve a more rapid onset of action overcoming the liver first-pass metabolism and avoiding gastrointestinal degradation (Song, Banov, Bassani, & Valdez, 2017), make the buccal mucosa an ideal target for the development of innovative micro/nano-systems. Although the drug absorption is enhanced by the high buccal vascularization and permeability, the residence time of the formulations is simultaneously influenced by saliva secretion, tongue movements, food intake and the problematic interaction between drug and the small surface area that constitute significant limits that may be surpassed (Salamat-Miller, Chittchang, & Johnston, 2005). Since mucoadhesion can be reached when bioadhesive materials come in close contact with mucosa and form interfacial bonds (Walicova, Gajdziok, Pavlokova, & Vetchy, 2017), the biological properties of the polymers employed in the design of novel drug delivery systems represent a crucial point to increase the drug efficacy (Song, Banov, Bassani, & Valdez, 2017) and to promote and prolong its buccal permanence.

Recently, the use of bioadhesive colloidal carriers has been considered an opportunity to modify the release and absorption of drugs, to exert protection against degradation and possibly administer hydrophobic drugs as an aqueous dispersion (Mazzarino, Borsali, & Lemos-Senna, 2014).

The mucoadhesive properties are positively influenced by different factors like the charge of the polymer and its molecular weight, the flexibility of the polymer chains and the capacity to form hydrogen bonds (Shtenberg, Goldfeder, Prinz, Shainsky, Ghantous, Abu El-Naaj, et al., 2018). Mucin is a glycoprotein that forms electrostatic, hydrogen, and hydrophobic interactions with different materials, and as far as mucin interactions happen, it has been routinely used to achieve bioadhesion (Bansil & Turner, 2006). Cationic polymers are involved in a non-covalent electrostatic interaction with anionic groups of mucins via polymeric chain entanglement (Morales & Brayden, 2017).

In this regard, the advantages of choosing natural biopolymers as carriers include the long history of their use as biocompatible and biodegradable excipients and their sensory attributes (Alqahtani, Islam, Podaralla, Kaushik, Reineke, Woyengo, et al., 2017). For instance, nanoparticles coated with the polysaccharide chitosan are widely employed for mucoadhesive

applications mainly because of its ability to interact with the negatively charged mucosal surface reorganizing the tight junctions between mucosal cells (Bernkop-Schnürch & Dünnhaupt, 2012).

Natural protein polymers play an essential role in designing novel mucoadhesive systems which can cargo either hydrophilic or lipophilic compounds and their chemical and structural diversity can be used to reach unique functional features (Wan, Guo, & Yang, 2015).

Recently, whey proteins were studied for their ability to interact with the epithelial membranes even if they are already used in a marketed formulation of buccal mucoadhesive tablets treating oral candidiasis (Loramyc®) (Lalla & Bensadoun, 2011). Since proteins can be employed to improve the residence time at the absorption site, bioadhesive cross-linked whey protein microparticles were found to interact *ex vivo* with rat intestine (Hsein, Garrait, Beyssac, & Hoffart, 2015). This property has been exploited to prepare bioadhesive food protein nanoparticles for pediatric oral drug delivery applications, formed by a hydrophilic shell of whey protein on a lipophilic core of zein (Islam, Reineke, Kaushik, Woyengo, Baride, Alqahtani, et al., 2019).

As mentioned in the general introduction to this chapter, Curcumin (CUR) has low water solubility, chemical instability, and poor oral bioavailability (Laffleur, Schmelzle, Ganner, & Vanicek, 2017). Once absorbed, it is subjected to extensive first-pass metabolism, mainly in the liver and intestinal mucosa, giving glucuronide and sulphate derivatives (Garcea, Jones, Singh, Dennison, Farmer, Sharma, et al., 2004). Therefore, CUR can be an excellent candidate for a buccal formulation (Hazzah, Farid, Nasra, El-Massik, & Abdallah, 2015; Mazzarino, Borsali, & Lemos-Senna, 2014).

Given that there are some benefits of antioxidants encapsulated in a zein-polysaccharide matrix (Purpura, Lowery, Wilson, Mannan, Munch, & Razmovski-Naumovski, 2018; Sun, Xu, Mao, Wang, Yang, & Gao, 2017; Tapia-Hernandez, Rodriguez-Felix, Juarez-Onofre, Ruiz-Cruz, Robles-Garcia, Borboa-Flores, et al., 2018), casein-covered zein nanoparticles (NPs) for CUR oral delivery have been developed and demonstrated to interact with both a mucus layer by an *in vitro* wash-off method and on Caco-2 cells (A. Patel, Hu, Tiwari, & Velikov, 2010). On the other hand CUR can form "host-guest inclusion complex" with the hydrophobic cavity of cyclodextrins increasing its solubility (Li, Uehara, Sawangrat, Morishita, Kusamori, Katsumi, et al., 2018; Rachmawati, Edityaningrum, & Mauludin, 2013). The combination between zein and β-cyclodextrin (CD) may represent a valid strategy to produce mucoadhesive NPs for buccal delivery.

Thus, zein/CD NPs become attractive not only as a tool to ameliorate CUR water solubility, chemical stability but also to prolong their residence time via mucin interactions.

1.2 Materials and methods

1.2.1 Materials

Corn zein (Z) (F4400C non-GMO/food grade) was a kind gift of Flo Chemical Corporation (Ashburnham, MA, USA). KLEPTOSE®/Beta-Cyclodextrin (CD) was purchased by Roquette Italia SpA (Alessandria, Italy). Curcumin (CUR) >94% (curcuminoid content) >80 % (Curcumin), sodium chloride, potassium phosphate monobasic, sodium phosphate dibasic, mucin from porcine mucosa were purchased by Sigma-Aldrich (Italy). Ethanol was purchased by Honeywell (Seelze, Germany). All the other chemicals were of analytical reagent grade. Ultrapure water was used for all experiments.

1.2.2 Production of CUR-loaded NPs

A colloidal dispersion (Z/CD) was formed by the anti-solvent co-precipitation method adding 50 mL of a water solution of CD (0.1% w/v) to 10 mL of a solution of zein (2% w/v) in ethanol/water 80% v/v at room temperature under magnetic stirring. 20 mg (Z/CD_CUR_{20}), 10 mg (Z/CD_CUR_{10}), and 5 mg (Z/CD_CUR_5) of CUR were dissolved in the hydroalcoholic solution with zein. Ethanol was eliminated from the formulations under vacuum (Rotavapor R-100 Büchi Labortechnik AG, Flawil Switzerland). Then NPs were purified by centrifugation (21700 *xg* for 30 min), collected and stored at 4°C. NPs loaded with CUR in the absence of CD (Z_CUR_{20}, Z_CUR_{10}, Z_CUR_5) were prepared too.

1.2.3 Characterization of CUR-loaded NPs

The hydrodynamic diameter (D_H), polydispersity index (PI), and zeta potential (ζ) of NPs were assessed on a Zetasizer Nano ZS (Malvern Instruments Ltd.). Results are reported as the mean of three separate measurements of three different batches (n=9) ± standard deviation (SD).

CUR loading inside NPs was evaluated by placing 2 mg of freeze-dried NPs in 1 mL of ethanol under magnetic stirring for 1 h. The spectrophotometric analysis of samples was carried out at λ=424 nm (UV-1800, Shimadzu) versus the calibration curve of CUR in ethanol plotted in a concentration range of 0.3–5 μg/mL (R^2> 0.99).

The stability of the formulations loaded with different amounts of CUR was evaluated for four weeks at room temperature monitoring the same parameters reported above on a Zetasizer

Nano ZS (Malvern Instruments Ltd.). Results are reported as the mean of three separate measurements of three different batches (n=9) ± standard deviation (SD).

The interaction between Zein and CD in Z/CD_CUR$_{10}$ was evaluated at λ_{EX}= 278 nm (zein aminoacids emission and collecting the emission spectra in the range of 290-450 nm (RF-6000, Shimadzu). Fluorescence spectra of CUR and CUR-loaded NPs were also collected at λ_{EX}= 424 nm (CUR excitation) and setting an emission range of 450-650 nm. The NPs concentration was 0.3 mg/mL.

FEI Tecnai G12 Spirit-Twin apparatus was used for Transmission Electron Microscopy (TEM) analysis to investigate the morphology of NPs Z_CUR$_{10}$ and Z/CD_CUR$_{10}$.

The amount of CUR released from NPs was evaluated, introducing 0.5 mL of NPs Z_CUR$_{10}$ and Z/CD_CUR$_{10}$ in a dialysis bag (MWCO 3.5-5 KDa) immersed in 5 mL of Tween 80 5 % w/v at 37 ° C under magnetic stirring. At predeterminate times, 1 mL of medium was withdrawn, replaced with fresh medium, and analyzed at λ 424 nm.

Free CUR was nanoprecipitated following the same protocol used for the preparation of the NPs as reference.

1.2.4 CUR delivery by medical device

As prepared, CUR-loaded NPs (10 mL) were placed in a spray device (Classic line equipped with SL pump, Aptar Pharma, France) and sprayed in Teflon dishes (three sprays). The liquid was recovered with 2 mL of water, and the samples were freeze-dried. The powders collected were treated with 2 mL of ethanol and analyzed at λ=424 nm to quantify CUR, as reported above.

1.2.5 Interaction of NPs with porcine mucin

The mucoadhesive properties of NPs in the presence of the mucin were tested by an UV-turbidimetric assay (Sunoqrot, Hasan, Alsadi, Hamed, & Tarawneh, 2017). Mucin dispersions (0.08 % w/v) in water or phosphate buffer saline pH=7.4 (PBS composed by 3.5 g NaCl, 0.1091 g KCl, 0.891 g Na_2HPO_4 in 500 mL H_20) were prepared by overnight magnetic stirring. Then the mucin dispersion was centrifuged at 3500 *xg* for 20 min (Microfuge 20, Beckman), and the supernatant was recovered. CUR-loaded NPs were added to the mucin dispersion (final concentration 0.3 mg/mL) and analyzed by UV at λ=600 nm to measure scattering. Emission spectra of the samples at λ_{EX}=278 nm (protein excitation) were collected in the emission range 280-450 nm.

1.2.6 Mucoadhesion of CUR NPs on the porcine buccal mucosa

The mucoadhesion of CUR-loaded NPs on porcine buccal mucosa was assessed by spraying NPs dispersion in water (2 sprays) on porcine buccal mucosa. After 40 min, one set of mucosa samples was washed with a solution of NaCl 0.9 % w/v for 15 min to evaluate the attachment of NPs on the tissue. Both samples were analyzed by confocal microscopy.

1.3 Results and discussion

1.3.1 Characterization of CUR-loaded NPs

NPs were characterized for hydrodynamic diameter (D_H) polydispersity index (PI) and zeta potential (ζ), as reported in table 1. All NPs show a hydrodynamic diameter (D_H) below 140 nm and a low polydispersity index (PI). As reported in Fig. 1 (A, B), the narrow peaks in size distribution curves of NPs Z_CUR$_{10}$ and Z/CD_CUR$_{10}$ demonstrate that the colloidal dispersions produced are homogeneous in terms of particle diameter without any evident sign of aggregation. The surface charge was positive for all the formulations due to the ability of zein to expose positive amino acids when processed through nanoprecipitation. Remarkably, no significant influence of CD on the surface charge of NPs was found, also when different CUR loadings were tested.

The actual loading of CUR inside NPs was almost complete. As visible in table 1, the encapsulation efficiency for both Z and Z/CD was remarkably high and close to the theoretical loading of CUR inside the NPs. This result confirmed the high capacity of zein NPs to deliver hydrophobic bioactive compounds and the possibility of polyphenols to interact with protein chains (A. Patel, Hu, Tiwari, & Velikov, 2010). Nevertheless, the solubility of CUR in water (which is reported in the range 3.14 - 18.12 μg mL^{-1}) increases at 400 μg mL^{-1} with formulations prepared at the highest CUR theoretical loading.

Table 1. Characterization of NPs.

Batch	D_H [a] (nm ± SD)	PI [a] (± SD)	ζ [a] (mV± SD)	Actual loading mg CUR/100 mg NPs [b] (mg± SD)	Loading efficiency (theoretical loading) (%) [c]
Z/CD_CUR$_5$	137±6	0.1±0.1	+44±7	2.0±0.3	100 (2.0)
Z_CUR$_5$	124±11	0.2±0.1	+48±3	2.2±0.1	92 (2.4)
Z/CD_CUR$_{10}$	127±1	0.1±0.1	+53±8	3.8±0.4	100 (3.8)
Z_CUR$_{10}$	118±7	0.1±0.1	+47±4	4.6±0.1	98 (4.7)
Z/CD_CUR$_{20}$	119±8	0.1±0.1	+60±6	7.4±1.0	100 (7.4)
Z/CUR$_{20}$	113±2	0.1±0.1	+47±1	8.5±1.0	93 (9.1)

[a] Evaluated by Zetasizer Nano ZS, [b] mg of CUR per 100 mg of NPs. [c] Theoretical loading is expressed as the amount of CUR/amount of CUR+zein+CD %.

The morphology of Z_CUR10 and Z/CD_CUR10 was investigated by Transmission Electron Microscopy showed that NPs had a spherical shape with a matrix core and were not aggregated (Fig 1C and 1D). At a closer examination, NPs embedding CD (Fig 1D) seemed denser than those made only of zein probably due to the formation of a matrix where CD was not uniformly dispersed.

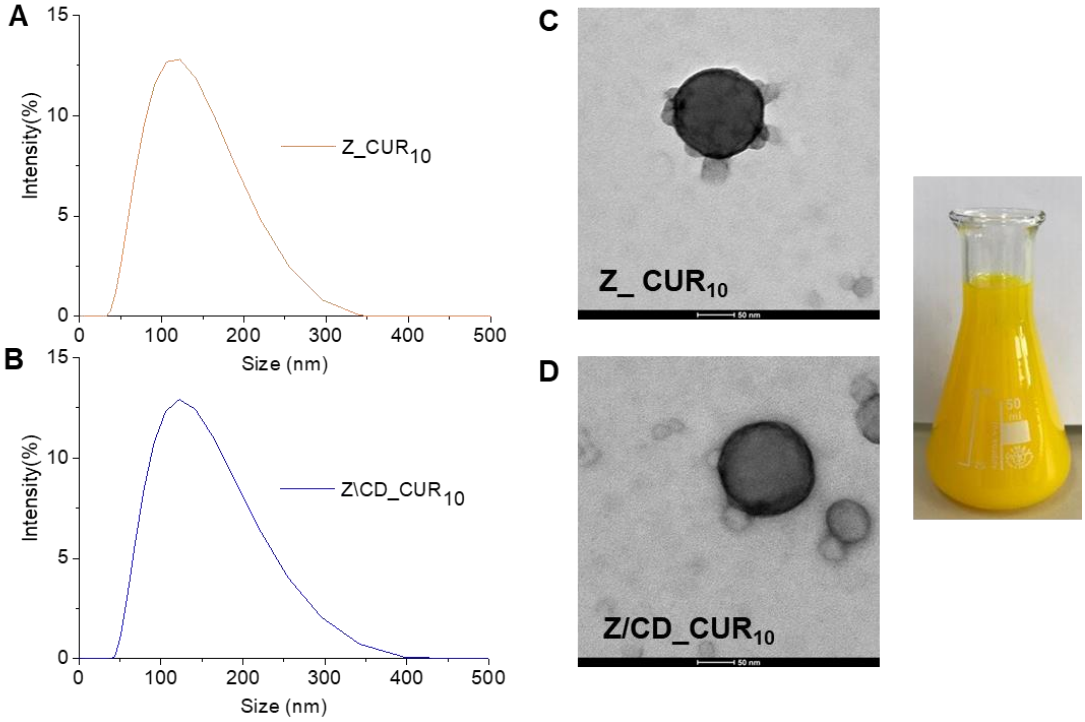

Fig. 1. Size distribution curves and TEM images of NPs Z_CUR10 (A, B) and Z/CD_CUR10 (C, D).

The stability of NPs was monitored at room temperature in the dark for four weeks. As shown in Fig. 2, no significant variation of NPs mean diameter was found in the time window of the experiment. In some cases, some aggregates were found at the bottom of the testing tube, but they could be rapidly redispersed under energic shaking. This behavior was independent of CUR presence and its theoretical loading. The PI of NPs remained constant even if it showed a slight tendency to increase in time as compared with the freshly prepared formulations. The surface charge remained positive and unaltered. The results were also reported in terms of Intensity (%) using the cumulative distribution curves of the NPs exported from Zetasizer Nano ZS (Supplementary material, Fig. S1). As visible in Fig. S1 C and D, NPs Z_CUR_{10}, and Z/CD_CUR_{10} showed a narrow peak of the cumulative distribution curves without evidence of aggregation.

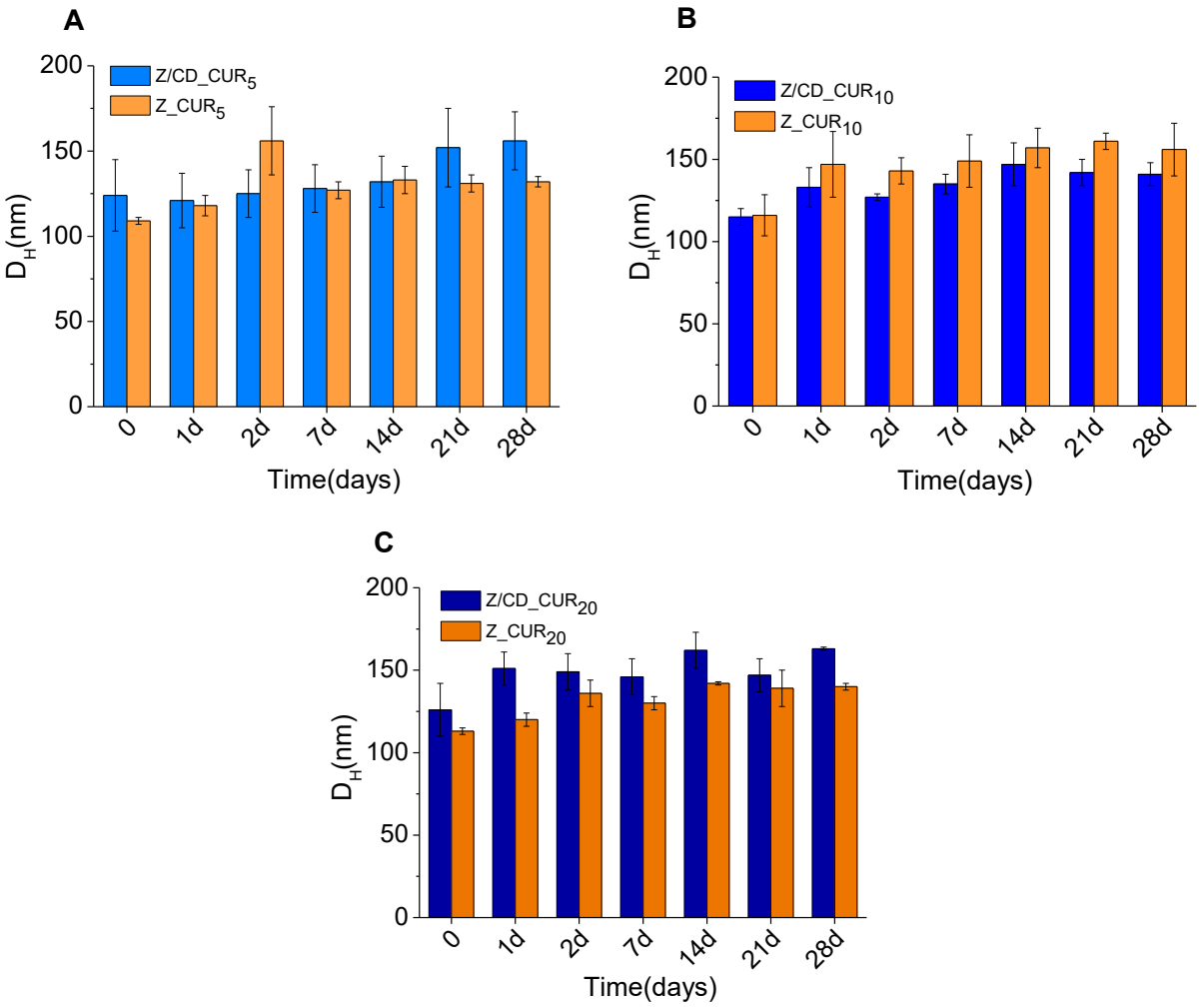

Fig. 2. Size of CUR-loaded NPs stored in the dark at room temperature.

The CUR dose delivered by an oral spray is reported in Fig. 3. The CUR delivered increased proportionally as the amount of CUR loaded in NPs did. The amount of CUR delivered was independent of the presence of CD in the formulations.

Nevertheless, the deliverability of NPs Z_CUR$_{20}$ and Z/CD_CUR$_{20}$ was worse than other formulations, so we selected the NPs loaded with 10 mg of CUR for further studies as the model formulation of this work.

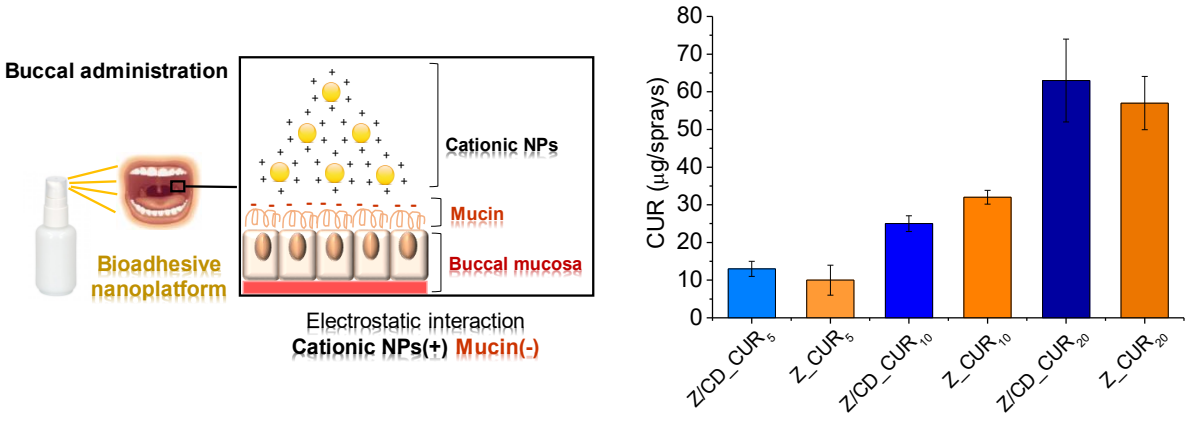

Fig. 3. The dose of CUR delivered by a spray device containing NPs with increasing CUR loading.

The spectroscopic behavior of the formulation was analyzed by UV-vis and fluorescence emission spectroscopy.

In Fig. 4A, we report the results obtained at λ_{ex} 278 nm, corresponding to the excitation wavelength of both zein and CUR. NPs prepared with CD showed a quenching of the fluorescence in the emission band with a maximum at 305 nm typical of tyrosine and tryptophan either for NPs unloaded or loaded with CUR. Fluorescence quenching, which is caused by an interaction between a fluorophore, such as a protein, and a quencher molecule, decreases the fluorescence intensity of the protein. Fluorescence quenching provides unique information about the interaction of CD with proteins because of the sensitivity of intrinsic fluorescence to the microenvironment changes around the protein. Since zein shows intrinsic fluorescence linked to amino acid residues containing aromatic moieties (phenylalanine, tryptophan, and tyrosine), fluorescence quenching confirms the presence of molecular interactions between CD and zein (Ren, Fu, Xiong, Cui, Ren, Guan, et al., 2018). This behavior is much more relevant since CUR fluorescence should, in some way, compensate quenching effect due to emission at the same wavelength.

Considering that CUR is intrinsically fluorescent when excited at λ_{ex} 424 nm after solubilization in an organic solvent like ethanol, the fluorescence emission spectra of CUR and CUR-loaded NPs were collected (Fig. 4B). In the case of CUR, its incorporation in colloidal NPs resulted in a blue shift of 10 nm and in a prominent hypochromic effect (A. R. Patel, Heussen, Dorst, Hazekamp, & Velikov, 2013).

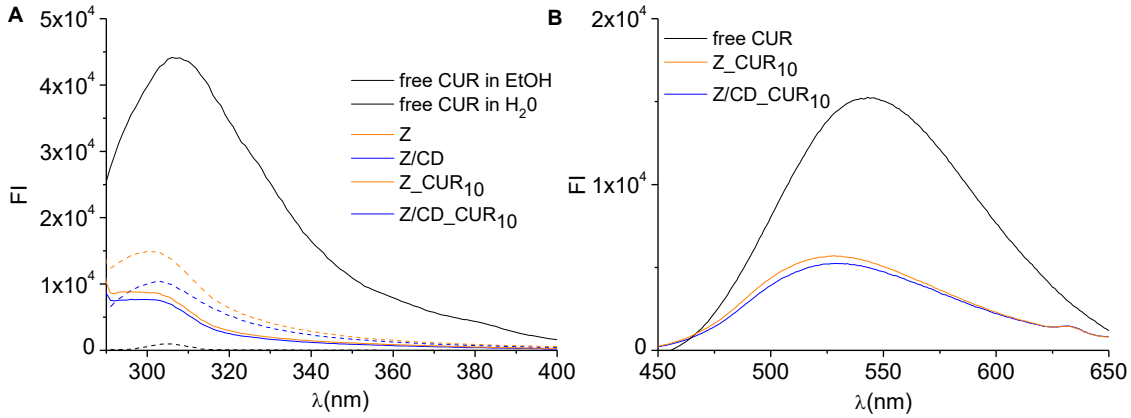

Fig. 4. Emission spectra of free CUR, CUR-loaded NPs, and unloaded NPs (dotted curves) at λ_{EX}= 278 nm (A) and λ_{EX}= 424 nm (B). CUR amount in the samples was fixed at 3 µg/mL.

The release properties of NPs Z_CUR$_{10}$ and Z/CD_CUR$_{10}$ were investigated to understand if NPs can allow a modified release of CUR in the buccal compartment.

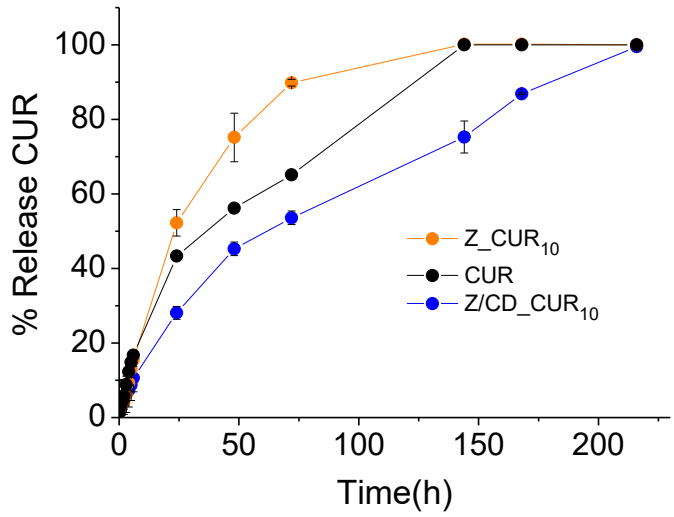

Fig. 5. CUR released from NPs Z_CUR$_{10}$ and Z/CD_CUR$_{10}$ as assessed by dialysis. The external medium was in 5 mL of Tween 80 5 %w/v at 37 ° C under magnetic stirring versus free CUR.

As shown in Fig. 5, NPs Z/CD_CUR$_{10}$ presented a prolonged release of CUR versus NPs Z_CUR$_{10}$ and free CUR confirming that CD is a useful excipient to modulate nanosystem features and to control the release of its cargo. This effect is surprising since, in general, CD class is shown to accelerate the release of poorly water-soluble compounds from matrices where

the release is activated by an initial hydration step. Due to their ability to increase the apparent solubility of lipophilic drugs, it is expected that when they are incorporated in an insoluble/slowly soluble polymer matrix, they increase the number of diffusive species and, in turn, increase the release rate. In the present case, the actual modification of matrix permeability to water entry and diffusant transport operated by CDs can slow down the release rate. Although CDs have been demonstrated to act as modifiers of small molecule release rates from different types of polymer matrices (Conte, Dal Poggetto, B, Esposito, Ungaro, Laurienzo, et al., 2019; d'Angelo, Fraix, Ungaro, Quaglia, & Miro, 2017; da Silva, 2018; Miro, d'Angelo, Nappi, La Manna, Biondi, Mayol, et al., 2013) to our knowledge this is the first report on CDs to modulate release features of a protein platform.

1.3.2 Interaction of NPs with porcine mucin

UV-absorption of Z_CUR_{10} and Z/CD_CUR_{10} was collected at 600 nm in water or a water dispersion of mucin (Fig. 6A).

NPs incubated with different mucin dispersions displayed absorbance values (scattering) higher than the corresponding NPs in water suggesting that NPs can remarkably interact with mucin. An increase in the scattering is generally related to extensive mucin-NPs interactions. As shown in Fig. 6A, there are no significant differences between zein NPs and zein/CD NPs since both demonstrate interaction with mucin. Moreover, the experiment was carried out in the presence of mucin in PBS, obtaining comparable results.

Fluorescence analysis of the NPs samples was useful to confirm this hypothesis further. As visible in Fig. 6B, a quenching of the emission band of mucin, was observed in the presence of NPs. The fluorescence quenching of mucin suggests its interaction with NPs, likely involving the formation of stable electrostatic bonds at the surface of NPs. The interaction of NPs with mucin was also evident in the cumulative distribution curves of the NPs in the presence of mucin. As shown in Fig. 6C, the shift of the NPs curves toward higher size values in the presence of mucin demonstrates the strong interaction between cationic NPs and anionic mucin.

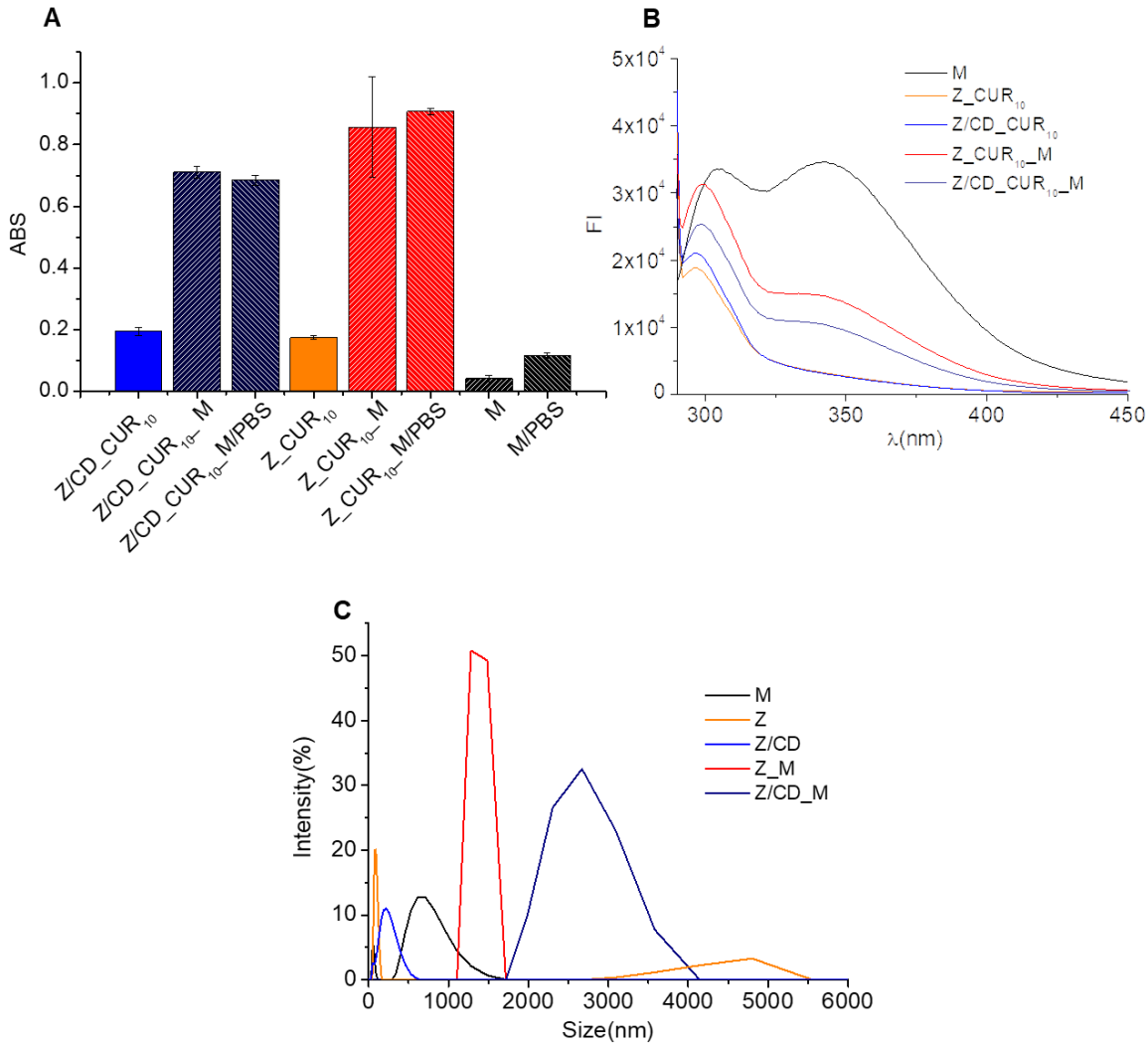

Fig. 6. ABS at 600 nm of NPs in water, in a mucin water or PBS dispersion (A) and emission spectra of NPs a mucin water dispersion versus free mucin (excitation of mucin at λ_{EX}=278 nm) (B). Cumulative distribution curves of the NPs Z_CUR$_{10}$ and corresponding NPS Z/CD_CUR$_{10}$ with/without addition of mucin versus mucin dispersion (M) (C).

1.3.3 Bioadhesion of NPs on the porcine buccal mucosa

The mucoadhesive features of the NPs were evaluated by using porcine buccal mucosa as a model tissue. The NPs and free CUR were first separately sprayed on the tissue, and then, each piece of the treated mucosa was washed with NaCl 0.9 % w/v and analyzed by confocal microscopy. The confocal images (Fig. 7) showed that the fluorescence of NPs Z_CUR$_{10}$ (panel B) and Z/CD_CUR$_{10}$ (panel C) is higher than the fluorescence of free CUR (panel A).

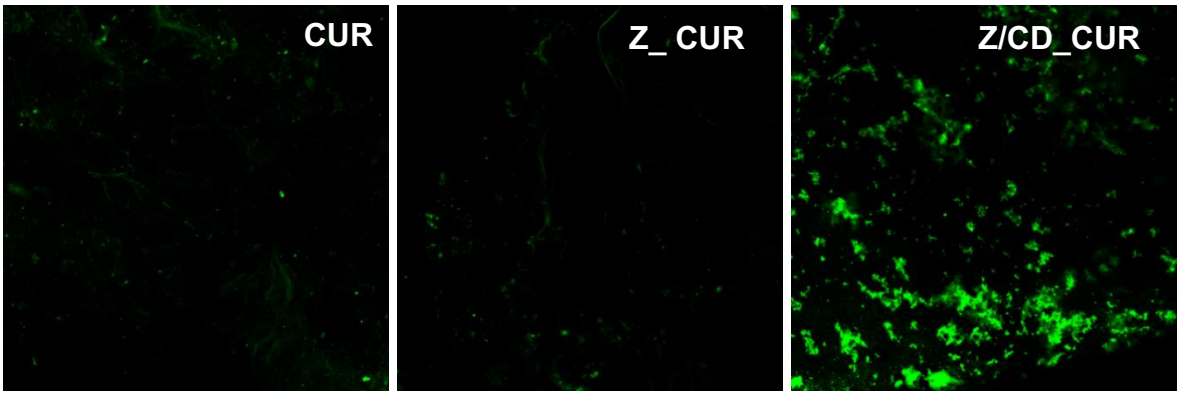

Fig. 7. Confocal images of porcine buccal mucosa treated with free CUR (A), NPs Z_CUR$_{10}$ (B), and Z/CD_CUR$_{10}$ (C) after washing step with NaCl 0.9 % w/v. The samples are representative of three experiments.

This piece of evidence confirms that zein/CD NPs allow CUR to lay on the mucosa and be adsorbed through the underlying buccal epithelium, while CUR is mainly swallowed and absorbed through the intestinal epithelium.

1.4 Conclusions

In this work, we propose zein-based NPs as a platform for buccal delivery of CUR to circumvent its poor bioavailability due to poor dissolution and high metabolization in the GI tract. NPs based on zein or zein /CD association were prepared by the anti-solvent co-precipitation method. NPs were spherical, positive, loaded CUR with high efficiency up to a theoretical loading of 10% and were stable upon storage. All NPs proposed could be delivered by a spray device on the biological area of interest. UV and fluorescence analysis confirmed the presence of interactions between CD and zein and their strong interaction with mucin. The critical role of CD in the NPs is highlighted by release studies and mucoadhesion to the porcine buccal mucosa. The presence of CD was found to slow down the release rate of CUR from NPs and to interact extensively with mucosa, possibly extending their permanence at the CUR absorption site.

In conclusion, zein/CD/CUR NPs could be employed as a novel platform to increase CUR permanence in the buccal compartment and, consequently, its efficacy in the treatment of local buccal diseases as well as to increase CUR absorption avoiding first-pass metabolism.

References

Alqahtani, M. S., Islam, M. S., Podaralla, S., Kaushik, R. S., Reineke, J., Woyengo, T., & Perumal, O. (2017). Food Protein Based Core-Shell Nanocarriers for Oral Drug Delivery: Effect of Shell Composition on in Vitro and in Vivo Functional Performance of Zein Nanocarriers. *Mol Pharm, 14*(3), 757-769.

Bansil, R., & Turner, B. (2006). Mucin structure, aggregation, physiological functions and biomedical applications. *Current Opinion in Colloid & Interface Science, 11*, 164-170.

Bernkop-Schnürch, A., & Dünnhaupt, S. (2012). Chitosan-based drug delivery systems. *European Journal of Pharmaceutics and Biopharmaceutics, 81*(3), 463-469.

Conte, C., Dal Poggetto, G., B, J. S., Esposito, D., Ungaro, F., Laurienzo, P., Boraschi, D., & Quaglia, F. (2019). Surface Exposure of PEG and Amines on Biodegradable Nanoparticles as a Strategy to Tune Their Interaction with Protein-Rich Biological Media. *Nanomaterials (Basel), 9*(10).

d'Angelo, I., Fraix, A., Ungaro, F., Quaglia, F., & Miro, A. (2017). Poly(ethylene oxide)/hydroxypropyl-β-cyclodextrin films for oromucosal delivery of hydrophilic drugs. *International Journal of Pharmaceutics, 531*(2), 606-613.

da Silva, A. M. (2018). Room at the Top as well as at the Bottom: Structure of Functional Food Inclusion Compounds. In P. A. a. N. Dhingra (Ed.), *Cyclodextrin - A Versatile Ingredient*): IntechOpen.

Garcea, G., Jones, D. J. L., Singh, R., Dennison, A. R., Farmer, P. B., Sharma, R. A., Steward, W. P., Gescher, A. J., & Berry, D. P. (2004). Detection of curcumin and its metabolites in hepatic tissue and portal blood of patients following oral administration. *British Journal of Cancer, 90*(5), 1011-1015.

Hazzah, H. A., Farid, R. M., Nasra, M. M., El-Massik, M. A., & Abdallah, O. Y. (2015). Lyophilized sponges loaded with curcumin solid lipid nanoparticles for buccal delivery: Development and characterization. *Int J Pharm, 492*(1-2), 248-257.

Hsein, H., Garrait, G., Beyssac, E., & Hoffart, V. (2015). Whey protein mucoadhesive properties for oral drug delivery: Mucin–whey protein interaction and mucoadhesive bond strength. *Colloids and Surfaces B: Biointerfaces, 136*, 799-808.

Islam, M. S., Reineke, J., Kaushik, R., Woyengo, T., Baride, A., Alqahtani, M. S., & Perumal, O. (2019). Bioadhesive Food Protein Nanoparticles as Pediatric Oral Drug Delivery System. *ACS Applied Materials & Interfaces, 11*(20), 18062-18073.

Laffleur, F., Schmelzle, F., Ganner, A., & Vanicek, S. (2017). In Vitro and Ex Vivo Evaluation of Novel Curcumin-Loaded Excipient for Buccal Delivery. *AAPS PharmSciTech, 18*(6), 2102-2109.

Lalla, R. V., & Bensadoun, R.-J. (2011). Miconazole mucoadhesive tablet for oropharyngeal candidiasis. *Expert Review of Anti-infective Therapy, 9*(1), 13-17.

Li, X., Uehara, S., Sawangrat, K., Morishita, M., Kusamori, K., Katsumi, H., Sakane, T., & Yamamoto, A. (2018). Improvement of intestinal absorption of curcumin by cyclodextrins and the mechanisms underlying absorption enhancement. *Int J Pharm, 535*(1-2), 340-349.

Mazzarino, L., Borsali, R., & Lemos-Senna, E. (2014). Mucoadhesive films containing chitosan-coated nanoparticles: a new strategy for buccal curcumin release. *J Pharm Sci, 103*(11), 3764-3771.

Miro, A., d'Angelo, I., Nappi, A., La Manna, P., Biondi, M., Mayol, L., Musto, P., Russo, R., Rotonda, M. I. L., Ungaro, F., & Quaglia, F. (2013). Engineering poly(ethylene oxide) buccal films with cyclodextrin: A novel role for an old excipient? *International Journal of Pharmaceutics, 452*(1), 283-291.

Morales, J. O., & Brayden, D. J. (2017). Buccal delivery of small molecules and biologics: of mucoadhesive polymers, films, and nanoparticles. *Curr Opin Pharmacol, 36*, 22-28.

Patel, A., Hu, Y., Tiwari, J. K., & Velikov, K. P. (2010). Synthesis and characterisation of zein–curcumin colloidal particles. *Soft Matter, 6*(24), 6192-6199.

Patel, A. R., Heussen, P. C., Dorst, E., Hazekamp, J., & Velikov, K. P. (2013). Colloidal approach to prepare colour blends from colourants with different solubility profiles. *Food Chem, 141*(2), 1466-1471.

Purpura, M., Lowery, R. P., Wilson, J. M., Mannan, H., Munch, G., & Razmovski-Naumovski, V. (2018). Analysis of different innovative formulations of curcumin for improved relative oral bioavailability in human subjects. *Eur J Nutr, 57*(3), 929-938.

Rachmawati, H., Edityaningrum, C. A., & Mauludin, R. (2013). Molecular inclusion complex of curcumin-beta-cyclodextrin nanoparticle to enhance curcumin skin permeability from hydrophilic matrix gel. *AAPS PharmSciTech, 14*(4), 1303-1312.

Ren, F., Fu, J., Xiong, H., Cui, L., Ren, G., Guan, H., & Jing, Q. (2018). Complexes of Felodipine Nanoparticles With Zein Prepared Using a Dual Shift Technique. *J Pharm Sci, 107*(1), 239-249.

Salamat-Miller, N., Chittchang, M., & Johnston, T. P. (2005). The use of mucoadhesive polymers in buccal drug delivery. *Advanced Drug Delivery Reviews, 57*(11), 1666-1691.

Shtenberg, Y., Goldfeder, M., Prinz, H., Shainsky, J., Ghantous, Y., Abu El-Naaj, I., Schroeder, A., & Bianco-Peled, H. (2018). Mucoadhesive alginate pastes with embedded liposomes for local oral drug delivery. *International Journal of Biological Macromolecules, 111*, 62-69.

Song, G., Banov, D., Bassani, A. S., & Valdez, B. C. (2017). Evaluation of the Safety, Cell Migration, and Mucoadhesive Properties of a Mucoadhesive Polymer Blend in Human Oral Mucosa. *AAPS PharmSciTech, 18*(5), 1617-1623.

Sun, C., Xu, C., Mao, L., Wang, D., Yang, J., & Gao, Y. (2017). Preparation, characterization and stability of curcumin-loaded zein-shellac composite colloidal particles. *Food Chemistry, 228*, 656-667.

Sunoqrot, S., Hasan, L., Alsadi, A., Hamed, R., & Tarawneh, O. (2017). Interactions of Mussel-inspired Polymeric Nanoparticles with Gastric Mucin: Implications for Gastro-retentive Drug Delivery. *Colloids and Surfaces B: Biointerfaces, 156*.

Tapia-Hernandez, J. A., Rodriguez-Felix, F., Juarez-Onofre, J. E., Ruiz-Cruz, S., Robles-Garcia, M. A., Borboa-Flores, J., Wong-Corral, F. J., Cinco-Moroyoqui, F. J., Castro-Enriquez, D. D., & Del-Toro-Sanchez, C. L. (2018). Zein-polysaccharide nanoparticles as matrices for antioxidant compounds: A strategy for prevention of chronic degenerative diseases. *Food Res Int, 111*, 451-471.

Walicova, V., Gajdziok, J., Pavlokova, S., & Vetchy, D. (2017). Design and evaluation of mucoadhesive oral films containing sodium hyaluronate using multivariate data analysis. *Pharm Dev Technol, 22*(2), 229-236.

Wan, Z.-L., Guo, J., & Yang, X.-Q. (2015). Plant protein-based delivery systems for bioactive ingredients in foods. *Food & Function, 6*(9), 2876-2889.

Supplementary material

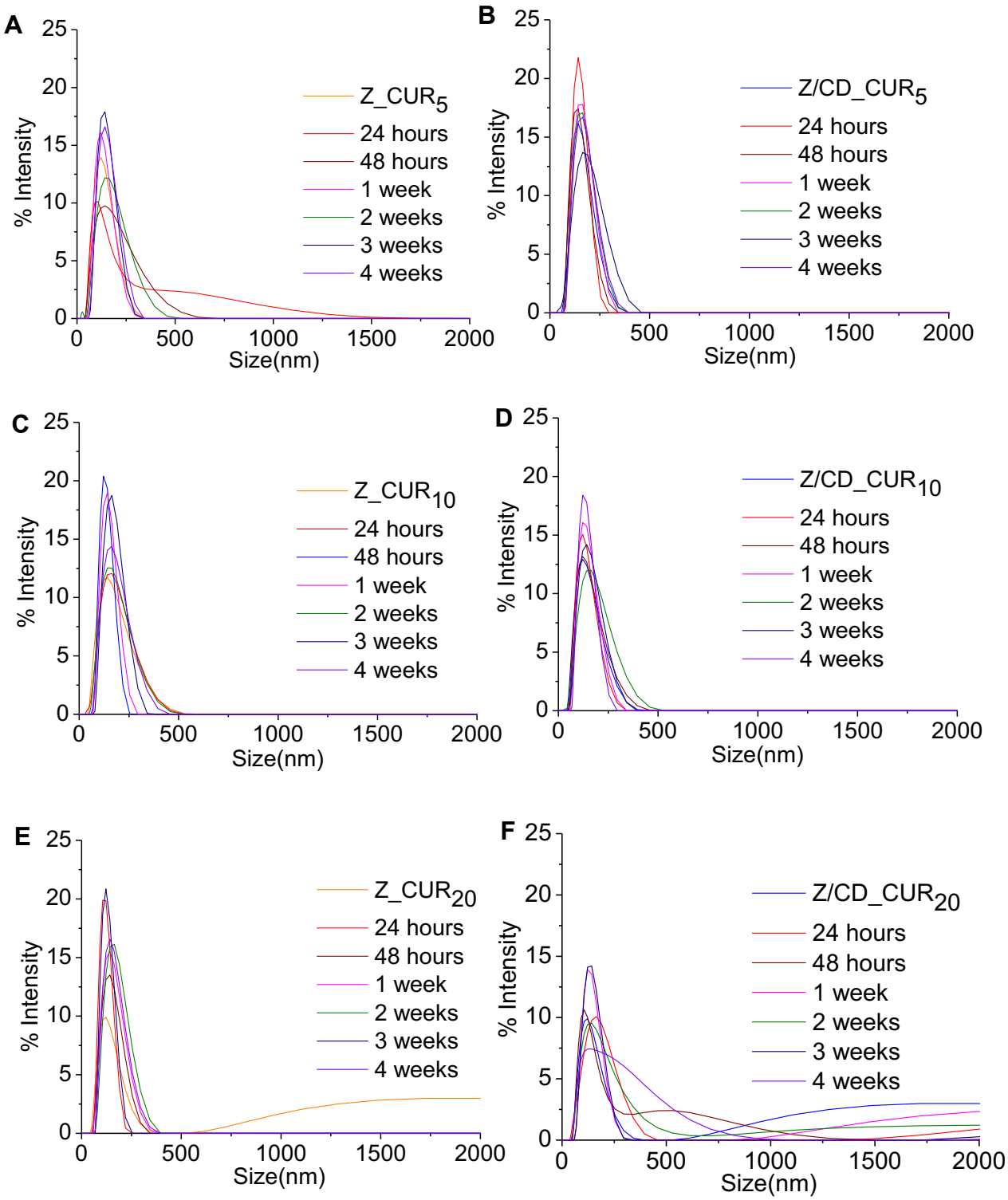

Fig. S1. Cumulative distribution curves of NPs Z_CUR$_5$(A), NPs Z_CUR$_{10}$ (C), NPs Z_CUR$_{20}$(E), and corresponding NPS embedded with CD (B, D, F) monitored at room temperature in the dark for four weeks.

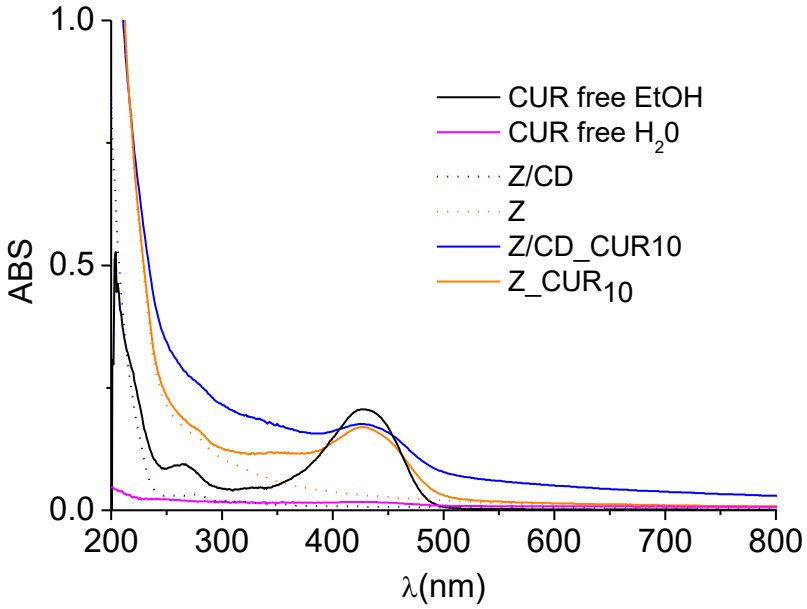

Fig. S2. UV-spectra of free CUR solubilized in EtOH, of free CUR precipitated in water, of CUR-loaded NPs and of unloaded NPs as control (dotted curves).

Chapter 4

From the bench to the market: industrial partnership and product development

1.1 Industrial PhD: an opportunity to merge academic knowledge and industrial expertise

The research was focused on the formulation of bioactive compounds that have a high impact in the food supplement field, with polymer materials, generally approved as food ingredients, opportunely processed through the application of nano-micro technology to get innovative oral delivery systems with implemented properties.

In the attempt to develop a formulated bioactive compound with potential as a food supplement, the collaboration with the industrial partners, Neilos s.r.l. and BUCHI Labortechnik AG has been envisaged to face the industrial transfer stage and the product launch in the market.

Along this line, we have identified through an in-depth marketing analysis a panel of bioactive compounds with high interest in the nutraceutical field and characterized by low stability and bioavailability. As ingredients useful to formulate the final product, zein, a plant-based protein insoluble in water, has been selected. The formulation approach was based on the use of zein alone or in combination with polysaccharides aimed to deliver bioactive compounds with different properties and to optimize their oral absorption. In particular, the research has been focused on the combination of zein and beta-cyclodextrin (CD), a carrier already employed in the pharmaceutical field and food science with different purposes.

As a processing method of bioactive compounds/polymer combinations, we have selected spray-drying, a green drying process proposed to produce powders in one-step with fine-tuning of process parameters. In this context, the partnership with BUCHI Labortechnik AG has been crucial to ameliorate processing and to check the quality of the formulated products.

1.2 Neilos s.r.l. internship

During the initial 4-month stage at Neilos s.r.l., some bioactive molecules of commercial interest, in compliance with the food supplements legislation, and corresponding raw materials suppliers were identified. Another formative activity was the study, drafting and filing of International (PCT), European (EP) and Italian (IT) patent applications for industrial inventions. In particular, the combination of zein/cyclodextrin was patented by Neilos s.r.l. as a versatile platform to deliver lipophilic/hydrophilic bioactive compounds in nutraceutical field (A system for the controlled release of active ingredients based on polymeric materials and its use in the nutraceutical field, WO2018203294A1).

1.2.1 Selection of the raw materials and bioactive compounds

Part of the internship at Neilos s.r.l. was dedicated to a careful study of the regulation of food supplements, and great attention was paid on the European regulations, published on the Official Journal of the European Union, for the product launch in the market.

EU legislation and EFSA guidance documents detail how to assemble a dossier for nutraceutical approval and the information and studies required for its evaluation. EFSA guidance is updated regularly, so applicants should check they are using the latest version before applying for new products. The objective of the harmonized rules on food supplements in Directive 2002/46/EC is to protect consumers against potential health risks from those products and to ensure that they are not provided with misleading information. With respect to the safety of food supplements, the Directive lays down a harmonized list of vitamins and minerals that may be added for nutritional purposes in food supplements (in Annex I to the Directive). Annex II of the Directive contains a list of permitted sources (vitamin and mineral substances) from which those vitamins and minerals may be manufactured.

This list has been amended by the following Regulations and Directive to include additional substances. Particular attention was paid to the regulations (UE) 1170/2009, 1129/2011, and 1169/2011. The regulation No 1170/2009 (30 November 2009) amended Directive 2002/46/EC and 1925/2006 as regards the lists of vitamin and minerals and their forms that can be added to foods, including food supplements. The EU regulation 1129/2011 (11 November 2011) amended Annex II to Regulation (EC) No 1333/2008 of the European Parliament and of the Council establishing a single list of food additives approved.

The regulation 1169/2011 (25 October 2011) on the provision of food information to consumers, amended Regulations 1924/2006 and 1925/2006 including the specifications of all additives which may be used to produce food products and establishing the rules for the right labeling/packaging of nutraceuticals including all responsibilities/requirements for the employees and for the companies involved in the manufacturing process.

Based on these premises, we have selected bioactive compounds with growing market interest but poorly explored so far for innovation purposes. We have paid particular attention to iron salts and curcumin (CUR) to demonstrate the versatility of the platform developed for the delivery of both hydrophilic and lipophilic compounds. Concerning the excipients, zein is a GRAS ingredient approved by the FDA, while β-cyclodextrin (CD) is approved in Europe as an additive in food supplements (E459).

1.2.2 Selection of iron source

After the development phase in the lab, aimed at setting-up conditions for bioactive compound entrapment in zein platforms, the attention was focused on the transfer of the product from a lab-scale to an industrial setting.

An in-depth analysis of the chemical properties of iron salts was performed to select suitable iron sources to employ in the formulation study and for the industrialization process. Among a series of iron (II) sources, iron sulphate heptahydrate was selected considering the iron supplements already launched in the market and its tolerability.

Under the regulation No 1170/2009 and 1169/2011, all iron sources which can be employed in the formulation of iron food supplements were taken into consideration exploring different aspects such as their solubility, their compatibility with the selected raw materials and their claimed use in the nutraceutical field. The following list includes all different forms of iron approved in food field:

- ferrous carbonate
- ferrous citrate
- ferric ammonium citrate
- ferrous gluconate
- ferrous fumarate
- ferric sodium diphosphate
- ferrous lactate
- ferrous sulphate
- ferric diphosphate (ferric pyrophosphate)
- ferric saccharate
- elemental iron (carbonyl + electrolytic + hydrogen reduced)
- ferrous bisglycinate
- ferrous L-pidolate
- ferrous phosphate
- iron (II) taurate

A comprehensive analysis was carried out to identify the iron sources readily available on the market and clinically relevant. Furthermore, the competitor product available on the Italian food supplements market was considered too.

After this market analysis, ferrous gluconate, ferrous fumarate, ferrous sulphate, ferrous bisglycinate, ferrous L-pidolate, ferric diphosphate (ferric pyrophosphate) and ferric saccharate were chosen from the list above.

Then the iron bioavailability in vivo was a crucial factor to eliminate the iron (III) sources (ferric diphosphate (ferric pyrophosphate) and ferric saccharate) considering the better absorption of iron (II) derivatives.

Further selection was based on the solubility of these bioactive compounds, considering the solvents involved in the formulation process for micropowder production described in chapter 2, namely ethanol and water.

Ferrous fumarate was poorly soluble in water, while ferrous gluconate was practically insoluble in ethanol, so they were excluded from the selection. Ferrous L-pidolate, ferrous bisglycinate, and sulphate passed each consequential screening. Ferrous L-pidolate was eventually excluded due to the presence of impurities of glutamic acid in the purchased raw materials, which could overcomplicate micropowder characterization. In conclusion, ferrous bisglycinate (FeBIS) and sulphate were the two leading candidates.

The results obtained with FeBIS (Chapter 2) highlighted two main issues for industrial scale-up:

- Low iron loading resulting in the use of too high amounts of iron-loaded micropowders;
- Presence of ethanol in the feeding liquid of the spray drying process;
- The low solid content in the feeding liquid of the spray drying process.

In an attempt to increase iron loading, our attention turned to Iron (II) sulfate as an alternative to FeBIS. The results are reported in the following section.

1.2.3 Production and characterization of iron (II) sulfate pseudolatexes

A colloidal dispersion (pseudolatex) was formed by the anti-solvent co-precipitation method adding 50 mL of a water solution of CD (0.1% w/v) to 10 mL of a solution of zein (2% w/v) in ethanol/water 80% v/v at room temperature under magnetic stirring. The volume ratio between the hydroalcoholic solution of zein 2% w/v and water solution of CD 0.1 % w/v was 1:5. The ratio between zein/CD is 4:1 by the weight of solid. An amount of 50, 100, 125, 150 mg of iron (II) sulfate corresponding to 10 (Z/CD_Fe_{10}), 20 (Z/CD_Fe_{20}), 25 (Z/CD_Fe_{25}), 30

(Z/CD_Fe_{30}) mg of Fe^{2+} were incorporated in the pseudolatex (PL) upon co-solubilization with zein in the hydroalcoholic solution.

PLs were characterized in terms of the hydrodynamic diameter (D_H), polydispersity index (PI), and zeta potential (ζ), and results are reported in Table 1.

All PLs show a hydrodynamic diameter (D_H) below 500 nm and a polydispersity index (PI) relatively low. The colloidal dispersions produced were homogeneous in terms of particle diameter without evident signs of aggregation. The surface charge was positive for all the formulations due to the ability of zein to expose positive amino acids when processed through nanoprecipitation, as explained in chapters 2 and 3.

Table 1. Characterization of MPs.

Batch	**D_H [a] (nm ± SD)**	**PI [a] (± SD)**	**ζ [a] (mV± SD)**	**Theoretical loading mg Fe^{2+}/ 100 mg MPs [b] (mg)**
Z/CD_Fe_{10}	319	0.1	+13	4.0
Z/CD_Fe_{20}	399	0.1	+11	8.0
Z/CD_Fe_{25}	422	0.2	+8	10
Z/CD_Fe_{30}	544	0.3	+10	12.0

[a] evaluated by Zetasizer Nano ZS, [b] mg Fe^{2+} in 100 mg of MPs.

Contrarily to the pseudolatexes loaded with FeBIS, it was possible to eliminate ethanol from the formulations of iron (II) sulfate under vacuum (Rotavapor R-100 Büchi Labortechnik AG, Flawil Switzerland). This step was certainly advantageous considering the issues linked to the use of the organic solvents during an industrial manufacturing process.

1.2.4 Scale-up of the process

Thus, several European companies, already successful in the scale-up of spray-dried powders, were contacted to perform the production process on a large scale (Table 2) and the designed flow chart for the industrial scale-up of the iron (II) sulfate -loaded micropowders (Fig. 1) was proposed.

Table 2. European companies successful in the scale-up of spray-dried powders.

Company	Country
BIO2 (LaBIOTRE)	Italy
Chemiferm Srl	Italy
DPHAR SpA	Italy
E-PHARMA	Italy
Ips srl	Italy
MB MED	Italy
Gea Niro	Denmark
HOVIONE	Portugal
Procept/Xedev	Belgium
Upperton	United Kingdom
Vitasquare	Netherlands

Among the companies reported above, some attempts to industrialize our platform were carried out by MB MED (Italy). During the first experimental trials some hurdles of the scale-up process such as nozzle blocking of spray-dryer or the complications in the solvent removal emerged. Other efforts will be necessary to optimize the process performed at industrial level.

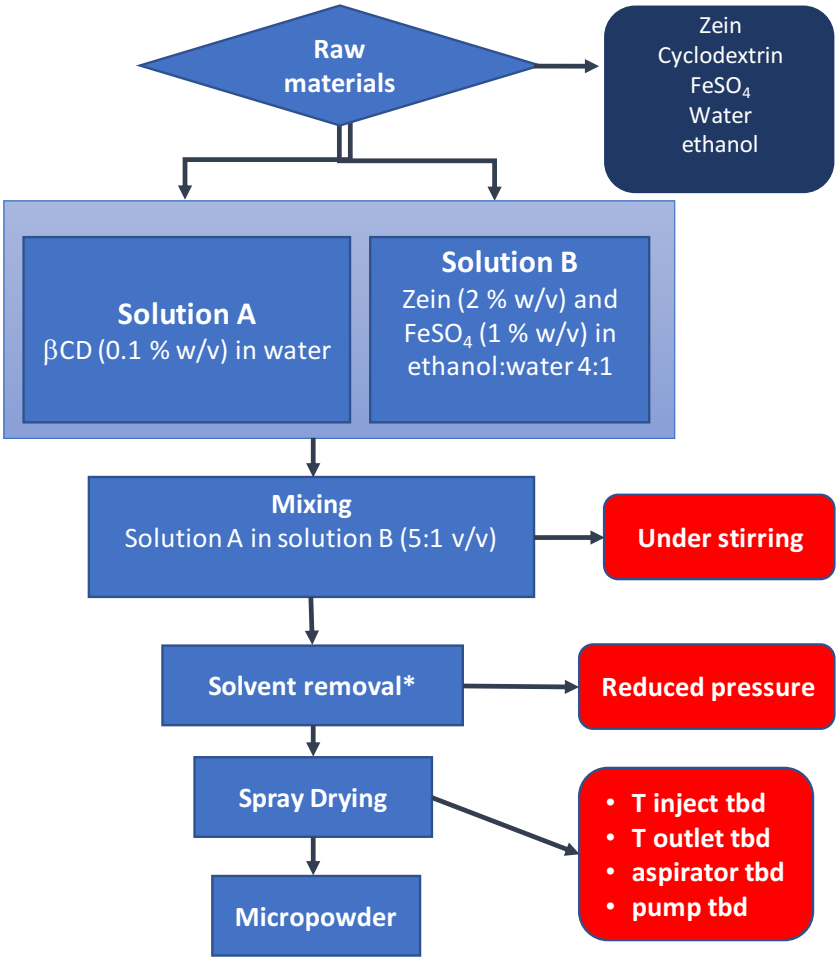

Fig. 1. Scheme proposed for manufacturing the product.

1.3 BUCHI Labortechnik AG internship

At BUCHI Labortechnik AG, after the BUCHI Basic Training on BUCHI Products&Solutions, the optimization of spray drying parameters, the encapsulation of different molecules with high impact in the nutraceutical field and the chemical characterization of the raw material/micropowders with different technologies as Kjeldahl and NIR spectroscopy were carried out. All the activities were performed under the supervision of the Product Specialist Dr Aurelie Demont and checked periodically during the scientific meetings. The results obtained will be reported in new application notes/booklets to improve BUCHI portfolio.

Results on micropowder development and characterization have been reported in chapters 2 and 3 while in the following, some additional aspects are reported. Furthermore, the use of zein as a coating for alginate beads produced by the Encapsulator® apparatus is described.

1.3.1 Optimization of Zein/CD micropowders by spray-drying

The first part of this stage was focused on the optimization process of the zein micropowders produced using the Mini Spray-Dryer B-290 in close-mode configuration due to the presence of a percentage of ethanol in the PL.

In this regard, the modulation of the process parameters was critical to reaching the maximum performance of the drying process. In Fig. 2, Buchi guidelines that describe the influence of the different process parameters on the dependent variable are reported in an intuitive scheme.

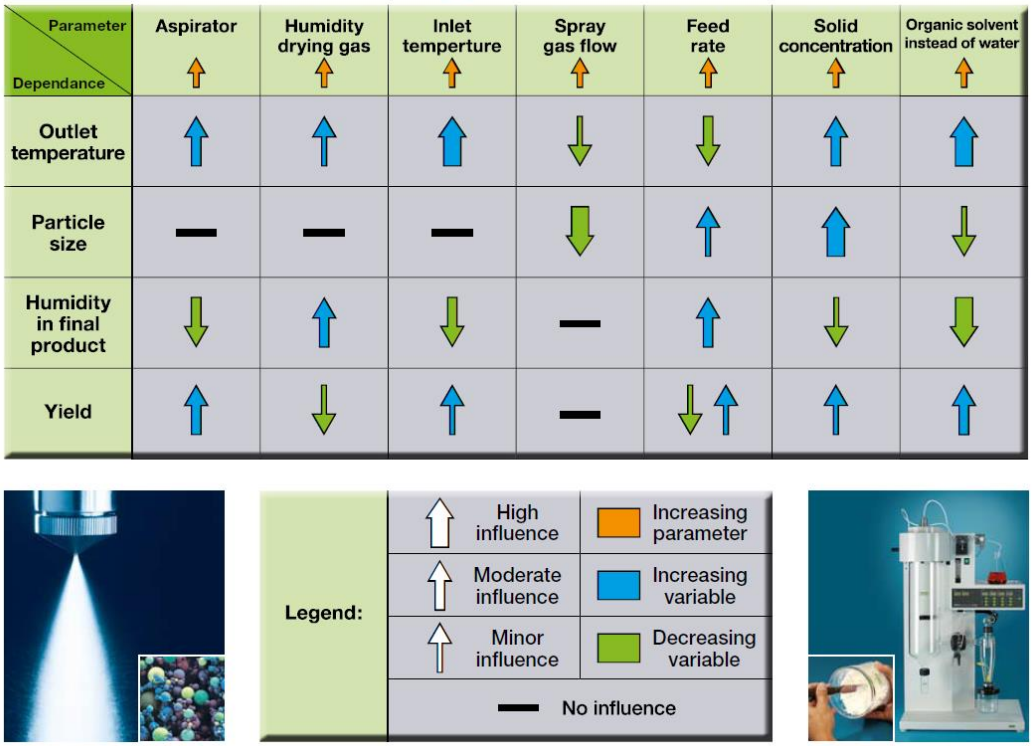

Fig. 2. Modulation of process parameters using Mini-Spray Dryer Buchi B-290.

The optimization process of the zein-based micropowders consisted of improving the yield of the final solid product by decreasing their adhesiveness inside the Mini Spray-Dryer cyclone. Thus, pseudolatex of zein/CD were processed in different experimental conditions highlighting the positive contribution of CDs on the quality of micropowders collected.

The first parameter monitored was the influence of the inlet temperature on the drying process. The increase of the inlet temperature provided a proportional increase of the outlet temperature reducing the relative humidity in the drying gas and allowed the formation of a dried powder, which was less sticky.

Another parameter that affected the outlet gas temperature was the aspirator rate, which offers more drying energy and causes a smaller amount of residual moisture in the product promoting a better degree of separation in the cyclone. The aspirator rate was set up around 90-100 % maximum value. A higher gas flow decreased the outlet temperature due to the presence of additional gas to heat up and produced smaller droplets from the nozzle, which correspond to smaller solid particles.

Increasing feed rate means more liquid to evaporate and increases the droplet size because more liquid must be dispersed. As a result, humid or moist products are obtained. For this reason, we tried to increase the pump rate only to demonstrate that the yield remarkably decreased due to the high humidity in the final solid products that resulted in adhesive powders on the glassware and to confirm that the pump rate (10 %) used for zein-based micropowders was appropriate.

1.3.2 Micropowder characterization techniques: Kjeldahl and NIR for solids

For more than 130 years, the Kjeldahl method has been internationally accepted as a standard protocol to determine the nitrogen/protein content for different fields of application (Pharma, Food & Feed). The Kjeldahl method consists of a procedure of catalytically supported mineralization of organic material in a boiling mixture of sulfuric acid and sulfate salts at a boiling temperature between 340-370 °C. In the digestion process, the organically bonded nitrogen is converted into ammonium sulfate. Alkalizing the solution liberates ammonia, which is quantitatively stem-distilled and determined by titration (Kjeldahl knowledge base, BUCHI LABORTECHNIK AG, 2017). In this research project, this method was used as a quality control method for zein (as raw material) and spray-dried products. The technical data sheet (TDS) of zein was used as the reference standard.

Based on the previous results obtained with ATR-FTIR, also NIR was explored to investigate the spectra of the selected raw materials and zein-based micropowders. The instrument used was the NIRFlex for Solids, and the measurements were performed in a range of frequency 4000–10000 cm^{-1} and reported as reflactance values.

These analytical techniques were employed to fully characterize the FeBIS and curcumin loaded micropowders described in chapters 2 and 3.

1.3.3 Encapsulator B-390 trials

To explore the possibility of employing zein as coating material, expanding the possibility of its application, we tried to prepare alginate beads coated with zein through Büchi Encapsulator B-390 to deliver selected bioactive compounds. The easy-to-use technology works on the principle of laminar jet break up of a liquid stream into equally sized beads/capsules by applying a controlled vibrational frequency to the liquid. The easy to adjust process condition, allow the production of a wide range of pre-selectable particle sizes (80 µm – 4 mm) due to the possibility to employ many different sized nozzles. The reliable and gentle technology also enables the reproducible production of mono-dispersed and homogenous particles, which have a very narrow size distribution (< 5% standard deviation from the average mean size for alginate solutions) using a simple, single-step process, which is also scalable.

To prevent coalescence of the droplets during jet break-up and/or when entering the gelling bath, an electrical charge is induced onto the surface of the droplets using an electrostatic voltage system. This system applies an electrical potential between the nozzle and an electrode, placed directly underneath the nozzle. As droplets fall through the electrode, they are charged and deflected from their vertical position resulting in their impact occurring over a larger area in the hardening solution.

The liquid jet break up process to form droplets can be viewed and monitored in the light of a stroboscopic lamp, which is placed directly behind the droplets. This enables optimal droplet formation to be obtained before landing in the gelling bath.

Upon landing in the agitated hardening bath, the droplets are converted into beads either by gelation or a polymerization reaction. The encapsulated material is entrapped within the matrix structure of the beads. After production the produced particles can be removed and used as required or pre-treated further (Fig. 3) (Encapsulator B-390/B-395 Pro Laboratory Guide, BUCHI LABORTECHNIK AG, 2014).

For the preparation of alginate beads, 3,0 g of sodium alginate were dissolved in 200 mL of water (1.5 % w/v) at room temperature using a mixer. The suspension was immediately dripped into 100 mM $CaCl_2$ solution (7,35 g in 500 mL) using the Buchi encapsulator B-390 (BÜCHI Labortechnik AG, Flawil, Switzerland) fitted with a nozzle (450 µm) at a vibration frequency of 800 Hz with an electrode voltage of 500 mV.

The air pressure was maintained at 500 mbar to generate beads. A curing time of 30 min was allowed for their crosslinking. After that, the beads were separated using a nylon mesh and washed several times with water to remove unreacted $CaCl_2$ and finally dried at 40 °C until constant weight. Dried beads were kept in glass vials and stored in the desiccator at room temperature.

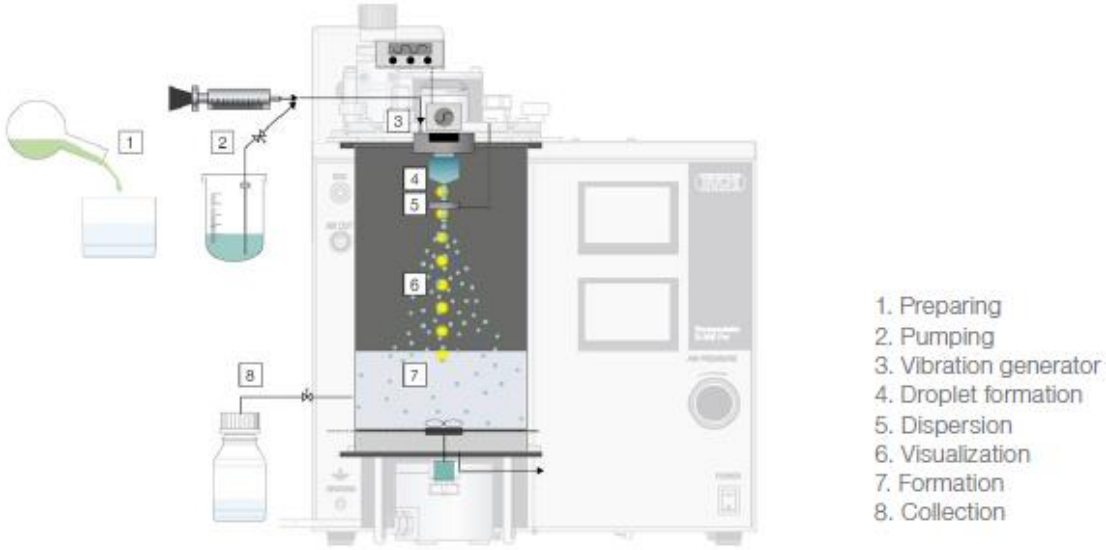

Fig. 3. Schematic displaying of the operation of Encapsulator B-390/B-395 Pro when using a single nozzle system to produce beads.

For the coating step, a 10 % w/v zein solution (5 g in 50 mL) in 80 % v/v of ethanol in water was prepared. Alginate beads (1 g) were placed on a nylon mesh strainer (14 cm diameter) with a holder to produce a uniform layer, and then 5 mL of the zein solution were sprayed at the surface of beads using a manual atomizer. The spraying was carried out to wet the entire surface of the beads, and the coating was dried, leaving the beads overnight at room temperature in order to obtain a uniform coating.

A picture of zein-coated and uncoated alginate beads is reported in Fig. 4. Prospectively these beads could represent another innovative platform for the delivery of the molecules of our interest.

Fig. 4. Zein-coated (left) and uncoated (right) alginate beads.

1.3.4 Additional activities

In addition to the scientific research activity, the marketing campaign for the launch of the last version of BUCHI R-300 was carried out under the responsibility of the BUCHI Marketing & Communication team and with the collaboration of my academic supervisor Fabiana Quaglia.

As Drug Delivery team, we sponsored this product through official videos/photos which will be shared on the BUCHI international website in the next future.

Another activity was the translation in Italian of the firmware for the BUCHI FatExtractor E-500.

References

Encapsulator B-390/B-395 Pro Laboratory Guide, BUCHI LABORTECHNIK AG, 2014.

Kjeldahl knowledge base, BUCHI LABORTECHNIK AG, 2017.

www.efsa.europa.eu

General Conclusions

Nowadays, nutraceuticals have become increasingly popular due to their potential nutritional and physiological effects. Recently, the scientific community has been not only focused on their beneficial properties but also the optimization of nutraceuticals delivery in the body.

This aspect is crucial to overcome the issues of their oral absorption and preserve their effect on human health. A major challenge for successful administration of micronutrients and nutraceuticals is the complexity involved in its stability and bioavailability in the gastrointestinal tract.

In this scenario, nanotechnologies are certainly a promising tool for addressing the inherent limitation posed in these products.

The development of oral delivery platforms for both a lipophilic (curcumin) and a hydrophilic compound (iron bisglycinate) with implemented properties and, potentially transferable to an industrial setting, was the main goal of the experimental work of this thesis.

The overall strategy encompasses the combined use of zein, a plant-based protein extracted from corn, with β-cyclodextrin (βCD) and the processing through the application of nano/micro technologies. Notably βCD held a crucial role in the formulation process due to its ability to form host-guest inclusion complexes with both zein and selected bioactive compounds.

An appropriate set-up of the experimental parameters allowed the fabrication of nanoparticles that can be used either as micropowders after spray-drying (Chapter 2 and Chapter 3 Section A) or as liquid formulation (Chapter 3 Section B).

To formulate a hydrophilic compound (iron bisglycinate), in Chapter 2 “Zein Beta-cyclodextrin micropowders for iron bisglycinate delivery” a two-step nano-in-micro strategy was set up where nanometer-size zein was formed in a first step and then spray-dried to get a micron-sized powder. The crucial role of beta-cyclodextrin as a helping excipient to process zein by spray-drying and to entrap a hydrophilic iron chelate effectively was demonstrated. Zein/βCD/FeBIS micropowders could allow efficient delivery of FeBIS which acquires desirable gastro resistance when formulated as micropowders, avoiding chelate destruction, occurring at the low pH values in the stomach, and prospectively promoting its intestinal absorption overcoming the issue related to its administration.

As reported in Chapter 3 “Zein platforms for curcumin oral delivery”, despite the potential beneficial activities and safety profile, CUR has not been approved yet as therapeutic agent

mainly because of its relatively poor bioavailability/stability. Based on these considerations, two different platforms based on zein and zein/βCD for CUR oral delivery aimed at increasing its bioavailability were developed.

In the Chapter 3 Section A "Zein beta-cyclodextrin micropowders for curcumin oral delivery", CUR was entrapped in micron-sized powders produced by the nano-in-micro strategy described in Chapter 2 to overcome CUR poor aqueous solubility. CUR-loaded micropowders with CD allow a full control of the release kinetics of the bioactive molecules providing its complete dissolution in a time-window typical for absorption in humans guarantying an improve of CUR bioavailability respect to CUR free. This delivery system represents an innovative tool to formulate CUR in a high-bioavailability nutraceutical product.

Mucoadhesive nanoparticles suitable for buccal delivery were developed and tested for their potential to improve CUR absorption and by-pass hepatic metabolism in the Chapter 3 Section B "Bioadhesive zein beta-cyclodextrin nanoparticles for the buccal delivery of curcumin". In this case, the critical role of βCD in the NPs is highlighted not only for the release studies but also for the mucoadhesion to the porcine buccal mucosa. The presence of βCD was found to slow down the release rate of CUR from NPs and to interact extensively with mucosa, possibly extending their permanence at the CUR absorption site. The remarkable interaction of the nanoparticles with mucus was useful to extend their residence time in the gastrointestinal tract and prospectively to improve absorption of the bioactive cargo.

Another goal of this research activity (Chapter 4 "From the bench to the market: industrial partnership and product development") was the industrialization of the developed products taking advantage of our industrial partners. In the attempt to develop a formulated bioactive compound with potential as a food supplement, the collaboration with the industrial partners, Neilos s.r.l. and BUCHI Labortechnik AG has been envisaged to face the industrial transfer stage and the product launch in the market.

To conclude, the research work carried out during three years of Ph.D. in Pharmaceutical Science, has demonstrated that zein/βCD platforms can be considered as a novel option for efficient oral delivery of nutraceutical compounds in the body, which could be potentially used in functional foods and dietary supplements.

ANNEX-I

Biodegradable nanoparticles bearing amine groups as a strategy to alter surface features, biological identity and accumulation in a lung metastasis model*

* this work has been published as:
Diletta Esposito, Claudia Conte, Giovanni Dal Poggetto, Annapina Russo, Antonio Barbieri, Francesca Ungaro, Claudio Arra, Giulia Russo, Paola Laurienzo, Fabiana Quaglia, **Journal of Material Chemistry B, 2018, 6, 5922–5930.**

ABSTRACT

Polymer-based nanoparticles (NPs) with a cationic charge have been emerged recently as a potent nanotool due to their unique ability to penetrate deeply inside tumor tissue and to interact preferentially with plasma membrane of cancer cells. In this paper, we propose a general strategy to obtain biodegradable cationic NPs of poly(ε-caprolactone) (PCL) based on an amine terminated PCL (NH_2-$PCL_{4.2k}$) or its mixture with monomethoxypoly(ethylenglycol)-PCL ($mPEG_{1k}$-PCL_{4k}). Positively-charged NPs were obtained, switching to net negative values through adsorption of low molecular weight hyaluronan (HA). NPs exposing both amine and PEG groups on the surface showed a larger Fixed Aqueous Layer Thickness as compared to fully PEGylated NPs, suggesting that PEG conformation/localization is affected by the presence of amino groups. Stability of positively-charged NPs was affected by the presence of ions, while interaction with human plasma protein pool indicated a time-dependent protein corona formation imparting an overall negative charge. NPs induced hemolysis was low while cytotoxicity against A549 and Calu-3 lung cancer cell lines was cell-specific as well as dose and time-dependent. Finally, the presence of amino groups greatly changed in vivo biodistribution of NPs in tumor-bearing mice (lung colonization of B16F10 cancer cells) allowing amine/PEGylated NPs to accumulate mainly at target organ. Overall, this study demonstrates that NPs with a mixed amine/PEGylated surface show peculiar biological identity that alters their interaction in the bioenvironment and thus worth of further investigation in chemotherapeutic delivery.

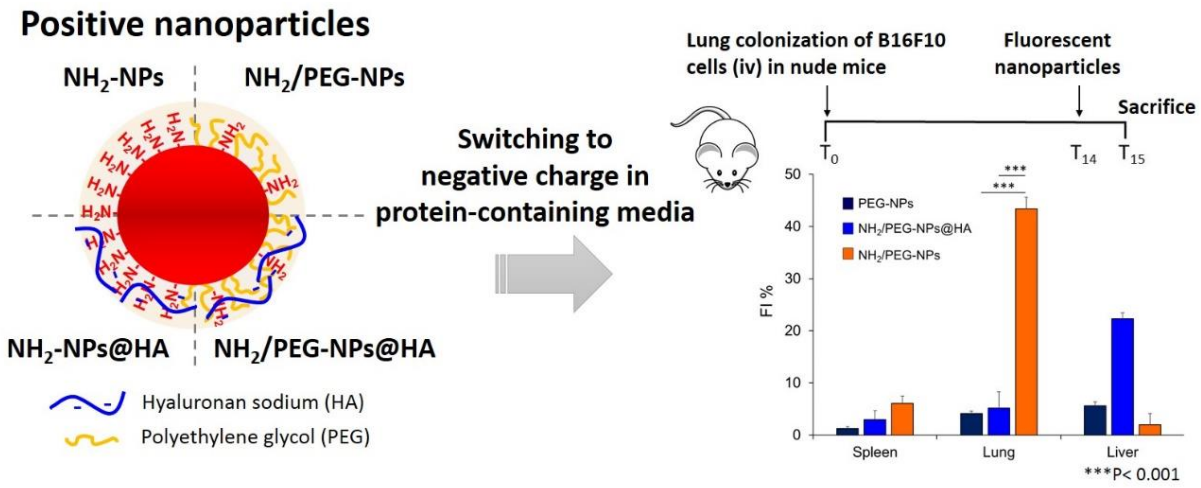

1.1 Introduction

Biodegradable polymer-based nanoparticles (NPs) are emerging in the treatment of several diseases, including cancer, due to the advantage to manipulate their features by selecting polymer type and tuning the mode of carrier assembly. [1-3] For a rational design of NPs, the size and surface properties are of key importance to control interactions with body environment at molecular, cell and tissue/organ level.[4-8] It is widely accepted that polymeric NPs surrounded by a hydrophilic shell of polyethylenglycol (PEG) are able to evade the mononuclear phagocyte system (MPS) and to long circulate once intravenously injected.[9-11] The presence of a hydrophilic fringe represents a surpassing tool also in the light of NPs stability in aqueous media since aggregation phenomena are efficiently limited. Despite these advantages, PEGylation critically affects NP/cell interaction acting as a 'steric' barrier to NPs internalization.[12]

In the context of biodegradable materials, PEGylated polyesters have been widely employed in drug delivery applications due to their biocompatibility and biodegradation to non-toxic products.[13-15] Block copolymers of PEG and poly(ε -caprolactone) (PCL) have gained attention due to possibility to tune PEG conformation on the surface. Through proper synthetic strategies, PEG-PCL copolymers with different copolymer architectures (diblock, triblock, star-shaped or branched) and hydrophilic/lipophilic balance are obtained and nanoassembled forming different delivery platforms (micelles, polymersomes, NPs, nanocapsules). This formulation versatility allows efficient entrapment of both hydrophilic and lipophilic drug cargo.[14] In the case of diblock copolymers, PEG/PCL chain length and the mode of copolymer assembly are crucial to drive the PEG orientation on the surface, eventually affecting interaction with proteins and biological response in vitro and in vivo.[16-18] In fact, PEG-PCL NPs were found mainly to alleviate toxicity profile of a lipophilic chemotherapeutic cargo as compared to commercial formulations due to increased circulation time.[14]

To promote accumulation in solid tumours, and in turn to improve therapeutic potential, pioneering studies have shown that PEGylated cationic liposomes demonstrated superior effectiveness in targeting tumour versus normal vascular networks.[19] More recently, it has been shown that PEGylated cationic NPs possess unique ability to penetrate deeply inside tumour tissue[20, 21] and, although slightly inferior in blood circulation and tumour accumulation as compared to their neutral and anionic counterpart, they are more effective in inhibiting tumour growth in subcutaneous CT26 and BX-PC3 tumour xenografts.[21, 22] In fact, an elevated glycolysis in different cancer cell lines leads to a higher level of lactate secretion as compared to normal cells, generating negative surfaces with high affinity toward cationic nanocarriers[20].

This has prompted a renewed interest in developing NPs with a positive charge to expand the arsenal of nanotools for the delivery of chemotherapeutics [23, 24].

Cationic NPs are usually prepared through adsorption of cationic surfactants, polymers or phospholipids on the surface of a preformed biodegradable nanotemplate[25], while only recently NPs prepared from amine-bearing biodegradable polymers have been proposed.[26]

In the attempt to extend the benefit of bearing a positive charge to PCL-based NPs through synthetic strategies, herein we have developed amine-functionalized NPs based on an amine terminated PCL ($PCL_{4.2k}$-NH_2) and its mixture with monomethoxy-PEG-PCL ($mPEG_{1k}$-PCL_{4k}) (Scheme 1). Further functionalization of amine NPs with hyaluronan (HA) has been carried out to modify the surface charge toward negative values and eventually to encourage uptake in CD44+ tumors through receptor-mediated endocytosis. In view of an intravenous administration, NPs interaction with human plasma has been investigated to get knowledge of their biological identity[27, 28]. Hereafter, haemolysis and cytotoxicity were carried out in different lung cancer cell lines. Finally, in vivo biodistribution of NPs in an experimental mice model of lung metastasis has been investigated.

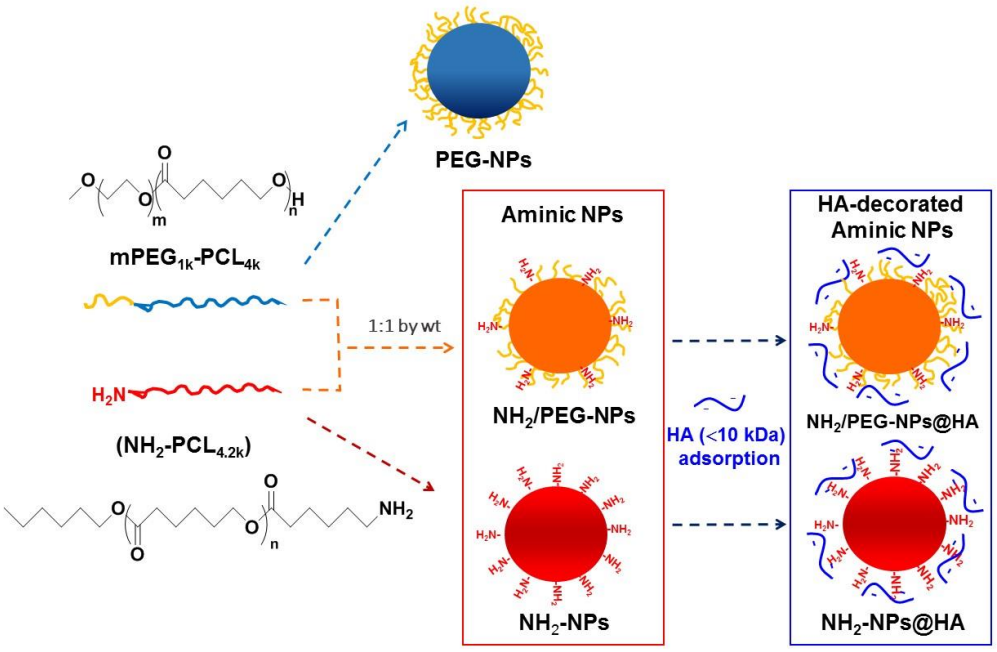

Scheme 1. Schematic representation of synthesized polymers and prepared NPs. NPs were designed to bear on the surface amine groups (NH_2-NPs) or amine/PEG groups (NH_2/PEG-NPs). To shield amines, sodium hyaluronan (HA) was adsorbed on the surface. PEG-NPs were also tested as reference formulation.

1.2 Experimental

1.2.1 Materials

Monomethoxy-poly(ethyleneglycol) with Mn 1,0 kDa ($mPEG_{1.0k}$, Nanocs Inc., New York, USA) was dehydrated by azeotropic distillation with dry toluene in a Dean-Stark trap. All reagents were purchased from Sigma-Aldrich (Milan, Italy). ε -caprolactone (CL) was distilled over CaH_2 under vacuum. Stannous-(2-ethylhexanoate)$_2$ ($Sn(oct)_2$), triethylamine (TEA), tosyl chloride (TsCl), triphenylphosphine (PPh_3) and sodium azide were used without further purification. 1-hexanol was dried according to a standard procedure. All solvents (analytical grade) were purchased from Sigma-Aldrich. N,N-dimethylformamide (DMF) and dichloromethane (DCM) were dried before use according to standard procedures (Armarego and Chai, Purification of Laboratory Chemicals, 7th Edition). Sodium hyaluronan (HA, MW < 10 kDa) was a kind gift of Magaldi Life S.r.l. Did-oil was provided by Sigma Aldrich. All other solvents were used as received.

1.2.2 Polymer characterization

FTIR analysis was performed with a Perkin-Elmer spectrometer (Paragon 500) equipped with a ZnSe attenuated total reflectance (ATR) crystal accessory. Samples were placed in direct contact with the ATR crystal and pressed with a pressure clamp positioned over the crystal/sample area to allow intimal contact between the material and the crystal. Spectra were acquired in the 4000 - 400 cm^{-1} range, at a resolution of 2 cm^{-1} (average of 20 scans). 1H NMR spectra were recorded with a Bruker Avance DPX400 apparatus operating at 400 MHz. For GPC analysis, samples were dissolved in THF and passed through a 0.22 μm PTFE membrane filter. Measurements were performed on an injected volume of 100 μL by using a Malvern-Viscotek GPC MAX/TDA 305 quadruple detector array equipped with a precolumn and two Phenogel columns (Phenomenex) with exclusion limits 106 and 103 Da, respectively. The GPC instrument was used at a flow rate of 0.8 mL/min and at columns and system temperature of 35 °C. Triple detectors calibration was based on a standard of polystyrene with molecular weight 104,959 Da.

1.2.3 Polymer synthesis

Synthesis of mPEG-PCL diblock copolymer

The linear diblock copolymer was prepared by ring-opening polymerization (ROP) of CL at 120 °C for 24 h using $mPEG_{1.0k}$ as initiator and $Sn(Oct)_2$ as catalyst (20% by mol).[18]

CL/initiator molar ratio = 36. 1H NMR ($CHCl_3$, δ in ppm), PCL block: 1.29–1.78 (m), 2.19–2.43 (t) 3.20 (m); 3.92–4.21 (t), 4.31(t); PEG block: 4.10 (t), 3.64 (s), 3.38 (t). GPC analysis: Mw = 6.74 kDa; Mn = 5.06 kDa; Mw/Mn = 1.33.

1.2.4 Synthesis of monoamino-PCL ($PCL_{4.2k}$-NH_2)

Step 1. Synthesis of monohydroxyl-PCL ($PCL_{4.2k}$-OH). 1-hexanol (100 mg, 0.98 mmol), CL (3.912 g, 34.3 mmol), Sn $(Oct)_2$ (79.0 mg, 0.196 mmol) was charged in a flask under dry nitrogen. The polymerization was carried out under stirring at 120°C for 24 h. The polymer was dissolved in 5 mL of DCM, precipitated in cold hexane, filtered and finally dried (yield 94%). 1H-NMR ($CDCl_3$, δ in ppm): 1.29–1.78 (123H, m), 2.19–2.43 (74H, m), 3.92–4.21 (74H, t), 3.64 (2H, t); Mn evaluated by 1H NMR = 4.2 kDa. Mw (GPC) =4.2 kDa; Mw/Mn=1.14.

Step 2. Synthesis of monotosyl-PCL ($PCL_{4.2k}$-Ts). $PCL_{4.2k}$-OH (4.00 g, 0.955 mmol) was dissolved in 40 mL of DCM, then TEA (506 mg, 5.0 mmol,) and TsCl (953 mg, 5.0 mmol) were added. The solution was stirred at room temperature for 24 h. The polymer was dissolved in 20 mL of DCM, precipitated in cold hexane, recovered and finally dried (yield 92%). 1H-NMR ($CDCl_3$, δ in ppm): 1.29–1.78 (123H, m), 2.19–2.43 (74H, m), 3.92–4.21(74H, t), 3.64 (2H, t), 7.79 (2H, d), 7.49 (2H, d), 2.43 (3H, s).

Step 3. Synthesis of monoazido-PCL ($PCL_{4.2k}$-N_3). $PCL_{4.2k}$-Ts (3.5 g, 0.88 mmol) dissolved in 15 mL of dry DMF was charged in a flask under nitrogen, then NaN_3 (229 mg, 3.52 mmol) was added, and the mixture was stirred at 90 °C overnight. The reaction was stopped by cooling to room temperature, the solution was filtered and DMF removed under vacuum. The residue was dissolved in 15 mL of DCM and the solution was extracted twice with brine and twice with water in a separating funnel. The organic phase was dried over anhydrous Na_2SO_4, concentrated and poured in cold hexane to precipitate the final polymer (yield 80%). 1H-NMR ($CDCl_3$, in ppm): 1.29–1.78, (123H, m), 2.19–2.43, (74H, m); 3.92–4.21(74H, t), 3.64 (2H, t). FTIR diagnostic band: 2107 cm^{-1} (N_3 stretching).

Step 4. Synthesis of $PCL_{4.2k}$–NH_2. $PCL_{4.2k}$-N_3 (2.0 g, 0.476 mmol) was dissolved in 50 mL of MeOH at 40 °C in a flask equipped with nitrogen inlet and refrigerator, then PPh_3 (N_3/PPh_3 molar ratio=1/3) was added and the reaction was carried out at 40 °C overnight. The solvent was removed by rotary evaporation and the product was dissolved in 10 mL of DCM, precipitated in cold hexane and dried under vacuum (yield 94%). The occurrence of the reaction was confirmed by FTIR through disappearance of the 2107 cm^{-1} N_3 stretching band. 1H-NMR

($CDCl_3$, in ppm): 1.29–1.78, (123H, m), 2.19–2.43, (74H, m); 3.92–4.21(74H, t), 3.64 (2H, t), 2.48 (2H, broad).

1.2.5 Preparation and characterization of NPs

PEGylated NPs (PEG-NPs), amine NPs (NH_2-NPs) and PEGylated amine NPs (NH_2/PEG-NPs) were prepared by solvent-diffusion method. In this latter case, $mPEG_{1k}$-PCL_{4k} and $PCL_{4.2k}$-NH_2 at 1:1 w/w ratio were mixed. Amine NPs were further decorated with a layer of HA thus obtaining NH_2-NPs@HA and NH_2/PEG-NPs@HA. Briefly, 10 mg of polymers were dissolved in 2 mL of acetone and added drop by drop in 4 mL water containing 4 mg Pluronic®F68 under stirring. Acetone was removed by rotavapor for 5 min. Then NPs were split in 4 Eppendorf tubes (1 mL) and immediately characterized. For HA-decorated NPs, 100 µL of HA (4 mg/mL) were added in each tube (2 mg/mL of NPs on the basis of yield).

Fluorescent NPs loaded with Did-oil at 0.2% w/w were prepared too. In particular, 20 µg of Did-Oil were solubilized in 200 µL of MeOH and added to polymer solution in acetone. NPs were formed as reported above. Thereafter, NPs were washed twice with water by centrifugation at 13000 x g for 30 min. The supernatant was finally collected, and the Did-Oil content quantified through spectrofluorimetry at λ ex/ λ em 644 and 680 nm, respectively (RF-6000-Shimadzu). As reference, a calibration curve of Did-Oil in methanol (concentration range 0.1-5.5 µg/mL) was constructed.

The hydrodynamic diameter (D_H), polydispersity index (PI) and zeta potential (ζ) of NPs were determined on a Zetasizer Nano ZS (Malvern Instruments Ltd.).

Results are reported as the mean of three separate measurements on three different batches (n=9) ± standard deviation (SD).

1.2.6 Evaluation of primary amines on NP surface

The evaluation of amine groups on NPs surface was carried out through fluorescamine assay. Briefly, a fluorescamine stock solution in DMSO was prepared (3 mg/mL) and 3 µL of this stock solution were incubated in 1 mL of NPs in water (500 µg/mL) for 15 min. Thereafter, emission spectra at λ ex 350 nm were collected.

1.2.7 FALT measurements

Fixed aqueous layer thickness (FALT) was measured by monitoring the influence of ionic strength on particle surface charge. Different amount of NaCl stock solutions at different

concentrations were added to a NP dispersion in water (0.5 mg/mL) and ζ of the samples was measured. A plot of ln (ζ) against 3.33·[NaCl]0.5 gives a straight line where the slope represents the thickness of the PEG shell in nm.

Stability studies of NPs

The stability of NPs under physiologically relevant conditions was assessed by dispersing a known amount of NPs (2 mg/mL) in either 10 mM phosphate buffer saline at pH 7.4 (PBS) or DMEM/FBS+ and incubating the sample at 37 °C under mild stirring. D_H and ζ of the samples were taken after 30 min of incubation.

1.2.8 Interaction with blood components

The behaviour of NPs in human plasma (Sigma Aldrich) was evaluated by monitoring D_H, ζ and scattering. Briefly, 500 µL of NPs (2 mg/mL) were added to 500 µL of human plasma and incubated at 37°C for different times (15 min, 24 h and 48 h). D_H and ζ were evaluated as reported above while for scattering measurements, the absorbance of the samples at 500 nm was collected on an UV spectrophotometer (Shimadzu UV 1800). Haemolysis of human red blood cells (RBC) was evaluated on EDTA-treated human blood from healthy volunteers (after informed ethical consent). The blood samples were collected from the student health care complex at University of Napoli Federico II, Italy. Blood was centrifuged at 880 x g for 5 min. RBC pellet was diluted with 0.1 M PBS up to a concentration of 10% v/v. The RBC dispersion (0.1 mL) was added to 0.9 mL of a NPs dispersion in PBS (0.5 mg/mL). The sample was incubated at 37 °C for 30 minutes and centrifuged at 1000 x g for 10 minutes. The supernatant was collected and analysed for haemoglobin release by spectrophotometry at 416 nm. To obtain 0 and 100% haemolysis, 0.1 mL of RBC dispersion was added to 0.9 mL of PBS and distilled water, respectively. The degree of haemolysis was determined by the following equation: Haemolysis (%) = (ABS-ABS0)/(ABS100-ABS0) x 100, where ABS100 and ABS0 are the absorbance of the solution at 100% and 0% haemolysis, respectively.

1.2.9 Cell cultures and treatments

A549 and Calu-3 cell lines were purchased from American Type Culture Collection (Rockville, MD, USA) and were authenticated by LGC Standards (Sesto San Giovanni, Italy). Cells were cultured in DMEM with glutamax (Invitrogen, Carlsbad, California) supplemented with 10% FBS, 2 mM L-glutamine and penicillin-streptomycin 50 U/mL. Treatments of cells were performed as previously reported [29].

1.2.10 MTT assay

A549 and Calu-3 cells were seeded onto 96-well plates (2 × 104 cells/well) and incubated with NPs (concentration range 0.1-0.75 mg/mL) for 24, 48 and 72 h. Then, cell viability was evaluated as metabolic activity using the MTT assay. The absorbance was measured at 540 nm using a microplate reader (Labsystems Multiskan, MS).

Biodistribution in mice

The biodistribution of NPs was tested in forty-eight weeks-old nude female mice obtained from Harlan (SanPietro al Natisone, Italy). Mice were housed five per cage and maintained on a 12 h light:12 h dark cycle (lights on at 7:00 a.m.) in a temperature-controlled room (22 ± 2 C°) and with food and water ad libitum. The present study was approved by the Animal Ethics Committee at National Cancer Institute - Foundation "G. Pascale", Naples - Italy, following the guidelines of Italian law (D.L. 26/2014) and in agreement with the European Union policy for experimental animal care and use (Directive 2010/63/EU). After one week of acclimation to the housing conditions, mice were distributed into three groups (10 animals/group) and injected with 3x105 B16F10 murine melanoma cells via tail vein (lung colonization model). Mice used in experiments were anesthetized with zolazepam (50 mg/Kg i.p.), xylazine (20 mg/Kg) and atropine sulphate (0.04 mg/Kg). All efforts were made to minimize animal suffering.

Mice received one intravenous administration into the caudal vein of NaCl 0.9% (control), PEG-NPs, NH_2/ PEG-NPs and NH_2/PEG NPs@HA loaded with Did-Oil 0.2% w/w. NP dose was 4 mg/Kg (corresponding to 8 μg Did-Oil/Kg). Mice were sacrificed 24 h post injection and the main organs were collected (liver, spleen, lung). Then each organ was weighted and homogenized as previously reported [29]. Fluorescence intensities of homogenized tissue sample were assessed by fluorimetry on a Cary Eclipse fluorescence spectrophotometer (Varian) at λ ex 650 nm and λ em 673 nm.

1.2.11 Statistical analysis

Unless otherwise stated, all data are shown as mean ± standard deviation (SD). Two-way analysis of variance (ANOVA) was applied for comparison of three or more group means (Tukey's multiple comparisons test). P value of <0.05 was considered statistically significant. ***, **, and * display $p< 0.001$, $p < 0.01$, and $p < 0.05$, respectively. Origin software was used for data analysis.

1.3 Results and discussion

1.3.1 Polymer characterization and synthesis

Monoamino-PCL was obtained by classical ROP using hexanol as initiator. The molecular weight was controlled by the CL/initiator molar ratio by designing a target value of around 4 kDa, close to the molecular weight of PCL block in the mPEG-PCL copolymer. The actual molecular weight was calculated by 1H NMR analysis by the ratio between the intensities of the resonance at 3.64 associated to the $–CH_2$-OH methylene protons, and those of the resonance at 2.31, associated to $-CH_2$-CO- units in the PCL chain. The experimental Mn value was 4.2 kDa, very close to the theoretical value calculated by the CL/initiator molar ratio in the feed. GPC analysis confirmed the molecular weight, with a polydispersity index of 1.14, indicating a narrow molecular weight distribution. Subsequently, PCL was modified at terminal hydroxyl following the same pathway already described in the literature in the case of PEG[30]. Briefly, monohydroxyl-PCL was first tosylated with tosyl chloride, then monoazide-PCL was obtained by substitution with sodium azide. The azide was finally reduced to amine with triphenylphosphine. The reduction was followed by FTIR, where the complete disappearance of the azide band at 2107 cm^{-1} was accounted for a complete conversion. The structure and purity of PCL-NH_2 and intermediates were confirmed by 1H NMR analysis.

mPEG-PCL diblock copolymer ($mPEG_{1k}$-PCL_{4k}) was synthesized according to a standard procedure widely reported in literature.[18]

1.3.2 Preparation and properties of amine-bearing NPs

NPs were designed with the aim to manipulate the amine surface density and to expose PEG for effective stabilization. NPs were prepared by nanoprecipitation of $mPEG_{1k}$-PCL_{4k} and NH_2-$PCL_{4.2k}$, alone or in 1:1 ratio by weight, thus obtaining respectively PEGylated NPs (PEG-NPs), amine NPs (NH_2-NPs) and PEGylated/amine NPs (NH_2/PEG-NPs). In a following step, a low molecular weight HA was spontaneously adsorbed on the top of the amine NPs (NH_2-NPs@HA and NH_2/PEG-NPs@HA (Scheme 1) taking advantage of electrostatic interactions.

NP codes and their properties are reported in Table 1 and in Fig. 1. In all the cases NPs with good yield and low PI were obtained. Sizes and zeta potential values in water were affected by the type of the polymer employed. PEG-NPs were below 100 nm and showed a negative ζ, whereas amine NPs were larger with a largely positive ζ. NPs prepared from a 1:1 mixture by wt of mPEG-PCL and NH_2-PCL had a size comparable to that of amine NPs but with intermediate charge presumably due to the presence of PEG chains shielding primary amine

groups. The larger size of amine NPs can be reasonably attributed to the poor hydrophilicity of amine PCL as compared to PEG-PCL, which slows down acetone diffusion in water during nanoprecipitation step.

Table 1. Properties of nanoparticles.

Formulation code	Size (nm ± SD) [b]	PI	ζ (mV ± SD) [b]	Yield (%)
PEG-NPs	83 ± 2	0.1	-2.5 ± 0.7	98
NH_2-NPs	120 ± 14	0.2	+33 ± 1.4	95
NH_2/PEG-NPs [a]	117 ± 3	0.1	+9.4 ± 4.8	97
NH_2-NPs@HA	178 ± 10	0.2	-28 ± 3.7	94
NH_2/PEG-NPs@HA [a]	141 ± 3	0.1	-10 ± 2.5	92

[a] Nanoparticles prepared with a NH_2 PCL/mPEG-PCL mixture at 1:1 ratio by weight.
[b] SD was calculated on three different batches.

The density of amino groups on NPs surface was assessed by a fluorescamine based assay (FA). Fluorescamine is a non-fluorescent molecule (ABS maximum at 350 nm) which emits fluorescence only in the presence of primary amines due to complex formation. As shown in Fig. 1C, only amine NPs induced FA emission due to formation of hydrogen bonds on NPs surface whereas no fluorescence was observed for PEG-NPs. As expected, the number of amine groups on NPs surface was higher for NH_2-NPs than NH_2/PEG-NPs, in line with composition and zeta potential values. These results further suggest that amine groups on the surface are accessible also in the presence of PEG thus giving a mixed amine/PEGylated surface.

Despite their net positive charge, cationic NPs are prone to aggregate in ion-rich media (and presumably also in biological fluids) due to perturbation of ionic double shell.[31] As shown in Fig. 1B, NH_2- NPs showed an apparent 3-folds increase of mean size in PBS, which was limited by the presence of PEG in NH_2/PEG-NPs. To alter ionic nanoenvironment around NPs due to the presence of amine groups, negatively charged HA was adsorbed on their surface as recently proposed to stabilize cationic NPs.[32] As shown in Fig. 1A, HA reversed ζ values of amine NPs from positive to negative values due to electrostatic anchoring on cationic NPs surface. HA decoration allowed to limit size increase in PBS only for NH_2/PEG-NPs due to the cooperative shielding effect of PEG.

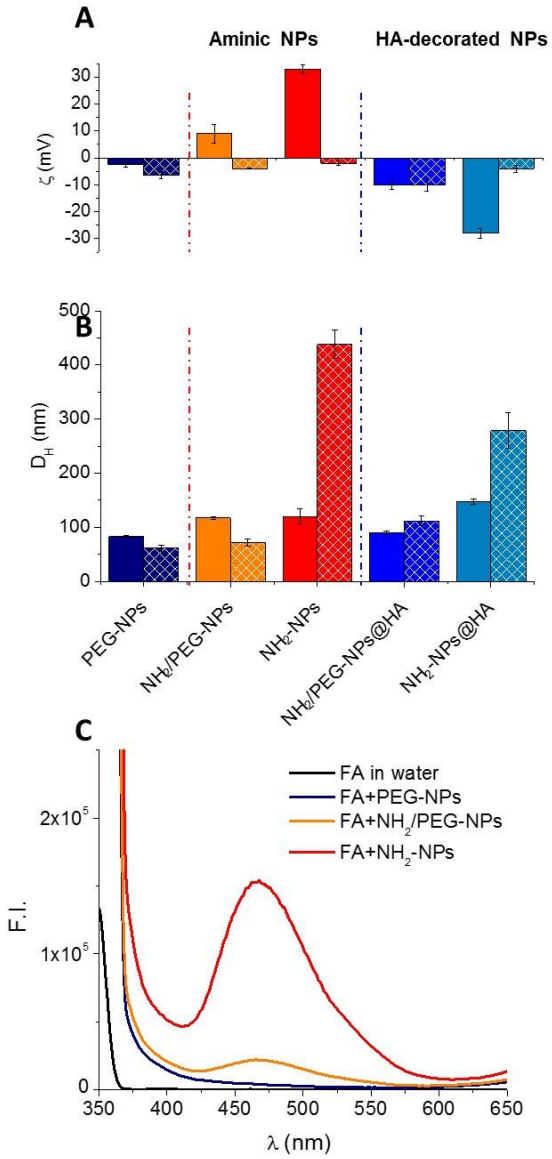

Fig. 1. NPs properties. A) Zeta potential (ζ) and B) Hydrodynamic diameter (D_H) of NPs in water (full bars) and PBS at pH 7.4 (square bars). Results are the mean of three measurements obtained on three different NP batches ±SD; C) Emission spectra (λ ex 350 nm) of fluorescamine (FA) (3 μg/mL) in the presence of NPs. F.I. maximum is dependent on the number of amine groups on the surface., the spectrum of FA is reported as control.

Fixed Aqueous Layer Thickness measurements were performed on PEGylated NPs to investigate the impact of composition on the orientation of PEG/HA chains in the shell (Fig. 2). PEGylated NPs showed the lowest PEG thickness whereas NH_2/PEG-NPs were characterized by a two-folds larger thickness, thus suggesting a more extended orientation of the PEG chains on NP shell. These results demonstrate that the presence of amino groups on NPs surface can critically affect PEG conformation offering a novel and additional tool to modulate NPs interface. The electrostatic interaction with HA macromolecules did not alter significantly the thickness of the hydrophilic shell, suggesting the intercalation of HA with PEG chains.

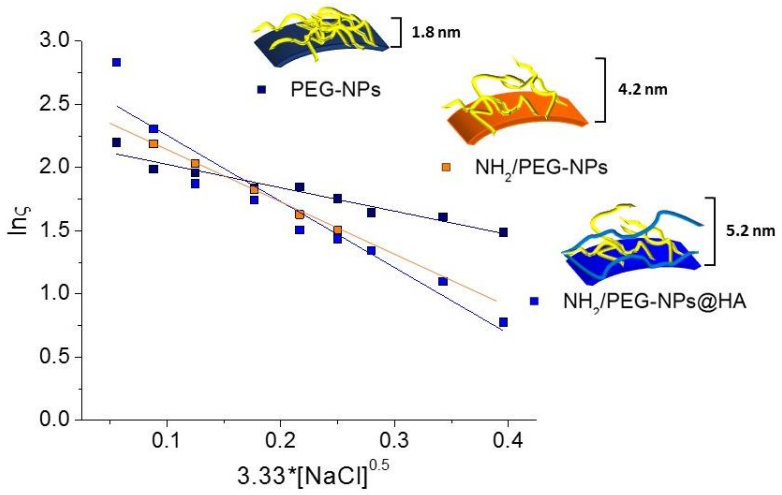

Fig. 2. FALT measurements on PEGylated NPs as assessed by monitoring ζ at different NaCl concentrations (representative curves are shown). The slope of the interpolated straight line represents the thickness of the PEG shell in nm (d shell). FALT values are the mean of three measurements obtained on three different NP batches (SD was below 0.2 nm).

1.3.3 Interaction with blood components

To get preliminary insights into the behavior of NPs after i.v. injection, their interaction with human plasma along time was investigated (Fig. 3). Indeed, the presence of ions and the formation of a protein corona may mask the surface of NPs imparting a specific biological identity. Consequently, these interactions should be considered since they have a huge impact on their journey in the body. As shown in Fig. 3A, amine-bearing NPs switched from net positive to negative values of ζ upon contact with plasma, which is suggestive of surface adsorption of protein pool. Thereafter, all NPs formulations displayed negative ζ stably around -10 mV. Accordingly, D_H of amine NPs in human plasma at 15 min slightly increased as compared to that in water while for HA-coated NPs, no significant change took place (Fig. 3B). Progressive increase of size was observed in the case of amine NPs and fully PEGylated NPs demonstrating that reorganization of protein corona can occur along time.[33] Scattering of NP samples (Fig. 3C) and size distribution curves were not altered up to 48 h, except for NH_2-NPs for which protein adsorption impacted remarkably on particle-to-particle interaction inducing aggregation. HA adsorption on amine NPs alleviated aggregation, as shown previously for PBS. No significant effect of NPs features on haemolysis of red blood cells was found (Fig. 3D).

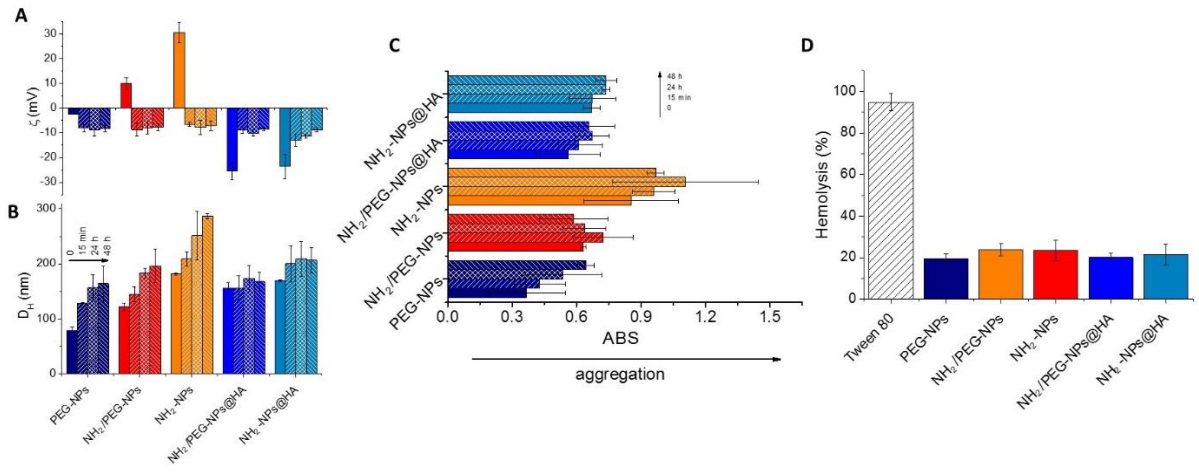

Fig. 3. NPs behaviour in human plasma A) zeta potential (ζ) and B) Hydrodynamic diameter (DH) of NPs dispersed in human plasma at 37°C; C) Scattering of NPs in human plasma (ABS at 500 nm); D) Haemolytic activity of NPs (Tween 80 is reported as positive control). Results are the mean of three measurements obtained on three different NP batches ±SD.

Overall, these results suggest that biological identity of amine NPs is far from the designed chemical identity and remarkably affected by interactions with plasma protein pool, as suggested previously for polyethylenimine-coated polymeric NPs and iron oxide NPs. Based on the stability results, PEGylated NPs (NH_2/PEG-NPs, its HA-coated counterpart and reference PEG-NPs) were selected for the following biological study. To track NPs in cells and in vivo, fluorescent NPs loading DiD-Oil were prepared and characterized (data not shown).

1.3.4 Cell studies

As far as the impact of surface modification on cytotoxicity is considered, colloidal properties (D_H, PI and ζ) of selected NPs in DMEM FBS+ were evaluated (data not shown). All NPs tested did not aggregate in the medium and maintained a size below 250 nm. In analogy to the behaviour in human plasma, NPs surface charge switched to negative values due to electrostatic/hydrophobic adsorption of FBS proteins.

Cytotoxicity was assessed by the MTT assay on Calu-3 and A549 lung cancer cells in a range of NP concentrations upon 24 h, 48 and 72 h of treatment. Results in Fig. 4 show a dose- and time-dependent toxicity at the tested concentrations, which was much more evident in Calu-3 cells (Fig 4B). These cells exhibited a higher sensitivity in response to NPs treatments, independently of NPs composition. In fact, their viability upon time exposure to NPs decreased much more than that of A549 cells at all tested NPs concentrations. These results suggest that

NPs are presumably partially covered with FBS proteins since their cytotoxicity is not fully attenuated as demonstrated for NPs coated with polyethyleneimine.[32] These differences of sensitivity to NPs treatments between cell types, which has been reported in the literature[34], could be attributed to the molecular specificity of each cell type and consequent biological response. A possible role could be played by p53 expression levels as we used two cell lines that express (A549) or not (Calu-3) p53. Since it is already known that intracellular signalling pathways activated in response to cellular stress depend on the presence of p53[35], it is possible to hypothesize that the differences in cell toxicity to NPs treatments are due to the p53 status.

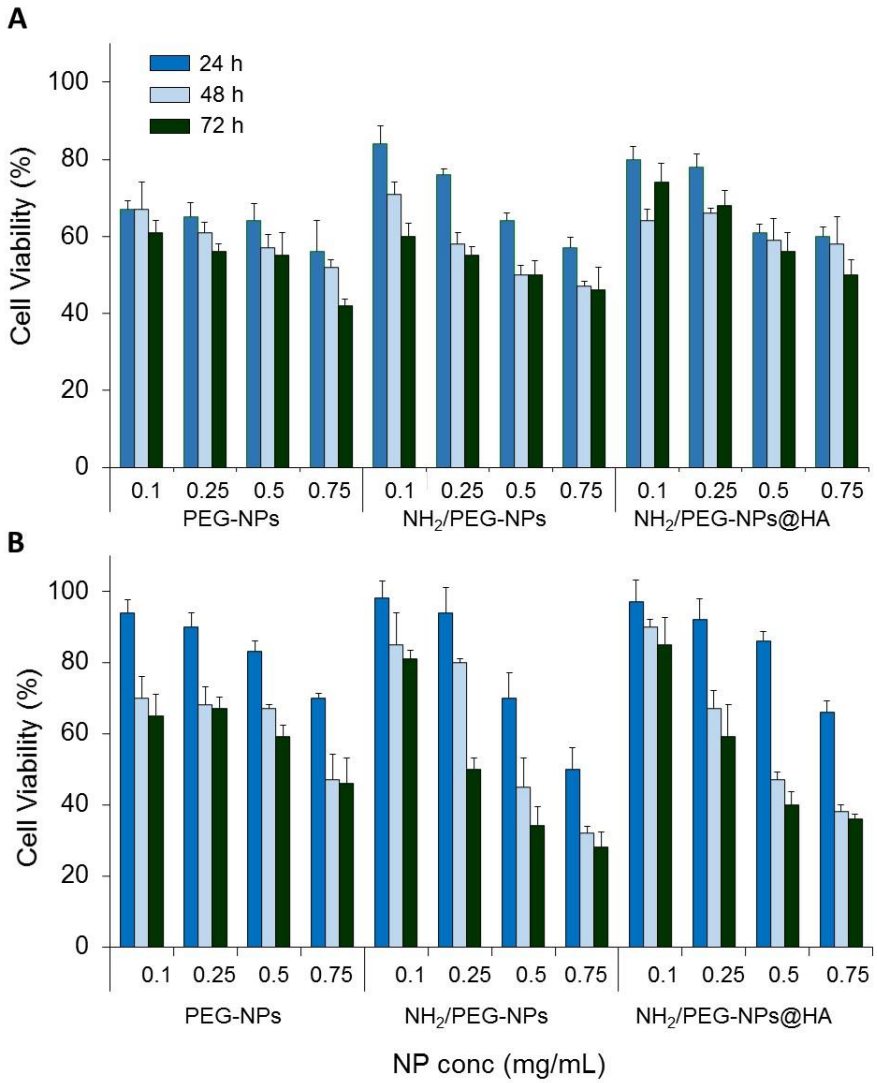

Fig. 4. Viability of A549 (A) and Calu-3 (B) lung cancer cells upon exposure to increasing concentrations of NPs for 24, 48 and 72 h. After incubation, cell viability was evaluated using the MTT assay. The cell viability from untreated control was set to 100%. Results are presented as percentage (mean ± SEM) (n = 3) of the control cells.

HA-coated NPs can be accumulated in cancer cells overexpressing CD44 receptor via receptor-mediated endocytosis. Since A549 express high levels of CD44, internalization of non-coated and HA coated NPs in this cell line was compared. Results demonstrated no benefit of HA surface decoration, suggesting no targeting ability of the HA coating adsorbed on NH_2/PEG-NPs and in line with the formation of a protein corona shielding HA-coated NPs/CD44 recognition.

1.3.5 Biodistribution in mice

After i.v. injections, PEGylated NPs are expected to long-circulate, to evade immune recognition altering the biodistribution of their drug cargo. Besides size and shape, the fate of spherical PEGylated NPs is strictly dictated by surface features which regulate blood protein adsorption and composition of protein corona and drive NPs to their final destination in the body.[36] It has been found that PEG-PCL NPs display different circulation time and, in turn, dose fraction reaching tumor in mice xenographts depends on size and PEG surface conformation.[37] In fact, although designed to accumulated in solid tumors via Enhanced Permeability and Retention (EPR) effect, PEGylated NPs accumulate greatly in non-target organs of MPS, i.e. spleen and liver. This aspect is of utmost importance when targeting solid tumors in general but much more relevant for lung metastasis since capillary bed at lung is the first area NPs encounter after i.v. injection.[38] .To understand the impact of NPs surface features on their lung accumulation, biodistribution of i.v. injected NPs in a mice model of B16F10 melanoma cells lung colonization, which is an experimental model for lung metastasis, was evaluated. DiD-Oil-loaded fluorescent NPs dispersed in saline were administered via tail vail and animals sacrificed after 24 h. Spleen, liver and lung (the target organ) were collected, processed and their fluorescence evaluated. As clearly evidenced in Fig. 5, the level of NPs into MPS organs and at lung was strongly depending on the NPs properties.

In fact, NH_2/PEG-NPs accumulated in higher extent in the lung, where cancer cells are disseminated, as compared to analogous HA-coated NPs, which preferentially distributed to liver. This behaviour could not be due to size, since NH_2/PEG-NPs and NH_2/PEG-NPs@HA display comparable size. On the other hand, smaller PEG-NPs were found in MPS organs and lung in comparable amounts. Thus, the presence of a cationic charge on NPs and switch to a new biological identity, driven by dynamics of plasma protein fouling, may be responsible of their accumulation in the lung and hopefully in situ delivery of therapeutic cargo.

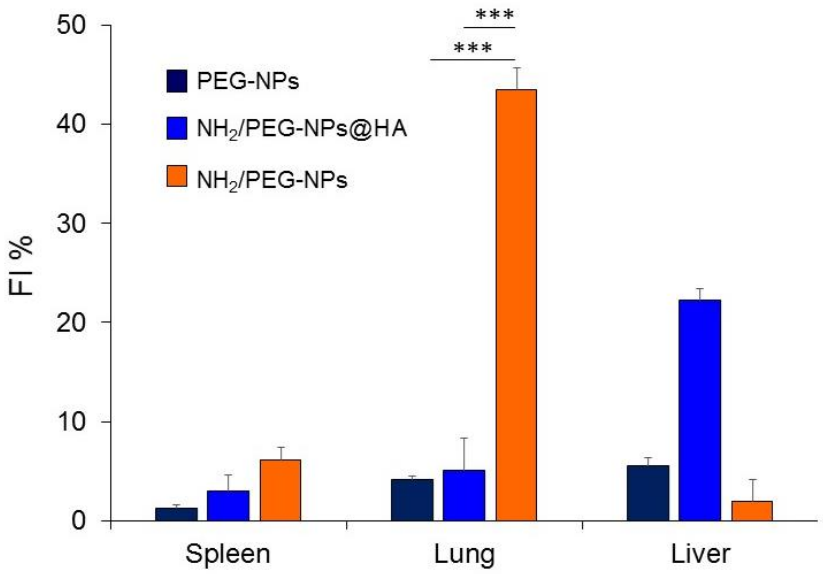

Fig. 5. Quantitative in vivo organ distribution of intravenously injected DiD-Oil loaded NPs. Mice were i.v. injected with 3x105 B16F10 murine melanoma cells via tail vein (lung colonization model). Fluorescence of treated organs was assessed at λ ex 650 nm and λ em 673 nm. Results are the mean of three measurements ±SD.

1.4 Conclusions

In this work, we have prepared a series of polymeric PCL-based amine NPs with different surface properties and charge densities, investigating their properties both in vitro and in vivo. Size, zeta potential, shell features and interaction with proteins were remarkably affected by the presence of primary amines, PEG chains and a HA coating on the surface NPs were well tolerated by human red blood cells while showing different cytotoxicity profile against lung cancer cells. Finally, in vivo biodistribution studies demonstrated a much higher accumulation of cationic/PEGylated NPs at the targeted organ. Taken together, the strategy proposed here paves the way to the development of a novel class of positively-charged PEGylated NPs with a great potential in the delivery of chemotherapeutics at different disease stage.

Acknowledgments

This work was supported by Italian Association for Cancer Research (IG2014#15764).

References

1. M. S. Singh, S. N. Tammam, M. A. Shetab Boushehri and A. Lamprecht, Pharmacological Research, 2017, 126, 2-30.

2. S. Wilhelm, A. J. Tavares, Q. Dai, S. Ohta, J. Audet, H. F. Dvorak and W. C. W. Chan, Nature Reviews Materials, 2016, 1, 16014.

3. E. Blanco, H. Shen and M. Ferrari, Nature Biotechnology, 2015, 33, 941.

4. N. Bertrand and J. C. Leroux, Journal of Controlled Release, 2012, 161, 152-163.

5. N. H. Abd Ellah and S. A. Abouelmagd, Expert Opinion on Drug Delivery, 2017, 14, 201-214.

6. N. Hoshyar, S. Gray, H. Han and G. Bao, Nanomedicine: nanotechnology, biology, and medicine, 2016, 11, 673-692.

7. A. Verma and F. Stellacci, Small, 2010, 6, 12-21.

8. C. Bantz, O. Koshkina, T. Lang, H.-J. Galla, C. J. Kirkpatrick, R. H. Stauber and M. Maskos, Beilstein Journal of Nanotechnology, 2014, 5, 1774-1786.

9. J. V. Jokerst, T. Lobovkina, R. N. Zare and S. S. Gambhir, Nanomedicine (London, England), 2011, 6, 715-728.

10. R. Gref, A. Domb, P. Quellec, T. Blunk, R. H. Muller, J. M. Verbavatz and R. Langer, Advanced Drug Delivery Reviews, 2012, 64, 316-326.

11. R. Gref, M. Lück, P. Quellec, M. Marchand, E. Dellacherie, S. Harnisch, T. Blunk and R. H. Müller, Colloids and Surfaces B: Biointerfaces, 2000, 18, 301-313.

12. S. Mishra, P. Webster and M. E. Davis, European Journal of Cell Biology, 2004, 83, 97-111.

13. C. Conte, I. d'Angelo, A. Miro, F. Ungaro and F. Quaglia, Current topics in medicinal chemistry, 2014, 14, 1097-1114.

14. P. Grossen, D. Witzigmann, S. Sieber and J. Huwyler, Journal of Controlled Release, 2017, 260, 46-60.

15. K. Zhang, X. Tang, J. Zhang, W. Lu, X. Lin, Y. Zhang, B. Tian, H. Yang and H. He, Journal of controlled release: official journal of the Controlled Release Society, 2014, 183, 77-86.

16. F. Ungaro, C. Conte, L. Ostacolo, G. Maglio, A. Barbieri, C. Arra, G. Misso, A. Abbruzzese, M. Caraglia and F. Quaglia, Nanomedicine-Nanotechnology Biology and Medicine, 2012, 8, 637-646.

17. C. Conte, I. Fotticchia, P. Tirino, F. Moret, B. Pagano, R. Gref, F. Ungaro, E. Reddi, C. Giancola and F. Quaglia, Colloids Surf B Biointerfaces, 2016, 141, 148-157.

18. A. Venuta, F. Moret, G. Dal Poggetto, D. Esposito, A. Fraix, C. Avitabile, F. Ungaro, M. Malinconico, S. Sortino, A. Romanelli, P. Laurienzo, E. Reddi and F. Quaglia, Eur J Pharm Sci, 2018, 111, 177-185.

19. R. B. Campbell, D. Fukumura, E. B. Brown, L. M. Mazzola, Y. Izumi, R. K. Jain, V. P. Torchilin and L. L. Munn, Cancer Research, 2002, 62, 6831.

20. B. Chen, W. Le, Y. Wang, Z. Li, D. Wang, L. Ren, L. Lin, S. Cui, J. J. Hu, Y. Hu, P. Yang, R. C. Ewing, D. Shi and Z. Cui, Theranostics, 2016, 6, 1887-1898.

21. H.-X. Wang, Z.-Q. Zuo, J.-Z. Du, Y.-C. Wang, R. Sun, Z.-T. Cao, X.-D. Ye, J.-L. Wang, K. W. Leong and J. Wang, Nano Today, 2016, 11, 133-144.

22. G. Wang, Y. Chen, P. Wang, Y. Wang, H. Hong, Y. Li, J. Qian, Y. Yuan, B. Yu and C. Liu, Acta Biomaterialia, 2016, 29, 248-260.

23. Q. Sun, T. Ojha, F. Kiessling, T. Lammers and Y. Shi, Biomacromolecules, 2017, 18, 1449-1459.

24. T. Stylianopoulos, K. Soteriou, D. Fukumura and R. K. Jain, in Annals of Biomedical Engineering, 2013, vol. 41, pp. 68-77.

25. E. Bilensoy, Expert Opinion on Drug Delivery, 2010, 7, 795-809.

26. A. Reisch, A. Runser, Y. Arntz, Y. Mély and A. S. Klymchenko, ACS nano, 2015, 9, 5104-5116.

27. G. Caracciolo, O. C. Farokhzad and M. Mahmoudi, Trends in biotechnology, 2017, 35, 257-264.

28. J. Lazarovits, Y. Y. Chen, E. A. Sykes and W. C. Chan, Chemical communications, 2015, 51, 2756-2767.

29. A. Russo, S. Maiolino, V. Pagliara, F. Ungaro, F. Tatangelo, A. Leone, G. Scalia, A. Budillon, F. Quaglia and G. Russo, Oncotarget, 2016, 7, 79670-79687.

30. R. Mahou and C. Wandrey, Polymers, 2012, 4, 561.

31. T. L. Moore, L. Rodriguez-Lorenzo, V. Hirsch, S. Balog, D. Urban, C. Jud, B. Rothen-Rutishauser, M. Lattuada and A. Petri-Fink, Chemical Society Reviews, 2015, 44, 6287-6305.
32. S. Maiolino, A. Russo, V. Pagliara, C. Conte, F. Ungaro, G. Russo and F. Quaglia, J Nanobiotechnology, 2015, 13, 29.

33. G. J. Pillai, M. M. Greeshma and D. Menon, Colloids and Surfaces B: Biointerfaces, 2015, 136, 1058-1066.

34. S. Lanone, F. Rogerieux, J. Geys, A. Dupont, E. Maillot-Marechal, J. Boczkowski, G. Lacroix and P. Hoet, Particle and Fibre Toxicology, 2009, 6, 14-14.

35. A. Russo and G. Russo, International Journal of Molecular Sciences, 2017, 18, 140.

36. H. R. Lakkireddy and D. Bazile, Advanced Drug Delivery Reviews, 2016, 107, 289-332.

37. X. J. Du, J. L. Wang, W. W. Liu, J. X. Yang, C. Y. Sun, R. Sun, H. J. Li, S. Shen, Y. L. Luo, X. D. Ye, Y. H. Zhu, X. Z. Yang and J. Wang, Biomaterials, 2015, 69, 1-11.

38. J. L. Perry, K. G. Reuter, J. C. Luft, C. V. Pecot, W. Zamboni and J. M. DeSimone, Nano letters, 2017, 17, 2879-2886.

ANNEX-II

Surface exposure of PEG and amines on biodegradable nanoparticles as a strategy to tune their interaction with protein-rich biological media*

* this work has been published as:

Claudia Conte, Giovanni Dal Poggetto, Benjamin J. Swartzwelter, Diletta Esposito, Francesca Ungaro, Paola Laurienzo, Diana Boraschi, Fabiana Quaglia, ***Nanomaterials*** **2019, *9*(10), 1354**

ABSTRACT

Nanoparticles (NPs) based on amphiphilic block copolymers of polyethylene glycol (PEG) and biodegradable polyesters are of current interest in drug nanodelivery due to easy manipulable properties. The interaction of these NPs with biological environments is highly influenced by shell features, which drive biological identity after administration. To widen the strategies available for tuning particle surface chemistry, here we have developed a panel of amine-bearing PEGylated NPs with a poly(ε-caprolactone) (PCL) core for the delivery of lipophilic drugs, and investigated the impact of NP modifications on their interaction with abundant circulating proteins (human serum albumin -HSA- and mucin), as well as their transport through biological barriers (artificial mucus -AM, extracellular matrix -ECM). We prepared NPs based on a diamino-terminated PCL (amine-NPs) and its mixture with PEG-PCL copolymers (amine/PEG-NPs) at different PEG molecular weights by nanoprecipitation, as well as corresponding NPs of PEG-PCL (PEG-NPs). The presence of an amine-bearing polymer resulted in NPs with a net positive charge and a zeta potential dependent on the length of PEG in the copolymer. Amine/PEG-NPs had a larger Fixed Aqueous Layer Thickness as compared to PEG-NPs, suggesting that PEG conformation is affected by the presence of positive charges. In general, amine-bearing NPs interacted promptly with the dysopsonic protein HSA, due to electrostatic interactions, and lose stability thereby undergoing time-related aggregation. On the other hand, amine/PEG-NPs interaction with mucin, induced switching to a negative surface charge but did not alter the quality of the dispersion. Transport kinetics of NPs through a layer of artificial mucus and tumor extracellular matrix was studied by means of fluorescent NPs based upon FRET. Amine/PEG-NPs did not cross the ECM but they were promptly transported through AM, with swifter transport noted at increasing MWs of PEG in the copolymer. Finally, we demonstrated that all the different NP types developed in this study are internalized by human monocytes and, despite the positive charge, they did not induce measurable inflammatory effect. In conclusion, we show that the concurrent presence of both PEG and amine groups on the NP surface is a promising strategy for directing their interaction with body compartments. While PEG-NPs are confirmed for their capacity to cross ECM-like compartments, amine/PEG-NPs are revealed as a powerful platform to widen the arsenal of nanotools available for overcoming mucus-covered epithelia.

1.1 Introduction

PEGylated biodegradable nanoparticles (NPs) based on amphiphilic block copolymers are earning increased attention in the nanodelivery field due to their complete degradability in the body, ease of processing, and synthesis scalability. Owing to their core-shell structure, the hydrophobic inner compartment can host single or multiple drug(s), protect the payload from the harsh environment in the body, and ensure sustained release. On the other hand, the hydrophilic outer shell can be tailored toward deliberate interactions with the biological environment, besides providing superior physical stability to the entire manufacturing process [1,2]. The effects of PEGylation are closely related to the PEG molecular weight, the number of PEG chains located on the NP surface, and the corresponding orientation (brush/mushroom), each of which can be affected by the preparation method [3,4]. For nanomedical approaches that imply intravenous NP administration, PEGylation is the most common strategy to extend their half-life, since the hydrophilic PEG fringe hinders adsorption of opsonin on the NP surface, thus avoiding prompt recognition by the mononuclear phagocyte system [5,6]. PEGylation is also useful for improving NP transport through protein-rich gel barriers in the body [7,8]. Precise PEG physico-chemical properties and conformation on the particle surface are needed to effectively evade interaction with mucins and facilitate NP transport through mucus-covered epithelial barriers. One of the drawbacks of PEGylated NPs is that cell internalization is impaired, which decreases the delivery of the drug payload to intracellular targets. To overcome poor cell uptake, the preeminent strategy is the decoration of NPs with ligands that target receptors on the cell surface, thereby allowing for internalization via receptor-mediated endocytosis [9]. Recently, we have explored the modification of the surface features of biodegradable PEGylated NPs made of poly(ε -caprolactone) (PCL) in view of their application as a drug delivery platform. The introduction of amine groups on the surface, which imparts a positive charge to NPs, could in fact become an additional tool to expand the possibility to manipulate NPs properties and their interaction with the bioenvironment. Advantages of cationic NPs are mainly related to their unique ability to penetrate deeply inside tumour tissue [10,11] and bacterial biofilms, which could expand the arsenal of nanotools for the delivery of drugs through different routes [12,13]. Despite their potential, the strategies proposed thus far to build cationic NPs are limited, mainly relying on the adsorption of cationic surfactants, polymers or phospholipids on the surface of preformed biodegradable nanotemplates [14]. Only recently NPs prepared from ammonia-terminated [15] and amine-terminated biodegradable polymers have been reported [16]. Envisaging an application of

amine-bearing NPs in cancer, we demonstrated that size, surface charge, shell thickness, and interaction with human serum of these NPs were remarkably affected by the presence of PEG chains on the surface [16]. In terms of interactions with the biophase, it is expected that manipulation of the NP chemical identity would result in dramatic variations of the biological behaviour. In fact, interaction with the biological environment results in the formation of a biomolecular corona around NPs which drives their in vivo behaviour, cytotoxicity, immunotoxicity and activity [17,18]. Proteins are key players in this phenomenon and the presence/absence of protein-NP interactions should not be overlooked. For instance, the great majority of NPs tested in cell cultures come in contact with a protein-rich medium (e.g., protein from fetal bovine serum), which can get adsorbed on their surface thereby changing their properties. This aspect is often poorly addressed or ignored when interpreting biological data. Consequently, linking chemical identity to biological behaviour becomes unreliable, making the design of NPs with a particular delivery requirement a challenging task. To fully understand the interaction of the amine-functionalized NPs with biological systems, we have developed a panel of amine-functionalized PEGylated NPs with different PEG lengths, and assessed their properties with specific regard given to their surface features, their behaviour in protein solutions, their ability to permeate through gel-like barriers (tumor extracellular matrix and artificial mucus), and eventually both their uptake by human innate immune cells and capacity to induce an inflammatory reaction [19].

1.2 Materials and Methods

1.2.1 Materials

Monomethoxy-polyethylene glycol with Mn 1.0 kDa ($mPEG_{1.0k}$, Nanocs Inc., New York, USA) and Mn 2.0 kDa ($mPEG_{2.0k}$, Sigma-Aldrich, Milan, Italy) were dehydrated by azeotropic distillation with dry toluene in a Dean-Stark trap. PEG_{5K}-PCL_{5K} was purchased from Sigma-Aldrich. ε -caprolactone (CL) was distilled over CaH_2 under vacuum. Stannous-(2-ethylhexanoate)$_2$ ($Sn(oct)_2$), triethylamine (TEA), tosyl chloride (TsCl), triphenylphosphine (PPh_3), and sodium azide were used without further purification. 1,4-butandiol was dried according to a standard procedure. All solvents (analytical grade) were purchased from Sigma-Aldrich. N,N-dimethylformamide (DMF) and dichlorometane (DCM) were dried before use. Sodium chloride (NaCl), potassium chloride (KCl), calcium chloride ($CaCl_2$), sodium acetate ($NaH_3C_2O_2$), sodium bicarbonate ($NaHCO_3$), sodium citrate dihydrate, magnesium chloride hexahydrate ($MgCl_2$. $6H_2O$), sodium sulfate (Na_2SO_4), disodium phosphate (Na_2HPO_4), poloxamer 188 (Pluronic® F68), Human Serum Albumin (HSA), Type II porcine mucin, ECM

gel from Engelbreth-Holm-Swarm murine sarcoma, diethylenetriaminepentaacetic acid (DPTA), RPMI 1640 amino acids solution, and egg yolk emulsion (microbiology) were purchased from Sigma-Aldrich. 3,3′-Dioctadecyloxacarbocyanine perchlorate (DiO) and 1,1′-Dioctadecyl-3,3,3′,3′- tetramethylindocarbocyanine perchlorate (DiL) were purchased from Thermo Fisher Scientific, Monza, Italy.

1.2.2 Polymer synthesis

Synthesis of mPEG-PCL diblock copolymers

The linear diblock copolymers were prepared by ring-opening polymerization (ROP) of CL at 120°C for 24 h using mPEG (1.0, or 2.0 kDa) as an initiator and $Sn(Oct)_2$ as a catalyst (20% by mol). CL/initiator molar ratio = 36. Copolymers were isolated through dissolution of the crude product in $CHCl_3$, precipitation in n-hexane and removal of solvent by vacuum. ^1H NMR ($CHCl_3$, δ in ppm), PCL block: 1.29–1.78 (m), 2.19–2.43 (t) 3.20 (m); 3.92–4.21 (t), 4.31(t); PEG block: 4.10 (t), 3.64 (s), 3.38 (t).

Synthesis of diamine-PCL (NH_2-PCL_{4k}-NH_2)

Step 1. Synthesis of PCL diol (HO-PCL4k-OH). 1,4-butandiol (500 mg, 5.55 mmol), CL (22.49 g, 197 mmol), $SnOct_2$ (449 mg, 1.1 mmol) were added in a flask under dry nitrogen. The polymerization was carried out under stirring at 120°C for 24 h. The product was dissolved in 20 mL of DCM and precipitated in cold hexane; the polymer was collected and dried under vacuum. ^1H NMR ($CHCl_3$, δ in ppm): 1.29–1.78 (123H, m), 2.19–2.43 (74H, m), 3.92–4.21 (74H, t), 3.64 (4H, t) (Mn evaluated by ^1H NMR = 4,344 dalton).

Step 2. Synthesis of ditosyl-PCL (Ts-PCL_{4k}-Ts). HO-PCL_{4k}-OH (4.0 g, 0.92 mmol) was dissolved in 40 mL of DCM, then TEA (506 mg, 5.0 mmol) and TsCl (953 mg, 5.0 mmol) were added. The reaction was carried out under stirring at room temperature for 24 h. The polymer was dissolved in 15 mL of DCM and precipitated in cold hexane, then collected and dried under vacuum. ^1H NMR ($CHCl_3$, δ in ppm): 1.29–1.78 (123H, m), 2.19–2.43 (74H, m), 3.92–4.21(74H, t), 7.79 (4H, d), 7.49 (4H, d), 2.43 (6H, s).

Step 3. Synthesis of diazide-PCL (N_3-PCL_{4k}-N_3). Ts-PCL_{4k}-Ts (1.0 g, 0.66 mmol) was dissolved in 15 mL of dry DMF, then NaN_3 (214 mg, 3.3 mmol) was added and the mixture was stirred overnight at 90°C under nitrogen stream. The reaction mixture was then cooled down to room temperature and filtered, and DMF was removed under vacuum. The crude product was dissolved in 10 mL of DCM and washed twice with brine and twice with water in a separating funnel. The organic phase was dried over anhydrous Na_2SO_4, concentrated, poured

into cold hexane, and the precipitated polymer was dried under vacuum. FTIR diagnostic band: 2107 cm^{-1} (N_3 stretching) ^1H NMR ($CHCl_3$, δ in ppm): 1.29–1.78, (123H, m), 2.19–2.43, (74H, m); 3.92–4.21(74H, t).

Step 4. Synthesis of diamine-PCL (NH_2-PCL_{4k}-NH_2). N_3-PCL_{4k}-N_3 (2.0 g) was dissolved in 50 mL of MeOH at 40°C in a flask equipped with a nitrogen inlet and refrigerator, then PPh_3 (N_3/PPh_3 molar ratio=1/3) was added and the reaction was carried out at 100°C overnight. After removing of solvent by rotary evaporation, the polymer was dissolved in 10 mL of DCM, precipitated in cold hexane, collected and finally dried under vacuum. The occurrence of the reaction was confirmed by FTIR through disappearance of the 2097 cm^{-1} N_3 stretching band. ^1H NMR ($CDCl_3$, in ppm): 1.29–1.78, (123H, m), 2.19–2.43, (74H, m); 3.92–4.21(74H, t), 3.64 (4H, t), 2.48 (4H, broad). GPC analysis: Mw 4.8 kDa; Mn 4.2 kDa; Mw/Mn 1.1.

1.2.3 Polymer characterization

FTIR analysis was performed with a Perkin-Elmer spectrometer (Paragon 500) equipped with a ZnSe attenuated total reflectance (ATR) crystal accessory. ^1H NMR spectra were recorded with a Bruker Avance DPX400 apparatus operating at 400 MHz at 25°C and 128 NS. GPC analysis was performed using a Malvern-Viscotek MAX/TDA 305 quadruple detector array equipped with a precolumn and two Phenogel columns (Phenomenex) with exclusion limits 10^6 and 10^3 respectively. THF solutions (100 μL) were filtered (PTFE 0.22 μm) and analysed at flow rate 0.8 mL/min and T 35°C. Calibration was based on a standard of polystyrene (Mw 104,959 Da).

1.2.4 Preparation and characterization of nanoparticles

PEGylated and amine/PEGylated NPs were prepared by the solvent-diffusion method. In particular, we prepared PEG-NPs series (PEG_{1K}-PCL_{4K}, PEG_{2K}-PCL_{4K} and PEG_{5K}-PCL_{5K}), amine-NPs (NH_2-PCL_{4k}-NH_2) and amine/PEG-NPs (NH_2-PCL_{4k}-NH_2 mixed with either PEG_{1K}-PCL_{4K} or PEG_{2K}-PCL_{4K} or PEG_{5K}-PCL_{5K} at 1:1 w/w ratio). Briefly, 10 mg of polymers were dissolved in 2 mL of acetone and added dropwise in 4 mL of water containing 4 mg of Pluronic® F68 as surfactant (0.1% w/v) under stirring. Acetone was removed under vacuum (5 min). Finally, the NP dispersion was transferred and stored in Eppendorf tubes at a final NP concentration of 2.5 mg/mL. NPs were tested shortly after preparation. Fluorescent NPs giving FRET (FRET-NPs) were prepared by nanoprecipitation as described above with minor modifications. DiO (λ_{ex} = 488 nm, λ_{em} = 505 nm) and DiL (λ_{ex} = 543 nm, λ_{em} = 575 nm) were

selected as FRET pair. Briefly, 100 μL from each DCM stock solution of DiO and DiL (1 mg/mL) were transferred to a clean vial and left to evaporate for 30 min until a colourless film was formed. Then, the copolymer solution in acetone was added. Nanoprecipitation was carried out as reported above. After preparation, NPs were filtered (RC 0.4 μm) to remove any free dye molecules. DiL and DiO loading inside NPs was assessed by dissolving 1 mg of freeze-dried NPs in 1 mL of DCM under stirring for 1 h. Samples were analysed for DiO and DiL quantification by UV spectrophotometry at 488 and 543 nm, respectively. The concentration of DiL and/or DiO was calculated by means of a standard calibration curve derived for DCM solutions of the specific dye at known concentrations (0.5–60 μg/mL). Potential interference from DiL on DiO absorbance and vice versa were assessed by spiking a DiO solution in DCM with different amounts of DiL, or a DiL solution in DCM with different amount of DiO. To verify a possible interference of copolymers on DiL/DiO quantitative analysis, a weighted amount of unloaded NPs was dissolved in DCM and analysed under the same conditions reported for the dyes. The hydrodynamic diameter (D_H), polydispersity index (PI) and zeta potential (ζ) of NPs were determined on a Zetasizer Nano ZS (Malvern Instruments Ltd.). Results are reported as the mean of three separate measurements of three different batches (n=9) ± standard deviation (SD). Pluronic® F68 associated to NPs was assessed by quantitative ^{1}H NMR. After preparation, NPs were centrifuged at at 2300 x*g* for 20 min and the supernatant containing unadsorbed surfactant was lyophilized. The obtained solid was dissolved in D_2O and analyzed by ^{1}H NMR. The quantitative determination of Pluronic® F68 was achieved by comparing the integral of $–CH_3$ protons at 1.23 ppm in the samples with the corresponding signal of a spectrum of pure Pluronic® F68 of known concentration (2 mg/mL). The amount of Pluronic® F68 absorbed on NP surface was determined indirectly by the difference between the initial amount of Pluronic® F68 (4 mg) and the calculated amount of residual Pluronic® F68 in solution. Stability studies of NPs as prepared (0.5 mg/mL) were conducted over a 24 h time span by monitoring size, z and scattering (absorbance at 500 nm on an UV-1800 spectrophotometer, Shimadzu Corporation, Japan).

1.2.5 Evaluation of NP surface features

Fixed aqueous layer thickness (FALT) measurements were based on the approximation of the Gouy-Chapman theory and carried out by monitoring the influence of ionic strength on particle surface [20,21]. Different amounts of NaCl stock solutions at different concentrations were added to a NP dispersion in water (0.5 mg/mL), and ζ of the samples was measured. A

plot of ln (ζ) against $3.33 \cdot [NaCl]^{0.5}$ results in a straight line where the slope represents the thickness of the PEG shell in nm.

The amount of PEG on NP surface was evaluated through ^1H NMR. Spectra were recorded for either NPs dispersed in D_2O (5 mg/mL) or dissolved in $CDCl_3$ (5 mg/mL). The amount was calculated by comparing the integral of -CH_2- resonance of PEG in D_2O with the corresponding signal in $CDCl_3$. The -CH_2- integral relative to PEG was calculated considering the contribution of –CH_2- from Pluronic® F68:

int. $CH_{2(PEG)}$ = int.$CH_{2(total)}$ - 8 x int.$CH_{3(poloxamer)}$

where 8 x int.$CH_{3(poloxamer)}$ was obtained from a pure Pluronic® F68 spectrum

(ratio -CH_3/CH_2 =1/8).

1.2.6 Interactions with proteins

Interaction of NPs with HSA or mucin was assessed by fluorescence spectroscopy, DLS measurements, and turbidimetry analyses. For interaction with HSA, 200 µL of NPs (2.5 mg/mL) were mixed with 100 µL of HSA stock solution in water (2 mg/mL) and 700 µL of water. The final concentrations of NPs and HSA in the samples were 500 µg/mL and 200 µg/mL, respectively. For interaction with mucin, mucin powder was dispersed in water (0.16% w/v) and stirred overnight. Then, the dispersion was centrifuged at 2300 x*g* for 20 min and the supernatant collected. Thereafter, 200 µL of NPs were mixed with 250 µL of mucin dispersion and water up to a final volume of 1 mL. The final concentrations of NPs and mucin in these samples were 500 µg/mL and 0.04% w/v respectively [22]. Control samples of HSA, mucin and NPs were run as control.

Fluorescence spectroscopy was used to assess the 'quenching' effect of NPs on the ability of certain residues of the protein to emit light. Following preparation, the samples were incubated at RT for 1 h. Then, the emission spectra were acquired (λ_{ex}= 278 nm) (RF-6000, Shimadzu Corporation, Japan)[3]. At different time points (0, 4 and 24 h), size, ζ, and scattering were measured as described above.

1.2.7 Permeation of NPs through gel-like barriers

The capacity of NPs to cross artificial mucus (AM) and a tumor ECM was investigated. The transport experiment was carried out by placing either artificial mucus (AM) (for composition see SI) or ECM gel (from a murine sarcoma) in the upper chambers of Transwell®

-12 well plates (12 mm diameter, polyester membranes with 3.0 μm pore size), applying NPs and monitoring the amount of NPs that have diffused in the lower chamber [23]. For transport through AM, the lower chamber was filled with 1 mL of Simulated Interstitial Lung Fluid (SILF) (for composition see SI). For transport through the ECM gel, the lower chamber was filled with 1 mL of 0.01 M PBS (Phosphate Buffer Saline, NaCl 0.138 M, KCl 0.0027 M), pH 7.4 at 25 °C. FRET-NPs (0.1 mL, 2.5 mg/mL) were placed on the top of gel layer (0.3 mL) and maintained at RT. At 0, 1, 4 and 24 h, the medium in the lower chamber was collected and the fluorescence emission spectra recorded at λ_{Ex}=488 nm and 543 nm to determine the FRET efficiency ratio and the NP concentration, respectively.

To calculate NP concentration in SILF and PBS, a calibration curve of DiL emission intensity at λ_{ex} =543 nm against different known concentrations of NPs was generated for each formulation. FRET efficiency was calculated for λ_{ex} = 488 nm emission spectra using the following equation [24]:

$$\text{FRET efficiency} = \frac{\text{Intensity at Em=575 nm}}{\text{Intensity at Em=575 nm} + \text{Intensity at Em=505 nm}}$$

Stability of FRET-NPs in SILF and PBS was monitored until 24 h through DLS measurements.

1.2.8 NP interaction with human immune cells

Monocyte Isolation

Human primary blood monocytes were isolated from healthy donors with informed consent. Briefly, peripheral blood mononuclear cells were separated from freshly obtained whole blood by gradient density centrifugation on Ficoll-Paque PLUS (GE healthcare, Bio-Sciences AB, Uppsala, Sweden). CD14+ monocytes were further isolated by magnetic cell sorting using CD14 microbeads following the manufacturer's protocol (Miltenyi Biotec, Bergisch-Galdbach, Germany). Cell viability was assessed by trypan blue dye exclusion and determined to be > 98%.

NP uptake

Freshly isolated CD14+ monocytes were seeded in 24-well plates (Corning® Costar®; Corning Inc. Life Sciences, Oneonta, NY, USA) at 2 x 10^5 cells/well in 0.5 mL of Phenol Red-

free RPMI 1640 medium (GIBCO by Life Technologies, Paisley, UK) supplemented with 5% heat-inactivated pooled human AB serum (Sigma-Aldrich) and 50 µg/mL gentamicin sulfate (GIBCO). After 24 h at 37°C, the cells were washed and exposed for 2 h to 50 µg/mL of DIL-loaded NPs (NPs pre-treated for 1 h with 70% HSA). The extracellular media were then collected and the fluorescence intensity of DiL was measured at $\lambda_{ex/em}$ = 543/575 nm in a microplate reader (Cytation 3 imaging reader, Biotek, Winooski, VT, USA). The concentration of NPs in the extracellular compartment was calculated by means of a standard calibration curve derived for NP dispersions in the cell medium at known concentrations (0.5-50 µg/mL). For confocal microscopy, monocytes were seeded on glass cover slips and treated as described above. Following NP incubation, cells were fixed for 20 minutes in 3.7% formaldehyde, washed 3 times with PBS, and cover slips were mounted on slides with Vectashield mounting medium containing 4′,6-diamidino-2-phenylindole (Vector Laboratories Inc., Burlingame CA, USA). Confocal microscopy was conducted using a Zeiss LSM 700 confocal microscope.

Monocyte activation

Isolated monocytes were seeded in 24-well culture plates at 5 x 10^5 cells/well in 1 mL of RPMI 1640 medium supplemented with 5% heat-inactivated human AB serum and 50 µg/mL gentamicin sulfate. Cells were exposed to NPs (pre-treated for 1 h with 10% human AB serum) 1 ng/mL LPS from Escherichia coli (E. coli, serotype O55:B5, Sigma-Aldrich) for 1 h. The concentration of NPs incubated in each well was calculated based upon the NP surface area. After 24 h of incubation, supernatants were collected and frozen at -20°C until use. Activation was assessed as release in the supernatant of the inflammatory/defensive cytokines IL-1 and TNF, measured by ELISA with commercially available kits (DuoSet ELISA, R&D Systems, Minneapolis, MN, USA) following the manufacturer's instructions.

1.3 Results and discussion

1.3.1 Synthesis and characterization of the polymers

The mPEG-PCL diblock copolymers were synthesized by classical ROP polymerization, using mPEG-OH of different molecular weights as an initiator. Theoretical molecular weights were in agreement with the values found by GPC and determined by ^{1}H NMR (Mn of PCL block was calculated from the ratio between intensities of the resonance associated to -O–CH_3 protons of mPEG end groups at 3.36 ppm and –CH_2–CO– units in the PCL chain at 2.31 ppm) (Table S2). Diamine-PCL (NH_2-PCL-NH_2) was synthesized according to the scheme reported in Fig. 1a.

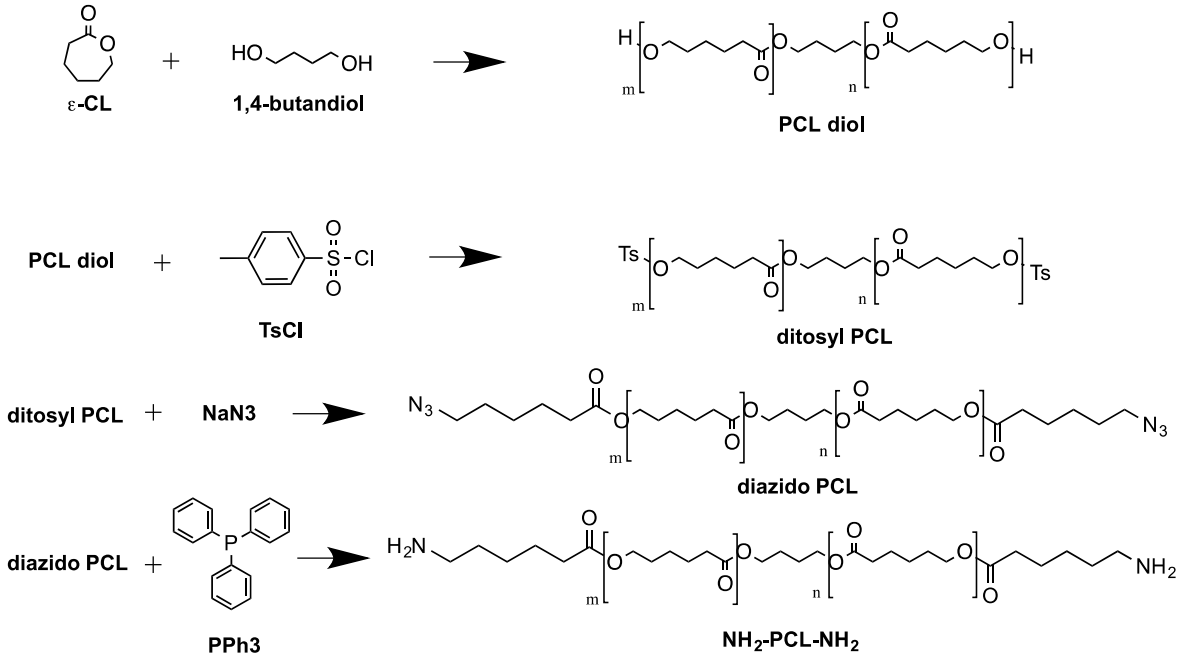

(**a**)

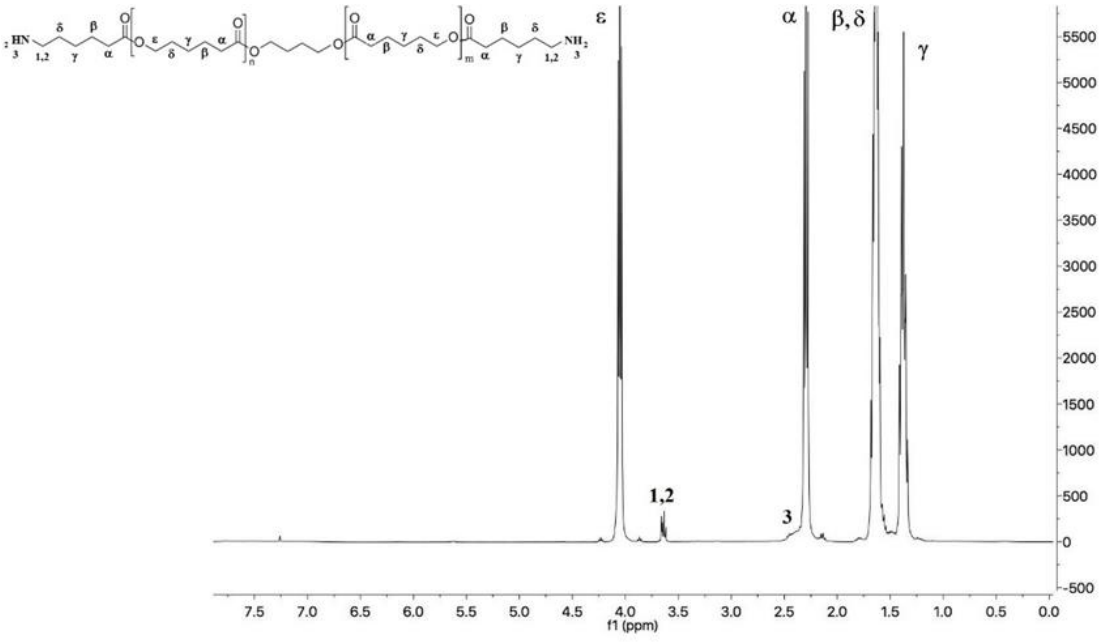

(**b**)

Fig. 1. (**a**) Steps for the synthesis of H_2N-PCL-NH_2. **(b)** ^{1}H NMR spectrum of H_2N-PCL- NH_2 in $CDCl_3$.

Full conversion of azide end-groups of N_3-PCL-N_3 precursor to amines was checked by FTIR through disappearance of the azide band at around 2100 cm^{-1}. The structure of the final polymer was confirmed by ^{1}H -NMR as reported in Fig. 1b.

1.3.2 Nanoparticle properties

A panel of core-shell NPs was obtained from 1:1 mixture of H_2N-PCL-NH_2 and PEG-PCL (amine/PEG-NPs), and single H_2N-PCL-NH_2 (Amine-NPs) or PEG-PCL (PEG-NPs) mixtures as shown in Fig. 2. PEGs of different molecular weights were employed in the study (1, 2, 5 kDa) while PCL moiety remained fixed (4 kDa).

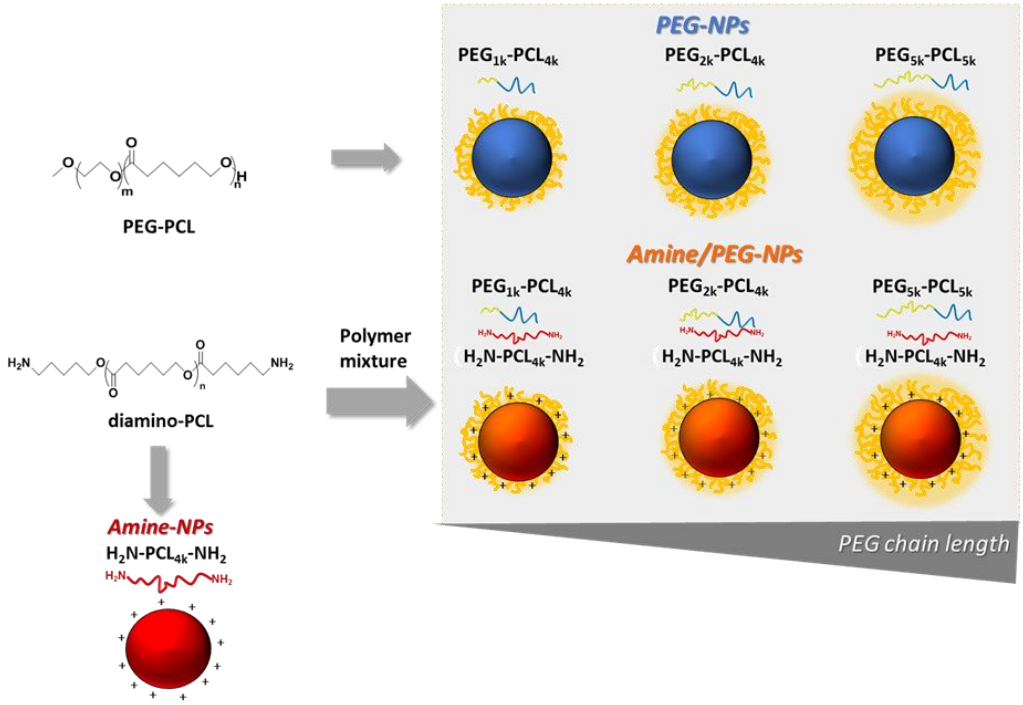

Fig. 2. Schematic representation of NPs tested in the study.

Pluronic F68 was needed to fabricate amine-bearing NPs with good yields yet avoiding their premature aggregation. For comparison purposes, its use was extended to all the formulations tested. Indeed, poloxamer was associated to all the types of PEGylated NPs and its surface amount decreased as PEG MW increased (Table 1). NPs had an average size below 150 nm and a monomodal distribution, a finding supported also by low PI values (Table 1). The increase of PEG MW in the copolymer decreased D_H for both PEG-NPs and amine/PEG-NPs. A positive ζ was observed in the amine-bearing variants which was decreased in the amine/PEG series, especially at increasing PEG MW. As expected, PEG-NPs had a negative ζ.

Short-term stability of NPs in water was observed up to 24 h by monitoring scattering, D_H and ζ (data not shown). Scattering analysis of NP suggested that no aggregation occurred over 4 h due to negligible changes in absorbance values at 500 nm. Amine-NPs and Am/PEG_{1K}-PCL_{4K} NPs showed an increase of D_H values and large fluctuations of ζ after 24 h while the

other NPs showed no significant differences in D_H. Size distribution curves in water (data not shown) clearly highlight that PEG_{1K} is not able to confer satisfactory colloidal stability to Am/PEG_{1k}-NPs in analogy to PEG_{1k}-NPs. Overall these results indicate that NPs should be tested within 4 h of preparation. From a clinical perspective, freeze-drying of the NPs dispersion, likely in the presence of a cryoprotectant, is needed to ensure suitable shelf-life and storage stability.

Table 1. Colloidal properties of NPs. Values are expressed as mean ± SD of three different batches.

	Code	**Composition[1]**	**Yield (%)**	**Poloxamer[2] (mg)**	**D_H[3] (nm±SD)**	**PI[3]**	**ζ[4] (mV±SD)**
PEG- NPs	PEG_{1K}-NPs	PEG_{1K}-PCL_{4K}	80	2.2	78 ± 0.3	0.224	-10.2 ± 2.0
	PEG_{2K}-NPs	PEG_{2K}-PCL_{4K}	95	1.3	44 ± 1.3	0.160	-17.1 ± 1.6
	PEG_{5K}-NPs	PEG_{5K}-PCL_{5K}	98	1.9	44 ± 3.6	0.175	-7.4 ± 1.9
Amine-NPs	Am-NPs	H_2N-PCL_{4K}-NH_2	82	-	134 ± 0.3	0.128	34.3 ± 1.3
Amine/PEG-NPs[1]	Am/PEG_{1K}-NPs	H_2N-PCL_{4K}-NH_2 / PEG_{1K}-PCL_{4K}	93	2.4	121 ± 2.8	0.191	28.6 ± 1.0
	Am/PEG_{2K}-NPs	H_2N-PCL_{4K}-NH_2 / PEG_{2K}-PCL_{4K}	95	1.0	99 ± 5.9	0.257	20.0 ± 2.3
	Am/PEG_{5K}-NPs	H_2N-PCL_{4K}-NH_2 / PEG_{5K}-PCL_{5K}	98	1.2	94 ± 6.8	0.250	21.3 ± 2.4

[1] Copolymer mixture was 1:1 by wt.; [2] Pluronic® F68 associated to NPs was derived from the amount found in the medium after NPs preparation. Quantitative ^{1}H NMR measurements were taken as described in 2.4.; [3] D_H and PI were measured in water by DLS; [4] measures the electrophoretic mobility of NPs.

1.3.3 Extent of nanoparticle PEGylation

FALT of the outer shell of NPs was determined by measuring ζ as a function of sodium chloride concentration at pH values of 7.0 where primary amines are expected to be ionized. As reported in Fig. 3, the slope value of the linear regression line obtained plotting Log ζ vs sodium chloride concentration gives the shell thickness (nm) for each NPs type. As expected, shell thickness increased as PEG MW increased. Interestingly, Am-PEG-NPs displayed a aqueous layers thicker as compared with the corresponding PEG-NPs counterparts (11.8 nm for Am/PEG$_{5K}$-NPs vs 4.0 nm for PEG$_{5K}$-NPs). The shell thickness for Amine/PEG-NPs increased with respect to increasing PEG chain length, as was the case for the PEG-NPs. However, the increase across the series was greatest for the Amine/PEG-NPs. The extent of shell thickness increase for Amine/PEG-NPs was steeper and more profound.

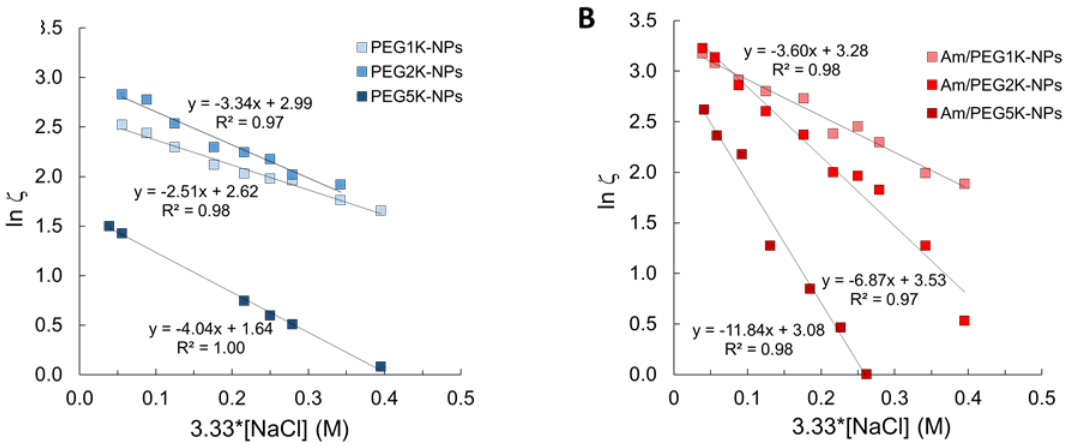

(**a**) (**b**)

Fig. 3. FALT measurements for (**a**) PEG-NPs and (**b**) Am/PEG-NPs.

The amount of PEG on the surface of NPs after washing out Pluronic® F68 was assessed by quantitative ^{1}H NMR (Table 2). As can be seen, NPs expose much less PEG than expected suggesting that during nanoprecipitation PEG chains are entangled in the PCL core. This result confirms that the preparation method has a major impact on PEGylation extent, and also on the conformation of the flexible hydrophilic cloud on the NPs surface.

Table 2. Shell thickness of NPs and percentage of PEG on NPs surface.

Type	Shell thickness[1] (nm)	Surface PEG[2] (wt %)
PEG_{1K}-NPs	2.5 ± 0.4	3
PEG_{2K}-NPs	3.4 ± 0.8	11
PEG_{5K}-NPs	4.0 ± 0.2	5
Am/PEG_{1K}-NPs	3.5 ± 0.2	2
Am/PEG_{2K}-NPs	6.8 ± 1.2	4
Am/PEG_{5K}-NPs	11.8 ± 0.9	2

[1] Slope of the regression line of FALT analysis in Fig. 3;

[2] Surface PEG calculated by ^{1}H NMR as described in 2.5.

1.3.4 Nanoparticle interactions with proteins in solution

Physical properties of NPs such as size, shape and surface composition strongly affect the interaction with proteins in complex media, which can alter the chemical identity of NPs and in turn their biological fate. HSA is a dysopsonic protein that can extend NP circulation time [25]and its mode of interaction with NPs can impact cell uptake [26]. On the other hand, mucin is a barrier protein which is relevant in the case of NP interactions with mucosal surfaces. Thus, we studied HSA and mucin interaction with the panel of NPs fabricated through the combination of fluorescence spectroscopy, turbidimetry and size measurements.

Protein adsorption onto the nanoparticles, which can affect their stability over time, was monitored by measuring the absorbance value (at λ = 500 nm) of NPs dispersions in the presence of HSA and mucin, over time. As the proteins absorb onto the NPs, light scattering occurs which changes the absorbance value over time. Only Am-NPs suffered from stability issues in the presence of proteins, showing a tendency to increase scattering of light over time, whereas no significant effect was found for the PEGylated series.

Fig. 4a and 4b show the fluorescence emission spectra of HSA in the absence and in the presence of NPs upon excitation at 278 nm. The black spectrum shows the typical dual band fluorescence spectrum of HSA, which reflects the contribution of the tyrosine (λ_{em} ca 310 nm) and tryptophan (λ_{em} ca 340 nm) fluorogenic centres. This strong emission is quenched upon addition of PEG-PCL NPs simply due to static quenching effects arising by the massive aggregation of HSA on the NPs [3]. This result suggests that: i) A PEG shell is unable to prevent

NP-protein hydrophobic interactions; ii) Am-NPs adsorb HSA, presumably due to electrostatic interactions, and iii) Amine-PEG NPs interact with HSA through combined hydrophobic/electrostatic interaction. These results are in line with those found for a series of PEGylated cationic liposomes that adsorbed human plasma proteins depending on PEG length[27].

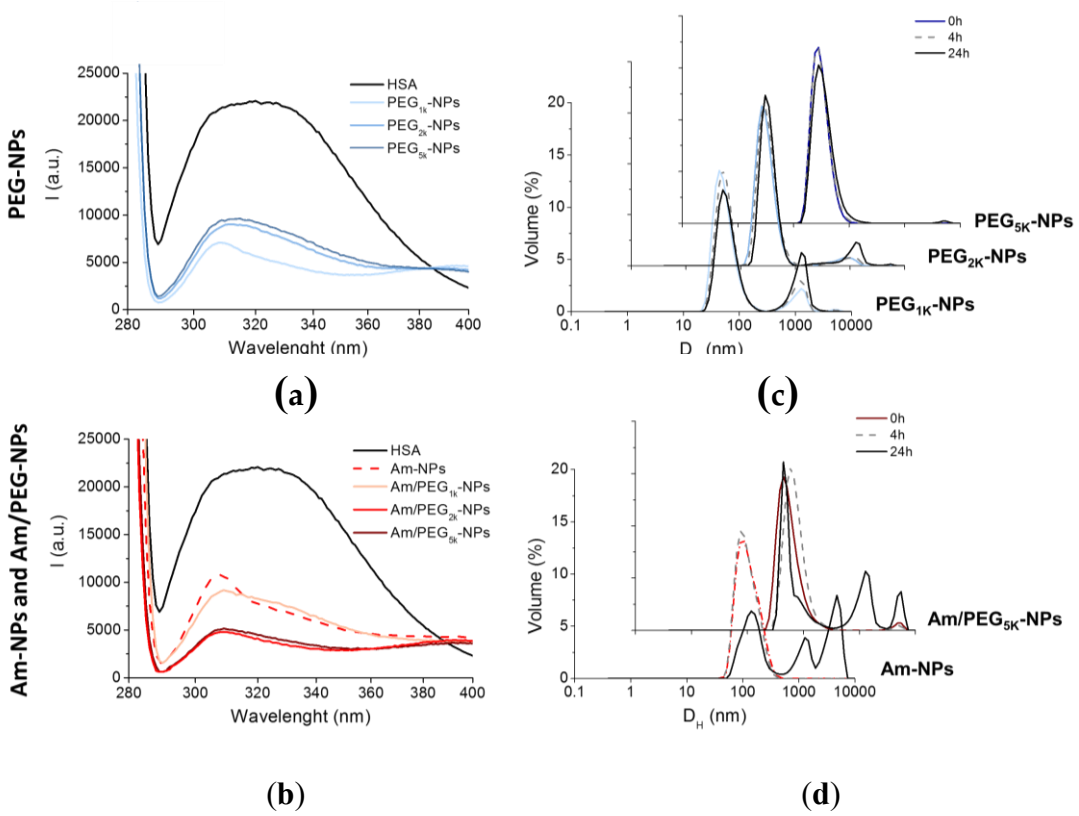

Fig. 4. Interaction of NPs with proteins. Fluorescence emission spectra of HSA (0.2 mg/mL) at Ex=278 nm in the presence of PEG-NPs (**a**) and Am-NPs or Am/PEG-NPs (**b**) (NPs=0.5 mg/mL). Spectrum of free HSA is reported as control. Representative size distribution curves of PEG-NPs (**c**) and Am-NPs or Am/PEG-NPs (**d**) incubated in HSA (0.2 mg/mL) (NPs=0.5 mg/mL).

Particle size in the presence of proteins was monitored over time using DLS, as shown in Fig. 4c and 4d. PEG-NPs experienced a high degree of protection from aggregation, especially for the PEG_{5k} variant (Fig. 4c). On the contrary, amine-bearing NPs showed a completely different behaviour, exhibiting a fast and time-dependent aggregation that even a PEG_{5k} copolymer was unable to hamper. These data demonstrate that PEGylated NPs are only partly capable of shielding HSA interaction, presumably due to the low amount of surface PEG and marginal effect of adsorbed poloxamer. As far as mucin interaction is concerned, its interaction with cationic NPs has been routinely used to achieve mucoadhesion [28]. Nevertheless, precise tuning of PEG grafting density and molecular weight is considered a strategic approach to minimize mucoadhesion and in turn promote NPs transport through a mucus layer [7].

Mucoadhesive behaviour of NPs can be estimated on the basis of an increased absorbance at 500 nm [29], while interactions between mucin and positively-charged NPs can be monitored by size measurements [8]. There was little quenching of mucin fluorescence in the presence of all NPs suggesting that mucin was not significantly interacting with the NPs. As shown in Fig. 5a, scattering in water increased only for Am-NPs, suggesting that such an interaction with the protein occurs. Nevertheless, ζ was unchanged for PEG-NPs and switched to negative values for all amine-bearing NPs. These results indicate that mucin negative chains adsorb onto positive Am-NPs via electrostatic interactions between opposite charges, which are not shielded by the concurrent presence of PEG chains. As evidenced by the corresponding size curves in Fig. 5c and 5d, the increase of PEG length is increasingly effective in ensuring satisfactory stability while avoiding interactions between NPs. Thus, PEG length and its surface conformation remains the main determinant for regulating behaviour at interface also for amine-modified NPs [8].

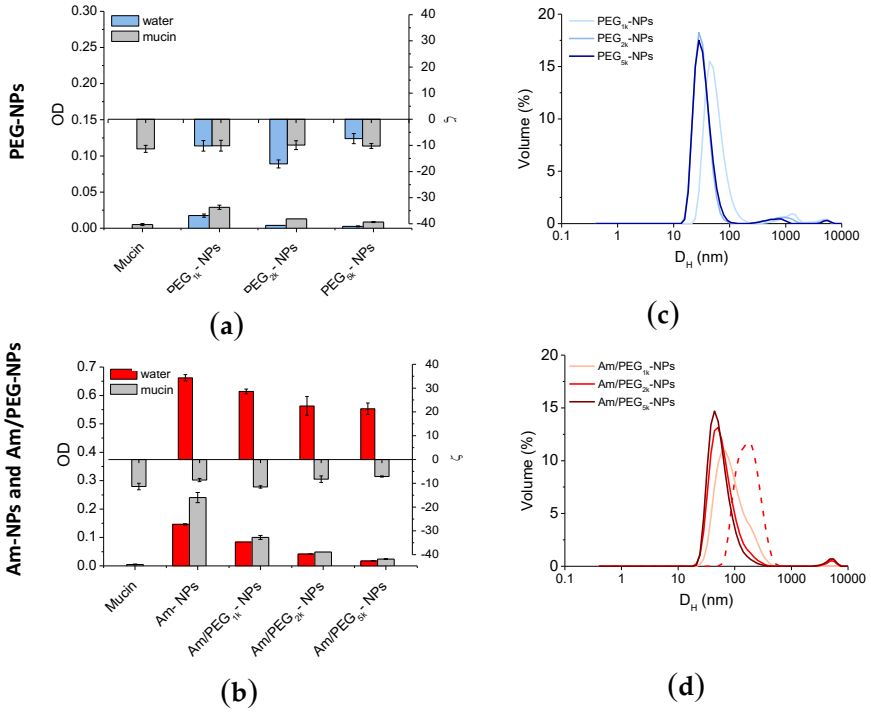

Fig. 5. Interaction of NPs with mucin. Scattering of PEG-NPs (**a**) or Am-NPs and Am/PEG-NPs (**b**) in water or in a mucin water dispersion (0.08% w/v) (NPs=0.5 mg/mL). Data are an average of triplicate measurements ± SD. Representative size distribution curves of PEG-NPs (**c**) or Am-NPs and Am/PEG-NPs (**d**) in a mucin water dispersion (0.08% w/v) (NPs=0.5 mg/mL).

1.3.5 Permeation through protein-rich gels

To ascertain if the developed NPs permeated differently through protein-rich gel-like barriers, we focused on a tumor ECM, which could mimic tumor stroma, and artificial mucus, which is representative of the bronchial secretion.

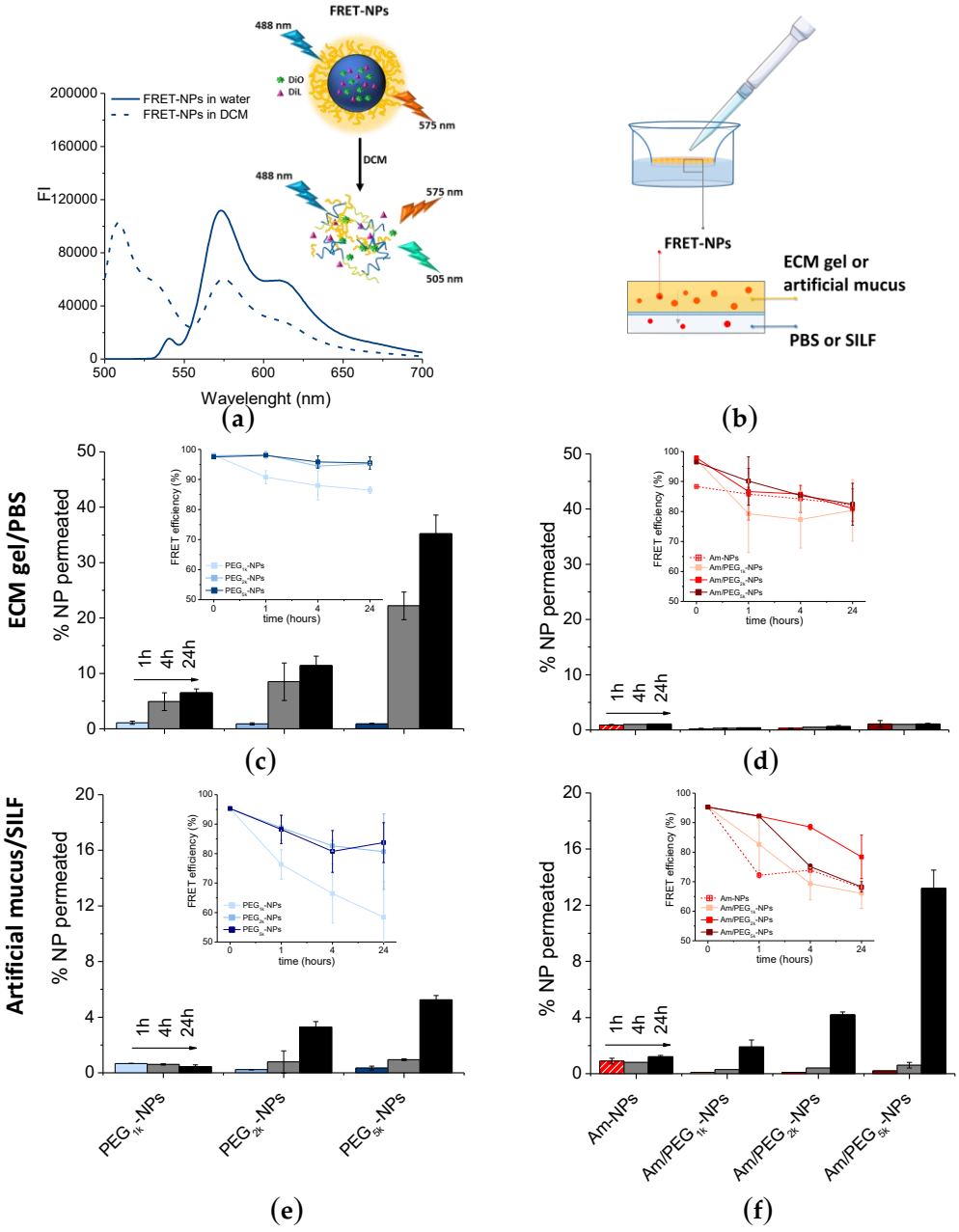

Fig. 6. Permeation of NPs through protein-reach gels over time. For this experiment, NPs were loaded with DiO/DiL as a FRET pair. (**a**) Emission spectra collected after DiO excitation (λ_{ex} = 488 nm) of DiO/DiL-loaded PEG5k-NPs dispersed in water or dissolved in DCM. (**b**) Set-up of the transport experiment. Amount of DiO/DiL-loaded PEG-NPs (**c, e**) and Amine-NPs and Amine/PEG-NPs (**d, f**) found in the acceptor chamber after crossing the ECM gel (**c, d**) and artificial mucus (**e, f**). The amount of NPs in the acceptor medium was evaluated by monitoring

DiL emission (λ_{ex} = 543 nm). In the inset FRET efficiency is reported (for calculation see 2.7). Data are an average of triplicate measurements ± SD.

For this experiment, FRET NPs were developed. FRET is a mechanism describing energy transfer between two light-sensitive molecules, a donor chromophore and an acceptor. The efficiency of this energy transfer is inversely proportional to the sixth power of the distance between donor and acceptor, making FRET extremely sensitive to small changes in distance. Measurement of FRET efficiency is a useful tool for determining if two fluorophores are released from a NP system and to monitor its disassembly in different biological conditions, in vitro and in vivo [23,30]. As donor and acceptor chromophores, we selected the hydrophobic dyes DiO ($\lambda_{ex/em}$ is 488/505 nm) and DiL ($\lambda_{ex/em}$ at 543/575 nm), respectively, since the DiO emission spectrum overlaps well with the DiL absorption spectrum. Fig. 6a reports emission spectra of PEG_{5k}-NPs loaded with DiO/DiL as a representative FRET formulation in both water and DCM. Upon excitation of NPs in water at 488 nm, DiO emission at 505 nm is quenched due to FRET and DiL emission is enhanced. When NPs are dissolved in DCM, DiO emission is restored and DiL emission is depressed since no FRET occurs. Mean particle size was doubled only in FRET-based PEG-NPs while λ of all NPs types were comparable to their unloaded counterparts (cfr D_H and ζ in Table 1). NP stability and constant FRET efficiency in the acceptor medium was demonstrated for all NP formulation; a fundamental prerequisite for validation of results in transport experiments. The percentage of NPs permeated through ECM or mucin over time was evaluated according the set-up described in Fig. 6b. At different time points, NPs amount in the acceptor chamber was evaluated by measuring DiL emission (λ_{ex} = 543 nm). As reported in Fig. 6c, PEG-NPs showed a time-dependent transport through ECM gel, with the extent of permeation clearly increasing as PEG MW increased. On the contrary, Am-NPs and Am/PEG-NPs did not show any capability to permeate through the ECM gel (Fig. 6d). In the case of artificial mucus, we found that increasing PEG MW allowed an increase of NP penetration for both PEG-NPs (Fig. 6d) and very surprisingly this was also the case for Am/PEG-NPs (Fig. 6e). In fact, the amount of transported Am/PEG_{5k}-NPs was higher than that corresponding to PEG_{5k}-NPs, highlighting that the presence of amine groups coupled with long PEG chains could even facilitate transport. Nevertheless, independently of the PEG MW, Am/PEG-NPs did not show any aggregation in SILF over time, as confirmed by DLS measurements. It is worth noting that permeation of Am-NPs was affected by their poor stability in both PBS and SILF (data not shown). Emission spectra of DiL collected at DiO excitation (data not shown) allowed calculation of FRET efficiency according to the equation reported in

2.7 (insets in Fig. 6c-e). A FRET efficiency higher than 80% for all the samples at different time points demonstrated that the fluorescence emission is due to intact fluorescent NPs and that only a limited contribution from FRET pair leaching is occurring.

1.3.6 Uptake and immune activation

The innate immune system is the first to come in contact with NPs entering the body. For this reason, we have investigated both the uptake and immunostimulatory capacity of our synthesized NPs in human primary monocytes, which are the main innate immune cells.

The extent of NP uptake by human monocytes was assessed by measuring the fluorescence of DiL in the extracellular compartment of cells, after exposing them to NPs for 2 h. The extent of NP uptake by human monocytes (Fig. 7a) was roughly related to PEG length in the copolymer (greater PEG length results in lower uptake) following a very general rule for PEGylated systems, while the presence of amine groups on NPs surface had no impact.

The production of IL-1 β and TNFα, which are indicators of inflammatory effects, was assessed by a commercially available ELISA kit following 24 h of NP incubation (Fig. 7b and d). In no cases were the levels of IL-1β or TNFα markedly elevated or suppressed compared to background cytokine production. To assess whether the NPs may modulate induced innate immune responses, cells were additionally stimulated with the gram-negative bacterial molecule lipopolysaccharide (LPS), in the presence and absence of each NP formulation (Fig. 7c and e). LPS stimulation resulted in elevated production of IL-1β and TNFα, a phenomenon that was not altered toward either increased or suppressed production in the presence of the NPs [19].

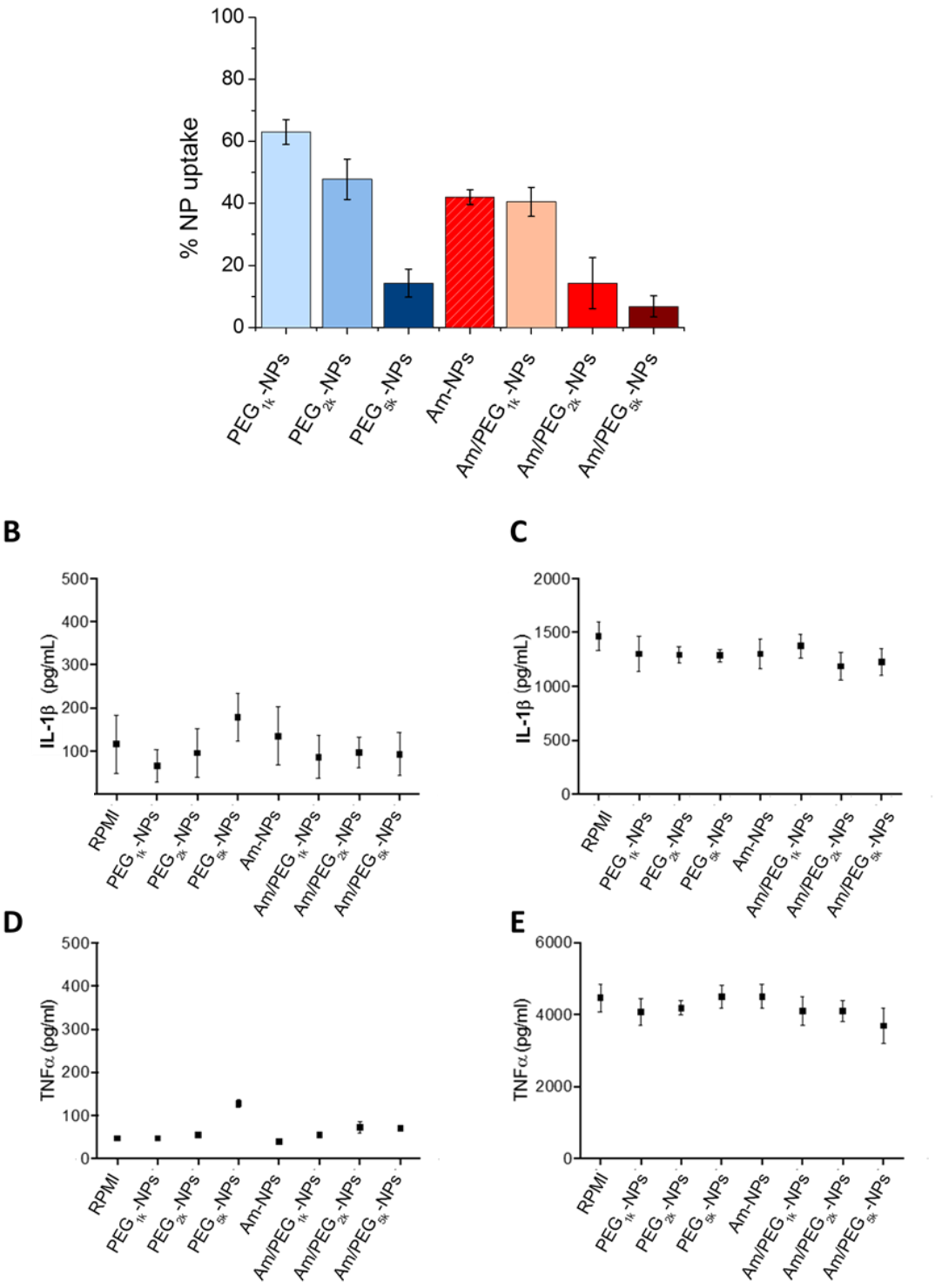

Fig. 7. Uptake and inflammatory response to NPs by human monocytes. (**a**) Quantification of NPs taken up by monocytes after 2 h incubation. Production of IL-1β (**b,c**) andTNFα (**d,e**) by human monocytes after 24 h of incubation with NPs as assessed by an ELISA kit. Panels (**c**) and (**e**) refer to LPS stimulated monocytes. Results represent mean ± SEM, n = 2.

1.4 Conclusions

In this work, we have prepared a panel of amine-functionalized PEGylated NPs (amine/PEG-NPs) with different PEG-chain length and evaluated their surface properties compared to corresponding PEG-NPs. The interaction of the NPs with human proteins, such as serum albumin and mucin, was studied using fluorescence spectroscopy, DLS and turbidimetry analysis. The results demonstrated that amine-bearing NPs interacted strongly with proteins, and that this was found to be dependent on PEG length and surface charge. Furthermore, differences in their ability to permeate through protein-rich biological barriers were also found. Amine/PEG-NPs were unable to cross ECM but were able to be transported through mucus, with transport facilitated by increasing MWs of PEG. Finally, the interaction of the different NP types with human innate immune cells (primary blood monocytes) was also studied. Cell uptake was found to decrease with increasing PEG MW and overall surface charge. Independently of uptake, NPs were found to not induce an inflammatory response, nor were they found to interfere with a normal defensive reaction to bacterial agents, thereby demonstrating high tolerability. In conclusion, we demonstrate that PEGylation extent and the presence of amine groups on NP surface are key elements that affect NP behavior in biological environments.

Funding: This research was funded by Italian Association for Cancer Research (IG2014 n.15764)" and "the EU H2020 project PANDORA (GA n. 671881)".

Acknowledgments: BJS and DB were supported by the EU H2020 project PANDORA (GA n. 671881). DB was also supported by the Cluster project MEDINTECH of the Italian Ministry of University and Research. The authors thank the Morpho-Functional Analysis and Bioimaging Unit of the Stazione Zoologica Anton Dohrn for assistance with confocal microscopy.

References

1. Grossen, P.; Witzigmann, D.; Sieber, S.; Huwyler, J. PEG-PCL-based nanomedicines: A biodegradable drug delivery system and its application. *Journal of controlled release: official journal of the Controlled Release Society* 2017, *260*, 46-60, doi:10.1016/j.jconrel.2017.05.028.

2. Conte, C.; d'Angelo, I.; Miro, A.; Ungaro, F.; Quaglia, F. PEGylated polyester-based nanoncologicals. *Current topics in medicinal chemistry* 2014, *14*, 1097-1114.

3. Venuta, A.; Moret, F.; Dal Poggetto, G.; Esposito, D.; Fraix, A.; Avitabile, C.; Ungaro, F.; Malinconico, M.; Sortino, S.; Romanelli, A., et al. Shedding light on surface exposition of poly(ethylene glycol) and folate targeting units on nanoparticles of poly(epsilon-caprolactone) diblock copolymers: Beyond a paradigm. *European journal of pharmaceutical sciences : official journal of the European Federation for Pharmaceutical Sciences* 2018, *111*, 177-185, doi:10.1016/j.ejps.2017.09.048.

4. Quaglia, F.; Ostacolo, L.; De Rosa, G.; La Rotonda, M.I.; Ammendola, M.; Nese, G.; Maglio, G.; Palumbo, R.; Vauthier, C. Nanoscopic core-shell drug carriers made of amphiphilic triblock and star-diblock copolymers. *Int J Pharm* 2006, *324*, 56-66, doi:10.1016/j.ijpharm.2006.07.020.

5. Harris, J.M.; Chess, R.B. Effect of pegylation on pharmaceuticals. *Nature Reviews Drug Discovery* 2003, *2*, 214-221, doi:10.1038/nrd1033.

6. Swierczewska, M.; Lee, K.C.; Lee, S. What is the future of PEGylated therapies? *Expert opinion on emerging drugs* 2015, *20*, 531-536, doi:10.1517/14728214.2015.1113254.

7. Xu, Q.; Ensign, L.M.; Boylan, N.J.; Schon, A.; Gong, X.; Yang, J.C.; Lamb, N.W.; Cai, S.; Yu, T.; Freire, E., et al. Impact of Surface Polyethylene Glycol (PEG) Density on Biodegradable Nanoparticle Transport in Mucus ex Vivo and Distribution in Vivo. *ACS nano* 2015, *9*, 9217-9227, doi:10.1021/acsnano.5b03876.

8. Huckaby, J.T.; Lai, S.K. PEGylation for enhancing nanoparticle diffusion in mucus. *Advanced Drug Delivery Reviews* 2018, *124*, 125-139, doi:https://doi.org/10.1016/j.addr.2017.08.010.

9. Shen, Z.; Nieh, M.-P.; Li, Y. Decorating Nanoparticle Surface for Targeted Drug Delivery: Opportunities and Challenges. *Polymers (Basel)* 2016, *8*, 83, doi:10.3390/polym8030083.

10. Chen, B.; Le, W.; Wang, Y.; Li, Z.; Wang, D.; Ren, L.; Lin, L.; Cui, S.; Hu, J.J.; Hu, Y., et al. Targeting Negative Surface Charges of Cancer Cells by Multifunctional Nanoprobes. *Theranostics* 2016, *6*, 1887-1898, doi:10.7150/thno.16358.

11. Wang, H.-X.; Zuo, Z.-Q.; Du, J.-Z.; Wang, Y.-C.; Sun, R.; Cao, Z.-T.; Ye, X.-D.; Wang, J.-L.; Leong, K.W.; Wang, J. Surface charge critically affects tumor penetration and therapeutic efficacy of cancer nanomedicines. *Nano Today* 2016, *11*, 133-144, doi:https://doi.org/10.1016/j.nantod.2016.04.008.

12. Sun, Q.; Ojha, T.; Kiessling, F.; Lammers, T.; Shi, Y. Enhancing Tumor Penetration of Nanomedicines. *Biomacromolecules* 2017, *18*, 1449-1459, doi:10.1021/acs.biomac.7b00068.

13. Stylianopoulos, T.; Soteriou, K.; Fukumura, D.; Jain, R.K. Cationic nanoparticles have superior transvascular flux into solid tumors: Insights from a mathematical model. In Proceedings of Annals of Biomedical Engineering, 2013; pp. 68-77.

14. Bilensoy, E. Cationic nanoparticles for cancer therapy. *Expert Opinion on Drug Delivery* 2010, *7*, 795-809, doi:10.1517/17425247.2010.485983.

15. Reisch, A.; Runser, A.; Arntz, Y.; Mély, Y.; Klymchenko, A.S. Charge-Controlled Nanoprecipitation as a Modular Approach to Ultrasmall Polymer Nanocarriers: Making Bright and Stable Nanoparticles. *ACS nano* 2015, *9*, 5104-5116, doi:10.1021/acsnano.5b00214.

16. Esposito, D.; Conte, C.; Dal Poggetto, G.; Russo, A.; Barbieri, A.; Ungaro, F.; Arra, C.; Russo, G.; Laurienzo, P.; Quaglia, F. Biodegradable nanoparticles bearing amine groups as a strategy to alter surface features, biological identity and accumulation in a lung metastasis model. *Journal of Materials Chemistry B* 2018, *6*, 5922-5930, doi:10.1039/C8TB01330F.

17. Monopoli, M.P.; Åberg, C.; Salvati, A.; Dawson, K.A. Biomolecular coronas provide the biological identity of nanosized materials. *Nature Nanotechnology* 2012, *7*, 779, doi:10.1038/nnano.2012.207.

18. Corbo, C.; Molinaro, R.; Parodi, A.; Toledano Furman, N.E.; Salvatore, F.; Tasciotti, E. The impact of nanoparticle protein corona on cytotoxicity, immunotoxicity and target drug delivery. *Nanomedicine* 2016, *11*, 81-100, doi:10.2217/nnm.15.188.

19. Boraschi, D.; Italiani, P.; Palomba, R.; Decuzzi, P.; Duschl, A.; Fadeel, B.; Moghimi, S.M. Nanoparticles and innate immunity: new perspectives on host defence. *Seminars in immunology* 2017, *34*, 33-51, doi:10.1016/j.smim.2017.08.013.

20. Shi, B.; Fang, C.; Pei, Y. Stealth PEG-PHDCA niosomes: Effects of Chain Length of PEG and Particle Size on Niosomes Surface Properties, In Vitro Drug Release, Phagocytic Uptake, In Vivo Pharmacokinetics and Antitumor Activity. *Journal of Pharmaceutical Sciences* 2006, *95*, 1873-1887, doi:https://doi.org/10.1002/jps.20491.

21. Abdelbary, A.A.; Li, X.; El-Nabarawi, M.; Elassasy, A.; Jasti, B. Effect of fixed aqueous layer thickness of polymeric stabilizers on zeta potential and stability of aripiprazole nanosuspensions. *Pharmaceutical Development and Technology* 2013, *18*, 730-735, doi:10.3109/10837450.2012.727001.

22. Ungaro, F.; d'Angelo, I.; Coletta, C.; d'Emmanuele di Villa Bianca, R.; Sorrentino, R.; Perfetto, B.; Tufano, M.A.; Miro, A.; La Rotonda, M.I.; Quaglia, F. Dry powders based on PLGA nanoparticles for pulmonary delivery of antibiotics: modulation of encapsulation efficiency, release rate and lung deposition pattern by hydrophilic polymers. *Journal of controlled release : official journal of the Controlled Release Society* 2012, *157*, 149-159, doi:10.1016/j.jconrel.2011.08.010.

23. Conte, C.; Mastrotto, F.; Taresco, V.; Tchoryk, A.; Quaglia, F.; Stolnik, S.; Alexander, C. Enhanced uptake in 2D-and 3D-lung cancer cell models of redox responsive PEGylated nanoparticles with sensitivity to reducing extra- and intracellular environments. *Journal of Controlled Release* 2018, *277*, 126-141, doi:10.1016/j.jconrel.2018.03.011.

24. Wan, F.; Nylander, T.; Klodzinska, S.N.; Foged, C.; Yang, M.; Baldursdottir, S.G.; H, M.N. Lipid Shell-Enveloped Polymeric Nanoparticles with High Integrity of Lipid Shells Improve Mucus Penetration and Interaction with Cystic Fibrosis-Related Bacterial Biofilms. *ACS applied materials & interfaces* 2018, *10*, 10678-10687, doi:10.1021/acsami.7b19762.

25. Takeuchi, T.; Kitayama, Y.; Sasao, R.; Yamada, T.; Toh, K.; Matsumoto, Y.; Kataoka, K. Molecularly Imprinted Nanogels Acquire Stealth In Situ by Cloaking Themselves with Native Dysopsonic Proteins. *Angewandte Chemie International Edition* 2017, *56*, 7088-7092, doi:10.1002/anie.201700647.

26. Fleischer, C.C.; Payne, C.K. Nanoparticle-cell interactions: molecular structure of the protein corona and cellular outcomes. *Acc Chem Res* 2014, *47*, 2651-2659, doi:10.1021/ar500190q.

27. Pozzi, D.; Colapicchioni, V.; Caracciolo, G.; Piovesana, S.; Capriotti, A.L.; Palchetti, S.; De Grossi, S.; Riccioli, A.; Amenitsch, H.; Laganà, A. Effect of polyethyleneglycol (PEG) chain length on the bio–nano-interactions between PEGylated lipid nanoparticles and biological fluids: from nanostructure to uptake in cancer cells. *Nanoscale* 2014, *6*, 2782-2792, doi:10.1039/C3NR05559K.

28. Prego, C.; Torres, D.; Alonso, M.J. The potential of chitosan for the oral administration of peptides. *Expert Opinion on Drug Delivery* 2005, *2*, 843-854, doi:10.1517/17425247.2.5.843.

29. d'Angelo, I.; Casciaro, B.; Miro, A.; Quaglia, F.; Mangoni, M.L.; Ungaro, F. Overcoming barriers in Pseudomonas aeruginosa lung infections: Engineered nanoparticles for local delivery of a cationic antimicrobial peptide. *Colloids and surfaces. B, Biointerfaces* 2015, *135*, 717-725, doi:10.1016/j.colsurfb.2015.08.027.

30. Chen, H.T.; Kim, S.W.; Li, L.; Wang, S.Y.; Park, K.; Cheng, J.X. Release of hydrophobic molecules from polymer micelles into cell membranes revealed by Forster resonance energy transfer imaging. *P Natl Acad Sci USA* 2008, *105*, 6596-6601, doi:10.1073/pnas.0707046105.